COO-2250-10
MITNE-164

GAMMA HEATING MEASUREMENTS IN FAST BREEDER REACTOR BLANKETS

by

P. A. Scheinert and M. J. Driscoll

August, 1974

Department of Nuclear Engineering
Massachusetts Institute of Technology
Cambridge, Massachusetts

AEC Research and Development Report
UC-34 Physics
Contract AT(11-1) - 2250
U. S. Atomic Energy Commission

MASSACHUSETTS INSTITUTE OF TECHNOLOGY
DEPARTMENT OF NUCLEAR ENGINEERING
Cambridge, Massachusetts

GAMMA HEATING MEASUREMENTS IN FAST BREEDER REACTOR BLANKETS

by

P. A. Scheinert and M. J. Driscoll

August, 1974

COO-2250-10
MITNE - 164

AEC Research and Development Report
UC-34 Physics

Contract AT (11-1) - 2250

U. S. Atomic Energy Commission

DISTRIBUTION

COO-2250-10 MITNE - 164

AEC Research and Development Contract

AT (11-1) - 2250
UC - 34 Physics

1-3. U. S. Atomic Energy Commission, Headquarters
Division of Reactor Development and Technology
Reactor Physics Branch

4,5. U. S. Atomic Energy Commission
Cambridge Office

6. Dr. Paul Greebler, Manager
Nuclear Energy Division
Breeder Reactor Department
General Electric Company
319 DeGuigne Drive
Sunnyvale, California 94086

7. Dr. Harry Morewitz, Manager
LMFBR Physics and Safety Projects
Atomics International
P. O. Box 309
Canoga Park, California 91305

8. Mr. Malcolm Dyos, Manager
Nuclear Development, LMFBR Project
Westinghouse Electric Corporation
Advanced Reactors Division
Waltz Mill Site
P. O. Box 158
Madison, Pennsylvania 15663

9. Dr. Robert Avery, Director
Reactor Physics Division
Argonne National Laboratory
9700 South Cass Avenue
Argonne, Illinois 60439

10. Dr. Charles A. Preskitt, Jr. Manager
Atomic and Nuclear Department
P. O. Box 608
San Diego, California 92112

ABSTRACT

Gamma heating measurements have been performed in a mockup of the blanket and reflector regions of an LMFBR using thermoluminescent dosimeters (TLD's). Supporting work was carried out on the use of cavity ionization theory to develop the spectral response factors necessary for the interpretation of the data.

Dose traverses were made using ^{7}LiF TLD rods encapsulated in stainless steel (to represent fuel rod cladding), aluminum (to simulate sodium coolant) and lead (to simulate UO_2 fuel). Absolute dose rates were determined using a Co-60calibration facility developed for the purpose, and the results were compared to state-of-the-art calculations using the ANISN computer program in the S_8, P_1 option and a 40 group (22 neutron, 18 gamma) coupled cross section set. Coolant and clad heating rates were underpredicted by roughly 50%, but the much larger fuel dose rates were predicted within the experimental uncertainty ($\pm 1\sigma = 8\%$), so that the overall gamma heating rate is only underestimated by about 20%.

Traverses made using stainless steel ionization chamber dosimeters confirm the TLD data within experimental uncertainty. It is concluded that TLD methods; with only slight and forseeable improvements, are satisfactory for gamma heating studies in fast breeder reactor assemblies.

ACKNOWLEDGMENTS

The work described in this report has been primarily performed by the principal author, Paul A. Scheinert, who has submitted substantially the same report in partial fulfillment of the requirements for the Nuclear Engineer Degree at M.I.T.

The financial support from the Atomic Energy Commission is deeply appreciated.

The advice and assistance of A. Supple on Experimental Work has been extremely helpful. J. Shin very capably carried out the ionization chamber experiments reported in Chapter 5. V. A. Miethe is gratefully acknowledged for her assistance with the many computer program runs which were performed at the M.I.T. Information Processing Center and the Laboratory for Nuclear Science. The typing of this report has been very ably handled by Miss Nina Robinson.

Finally, the principal author wishes to thank his family for their encouragement during the difficult period prior to completion of this work.

TABLE OF CONTENTS

LIST OF FIGURES

LIST OF TABLES

Chapter 1
INTRODUCTION

1.1 FOREWORD

The United States and a number of foreign countries are presently developing the Liquid Metal Fast Breeder Reactor (LMFBR) as a means of supplying future energy demands. When this reactor becomes a commercial reality it will produce an excess of Pu-239 from U-238 and thereby vastly expand usable nuclear fuel resources. A considerable portion of the conversion of U-238 to Pu-239 occurs in the radial and axial blankets of the LMFBR.

A significant period of time is required before bred plutonium generates a substantial amount of fission energy in the blanket. During this period gamma ray interactions are the primary source of heating in the outer rows of the radial blanket. The gamma photons are contributed by leakage from the core, and by neutron absorption in the blanket's fuel, structure, and coolant.

Therefore, in order to perform adequate thermal and hydraulic analyses for fuel assembly and reflector design, the spatial distribution of the energy deposited by gamma photons must be calculated. Furthermore, in order to develop and validate design methods, it is necessary to acquire benchmark experimental data for realistic configurations. The purpose of the present work was to measure such data in a mockup of the radial blanket and reflector regions of an LMFBR, and in particular to compare state-of-the-art experimental methods and calculational techniques. Particular emphasis has been placed upon the use of thermoluminescent dosimeters (TLD's) which have become the most widely accepted devices for gamma dosimetry in applications of the present type, due to their small size and relative insensitivity to neutrons. Considerable effort has also been made to provide independent

experimental verification of the results using other approaches, and to critically examine all aspects of the TLD method.

1.2 BACKGROUND

1.2.1 Survey of Methods for Measuring Gamma Heating

There are several approaches which have proven useful for the measurement of gamma energy deposition in the mixed neutron-gamma environment of nuclear reactors:

(a) Thermoluminescent dosimeters

(b) Ionization chambers

(c) Radiophotoluminescent dosimeters

(d) Microcalorimeters

Thermoluminescent dosimetry has been used in the past primarily for health physics applications (A, 3). Recently, other investigators (S, 4)(K, 1)(B, 6)(T, 3) have looked into using TLD's in critical facilities and shielding analysis. As noted in several excellent reviews (D, 1)(T, 2) (C, 1)(B, 1) TLD's are crystals of solid state material which trap electrons in lattice imperfections. These electrons are produced from gamma interactions (photoelectric effect, compton scattering, and pair production). These primary electrons in turn produce secondary electrons. When the crystals are heated, the electrons are released from their traps and fall back into their ground state. This process emits visible-spectrum light photons. The amount of light given off during this process can be measured with a photomultiplier tube. Both the total light given off and the glow curve of the dosimeter may be used to determine the gamma dose received by the dosimeter crystal. (The glow curve is the light emission as a function of temperature).

Ionization chambers can also be used for gamma heating. These chambers are nothing more than capacitors with a gaseous "dielectric," consisting of outer and inner electrodes held apart by insulation. The

space between the electrodes may be filled with a variety of gases, selected to suit the application. A charge is placed on the chamber to create a potential difference between the shell and inner electrode. When gamma photons interact with the shell, energetic primary and secondary electrons are produced. These in turn move to the central anode. This process reduces the potential difference between the outer shell and inner anode. Several modes of operation are possible: on-line instruments used in either the current or the pulse mode, or as passive dosimeters. Argonne National Laboratory (Y, 1) (S, 5) is currently using on-line instruments in the pulse mode, because the pulse shape can be used to distinguish between neutron and gamma-initiated events. Passive dosimetry was used in the present work. Ion chambers were used as integrating dosimeters - somewhat similar in concept to the pocket dosimeter commonly used for personnel monitoring. An initial voltage difference was imposed on the chambers: they were then irradiated and an electrometer was used to determine the final voltage. A calibration curve (plot of voltage change vs. total dose) was used to find the absolute gamma dose received by the Ionization Chamber Dosimeters (ICD's).

Radiophotoluminescent (RPL) dosimeters have also been used in critical facilities (D, 2). Luminescence involves the absorption of energy in matter and its re-radiation in the visible or near-visible spectral range. The ability of a particular RPL material to luminesce efficiently frequently depends on so-called activators, or special foreign atoms present in small quantities (Luminescence Centers). The energetic state of these luminescence centers (and hence the position of the absorption and emission bands corresponding to luminesence) can change under the effect of ionizing radiation. This change in the photoluminescence due to ionizing radiation is called radiophotoluminescence (RPL). This RPL effect can be used to detect and measure the dose from ionizing radiation such as gamma rays.

After exposing RPL materials to a gamma dose they must be read

out. This is done by exposing them to a light source which has been filtered so that only the proper range of wave lengths reach the RPL material. This excitation light causes the RPL to radiate at a different wavelength than the excitation light. This re-emitted light is viewed through a filter so that only the re-radiated light from the RPL is detected. The intensity (measured with a photomultiplier tube) can then be related to the dose received by the RPL through calibration.

Direct measurement of heating rates using calorimeters is an obvious approach. However, in a zero power critical facility the heating rates are so small, on the order of 5×10^{-5} °C/sec, that they are very hard to measure. Microcalorimetry is therefore required to measure these small temperature differences. In addition to this requirement the calorimeters must be small so that the neutron and gamma fluxes in the critical are not greatly perturbed. Atomics International engineers have designed, built, and used microcalorimeters (S, 10)(A, 1)(A, 2) in FBR criticals to directly determine the amount of heating which occurs in samples. The AI calorimeter consists of a stainless steel tube 5.08 cm. in diameter. The tube is evacuated to a pressure on the order of 10^{-6} torr and the sample is placed inside. A tubular copper heat shield is placed in the annulus between the sample and outer steel tube. An electric heating coil surrounding the copper tube is controlled by a differential thermocouple which monitors the temperature difference between the sample and copper shield. The thermocouple and its controller keep this temperature differential less than 0.003 °C, thereby creating an extremely stable thermal environment.

The most important parts of the microcalorimeter are the temperature measuring devices. The AI calorimeter uses both a quartz crystal thermometer and a platinum resistance thermometer. Both have yielded essentially identical results.

Several experiments have been completed in the Atomics International

FCEL critical assembly and in the Zero Power Plutonium Reactor (ZPPR). In general, the ratio of measured values to calculated values has been in the range of 0.7 to 0.9 for the FCEL experiments. The heating rates in these facilities have also been determined with TLD's. The TLD results have generally spanned the calorimeter results.

Table 1.1 summarizes the techniques discussed and lists advantages and disadvantages of each method.

TABLE 1.1

Comparison of techniques used for gamma heating measurements

TLDs	1. Very small size 2. Can measure high doses 3. Good readout systems are available. 4. TLD's are easily obtained	1. Response destroyed upon Readout. 2. Sensitive to annealing procedure. 3. Response to neutrons not well known.
RPL	1. Very small. 2. Readout devices are available or simple to build. 3. Signal not destroyed on readout 4. Can measure high doses.	1. Response to neutrons not well known, but greater than TLD's. 2. Signal may fade with time 3. Sensitive to annealing procedure.
Ionization Chamber Dosimeters (ICD)	1. Easy to construct 2. Readout method is very simple.	In dosimeter mode 1. Can take only low doses before complete discharge 2. Sensitive to dirt (causes charge leakage. 3. Neutron Response is unknown.
Microcalorimeter	1. Measures direct temperature changes. 2. The higher the heating rate the more accurate it gets.	1. Large (perturbs flux) 2. Temperature measuring devices are very sensitive. This requires a sophisticated and hard to build reader. 3. Calorimeter is difficult to build.

TLD's were chosen for use in the M.I.T. blanket test facility primarily because they were readily available, operated well in the dose range encountered, were small in size and this did not perturb the gamma or neutron fluxes greatly. Also, enough is known about the neutron responses of TLD's so that neutron effects can be estimated. RPL's and ionization chambers are also fairly simple to construct and use and were therefore used at M.I.T. to provide independent verification. Microcalorimeters have not been used at M.I.T. to date because they are difficult to construct and because the heating rate in the M.I.T. blanket mock-ups is at the lower boundary of the region of feasibility for state-of-the-art devices of this type.

1.2.2 Prior Fast Breeder Reactor Applications of TLDs

TLD's have been used in several particularly important experiments recently. They are

(1) Axial dose traverses in ZPPR (S, 4)

(2) Axial dose traverses in ZPR-9 (B, 6)

(3) Iron block experiments at ORNL (K, 1)

(4) Control rod studies in Atomic International's Fast Critical Experiment Laboratory. (T, 3)

At Argonne National Laboratory ^{7}LiF TLD's were encapsulated in stainless steel and used to make axial gamma dose measurements in the Zero Power Plutonium Critical Facility. The ^{7}LiF TLDs were enriched in lithium-7 so that the effect of the large Li^{6} neutron absorbtion cross section would be greatly reduced. The dose traverses extended throughout the inner and outer core, blanket, and reflector regions. The dosimeters were calibrated with various doses from a Ra^{226} cell. The standard deviation of the calibrated TLD's was found to be 3.5%. Once spectral corrections were applied, the experimental results were

assigned an overall error of ±5%.

The measured heating rates were compared against heating rates calculated by the transport code POPOP4 (F, 3). The cross sections which were used as input to POPOP4 were prepared using the code MUG (K, 2).

The agreement between the calculated and experimental results was generally within the limits of experimental error in the core regions. The shape of spatial distributions for measured heating rates in the blanket and reflector generally agreed well with calculations. However, the absolute doses were not in as good agreement, experimental data generally exceeding calculated values.

TLD runs were also conducted in control rod mock-ups constructed of B_4C and tantalum. In both of these materials , the results predicted by calculations were within the probable errors assigned to the experimental values.

Over 400 LiF^7 TLD's were used in axial dose traverses in the FTR-9 engineering mock-up critical. The TLD's used had dimensions of 1mm. x 1mm. x 6mm. and were enclosed in stainless steel sleeves. The capsule design was identical to that in the ZPPR experiments. A similar calibration technique and spectral correction process was employed, again resulting in overall errors of ±5%.

The ANISN computer code along with cross sections generated by MUG supplied calculated heating rates for comparison.

As was the case in ZPPR, the absolute agreement was very good in the core region: well within experimental errors. Again in the blanket, and especially in the reflector regions, the experiment gave values greater than the calculation predicted, suggesting a similar outcome in M.I.T.'s blanket experiments.

At Oak Ridge National Laboratory a particularly clean experiment has been performed to measure gamma heating dose rates. In this work a cobalt-60 source was embedded in iron and placed at the rear of

several slabs of iron having an overall thickness of 12.3 cm. Thermoluminescent dosimeters ($CaSo_4$; Dy or CaF_2: Dy powder in iron capsules) were placed in several positions on the front of the iron slabs and thereby subjected to a range of doses. The computer codes DOT and ANISN were then used to calculate the gamma spectrum. The two computed results agreed very well. This spectrum and current TLD techniques were then used to determine experimental values for gamma heating rates at each dosimeter location.

The ANISN and DOT codes were also used to calculate the heating rates.

Both TLD data analyses and gamma heating transport calculations require an accurate knowledge of the gamma spectrum. To insure that the gamma spectrum was calculated properly a sodium iodide spectrometer was used to experimentally determine the gamma spectrum in the Oak Ridge facility. Since the spectrometer is placed at some distance from the slab the gamma spectrum at the NaI crystal is not the same as that in the slab of iron. Given a multigroup spectrum in the iron slabs the FALSTF code calculates the spectrum at the NaI crystal. The DOT-FALSTF calculations agreed very well with the spectrometer measurements at small angles where the photons passed through the minimum thickness of iron. However, at large angles where the gammas had to pass through a large thickness of iron the spectral calculations did not agree quite so well. At these large angles the integrals of the calculated and the measured spectra were determined. The measured integral was larger by approximately 27%.

The heating rates measured with TLD's also agreed well with calculations when the distance through the iron was small, however, at large distances the TLD values were larger by as much as 30%. The discrepancies in the heating rates and spectral comparisons suggest that the calculations at large distances from the source are in error.

As in the ZPPR, and ZPR experiments, the Oak Ridge TLD results at the outer edges of the facility were larger than the calculated dose rates. Again this makes the M.I.T. study in the reflector mock-up particularly interesting.

TLD's were used to measure gamma heating rates in tantalum control rods at the Atomics International Fast Critical Experiment Laboratory. In this facility tantalum control rod clusters were studied. Holes were drilled into the control rods for LiF^7 TLD's (1 mm diam. by 6 mm).

This AI study undertook only to determine the heating rates with TLD's. No calculational comparisons were made. The results indicate that the largest areas of uncertainty deal with spectral response factors and fast neutron effects. The response factor uncertainty was a result of the uncertainty in the ambient gamma spectrum. The study also shows that lead sheaths for TLD's are a reasonable substitute for tantalum.

The computer code RESPOND, developed by R. J. Tuttle (T, 3) at Atomics International, presents a fairly simple and useful way to calculate spectral response factors based on T. E. Burlin's theory of ionization (B, 8). This code is valuable for TLD work.

The previous work cited above has laid a very good base for the gamma heating work at M.I.T. For the most part the prior experimental results have been in good agreement with calculations. However, the largest discrepancies have appeared in blanket and reflector regions. This circumstance makes the present investigation a particularly interesting and challenging one.

1.3 ORGANIZATION OF THIS WORK

1.3.1 Preface

The objectives of this work were threefold:

(1) To acquire a state-of-the-art experimental capability for using

thermoluminescent dosimeters to make gamma heating measurements in the LMFBR blanket/reflector mock-ups irradiated in the M.I.T. research reactor Blanket Test Facility.

(2) To acquire independent verification of the TLD results with Ionization Chamber Dosimeters (ICDs) and Radio Photoluminescent Dosimeters (RPL's).

(3) To compare the experimental heating results against neutron-gamma transport calculations.

In order to achieve these objectives, work was carried out in four main areas, each dealt with in a separate chapter of this report.

Chapter 2: Analytical Considerations

Chapter 3: Calibration facilities

Chapter 4: Experimental procedures and results

Chapter 5: Comparison with other gamma measurement techniques

In the following sections each of these chapters will be previewed briefly to show their relation to the objectives.

1.3.2 Analytical Considerations

Chapter 2 describes the analytical methods, mathematical models, and general procedures which are involved in gamma heating analysis. A description of the experimental mock-up facility (Blanket No. 4) is also presented. The key problems in determination of gamma spectra and gamma heating rates are discussed. Section 2.4 gives background information to provide an understanding of how a TLD behaves when irradiated and what equipment is used for TLD readout. The last four sections of Chapter 2 are concerned with the design of a TLD capsule for which the dose in the sleeve material may be determined accurately. This requires consideration of a number of items, such as cavity ionization theory, neutron effects, sleeve material selection, and

thermoluminescent material selection.

1.3.3 Calibration Facility

To obtain absolute dose rates in any gamma field the gamma detectors must be calibrated with a gamma ray source from which the dose rate is well known. For the present work the calibration of dosimeter capsules must be carried out over a wide range of absorbed doses: The dose rates in a typical blanket in the M.I.T. blanket test facility range from 300 rads per hour at the converter/blanket interface to 0.1 rads per hour in the reflector region. Two cobalt-60 gamma sources were used for calibration. The first source contained approximately 4400 curies and was located at Massachusetts General Hospital. The second source was a "Point" source encapsulated in a 3/4 in. O.D. by 1 in. steel slug. The source activity was approximately 70 mc . The procedures involved in using these sources and the construction of various auxiliary apparatus is described in Chapter 3.

1.3.4 Experimental Results and Comparison with Calculation

In Chapter 4 the experiment and its results are discussed. The actual procedure used is described early in the chapter. Comments are made on the bookkeeping strategy and run length determination. Once the raw TLD readouts have been converted to a gamma heating rate, the results must be normalized to some standard for comparison. This normalization scheme is presented in section 4.3. Section 4.4 presents the actual results. These results include the comparison of experimental and calculated dose rates for radial traverses. Results of and conclusions drawn from vertical and horizontal dose traverses used to determine a transverse buckling for leakage calculations are also discussed.

Chapter 4 also contains the dose rates measured in six sleeve materials. (Aluminum, stainless steel, tin, zirconium, tungsten, and lead). The heating rates from these materials were used to unfold the ambient gamma spectrum at the center of the blanket.

In section 4.4.4 the results of an experiment using TLD's encapsulated in a teflon sleeve are discussed. Since teflon's gamma absorption properties are very similar to those of lithium fluoride the ratio of the dose received by the teflon to that received by the TLD's will be 1.0 regardless of gamma energy. This constitutes a "Matched Cavity" dosimeter. When the TLD readouts of a "Matched Cavity" dosimeter and an unmatched cavity dosimeter are compared with calculations, the accuracy with which spectral response factors are calcuated can be determined. An experiment of this type using ^{7}LiF TLD's encapsulated in teflon, stainless steel, and lead is described in section 4.4.4.

1.3.5 Comparison with other Experimental Methods

Ionization chamber dosimeters were used to make independent dose measurements in the blanket mock- up. These results are compared to the TLD results in Chapter 5. Work is also reported on the use of lithium fluoride as a radiophotoluminescent material.

1.3.6 Summary and Appendices

The final chapter summarizes the highlights and major conclusions of the work. Also, recommendations for future work are offered. The report concludes with five appendices. The first contains a listing of symbols and nomenclature used throughout the report. Appendix B lists all of the cross sections which have been used in this study, with the

exception of the 40 group coupled set from Oak Ridge National Laboratory. This set is described in reference (M,1) and discussed further in section 2.3.1. Appendix C contains much of the intermediate data, including raw data, readouts for calibration runs, and dose traverses. Appendix D deals with computer analyses. The first section documents modifications which were made to RESPOND (which calculates Burlin "S" Factors). Appendix D2 presents a sample problem for the modified version of RESPOND.

Appendices D3 and D4 discuss the small programs INTERP and GAMRE. INTERP interpolates gamma energy absorbtion coefficients and punches them on cards in a suitable format for input to respond. GAMRE is a short program which uses the 18-group gamma spectrum from ANISN to prepare and punch the input spectrum for RESPOND.

Appendix D5 presents a sample problem for MITSPECTRA. A computer program which, while developed for foil-method neutron spectrometry, can be used to unfold a gamma spectrum from a set of measured gamma heating rates.

The last appendix lists all references.

Chapter 2
ANALYTICAL CONSIDERATIONS

2.1 INTRODUCTION

The use of TLD's to determine accurate gamma heating rates requires careful consideration of the characteristics of the TLD and its environment, both local and global. Thus, this chapter deals with two major topics: The pertinent characteristics of the blanket mockup in which gamma heating traverses are to be measured; and the many factors involved in the appropriate choice and use of the TLD and its capsule.

Section 2.2 presents a brief description of blanket mockup No. 4 and the M.I.T. Blanket Test Facility. Section 2.3 discusses the application of state-of-the-art methods to compute assembly photonics, emphasizing aspects pertinent to the selection of the TLD and its capsule.

Sections 2.4 through 2.8 discuss the physical phenomena underlying TLD behavior, the theoretical basis for relating TLD response to dose, neutron interference, and selection and design of the capsules.

2.2 DESCRIPTION OF BLANKET MOCKUP NO. 4

The Blanket Test Facility (BTF) at the M.I.T. reactor has been designed to test simulated fast reactor blankets. Detailed descriptions are given in references (L,1) and (F,1). A brief description follows.

Highly thermalized neutrons from the thermal column of the M.I.T. reactor enter the graphite-lined hohlraum. This arrangement is shown in Fig. 2.1. The BTF is located at the outer end of the hohlraum, and consists of a converter assembly, and a boral-lined cavity in which fast reactor blankets can be irradiated. The converter

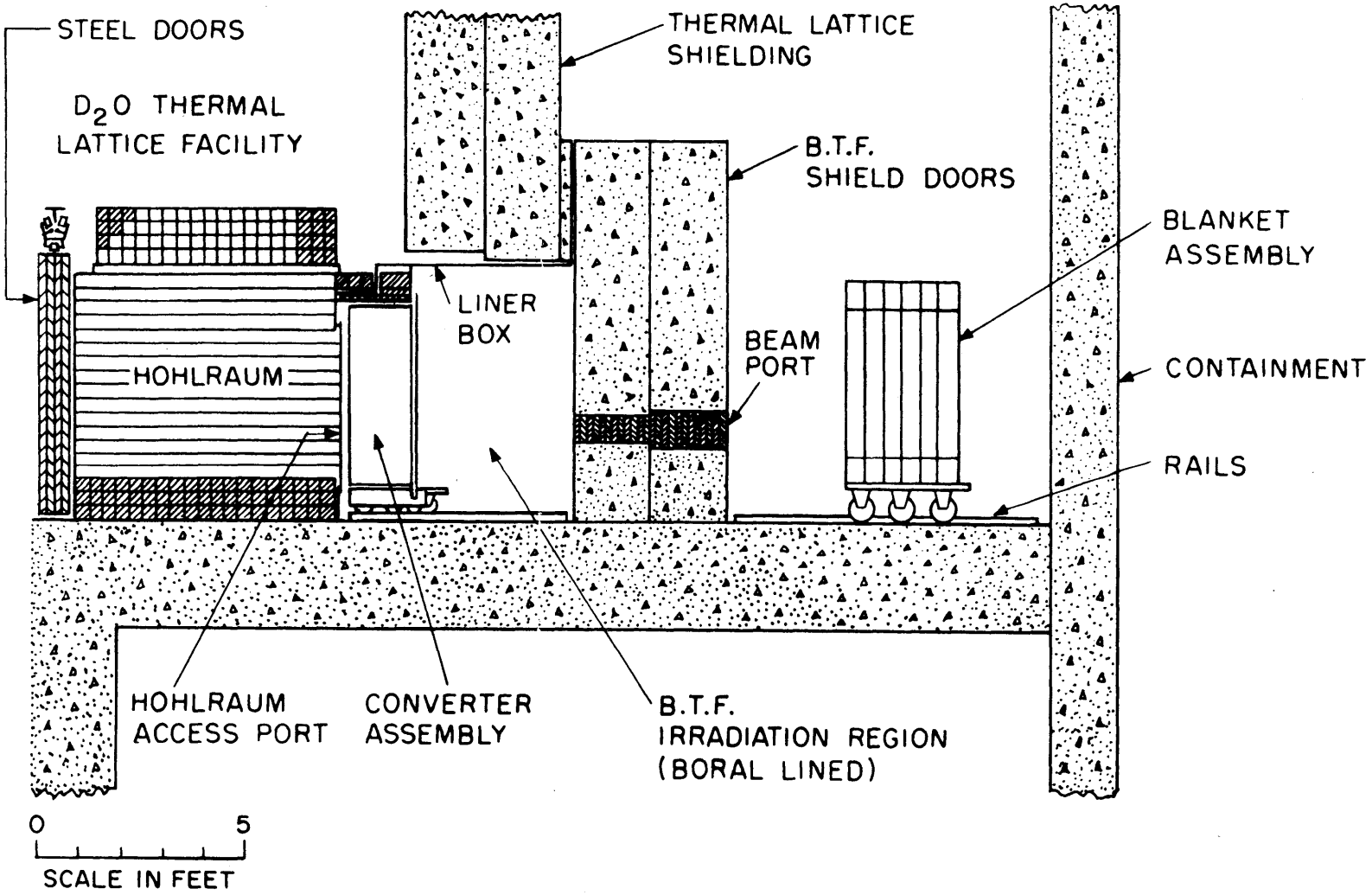

FIG. 2.1 SCHEMATIC CROSS SECTION VIEW OF HOHLRAUM AND BLANKET TEST FACILITY

assembly consists of successive layers of graphite and aluminum-clad UO_2 fuel designed to produce a driving spectrum similar to that leaking from a real LMFBR core. During the work reported in this thesis the converter composition was tailored to deliver a leakage spectrum simulating that of a demonstration plant sized core. All irradiations were carried out in Blanket Mockup No. 4, a 3 sub-assembly row, steel reflected simulation of a typical LMFBR blanket.

Figures 2.2 and 2.3 show isometric and top views of the blanket assembly. The assembly contains 25 sub-assemblies. Each sub-assembly contains 121 fuel rods. The fuel is slightly enriched uranium metal clad in mild steel tubing. The space between the fuel rods is filled with anhydrous sodium chromate. The exact composition and construction is described in reference (L,1).

The blanket is designed to simulate a fast reactor blanket employing UO_2 fuel, stainless steel cladding and sodium coolant. The homogenized atom densities for both Blanket No. 4 and an "equivalent realistic blanket" are shown in Table 2.1. The "equivalent realistic blanket" is composed of 37.0 v/o depleted UO_2 (at 90% of theoretical density), 20.7 v/o type 3/6 stainless steel (71.2 W/o Fe, 20.0 W/o Cr, and 8.8 W/o Ni), 32 v/o sodium, and 10.3 v/o void. The excellent simulation on a homogeneous basis is shown in the table; close equivalence of important heterogeneous effects has also been confirmed (G,1).

There are eighteen radial test positions located within the blanket and reflector regions: the first nine in the blanket region (see fig. 2.3) and the outer nine in a 2 in. diameter steel plug which slides into a hole in the reflector (see fig. 2.3). The experimental work discussed in this report is concerned primarily with measurement of gamma doses in these radial positions.

In addition to the radial positions there are seventeen test positions distributed across the width of the blanket. These posifions have been used to characterize transverse leakage from the blanket.

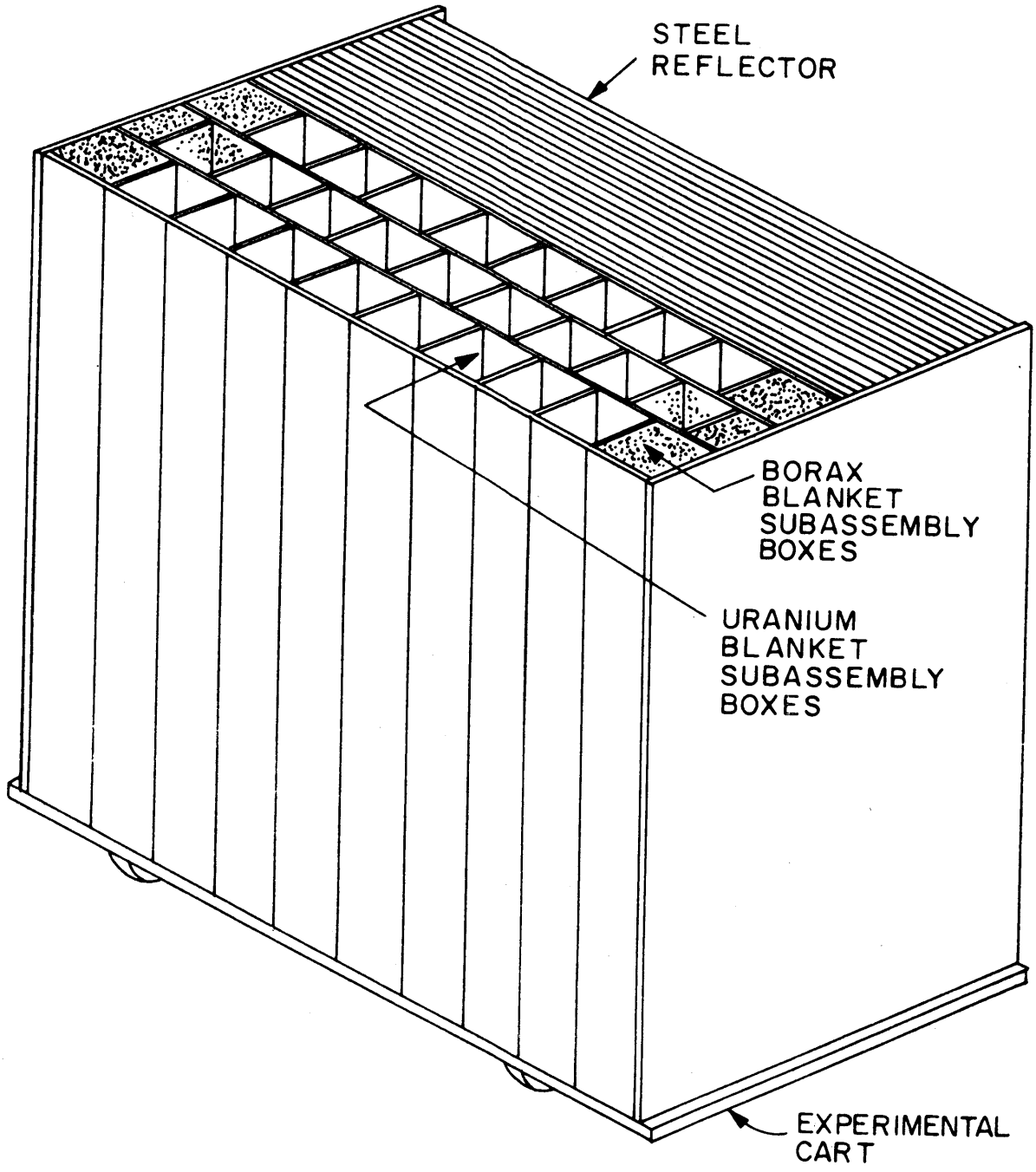

FIG. 2.2 SCHEMATIC VIEW OF BLANKET ASSEMBLY NO. 4

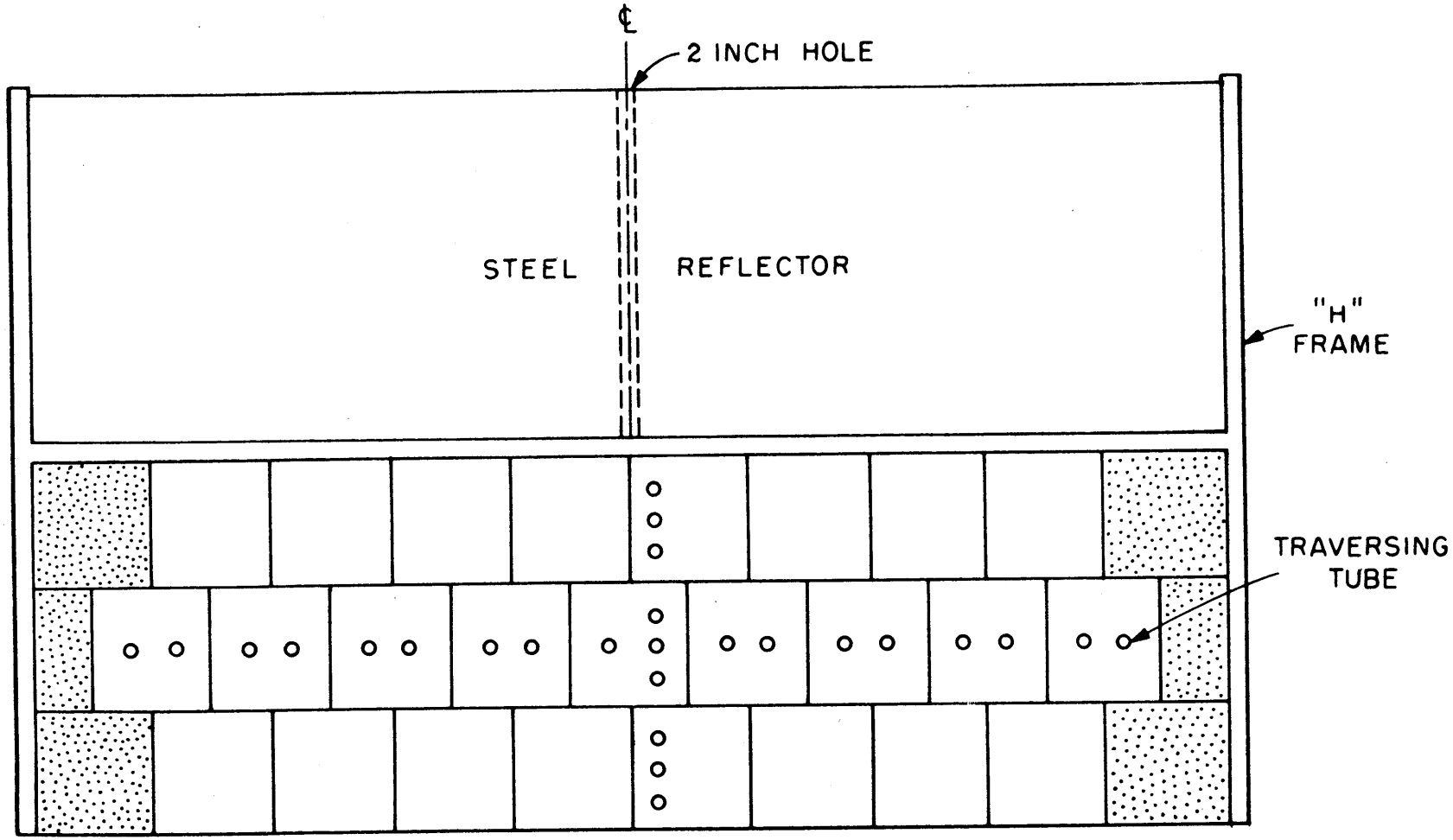

FIG. 2.3 PLAN VIEW OF BLANKET ASSEMBLY SHOWING THE TRAVERSING TUBE POSITIONS

TABLE 2.1 Homogenized Atom Densities of Blanket Mockup No. 4 (Nuclei/barn-cm)

Nuclide	Blanket Mockup No. 4		Equivalent Realistic Blanket	
U^{235}	0.000088		0.000016	
U^{238}	0.008108		0.008131	
0	0.016293		0.016293	
Na	0.008128		0.008128	
Cr	0.004064	0.017814	0.003728	0.017814
Fe	0.013750		0.012611	
Ni	0.000000		0.001475	
H	0.000073		0.000000	
C	0.000096		0.000082	

Nuclide	Steel Reflector
C	0.000590
Fe	0.084570

2.3 CALCULATION OF GAMMA SPECTRA AND HEATING RATES

Calculations of gamma spectra and heating rates are an important part of the present work. Spectra are needed to determine correction factors for TLD response; and calculated heating rates are required for comparison with the experimental results. In the present work the ANISN (E,1) one-dimensional transport program was used to carry out multigroup S_n calculations (P_0, P_1 or P_3) employing a coupled neutron-gamma cross section set.

2.3.1 Cross Sections

ANISN requires a set of multigroup cross sections for all of the materials making up an assembly. For this purpose a set of cross sections from Oak Ridge National Laboratory (M,1) was used: a coupled cross section library containing 22 neutron groups and 18 gamma groups for each material. The great advantage to using a coupled cross section library is that both neutron and gamma distributions and spectra are found simultaneously and consistently.

ANISN also requires an input of "foil activation" cross sections which are used to calculate gamma dose rates in individual materials according to the prescription:

$$D_j = \frac{KN_j}{\rho_j} \sum_{g=1}^{18} \phi_g (\sigma_j E)_g \qquad (2.1)$$

where D_j = Dose rate in material j (rads/hr.)

g = Group gamma flux (photons/cm^2 sec)

$(\sigma jE)g$ = Group absorption cross section (calories · barns/atom)

ρj = Density (gm/cm^3)

Nj = Number density ($atoms/cm^3$)

K = Conversion factor

The computer program GAMLEG 69 (R, 3) was used to calculate the cross sections $(\sigma_j E)_g$. Four materials were used for dose rate determinations: Iron, sodium, uranium metal, and uranium dioxide, representing the three major components of the blanket: structure, coolant, and fuel.

2.3.2 The ANISN Program

The ANISN computer program solves the Boltzman transport equation in one dimension using an S_n discrete ordinate technique. In this work the code has been used to calculate both neutron and gamma spectra, flux distributions, and gamma absorption rates. In addition to making calculations for the BTF, the code was used to calculate flux distributions and spectra throughout a cylindrical LMFBR for comparison.

The standard ANISN run for BTF blankets uses an S_8 approximation and a P_1 expansion. The facility is divided into eight zones. These zones are shown in Fig. 2.4. Zone 1 is the inboard layer of the converter. The left edge of this zone contains a plane source of isotropic thermal group neutrons. The next two zones, behind the graphite, are converter fuel zones consisting of aluminum-clad slightly-enriched uranium dioxide fuel rods arranged in a tightly packed slab array. A boral plate on the rear of the converter comprises zone 4.

The blanket region has been divided into three zones corresponding to the three rows of fuel boxes shown in Fig. 2.4. The homogenized nuclide concentrations used as ANISN input for these regions have already been presented in Table 2.1.

Finally, zone 8 is the mild steel reflector.

ANISN calculates neutron and gamma spectra and "foil activities" at each of 50 intervals. These intervals are distributed through the

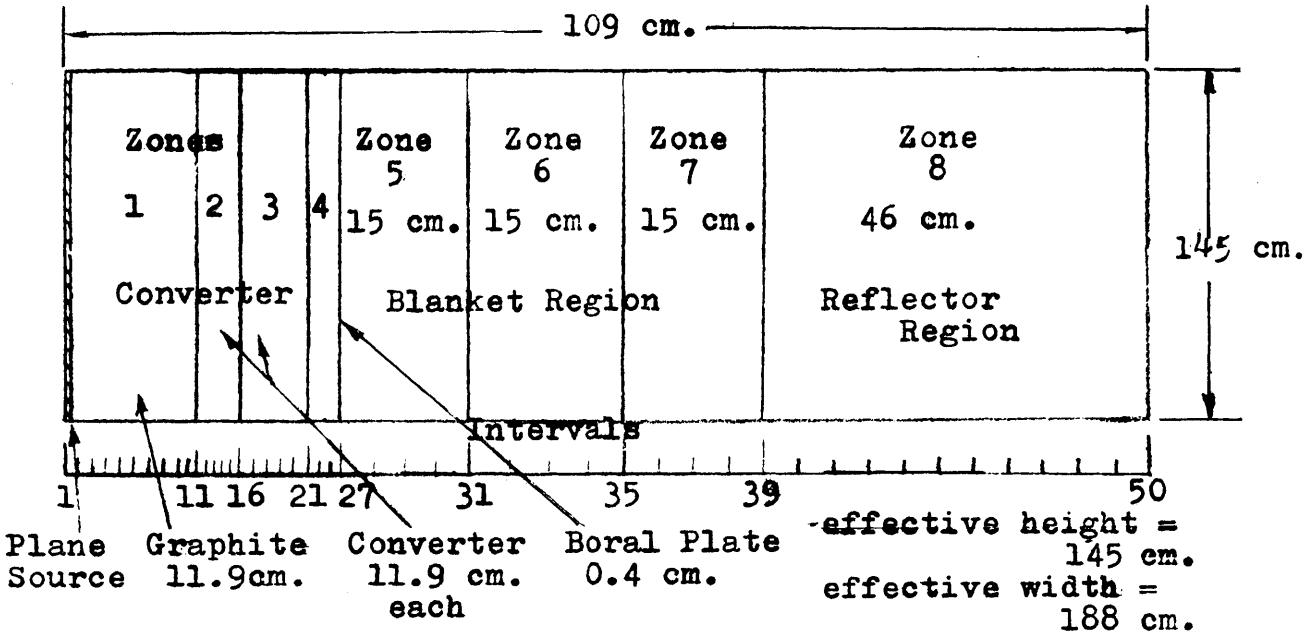

Fig. 2.4. Layout of Eight Zones Used to Describe the BTF Setup in ANISN.

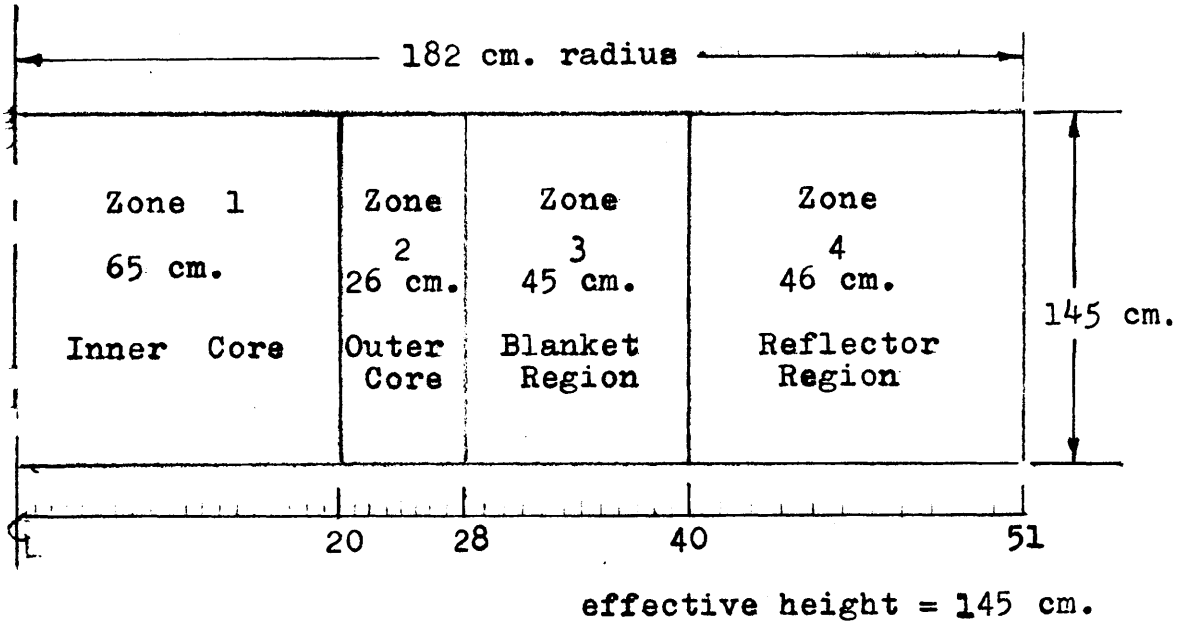

Fig. 2.5. Layout of the Four Zones Used to Describe an Actual Fast Reactor in ANISN.

ANISN calculates neutron and gamma spectra and "foil activities" at each of 50 intervals. These intervals are distributed through the assembly as follows; 1-26 in the converter, 27-38 in the blanket, and 39-50 in the reflector. Their positions are shown more exactly in Fig. 2.4. Table 2.2 shows normalized gamma spectra at 3 intervals in the BTF; the blanket mid-point, the blanket-reflector interface, and the reflector mid-point. The spectra are also plotted in Fig. 2.6.

If the Blanket Test Facility is to act as a good mockup for gamma heating it must compare favorably to an actual fast reactor. To perform this comparison ANISN was used to calculate gamma photon characteristics of an actual fast reactor. The material composition of the core has been selected (F,1) to be representative of typical fast reactor cores. The core was surrounded by a blanket and reflector with the same material compositions as Blanket Mockup No. 4. In this problem the S_8 approximation was employed, using the 40 group coupled neutron and gamma cross section set, however, only P_0 scattering was considered. The layout for this problem is shown in Fig. 2.5. The fast reactor and BTF results are compared in section 2.3.3.

ANISN was also used to determine the relative contributions of various sources to the gamma flux present in the blanket. These sources are in-leakage from the converter and production from absorption in the fuel, coolant, and structural materials. In order to make this study the cross sections input to ANISN were changed. In any coupled neutron/gamma cross section set, gamma production is accomplished through scattering from neutron groups to gamma groups. This allows a neutron to be absorbed and a gamma to be born, such as occurs in (n,γ), (n,f) or (n,n') reactions. Thus it is possible to eliminate gamma ray production by changing these particular scattering cross sections to zero. In this way one can eliminate all gamma ray production

TABLE 2.2 Normalized Gamma Spectra in Blanket and Reflector

Group	E_{max}(MEV)	Blanket Mid-Point INT 33	Blanket-Reflector Interface INT 39	Reflector Mid-Point INT 45
23	10.0	0.00095	0.00547	0.01443
24	8.0	0.00644	0.04154	0.12198
25	6.5	0.00442	0.01973	0.05559
26	5.0	0.01237	0.02052	0.04292
27	4.0	0.04316	0.03892	0.05124
28	3.0	0.07087	0.04227	0.03245
29	2.5	0.11900	0.06235	0.03108
30	2.0	0.10936	0.05737	0.02816
31	1.66	0.06784	0.04593	0.02824
32	1.33	0.13836	0.07652	0.03554
33	1.0	0.09408	0.06008	0.03052
34	0.8	0.10156	0.07273	0.03942
35	0.6	0.14325	0.14348	0.15344
36	0.4	0.04618	0.08209	0.08325
37	0.3	0.03053	0.11956	0.12131
38	0.2	0.01078	0.10612	0.12073
39	0.1	0.00078	0.00520	0.00585
40	0.05	0.00006	0.00010	0.00018

*Normalization: $\sum_{g=1}^{18} \phi_{\gamma g} = 1.0$

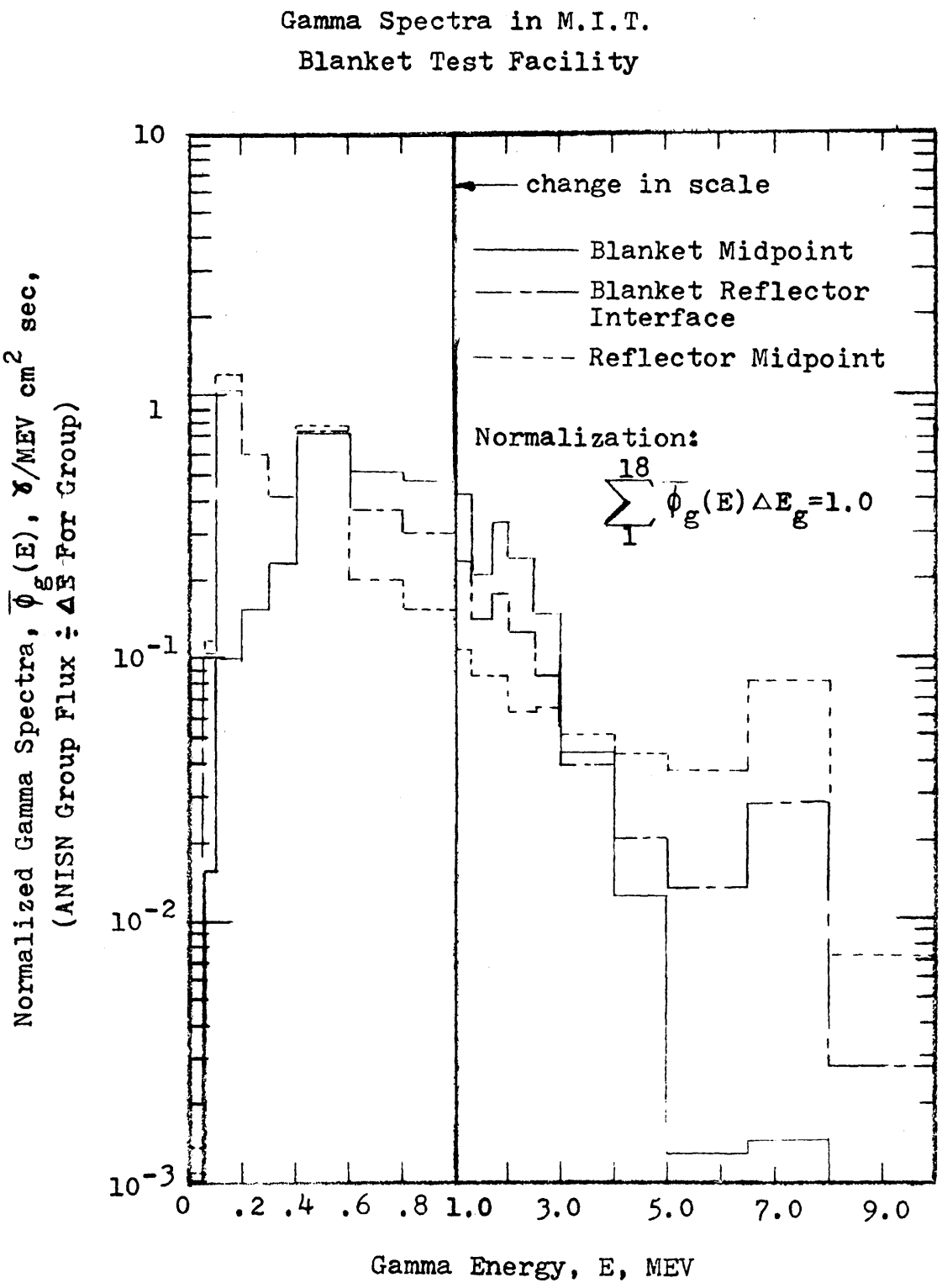

Fig. 2.6 Gamma Spectra in the M.I.T. Blanket Test Facility

from one or more materials in a mixture of materials. If in the blanket region all gamma production cross sections are zeroed-out the flux present can only be due to in-leakage from other regions. Also, if all gamma production cross sections from all materials in all zones are zeroed-out, except for one material whose cross sections are left intact then the gamma flux present is due only to that material. By making several ANISN runs with these changed cross sections, gamma flux contributions from each source may be found. The percentages of the ambient gamma flux from the four sources mentioned above are shown in Table 2.3. A similar analysis was done for the cylindrical fast reactor problem. The only difference is that the in-leakage was from the reactor core instead of from the converter. These results are shown in Table 2.4. In these two tables it is important to note that by far the largest portion of gammas are produced by neutron absorptions in blanket fuel (U-238). In section 2.3.3 it will be shown that fuel also dominates gamma absorption, indicating the major role of fuel in blanket photonics.

Nearly all ANISN calculations for the Blanket Test Facility were done with a P_1 order of scattering. To assess the adequacy of this level of approximation for gamma heating calculations the dose rate in stainless steel was calculated using ANISN for P_o, P_1 and P_3 expansions at all intervals throughout both the blanket and reflector. The results of this calculation are shown in Table 2.5. The differences between P_0 and P_1 are large enough to be of concern; but the difference between P_1 and P_3 is less than one percent. Therefore P_1 calculations are adequate for gamma heating calculations in the blanket and reflector regions of LMFBR's.

TABLE 2.3 Contribution to Gamma Flux in BTF From Various Sources

Distance from Core Interface	% from Core	% from Fuel	% from Clad(Fe)	% from Coolant
0.0 cm.	33.6%	59.6%	4.1%	2.6%
3.76 cm.	13.1%	78.7%	5.1%	3.1%
7.52 cm.	6.2%	85.7%	5.1%	3.0%
11.28 cm.	2.8%	89.4%	5.1%	2.8%
15.04 cm.	1.4%	91.1%	4.9%	2.6%
18.80 cm.	0.6%	92.3%	4.8%	2.4%
22.56 cm.	0.3%	92.8%	4.6%	2.3%
26.31 cm.	0.2%	93.2%	4.5%	2.1%
30.07 cm.	0.1%	93.5%	4.4%	2.0%
33.83 cm.	0.04%	93.8%	4.3%	1.9%
37.59 cm.	0.02%	94.3%	4.0%	1.7%
41.35 cm.	0.01%	94.8%	3.6%	1.9%

TABLE 2.4 Contribution to Gamma Flux in LMFBR Blanket from Various Sources

Distance From Converter Interface	% from Core	% from Fuel	% from Clad (Fe)	% from Coolant
0.00 cm.	39.0%	55.2%	3.57%	2.26%
7.57 cm.	7.16%	85.5%	4.72%	2.59%
22.56 cm.	0.324%	93.5%	4.28%	1.91%
30.07 cm.	0.076%	94.1%	4.13%	1.71%
41.35 cm.	0.016%	91.6%	6.22%	2.81%

TABLE 2.5 Calculated Dose Rates in Stainless Steel for Various P_n (rads /hr.)

Distance From Converter Interface	P_0	P_1	P_3
0.0 cm.	299.6	310.5	308.7
3.76 "	321.5	243.8	243.5
7.52 "	189.1	201.6	200.7
11.28 "	151.5	164.6	163.9
15.04 "	120.5	133.6	133.1
18.80 "	95.1	107.8	107.4
22.56 "	74.7	86.6	86.4
26.31 "	58.6	69.6	69.5
30.07 "	46.2	56.2	56.1
33.83 "	36.6	45.6	45.5
37.59 "	30.6	38.8	38.8
41.35 "	23.4	30.1	30.1
Reflector			
45.11 cm.	12.9	17.8	17.7
48.92 "	9.81	13.35	13.38
52.73 "	7.91	10.83	10.87
56.54 "	6.76	9.26	9.29
60.35 "	5.81	8.00	8.02
64.16 "	4.84	6.72	6.74
67.97 "	3.95	5.54	5.55
71.78 "	3.11	4.40	4.41
75.59 "	2.37	3.38	3.38
79.40 "	1.68	2.41	2.42
83.21 "	1.05	1.53	1.54
87.02 "	0.482	0.735	0.735

2.3.3 Comparison of the BTF to a Cylindrical LMFBR

In this section the ANISN results for the BTF blanket and an actual fast reactor are compared in several categories:

(1) Spatial distributions of total gamma flux

(2) Neutron absorption rates in U-238

(3) Gamma spectra in the blanket

(4) Gamma absorption in blanket materials

(5) Gamma to neutron flux ratios

This comparison gives an excellent understanding of how well the slab geometry of blanket No. 4 simulates an actual LMFBR.

The total gamma flux distribution has been calculated and is shown in Fig. 2.7 for both cases. For the most part the agreement is fairly good. However, there are differences at the front and rear of the blanket and in the reflector, ranging up to 20% which we attribute to the difference between slab and cylindrical geometry. It is important to note that the flux shapes are the same basic shape. On the whole therefore, we may conclude that the BTF blankets will provide a good simulation for a fast reactor.

The U-238 neutron absorption rates in both facilities are shown in Fig. 2.8. This quantity is very important because U-238 absorptions provide more than 90% of the gamma flux in the blanket. This was shown in Tables 2.3 and 2.4. It is therefore obvious that any valid fast reactor mockup must have U-238 capture rates which closely resemble those in the actual fast reactor. Fig. 2.6 shows that the comparison is good in the present case. In particular note that the LMFBR results compare to the BTF results, consistent with the gamma flux results in Fig. 2.7.

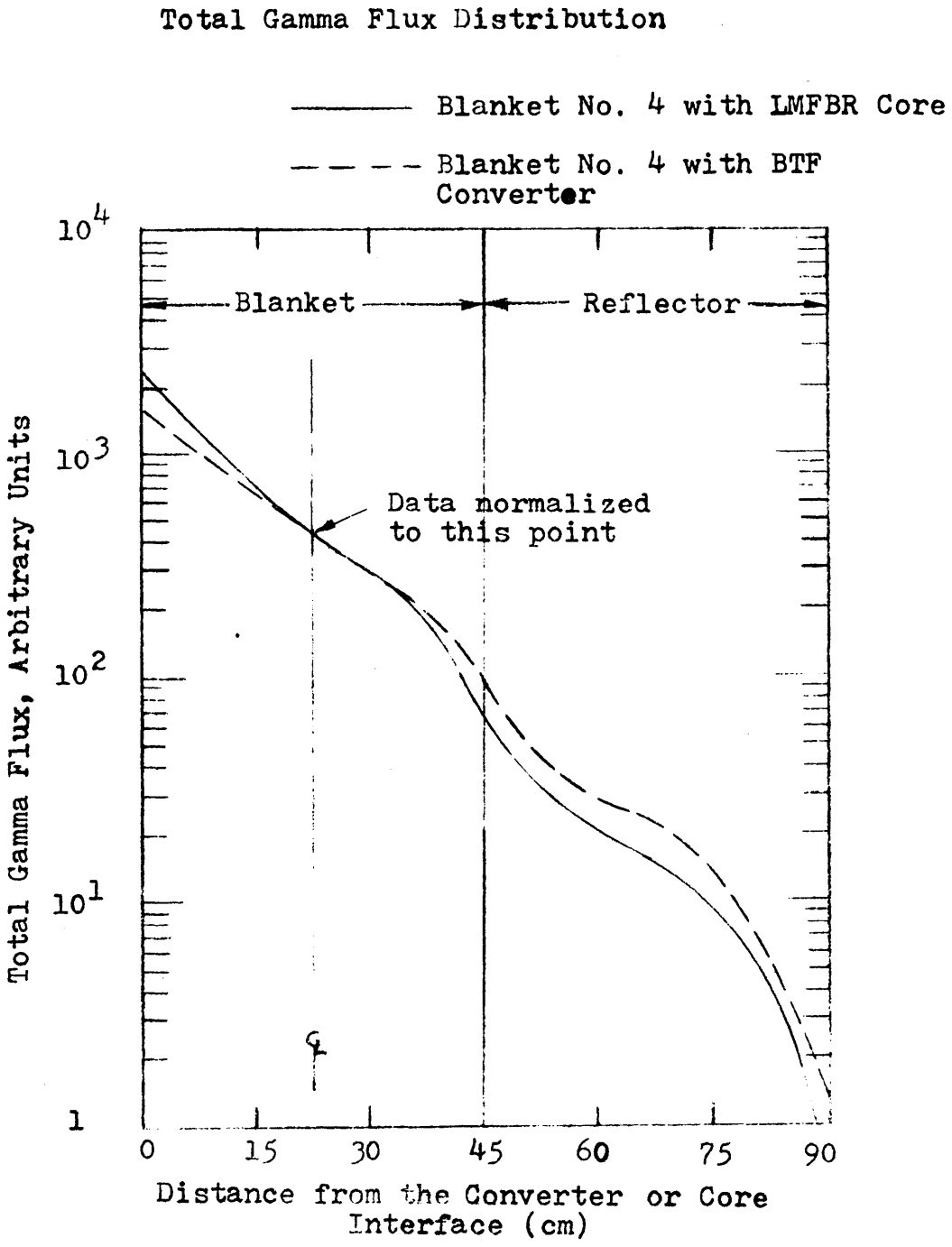

Fig. 2.7. Comparison of Total Gamma Flux in Blankets Driven by LMFBR Core and BTF Converter

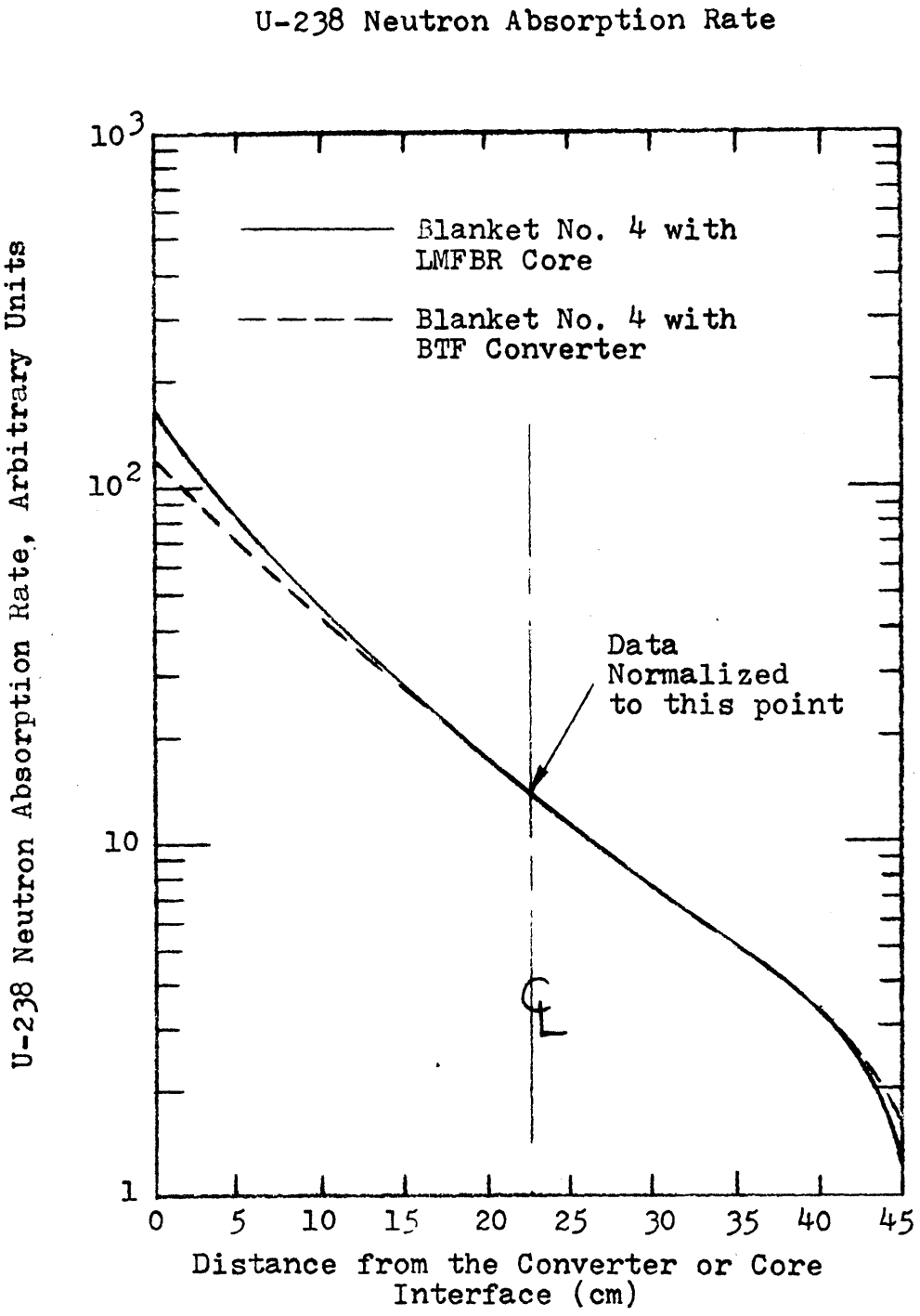

Fig. 2.8 Comparison of U-238 Absorption Rates in Blankets Driven by LMFBR Core and BTF Converter

Figure 2.9 shows the gamma spectra for the two cases. Here the agreement is very good, with all differences less than 3.5%.

Table 2.6 gives a breakdown showing where gamma energy is deposited in each of three major materials comprising the blanket. The fuel in the BTF blanket is composed of uranium metal. However, there is enough oxygen distributed through the facility such that on a homogenized basis there is an equivalent amount of oxygen to that in an LMFBR UO_2 fueled blanket. Thus, two cases of gamma absorption were considered for the BTF blanket. One fueled with uranium metal and one with UO_2. The table shows three important things: first, that over 80% of all gamma energy is deposited in fuel; secondly the difference in a U-Metal and UO_2 fueled blanket is very small, and thus gamma absorption in uranium metal serves as an excellent approximation to that in UO_2 absorption. This difference is less than 2.5% in all cases in Table 2.6. Finally the comparison between the BTF converter-driven blanket and the LMFBR-driven blanket is excellent, with differences less than 3.5%.

Figure 2.10 shows a plot of the ratio of the total gamma flux to the total neutron flux. This curve gives an excellent overall idea of how good a mockup Blanket No. 4 is, because both neutron and gamma distributions are factored into the comparison. As can be seen the agreement is good. The differences can again be attributed to the differences between slab and cylindrical geometry. Forbes showed in his original BTF design calculations that it would be necessary to employ a tapered (wedge-shaped) blanket to obtain exact geometric similitude (F,1). Calculations of the present type can be used to correct BTF data to cylindrical reactor equivalent results.

The sources of gamma flux in the blanket, previously presented in Tables 2.3 and 2.4, also compare quite well. These calculations also show that the gammas which leak in from the core, or converter,

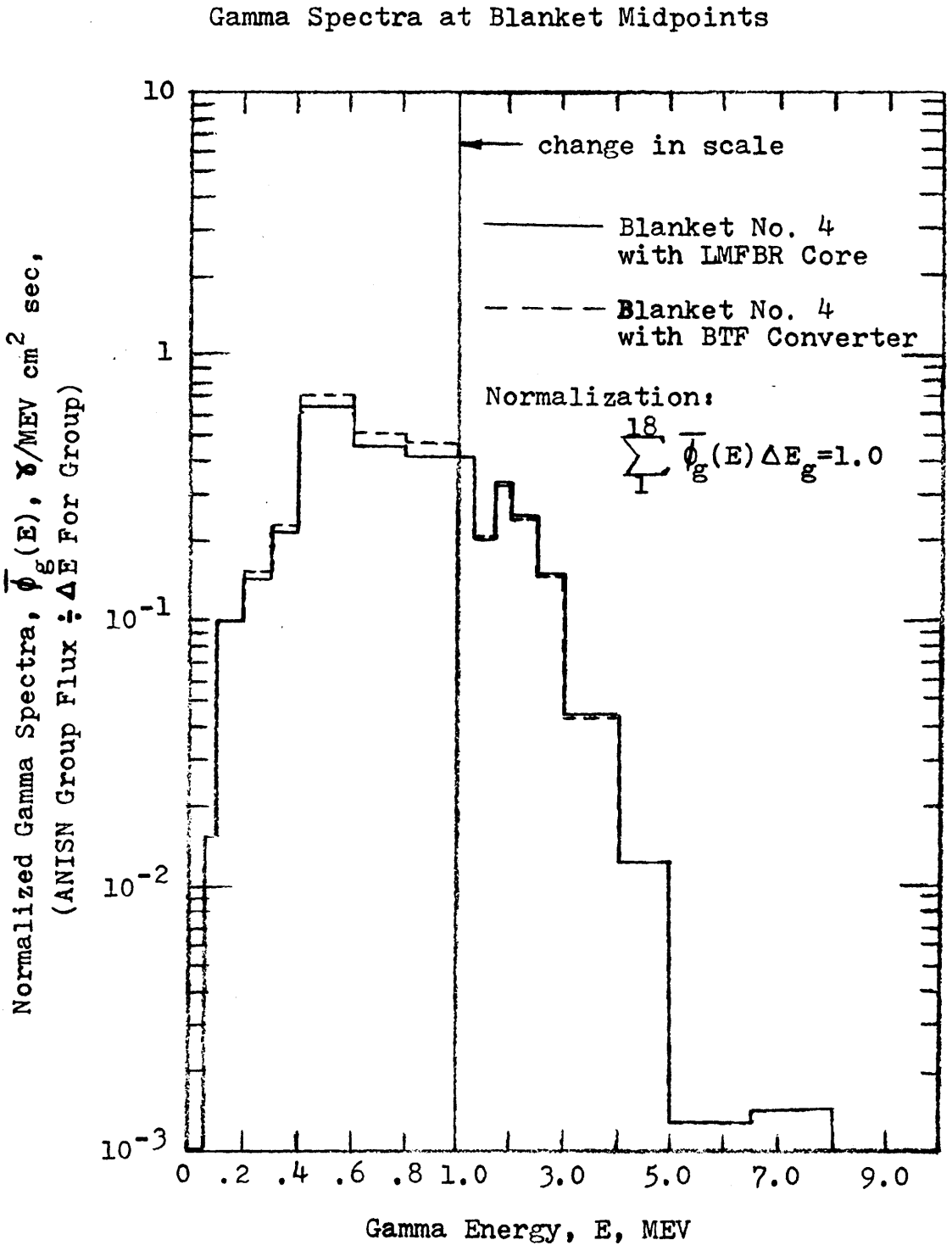

Fig. 2.9 Comparison of Blanket No. 4 Gamma Spectra When Driven by LMFBR Core and BTF Converter

TABLE 2.6 Percentage of Gamma Energy Absorbed in the Three Major Blanket Materials

Distance from Converter Interface BTF-Driven Blanket	Coolant		Clad		Fuel	
	U Fueled	UO_2 Fueled	U Fueled	UO_2 Fueled	U	UO_2
0.0 cm.	3.51%	3.25%	14.85%	13.73%	81.64%	83.03%
3.76 "	3.55	3.28	15.05	13.92	81.40	82.81
7.52 "	3.58	3.31	15.19	14.04	81.23	82.65
11.28 "	3.60	3.33	15.29	14.13	81.10	82.54
15.04 "	3.63	3.35	14.41	14.23	80.96	82.42
18.80 "	3.64	3.37	15.47	14.28	80.88	82.35
22.56 "	3.66	3.38	15.55	14.36	80.78	82.26
26.31 "	3.68	3.39	15.59	14.39	80.73	82.22
30.07 "	3.70	3.41	15.68	14.46	80.62	82.21
33.83 "	3.70	3.41	15.69	14.48	80.61	82.11
37.59 "	3.72	3.44	15.82	14.60	80.45	81.97
41.35 "	3.64	3.36	15.62	14.42	80.74	82.21
LMFBR Driven Blanket						
Distance From Core Interface						
0.0 cm.	3.52%	3.24%	14.95%	13.76%	81.53%	83.0%
3.76 "	3.56	3.28	15.11	13.92	81.33	82.80
7.52 "	3.61	3.32	15.34	14.09	81.05	82.59
11.28 "	3.62	3.32	15.34	14.10	81.04	82.57
15.04 "	3.67	3.36	15.56	14.26	80.77	82.38
18.80 "	3.66	3.36	15.55	14.26	80.79	82.38
22.56 "	3.71	3.39	15.72	14.39	80.57	82.21
26.31 "	3.70	3.39	15.69	14.38	80.61	82.23
30.07 "	3.73	3.42	15.83	14.50	80.44	82.08
33.83 "	3.72	3.41	15.80	14.47	80.48	82.13
37.69 "	3.76	3.44	15.95	14.62	80.29	81.93
41.35 "	3.67	3.28	15.72	14.44	80.61	82.28

rapidly attenuate, and that the blanket fuel supplies most of the gammas; clad supplies only to 6 percent, and coolant only 2 to 3 percent.

In summary, the comparisons which have been presented here show that on a calculational basis, Blanket No. 4 is an excellent mock-up of an LMFBR blanket and reflector. In addition this work establishes the dose rates, gamma absorption shapes, and other parameters against which later experiments can be compared.

2.3.4 Effect of Transverse Leakage

Blanket mockups in the BTF are finite in the transverse (vertical and horizontal) dimensions, with size carefully chosen to match transverse leakage to that in a cylindrical reactor. Moreover, the ANISN program used for all of the blanket analyses in the present work is one-dimensional. Hence it is important to characterize the transverse leakage using a buckling-type formulation, and to assess the sensitivity of the results to the buckling values used. In the present instance the sensitivity was evaluated by varying the effective extrapolated height, H, and width, W, of the assembly in a series of ANISN calculations. The extrapolated width, W, and Height, H, of the prism were changed over a wide range in ANISN. These values are used to generate a leakage correction in the form of a pseudo-absorption, DB^2, where

$$B^2 = \left(\frac{\pi}{H}\right)^2 + \left(\frac{\pi}{W}\right)^2 \qquad (2.2)$$

Two ANISN runs were made for the standard Blanket No. 4; one used both W and H equal to 10^6 cm. This approximates a semi-infinite slab in which there is no transverse leakage. The second used the values, H = 140 cm (55.1 in.) and W = 150 cm (59.0 in). The results of these

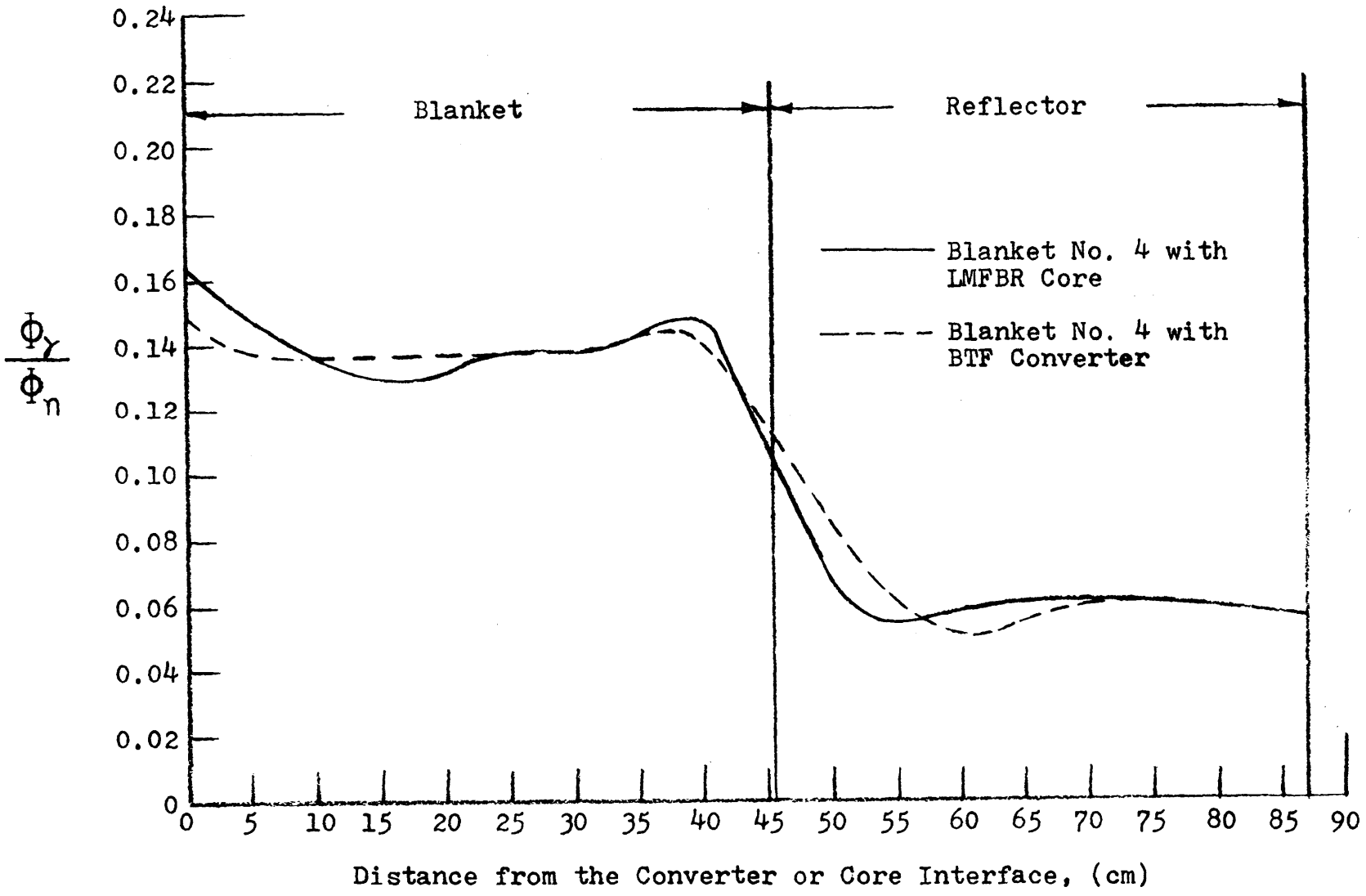

Fig. 2.10 Comparison of Ratio of Gamma to Neutron Flux in Blankets Driven by LMFBR Core and BTF Converter

runs show little difference between the two cases. There is no difference in either neutron or gamma spectra. The total neutron and gamma flux distributions are plotted in Figs. 2.11 and 2.12. In both figures the flux in the actual blanket is virtually identical to the case with W = H = 10^6cm. These calculations show that transverse leakage has a very minor effect, if any, on the reactions that occur in the middle of the blanket.

The transverse buckling of the blanket was also determined experimentally using thermoluminescent dosimeters. In this experiment two dose traverses were made; one in the horizontal direction and one the vertical direction. The points were then fit to a cosine distribution

$$D_\gamma(x,y,z) = D_\gamma(0,0,z)\cos\frac{\pi x}{W}\cos\frac{\pi y}{H} \qquad (2.3)$$

The best cosine fit for the horizontal flux traverse is shown in Fig. 2.13; the equivalent curve for the vertical direction is shown in Fig. 2.14. The respective H and W values for the vertical and horizontal directions were found to be 144.8 cm. (57.0 in) and 156.7cm (61.7 in.). These values are within the range covered in the leakage sensitivity study described above and are in fairly good agreement with previously determined values from similar experiments in which neutron-induced foil activities were employed. For example Leung (L, 1) found H = 152 cm. (59.8 in.) and W = 188 cm. (74.0 in.). It is thus concluded that the gamma leakage from the facility does not effect the spectral shape, spatial distribution, or reaction rates at the center of the blanket and for this reason all leakage effects could be ignored.

2.4 THERMOLUMINESCENT MATERIALS, PHYSICS, AND PROPERTIES

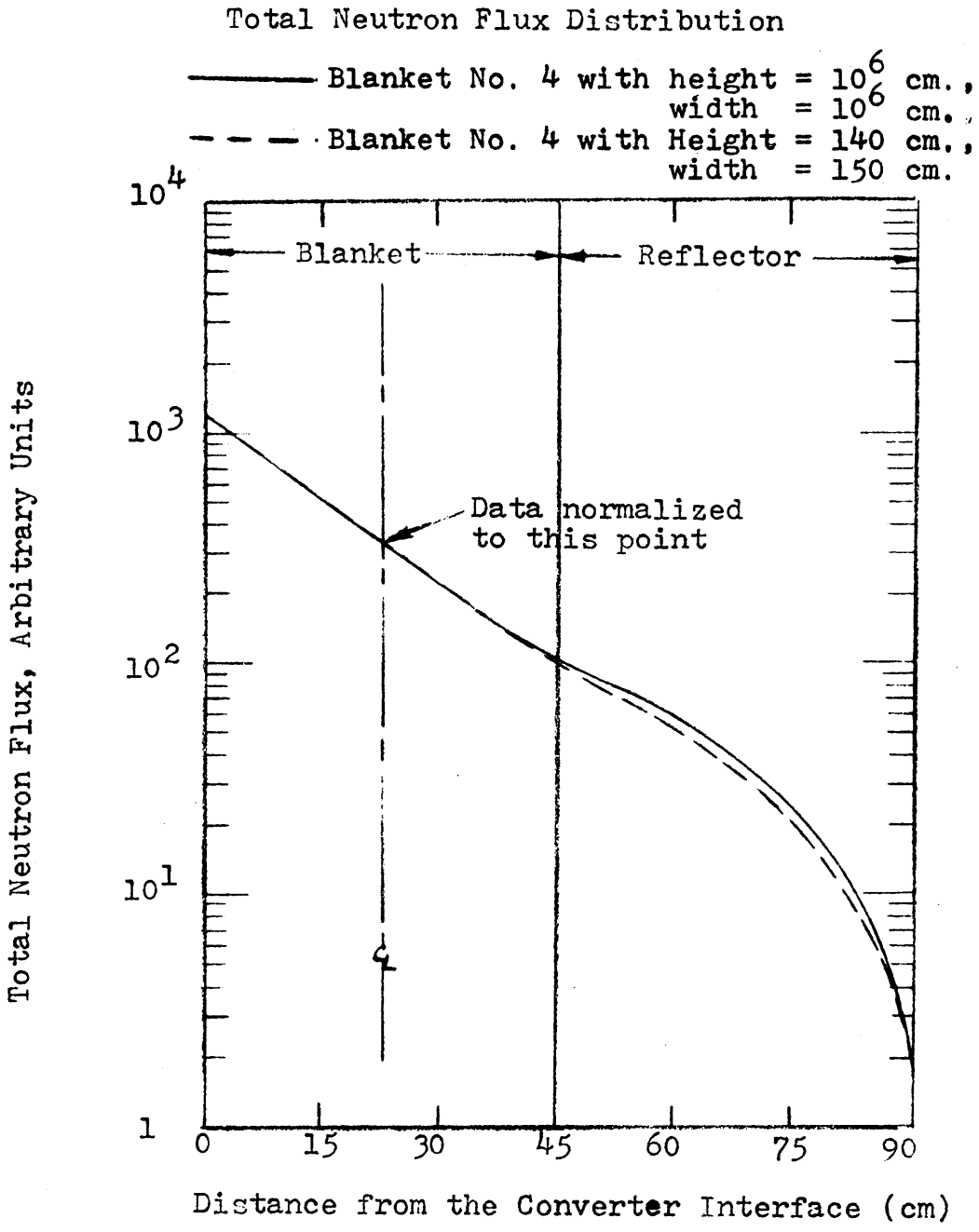

Fig. 2.11. Effect of Assembly Height (Transverse Leakage) on Blanket Neutronics

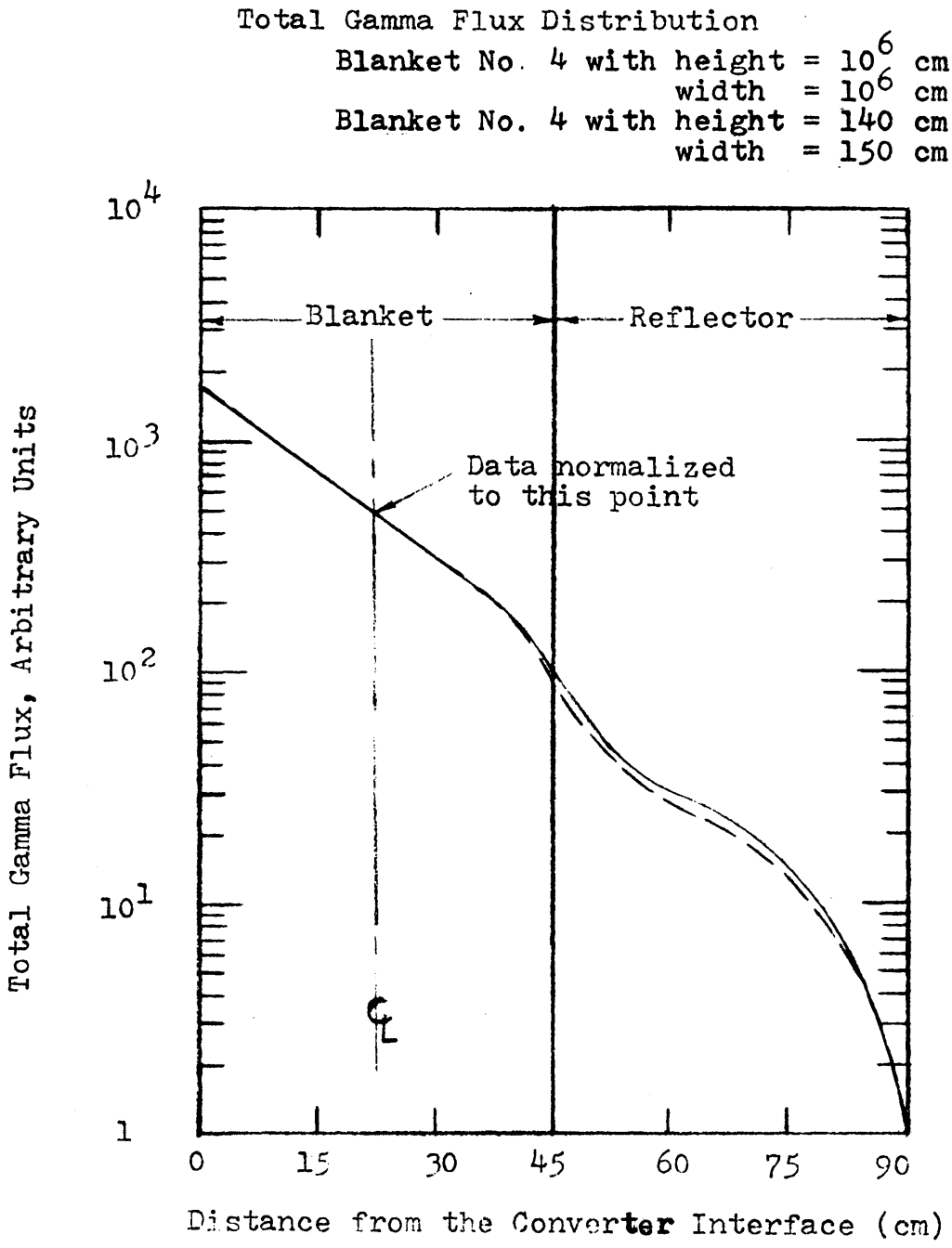

Fig. 2.12 Effect of Assembly Height (Transverse Leakage) on Blanket Photonics

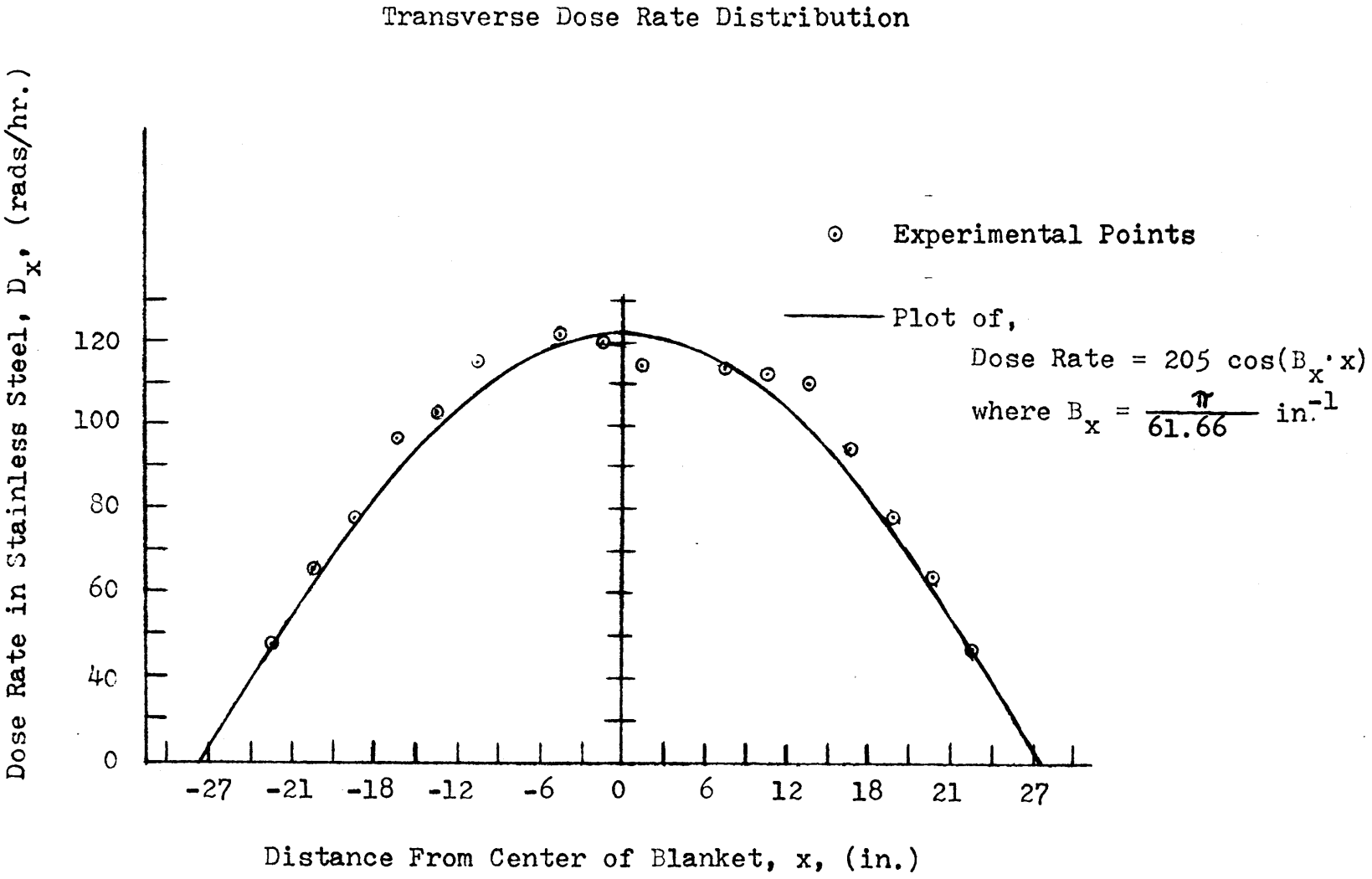

Fig. 2. 13. Blanket No. 4 Transverse Dose Rate (Stainless Steel) Distribution

Vertical Dose Rate Distribution

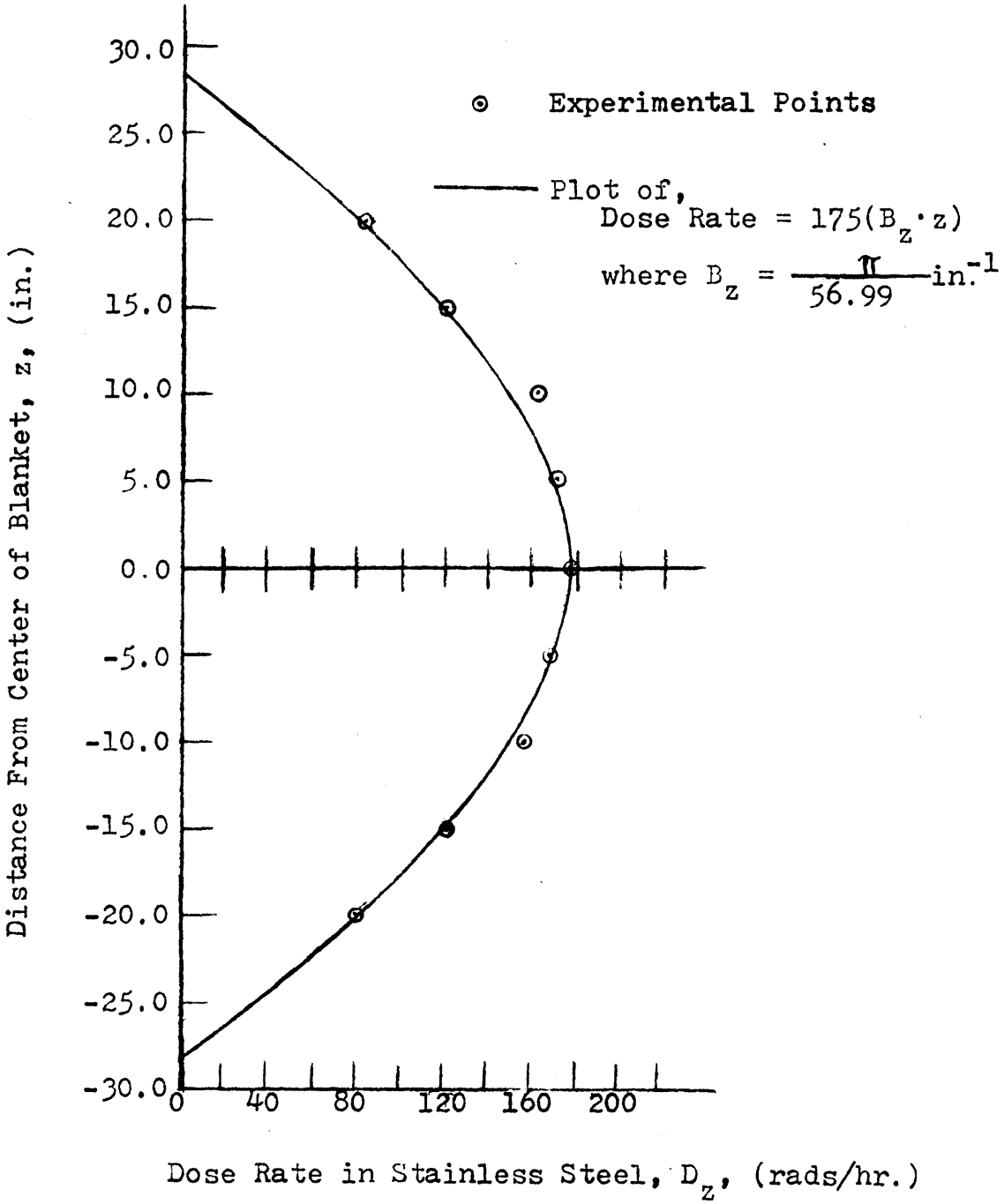

Fig. 2.14. Blanket No. 4 Vertical Dose Rate (Stainless Steel) Distribution

This section is concerned with explaining how thermoluminescent dosimeters function and what must be done to use them. This basically involves the phenomena involved in production, trapping, and release of electrons, with the resultant emission of light in the visible range. A discussion of the readout device and how it works is included. This is followed by an outline of cavity ionization theory and the necessary corrections required when using any electron-ionization monitoring device.

2.4.1 Thermoluminescent Phosphor Characteristics

TLD's are integrating gamma ray dosimeters. Solid-state dosimetery (radiophotoluminescence and thermoluminescence) depends entirely on crystal lattice imperfections. A luminescent material generally consists of solid insulators with a wide range of optical transparency. The alkali halides (Na Cl, Li F, etc.) are good examples because of their ionic structure. The ideal structure consists of alternating ions of Li^+, F^-, Li^+, F^-, as shown in Fig. 2.15. Such ideal lattices do not exist in nature. Actually there are many imperfections which consist primarily of vacancies and interstitials. A vacancy is a position in a lattice where an ion is missing and an interstitial is a place where an extra ion exists. These are also shown in Fig. 2.15. In a pure crystal the number of positive ion vacancies must equal the negative ion vacancies in order for the lattice to be electrically neutral. These lattice imperfections are very important because they create a region of localized charge . For example, if a negative ion is missing, a region of positive charge from the four remaining ions around it is set up. Likewise, wherever a positive interstitial exists there is also a region of positive charge. When radiation such as X or gamma rays interact with lattice atoms, free

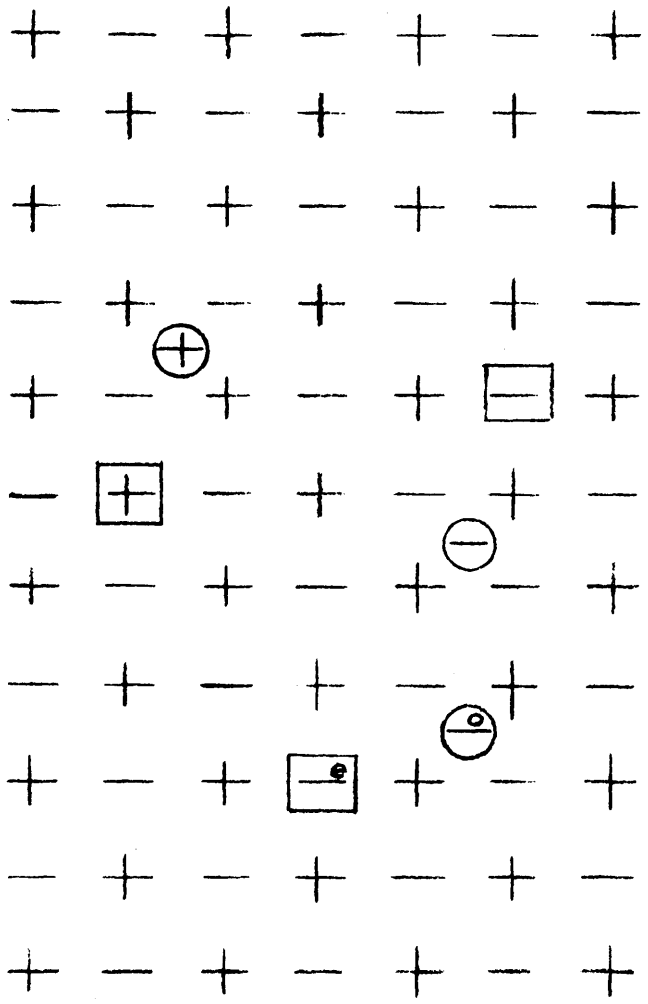

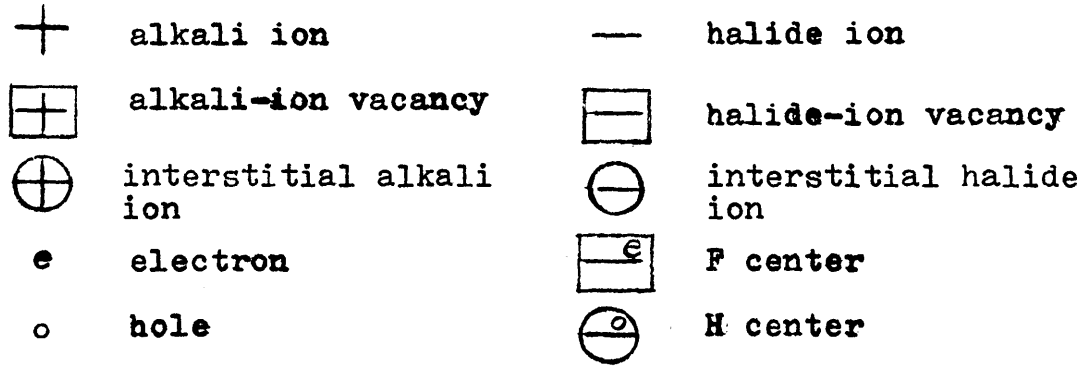

Fig. 2.15. Schematic representation of lattice imperfections in alkali halide materials.

electrons are produced. The birth of the free electron also creates an electron hole. The electron and electron hole are then free to migrate through the lattice. When the electron reaches an area of positive charge or the hole reaches an area of negative charge they can become trapped. These trapped electrons and holes form "color centers." An electron trapped in a positively charged area is called an "F" center and a trapped vacancy is called an "H" center. The existence of "F" centers is responsible for the luminescence phenomenon. "F" is derived from "Farbzentrum" the German word for color center.

The energetics of the electron migration will explain why the re-radiation of light occurs. Before the alkali-halide crystal interacts with X or gamma radiation all the electron-forming crystaline bonds are contained in the valence band. In this energy state they are bound to their nuclei and are not free to move through the lattice. When X or gamma radiation interact, they impart energy to valence band electrons and move them into the conduction band. This is shown in Fig 2.16 in step 1. In step 2 the electrons migrate through the lattice via the conduction band. In step 3 the electron becomes trapped and forms an "F" center. At the same time as the electron migrates through the lattice, the electron hole migrates through the valence band as in step 4. When it reaches a negative trap it forms an "H" center. This occurs in step 5.

The remaining processes occur when the lattice is heated. In step 1' the addition of heat imparts enough energy to the electron to cause it to excape from its trap back to the conduction band, where it migrates as in step 2'. In step 3' the electron passes near enough to a trapped hole to "fall" into it. In this process energy is given off in the form of visible light photons. Step 1" of Fig. 2.16 also occurs when the lattice is heated. Here the "hole" is given enough energy to return to the valence band. It then migrates through the lattice

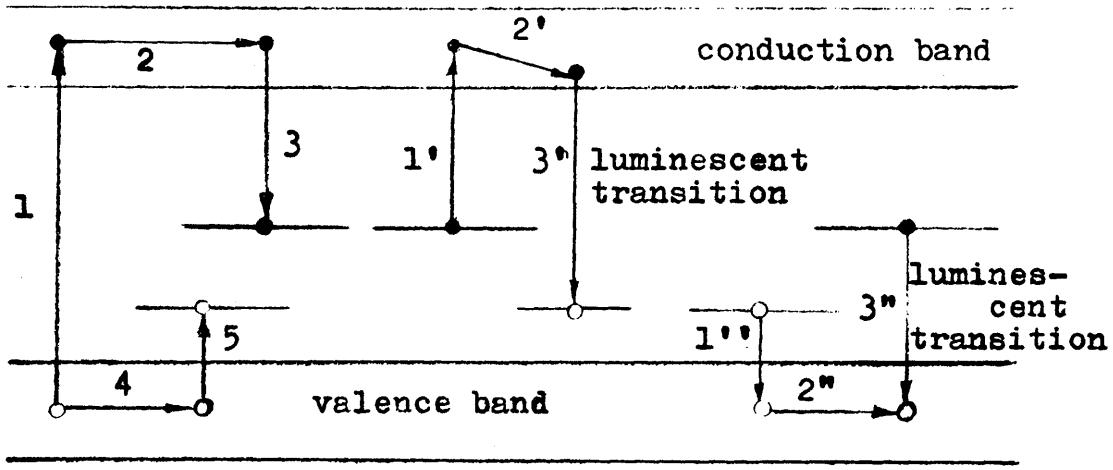

1. ejected primary or secondary electron
2. electron moves through conduction band
3. electron forms F center
4. electron hole moves through valence band
5. electron hole forms H center

1' electron removed from trap by heat

2' electron moves through conduction band

3' electron is trapped by H center

1" electron hole removed from trap by heat

2" electron hole moves through valence band

3" electron falls out of trap into nearby electron hole

Fig. 2.16 Energetics of electron transitions

(Step 2''). When it nears an "F" center the trapped electron falls into the "hole" and light is emitted. The total number of luminescent transistions is then proportional to the number of "F" centers which have formed. This is inturn proportional to the number of electrons which were liberated by gamma or X radiation. As a primary electron slows down it dissipates energy by stripping off other lattice electrons which inturn become trapped. Thus the total number of trapped electrons, and hence luminescent transitions, is proportional to the total gamma energy deposition.

In principle, then, a dosimeter could be made from a lattice of a pure salt. However, neither the efficiency nor reproducibility of pure salt "F" center formation is adequate to perform dosimetry. Radiation-induced centers which do have good reproducibility, high yield, good sensitivity to radiation, and useful luminescence are found only in alkali-halides which have been doped with additives which form solid solutions. In lithium fluoride and calcium fluoride, magnesium is used. This divalent impurity occupies positions in the lattice where alkali ions are otherwise located. Because of the impurity's excess charge, positive alkali atoms must be omitted from the lattice to maintain overall neutrality. This system of impurities and vacancies is shown in Fig.2.17. An impurity of this type creates a great many more potential "F" centers by virtue of its excess positive charge. The positive ion vacancies also create electron "hole" traps or potential "H" centers. The traps formed by these impurities are much more stable than the pure salt lattice imperfections.

When electrons are "caught" in traps, some are bound more tightly than others. Therefore, more thermal energy is required to get them out. Thus, the TLD's are heated on a constant temperature ramp and the light from the TLD is then monitored by a photomultiplier tube. The plot of this current versus temperature (or, equivalently, time) is

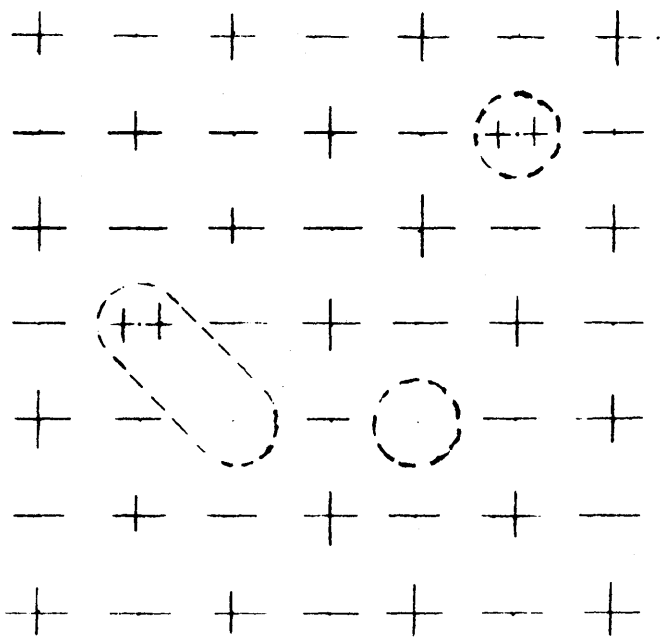

Fig. 2.17 Schematic Representation of Substitutional Impurity Atoms and Their Vacancies

called a glow curve. A typical glow curve for lithium fluoride is shown in Fig. 2.18. If lithium fluoride TLD's are used, the integrated area under the curve is commonly related to the gamma dose. For calcium fluoride TLD's the peak is generally used because it has been found to be more reproducible than the area under the curve.

2.4.2 TLD Readout Analyzer

The Harshaw 2000 TLD analyzer was found quite suitable for reading out TLD's. The unit consists of two discrete components, the model 2000-A TL Detector and the model 2000-B Automatic Integrating Picoammeter. In the 2000A TL detector the TLD is placed in a planchet which is mounted in a slide out drawer. When the drawer is inserted all the way into the 2000A unit the planchet is shielded from all ambient light. To initiate readout the TLD is placed in the planchet, the drawer is closed and the TLD is heated on a constant temperature ramp between 100 °C and 240°C. During the heating, luminescent transitions occur and light photons are emitted. These photons are inturn detected by a photomultiplier tube and associated electronics to create a glow curve.

The 2000A TL detector has several features which discriminate against erroneous signals. A nitrogen gas flow provides an inert atmosphere around the planchet. Also, light traveling from the TLD to the photo-tube must pass through "Black Body" filters which reduce non-signal light from the incandescent planchet to near zero levels. Also, magnetic and electrostatic shielding of the photomultiplier tube is used to stabilize gain and minimize dark current.

The associated Harshaw 2000B unit is basically a picoammeter. The unit can be connected to an X-Y plotter to produce glow curve plots. There is also a current-integration feature which is used to find the area under a glow curve. This area is proportional to the dose

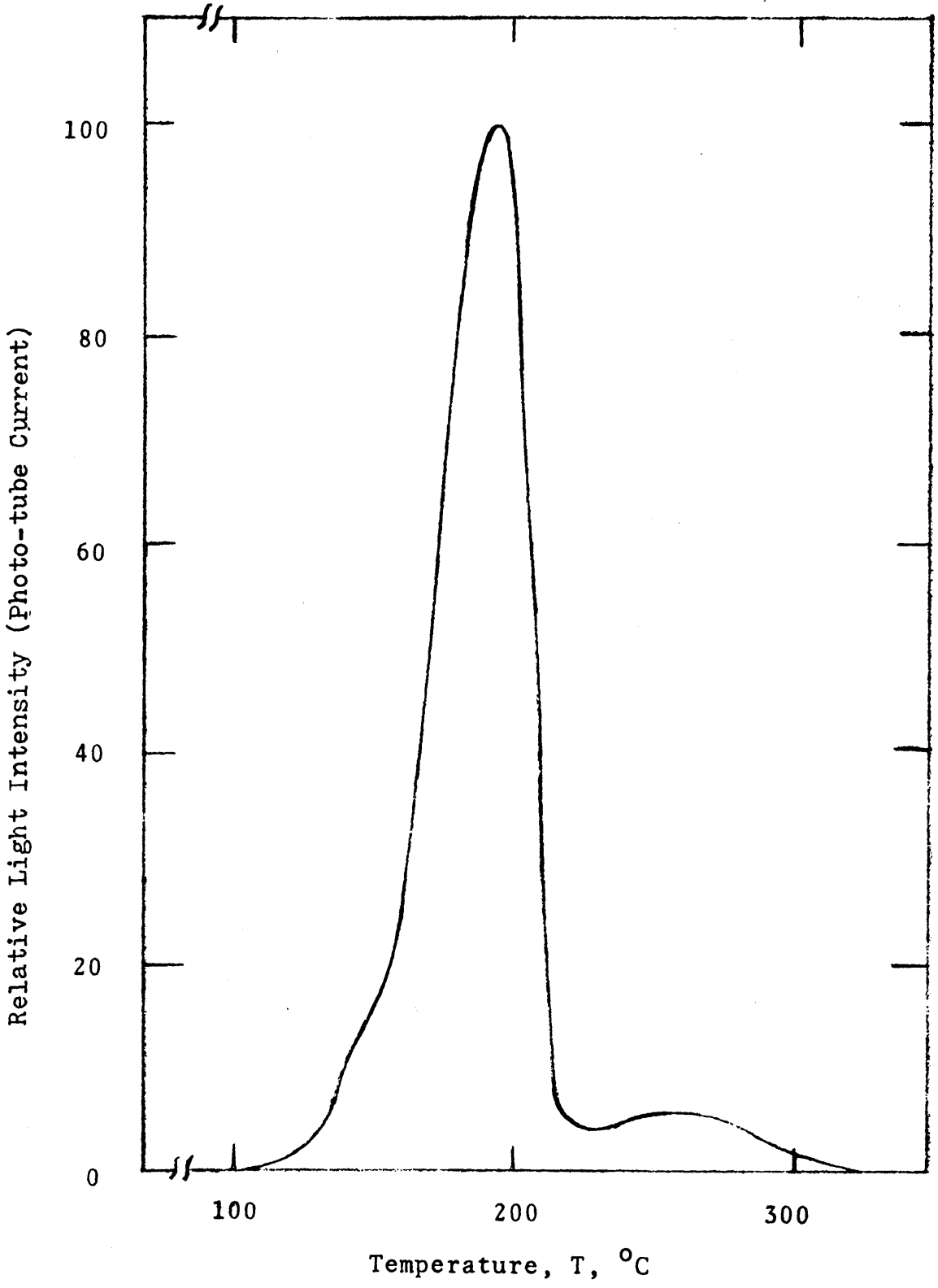

Fig. 2.18. Typical ^{7}LiF Glow Curve

absorbed by the dosimeter. This unit also contains the high voltage source for the photomultiplier tube.

In all TLD work at the M.I.T.Blanket Test Facility, the integrated current from the photo-tube (in nanocoulombs) was measured and then related to the total dose received by the capsule.

2.5 CAVITY IONIZATION THEORY

It is not very helpful to know only the gamma dose received by the TLD itself, when the key design data are the dose rates (energy deposition rates) received by blanket materials. The two doses, however, can be related IF the right dosimeter capsule design is used and appropriate correction factors applied to the raw data. The theoretical treatments underlying capsule design analysis and the development of spectral response factors are the subjects of this section.

2.5.1 Energy Deposition by Gamma Rays

When gamma rays interact with matter they dissipate energy. This occurs in two steps. The first consists of gamma interactions with electrons through the three processes of photoelectric, compton, and pair production interactions. In all of these processes energetic free electrons are produced with the loss of some or all of the incident gamma energy. This energy transfer can be expressed quantitatively in terms of the so-called kerma rate:

$$K = C \int_{E_1}^{E_2} \phi(E) \frac{\mu_{en}(E)}{\rho} \, dE, \frac{ergs}{gm.sec.} \qquad (2.4)$$

where $\phi(E)$ = Gamma Ray Energy Flux, MEV/MEV cm^2 sec.

$\frac{\mu_{en}(E)}{\rho}$ = Mass Energy Absorption Coefficient

C = Conversion Factor, ergs./MEV = 1.6021×10^{-6}

In this expression the flux ϕ (E) is the energy flux (per unit energy): The product of the normal photon flux (which is a function of energy and has units of photons per MEV per square centimeter per second) and the energy of the gamma photon.

The second step of the energy transfer occurs when the energetic electrons produced from the gammas slow down and give up their energy through coulomb-force interactions with other electrons. The energy dissipated per unit path length is called the stopping power, $\left|\frac{dT}{dx}\right|$, and has units of MEV per cm.

The total amount of energy deposited per unit volume is

$$D = C \int_{x_1}^{x_2} \left|\frac{dT}{dx}\right| dl \ , \quad \text{ergs} \tag{2.5}$$

where D = Total energy deposited, ergs

$\left|\frac{dT}{dx}\right|$ = Stopping power $\frac{\text{MEV}}{\text{cm}}$

dl = Differential element of electron range, cm

C = Conversion factor, $\frac{\text{ergs}}{\text{MEV}} = 1.6021 \times 10^{-6}$

and x_1 = Point of electron's birth

x_2 = Point of departure from the unit volume

This equation is merely the integral of the energy loss over the electron's track inside the unit, or control volume. Now if $n(T_o)dT_o$ is the number of electrons born per second within the unit volume in a small energy interval dT_o about T_o the energy deposition rate will be

$$dR = Cn(T_o)\, dT_o \int_{x_1}^{x_2} \left|\frac{dT}{dx}\right| dl \ , \quad \text{ergs/cm}^3 \text{ sec.} \tag{2.6}$$

If this expression is integrated over all electron birth energies, T_o, the total energy deposition rate is found.

$$R = \frac{C}{\rho} \int_o^{\infty} n(T_o)\ dT_o \int_{x_1}^{x_2} \left|\frac{dT}{dx}\right| dl \ , \ \text{ergs/gm. sec.} \tag{2.7}$$

Here the right side of this equation has been divided by the density, ρ, to obtain a mass/energy deposition rate. Standard gamma detectors such as calorimeters or a Bragg-Gray chamber can be used to measure the dose rate of Eq. (2.7.).

At first glance it may appear the energy deposition rate of equation 2.7 and the kerma rate of equation 2.4 are the same but they are conceptually quite different. The kerma rate assumed that all gamma energy was deposited at the point where the electron was born. This means that in the above example all energy is deposited within the control volume, however, some electrons escaped this control volume and deposited their energy elsewhere. Thus the two cases are equal only when as many electrons carrying an equal amount of energy leak into the control volume as leaked out. If this condition exists, charged particle equilibrium is said to exist, and the kerma rate and energy deposition rates are considered equal, or;

$$C\int_{E_1}^{E_2}\phi(E)\frac{u_{en}(E)}{\rho}\,dE \approx \frac{C}{\rho}\int_0^{\infty} n(T_o)\,dT_o\int_{x_1}^{x_2}\left|\frac{dT}{dx}\right|dl \ , \ \frac{ergs}{gm.\ sec.}$$

(2.8)

If charged particle equilibrium exists in a medium the assumption is made that the dose from gammas is deposited at the point where the gammas interacted. This avoids the necessity of using complicated electron transport theory to find where the electrons actually deposit their energy. Therefore, satisfying the requirement of charged particle equilibrium in a gamma detector greatly simplifies the work required to interpret results obtained with the detector.

2.5.2 Bragg-Gray Theory

A dosimeter capsule is designed by surrounding a cavity/TLD which detects electrons with a medium which is in charged particle equilibrium. When the medium is placed in a photon spectrum it may be used to measure the gamma energy deposited by the photon spectrum. However, the medium must be small so as not to significantly perturb the photon spectrum. When this situation exists, an electron spectrum, characteristic of both the gamma photon spectrum and medium will be established in the medium. If the medium is large enough, charged particle equilibrium is established and the electron spectrum will be the same throughout the medium. Now if a small cavity (filled with electron sensitive material, ie. TLD, ion chamber gas, etc.) exists in the medium it can be used to measure the energy deposition in the medium due to the slowing down of electrons. Bragg-Gray Theory assumes that the electron slowing down spectrum in the

cavity/TLD is identical to that in the surrounding medium. To understand this concept, consider the following example. The mass stopping power, $\frac{1}{\rho}\left|\frac{dT}{dx}\right|$, is the differential change in an electron's energy as it moves through a thickness, measured in gm/cm^2, of medium. Now if $I(T_o,T)$ is a slowing down spectrum of electrons with a unit source at energy T_o, then the amount of energy deposited by all electrons with energies in dT about T is

$$dD = I(T_o,T)\left(\frac{1}{\rho}\left|\frac{dT}{dx}\right|\right) dT \text{ , MEV/gm. sec.} \tag{2.9}$$

The integral of this expression over all electron energies between 0 and T_o gives the total energy lost by all electrons with intial energy T_o per gram of material per second.

$$D = \int_o^{T_o} I(T_o,T)\left(\frac{1}{\rho}\left|\frac{dT}{dx}\right|\right) dT \text{ , MEV/gm. sec.} \tag{2.10}$$

Thus the electron energy deposition rate is dependent upon both the electron spectrum, $I(T_o,T)$, and the mass stopping power. Bragg-Gray Theory assumes that in the small electron sensitive cavity, the slowing down spectrum is characteristic of the surrounding medium and the stopping power is characteristic of the cavity material. Thus, using the subscripts z to denote medium material and c to denote cavity material the energy deposition rate in the cavity/TLD becomes

$$D_c = \int_o^{T_o} I_z(T_o,T)\left(\frac{1}{\rho}\left|\frac{dT}{dx}\right|\right)_c dT \text{ , MEV/gm. sec.} \tag{2.11}$$

In order to use equation 2.11, the cavity/TLD must be small enough that it does not significantly perturb the medium's electron spectrum

2.5.3 Small Cavity Theory

The objective of small cavity theory is to find an expression for the ratio of energy deposited in the cavity/TLD to the energy deposited in the wall or medium. This theory only applies to small cavities in which Bragg-Gray Theory and equation 2.11 may be used.

Now recall that the stopping power for electrons is $\left|\frac{dT}{dx}\right|$ and let $N(T_o,T)$ (Electrons/MEV/sec) is the slowing down spectrum of electrons. Then $N(T_o,T)\,dT$ is the number of electrons in a small energy range dT about T which slow down past T every second due to a unit source of electrons at energy T_o. If an electron is traveling with a certain velocity, v, then its time rate of energy deposition will be

$$\left|\frac{dT}{dx}\right| v \text{ , MEV/sec} \tag{2.12}$$

Furthermore, the total energy loss for the electrons in dT about T is

$$N(T_o,T)\,dT \left|\frac{dT}{dx}\right| v \text{, MEV} \tag{2.13}$$

Thus, for every electron born at T_o the amount of energy deposited will be

$$\int_0^{T_o} N(T_o,T)\left|\frac{dT}{dx}\right| v\, dT \ , \ \text{MEV} \qquad (2.14)$$

The source spectrum of electrons with initial energy T_o is produced by various γ-electron processes. A unit energy source of gammas at energy E will produce a spectrum of initial primary electrons $Q(E, T_o)$ (Electrons per MEV) that is, $Q(E, T_o)\, dT_o$ is the number of primary electrons at energy T_o produced by one unit of available gamma energy. Available gamma energy is the total amount of energy which is imparted to electrons in a gamma-electron reaction. There are three processes by which electrons are produced; the Photoelectric Effect (PE), Pair Production (PP), and The Compton Effect (CE). The fraction of the available energy deposited by each process is given by $\frac{en\mu_\alpha}{en\mu\ tot}$. In this expression $en\mu_\alpha$ is the linear energy absorption coefficient for process α, either, PE, CE, or PP; and $en\,u_{tot}$ is the total linear energy absorption coefficient and equal to the sum of the $en\,u$ for each of the three processes. Thus the experssion for $Q(E,T_o)\, dT_o$ becomes

$$Q(E,T_o)\, dT_o = \frac{1}{en\mu\ tot}\left(en\mu_{PE}\, Q_{PE} + en\mu_{CE}\, Q_{CE} + en\mu_{PP}\, Q_{PP}\right)dT_o, \quad \text{electrons/MEV} \qquad (2.15)$$

In this expression Q_{PE}, Q_{CE}, and Q_{PP} are the shapes of the electron spectra arising from the three processes. Thus the fraction of available gamma energy, at energy E, which is actually deposited in a material can be expressed as

$$\int_0^E dT_o \; Q(E,T_o) \int_0^{T_o} N(T_o,T) \left|\frac{dT}{dx}\right| v \; dT \;, \; MEV/MEV$$

(2.16)

The final step in determining the dose caused by gamma rays is to mulitply Eq. (2.16) by the source of available gamma energy. At a particular gamma energy E the available energy is given by

$$E_{avail} = E \, \phi(E) \, {}_{en}\mu_{tot} \, dE \;, \; MEV/cm^3 \cdot sec.$$

(2.17)

Thus the total amount of energy deposited per unit volume of material is

$$D = \int_0^\infty E \, \phi(E) \, {}_{en}\mu_{tot} \, dE \int_0^E dT_o \; Q(E,T_o) \int_0^{T_o} N(T_o T) \left|\frac{dT}{dx}\right| v \; dT \;,$$

$$MEV/cm^3 \cdot sec \qquad (2.18)$$

The next step in the development of small cavity theory is to find an expression for the electron equilibrium spectrum $N(T_o \;, T)$. This may be obtained by considering the slowing down of electrons in the approximation of continuous slowing down. At each energy, T, a unit source of one electron per second slows down to a lower energy. Since the electrons lose energy at the rate $v\left|\frac{dT}{dx}\right|$ (MEV/sec.) , it takes them $\Delta T / v\left|\frac{dT}{dx}\right|$ seconds to cross an energy interval of width ΔT. Further, $N(T_o,T)\Delta T$ is the number of electrons in

that interval at any time. If $N(T_o,T)\Delta T$ is divided by the length of time required for an electron to pass through ΔT, the slowing down rate is found. This is the rate at which electrons pass energy T. For a unit source this slowing down rate is unity since no electrons are destroyed in the slowing down process. Thus,

$$\frac{N(T_o,T)\Delta T}{\frac{\Delta T}{v\left|\frac{dT}{dx}\right|}} = 1 \; ; \text{ or } \quad N(T_o,T) = \frac{1}{v\left|\frac{dT}{dx}\right|} \; , \; \frac{\text{electrons}}{\text{MEV/sec.}} \tag{2.19}$$

(This is analogous to the results for slowing down theory for neutrons in the absence of absorption).

To apply the theory developed this far to a dosimeter capsule, the Bragg-Gray assumption for a small cavity is used. It is assumed that the cavity/TLD is so small that the equilibrium spectrum established in the medium will also exist in the cavity/TLD. When this approximation is made the expression for the dose received by the cavity/TLD becomes

$$D_c = \int_o^\infty E\phi(E)\, {}_{en}\mu_{tot}^{z}\, dE \int_o^E dT_o Q_z(E,T) \int_o^{T_o} \frac{v\left|\frac{dT}{dx}\right|_c}{v\left|\frac{dT}{dx}\right|_z}\, dT \; , \; \frac{\text{MEV}}{\text{cm.}^3 \text{ sec.}} \tag{2.20}$$

In this relation the subscripts denote

z = Surrounding medium material

c = Cavity Material

When applied to the medium we have

$$D_z = \int_o^\infty E\phi(E)\, {}_{en}\mu_{tot}^{z}\, dE \int_o^E dT_o Q(E,T_o) \int_o^{T_o} \frac{\left|\frac{dT}{dx}\right|_z}{\left|\frac{dT}{dx}\right|_z}\, dT \; , \; \frac{\text{MEV}}{\text{cm.}^3 \text{ sec.}}$$

which reduces to

$$D_z = \int_0^{\infty} E\,\phi(E)_{en}\mu^z_{tot}\,dE \int_0^E Q(E,T_o)\,T_o\,dT_o\,, \quad \frac{MEV}{cm^3\ sec.} \tag{2.21}$$

Now recall that $Q(E,T_o)dT_o$ is the number of electrons produced at energy T_o due to a unit of available gamma energy at energy E. Therefore

$$\frac{\left\{\begin{array}{l}\text{Total energy deposited}\\ \text{by electrons in the}\\ \text{medium}\end{array}\right\}}{\left\{\begin{array}{l}\text{Total } \gamma \text{ energy imparted}\\ \text{to electrons}\end{array}\right\}} = \int_0^E T_o Q(E,T_o)\,dT_o = 1.0 \tag{2.22}$$

And the expression for the volumetric energy deposition rate in the medium becomes

$$D_z = \int_0^{\infty} E\phi(E)_{en}\,\mu^z_{tot}\,dE, \quad \frac{MEV}{cm^3\ sec.} \tag{2.23}$$

An equation can now be written for the ratio of the dose in the dosimeter to the dose in the surrounding medium.

$$\frac{D_c}{D_z} = \frac{\int_0^{\infty} E\phi(E)_{en}\mu^z_{tot}\,dE \int_0^E Q_z(E,T_o)dT_o \int_0^{T_o} \frac{\left|\frac{dT}{dx}\right|_c}{\left|\frac{dT}{dx}\right|_z}\,dT}{\int_0^{\infty} E\phi(E)_{en}\,\mu^z_{tot}\,dE} \tag{2.24}$$

In this equation the energy despostion rates are in units of (MEV/cm^3 sec). These energy deposition rates can be changed to mass energy deposition rates in units of (MEV/gm sec) by dividing the stopping powers by their respective densities and dividing both numerator and

denominator by the density of the medium. Thus if $_{m}D$ is the mass energy deposition rate, or dose rate, Eq. 2.24 can be rewritten as

$$\frac{m^{D}c}{m^{D}z} = \frac{\int_{o}^{\infty} E\phi(E) \frac{en\mu^{z}_{tot}}{z} dE \int_{o}^{E} Q_{z}(E,T_{o})dT_{o} \int_{o}^{T_{o}} \frac{(\frac{1}{\rho_{c}} \left|\frac{dT}{dx}\right|)_{c}}{(\frac{1}{\rho_{z}} \left|\frac{dT}{dx}\right|)_{z}} dT}{\int_{o}^{\infty} E\phi(E) \frac{en\mu^{z}_{tot}}{\rho_{z}} dE} \tag{2.25}$$

The basic philosophy used in arriving at Eq. 2.25 was to find expressions for the dose rate in the cavity/TLD and sleeve material (the medium) and set up the ratio of these expressions. This represents a departure from the traditional treatment where the ratio of the energy deposited by electrons with initial energy T_{o} in both cavity/TLD and medium is found. This ratio which, Burlin (B, 8) labels $(1/_{m}\bar{\bar{S}})$, is then averaged over the spectrum of initial electron energies. The result of this averaging is called the averaged reciprocal of the mass stopping power ratio. And is expressed by,

$$\frac{1}{m\bar{\bar{S}}} = \frac{\int_{o}^{E} A(E,T_{o})\, T_{o}(dT_{o}/_{m}\bar{S})}{\int_{o}^{E} A(E,T_{o})\, T_{o}dT_{o}} \tag{2.26}$$

Where $A(E, T_{o})$ is the spectrum of electrons with initial energies. When Burlin's expression for $1/_{m}\bar{S}$ is substituted, Eq. 2.26 becomes

$$\frac{1}{m\bar{\bar{S}}} = \frac{\int_{o}^{E} A(E,T_{o})dT_{o} \int_{o}^{T_{o}} \frac{(\frac{1}{\rho_{c}} \left|\frac{dT}{dx}\right|)_{c}}{(\frac{1}{\rho_{z}} \left|\frac{dT}{dx}\right|)_{z}} dT}{\int_{o}^{E} A(E,T_{o})\, T_{o}\, dT_{o}} \tag{2.27}$$

This quantity is merely the ratio of the energy deposited in the cavity/TLD to that deposited in the medium. Burlin goes on to say "If the

photon source is not momenergetic, then the stopping power ratio must be further averaged over the spectrum of photon energies. The spectrum of photon energies is merely $E\phi(E)$. To average with $E\phi(E)$ is to average with the total amount of gamma energy. However, not all of this energy is imparted to electrons in the medium, only the portion $E\phi(E)(_{en}\mu^{z}_{tot}/\rho)_z$ (MEV/gm sec) is. This is the gamma energy AVAILABLE for deposition in the medium. Now if $\mathbf{A}(E, T_o)$ is equivalent to $Q(E, T_o)$ and Eq. 2.27 is averaged over the AVAILABLE gamma energy the result is analogous to Eq. 2.25. Thus averaging should be performed over the quantity $E\phi(E)(_{en}\mu^{z}_{tot}/\rho)_z$ and not $E\phi(E)$.

In order to use Eq. 2.25, expressions for the mass stopping power and $Q_z(E, T_o)$ must be found. The relation for the mass stopping power (S, 8) is

$$\left(\frac{1}{\rho}\left|\frac{dT}{dx}\right|\right) = 2\pi r_o^2 N_o\left(\frac{Z}{A}\right) m_o c^2 \left\{\ln \frac{m_o c^2 T}{2I^2}\left(\frac{\beta^2}{1-\beta^2}\right) - \left[2\sqrt{1-\beta^2} - (1-\beta^2)\right]\ln 2 + (1-\beta^2) + \frac{1}{8}\left(1-\sqrt{1-\beta^2}\right)^2\right\} / \beta^2 \qquad (2.28)$$

where
- r_o = electron radius
- β = v/c
- N_o = Avogadro's Number
- m_o = Electron Rest Mass
- v = Electron Speed
- A = Atomic Number of Material
- Z = Atomic Mass of Material
- T = Electron Kinetic Energy
- I = Geometric Mean Ionization Potential

For compounds $(\overline{Z/A})$ in the above equation is found by Bragg's additivity rule (B, 4)

$$(\overline{Z/A}) = \sum w_i \, (Z/A)_i \, , \tag{2.29}$$

where w_i is the weight percent of each element. The mean ionization potential for elements is found by determining k in Fig. 2.19 (T, 3). k is then related to I by

$$I = kZ \tag{2.30}$$

The mean ionization potential for elements is found using (B, 4)

$$\ln I = \sum w_i \, (Z/A)_i \, \ln I_i/(\overline{Z/A}) \tag{2.31}$$

With Eq. 2.28 the integral of the mass stopping power ratios at the right of the numerator of Eq. 2.25 may now be evaulated. This was done at M.I.T. with the use of a modified version of the computer program RESPOND (T, 3). This code evaluates the integral by evaluating Eq. 2.28 at several points and employing the trapezoidal rule. RESPOND then divides this integral by T_o to obtain a numerical value for the quantity

$$\frac{1}{T_o} \int_o^{T_o} \frac{\frac{1}{\rho_c} \left|\frac{dT}{dx}\right|_c}{\frac{1}{\rho_z} \left|\frac{dT}{dx}\right|_z} \, dT \, , \tag{2.32}$$

which is the same as the Burlin expression for $(1/\overline{S}_m)$. Other workers in the field (S, 3) use an expression for this quantity which was developed by the National Committee on Radiation Protection (N, 1) (NCRP), based on a theoretical model by Laurence. Spencer and

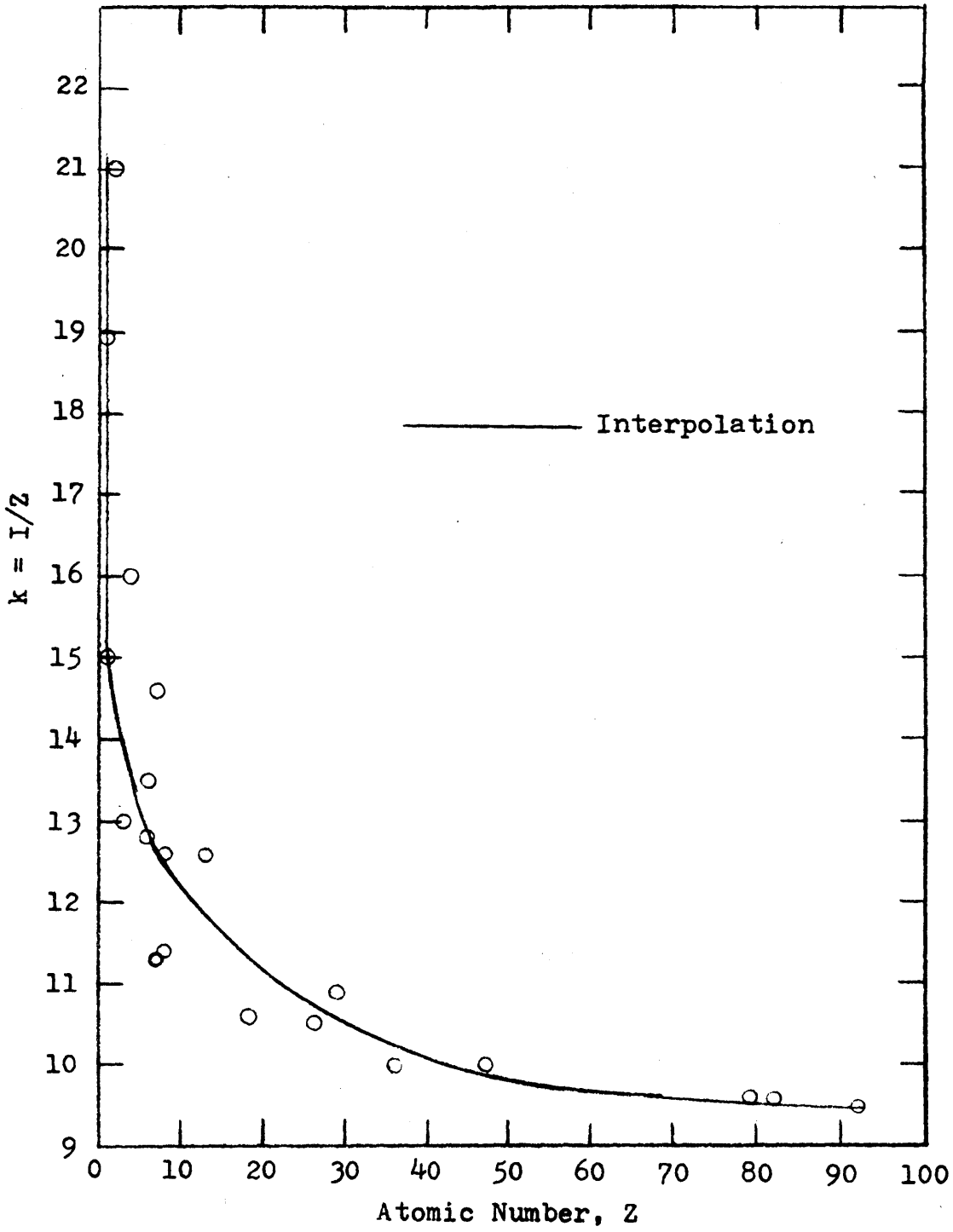

Fig. 2.19 Determination of Geometric Mean Ionization and Excitation Potential, I

Attix (S, 7) also developed an expression for the quantity in Eq. 2.32 which takes secondary electrons into account.

The results from RESPOND were found to be adequate; thus the Spencer and Attix and NCRP relations were not used.

In order to complete evaluation of Eq. 2.25, an expression for $Q(E,T_o)$ must be found. The spectral shape functions $\psi_\alpha(E,T_o)$ are used for this purpose: $\psi_\alpha(E,T_o)$ is the shape of the electron energy spectrum resulting from photons at energy E interacting via process α. Here α refers to either the photoelectric effect, pair production, or the compton effect. This spectrum is normalized so that

$$\int_0^E \psi_\alpha(E,T_o)\,dT_o \equiv 1 \qquad (2.33)$$

Equation 2.33 is equivalent to stating that the sum of the energy contained by all primary electrons arising due to process α is equal to the total amount of energy imparted to process α by gamma rays. Also, $\psi_\alpha(E,T_o)\,dT_o$ is the ratio of the energy imparted by process α to electrons in the energy range dT_o about T_o to the total amount of energy imparted to electrons by gammas at energy E which enter into process α. To find the actual number of electrons in energy dT_o we simply divide by T_o:

$$\left\{\begin{array}{l}\text{\# of electrons in } dT_o \\ \text{about } T_o \text{ per unit of} \\ \text{gamma energy imparted} \\ \text{in process } \alpha\end{array}\right\} = \psi_\alpha(E,T_o)\,\frac{dT_o}{T_o} \qquad (2.34)$$

At this point we can readily find an expression for $\psi_{PE}(E,T_o)$ from the definition of $\psi_\alpha(E,T_o)$ and the characteristics of the photoelectric process. Gamma rays which interact via the photoelectric effect kick out electrons whose energy is equal to that of the original

gamma minus the photoelectric work function. Thus in any given material photoelectric effect interactions with monoenergetic gammas will produce monoenergetic electrons. This is represented by equating $\psi_{PE}(E,T_o)$ to a delta function:

$$\psi_{PE}(E,T_o) = \delta(E - T_o) \tag{2.35}$$

The integral of this equation over the range of electron initial energies gives 1.0 in accordance with Eq. 2.33.

In order to find a relation for $Q(E,T_o)$, recall that $({}_{en}\mu_\alpha/{}_{en}\mu_{tot})$ is the fraction of gamma energy at E dissipated by process α. Thus the expression for $Q(E,T_o)$ is:

$$\begin{aligned} Q(E,T_o)dT_o = {} & (\psi_{CE}(E,T_o)\frac{dT_o}{T_o})({}_{en}\mu_{CE}/{}_{en}\mu_{tot}) + \\ & (\psi_{PP}(E,T_o)\frac{dT_o}{T_o})({}_{en}\mu_{PP}/{}_{en}\mu_{tot}) + \\ & (\psi_{PE}(E,T_o)\frac{dT_o}{T_o})({}_{en}\mu_{PE}/{}_{en}\mu_{tot}) \end{aligned} \tag{2.36}$$

this reduces to

$$\begin{aligned} Q(E,T_o)dT_o = \frac{dT_o}{T_o\ {}_{en}\mu_{tot}}\Big[& \psi_{CE}(E,T_o)\,{}_{en}\mu_{CE} + \psi_{PP}(E,T_o)\,{}_{en}\mu_{PP} + \\ & \psi_{PE}(E,T_o)\,{}_{en}\mu_{PE}\Big] \end{aligned} \tag{2.37}$$

Now when multiplied by T_o and integrated from $T_o = 0$ to $T_o = E$ Eq. 2.37 becomes

$$\begin{aligned} \int_o^E T_o Q(E,T_o)dT_o = \int_o^E \frac{T_o}{T_o\ {}_{en}\mu_{tot}}\Big[& \psi_{CE}(E,T_o)\,{}_{en}\mu_{CE} + \\ & \psi_{PP}(E,T_o)\,{}_{en}\mu_{PP} + \psi_{PE}(E,T_o)\,{}_{en}\mu_{PE}\Big] \end{aligned}$$

or,

$$\frac{1}{en\mu_{tot}}\left(en\mu_{CE} + en\mu_{PP} + en\mu_{PE} \right) = \frac{en\mu_{tot}}{en\mu_{tot}} = 1.0 \tag{2.38}$$

This shows that the expression for $Q(E,T_o)$ in Eq. 2.37 satisfies Eq. 2.33.

Now $\Psi_\alpha(E,T_o)$ must be evaulated. To find this quantity the expression for the spectrum of scattered electrons is used. For Compton scattering this spectrum is given by Evans (E, 3) as

$$N_{CE}(E,T_o) = \frac{\pi r_o^2}{\alpha^2 m_o c^2}\left\{ 2 + \left(\frac{T_o}{h\nu_o - T_o}\right)^2 \left[\frac{1}{\alpha} + \frac{h\nu_o - T_o}{h\nu_o} - \frac{2}{\alpha}\frac{(h\nu_o - T_o)}{T_o}\right]\right\} , \frac{cm^2}{KEV\ electron} \tag{2.39}$$

When rearranged, Eq. 2.37 becomes

$$N_{CE}(E,T_o) = \frac{r_o^2 m_o c^2}{E^2}\left\{ 2 + \left(\frac{T_o}{E-T}\right)^2 \left[\frac{(m_o c^2)^2}{E^2} + \frac{(T_o - 2m_o c^2)(E-T)}{E T_o}\right]\right\}, \frac{cm^2}{KEV\ electron} \tag{2.40}$$

In these equations

r_o = Electron Radius
α = $h\nu_o / m_o c^2$
m_o = Electron Rest Mass
c = Speed of Light
h = Plancks Contant
ν_o = Frequency of Gamma Radiation
T_o = Electron Energy
E = Gamma Energy = $h\nu$

For pair production electrons, $N_{pp}(E, T_o)$ is given by (B, 3)

$$N_{PP}(E, T_o) = \frac{d({}_e\sigma)}{dT_o} = \frac{4\sqrt{\frac{1}{4} - (\frac{T_o}{E - 2m_oc^2} - \frac{1}{2})^2}}{1.4 + 0.1T_o - (0.6 + 0.1T_o)\sin(1.4 + 0.1T_o)}, \quad \frac{cm^2}{MEV\ electron} \tag{2.41}$$

To obtain an expression for $\Psi_\alpha(E, T_o)$ we first multiply Eqs. 2.40 and 2.41 by $T_o dT_o$ to obtain $N_\alpha(E, T_o)T_o dT_o$ which is the amount of energy possessed by electrons with initial energies between T_o and $T_o + dT_o$ due to process α. This quantity can be normalized to unity by dividing by

$$\int_o^E N_\alpha(E, T_o)T_o dT_o \tag{2.42}$$

The expression for $\Psi_\alpha(E, T_o)dT_o$ then becomes

$$\Psi_\alpha(E, T_o)dT_o = \frac{N_\alpha(E, T_o)T_o dT_o}{\int_o^E N_\alpha(E, T_o)T_o dT_o} \tag{2.43}$$

Thus $\Psi_\alpha(E, T_o)dT_o$, as described earlier, is the fraction of the available energy imparted to electrons with initial energies between T_o and $T_o + dT_o$. This may then be inserted into Eq. 2.37 to find the expression for $Q(E, T_o)$. Now all relations which are required for the solution of Eq. 2.25 have been developed. Thus one can calculate the ratio of the dose in the cavity/TLD to the dose in the medium.

To recap, we desire to evaluate the dose ratio of Eq. 2.25.

In the first step Eq. 2.28 is used to evaluate the mass stopping power ratio. This is then integrated (using the trapezoidal rule). Next $Q_z(E,T_o)$ must be evaluated. This is done by finding expressions for $\psi_\alpha(E,T_o)$ and substituting them into Eq. 2.37. These spectral shape functions are evaluated according to Eq. 2.43 The electron spectra for Eq. 2.43 are found with Eqs. 2.40 and 2.41. The integration in the denominator of Eq. 2.43 is evaluated, again using the trapezoidal rule in the case of the RESPOND program.

RESPOND then multiplies the quantity in 2.32 by a function $\chi(E,T_o)$ and divides by the integral of $\chi(E,T_o)$ over all electron energies. $\chi(E,T_o)$ is the fortran variable called SOURCE and is defined as

$$\chi(E,T_o) \equiv \psi_{CE}(E,T_o)\left(\frac{en}{\rho}u_{CE}\right) + \psi_{PP}(E,T_o)\left(\frac{en}{\rho}u_{PP}\right) + \psi_{PE}(E,T_o)\left(\frac{en}{\rho}u_{PE}\right) \qquad (2.44)$$

Comparison of this Eq. and Eq. 2.37 shows that

$$\chi(E,T_o) = T_o\left(\frac{en}{\rho}\mu_{tot}\right) Q(E,T_o) \qquad (2.45)$$

Thus the integral of $\chi(E,T_o)$ over all electron energies is

$$\int_o^E \chi(E,T_o)dT_o = \frac{en}{\rho}\mu_{tot}\int_o^{T_o} T_o Q(E,T_o)dT_o = \frac{en}{\rho}\mu_{tot} \qquad (2.46)$$

In RESPOND, Tuttle evaluates the quantity

$$\frac{\chi(E,T_o)\left\{\frac{1}{T_o}\int_o^{T_o}\frac{\frac{1}{\rho_c}\left|\frac{dT}{dx}\right|_c}{\frac{1}{\rho_z}\left|\frac{dT}{dx}\right|_z}dT\right\}dT_o}{\int_o^E \chi(E,T_o)dT_o} \qquad (2.47)$$

When 2.45 and 2.46 are substituted, 2.47 reduces to

$$Q(E,T_o)dT_o\int_o^{T_o}\frac{\frac{1}{\rho_c}\left|\frac{dT}{dx}\right|_c}{\frac{1}{\rho_z}\left|\frac{dT}{dx}\right|_z}dT \qquad (2.48)$$

This, then, is identical to the quantity in the second integral in the numerator of Eq. 2.25. Tuttle, however defines as

$$\psi_\alpha(E,T_o)dT_o = \frac{N_\alpha(E,T_o)dT_o}{\int_o^E N_\alpha(E,T_o)dT_o} \qquad (2.49)$$

This differs from Eq. 2.43 in the omission of a T_o weighting. Therefore in the present work RESPOND was modified to comply with Eq. 2.43.

The next step in the evaluation of Eq. 2.25 requires the integration of 2.48 over all electron energies between 0 and E. This is done in RESPOND using the trapezoidal rule.

The final step is to average the quantity

$$\int_0^E Q(E,T_o)\,dT_o \int_0^{T_o} \frac{\frac{1}{\rho_c}\left|\frac{dT}{dx}\right|_c}{\frac{1}{\rho_z}\left|\frac{dT}{dx}\right|_z}\,dT \qquad (2.50)$$

over the available gamma energy,

Tuttle, however, averages over ϕ (E). Therefore RESPOND was again modified to comply with Eq. 2.25. Once the final integrals in Eq. 2.25 have been evaluated and the division performed, the ratio of the dose in the TLD/cavity to that in the medium has been evaluated.

2.5.4 Correction for Large Cavities

Up to this point in the derivation it has been assumed that the dose in the dosimeter was caused by an equilibrium spectrum of electrons slowing down in the medium or wall surrounding the TLD cavity. This spectrum was assumed to remain unchanged in the TLD cavity. This would only by the case if the cavity/TLD were small with respect to the range of an electron in the cavity material (LiF). In actuality the range of an electron in most TLD materials is very small and the small cavity approximation is a bad one. T. E. Burlin (B,8) has developed a correction factor based on the assumption that the electron spectrum in the cavity does not change, but merely decreases in intensity up to the limit of the electron range in the cavity material. Burlin's weighting factor is given by

$$d(E) = \frac{1.0}{l}\int_0^l e^{-\beta x}\,dx = \frac{1.0 - e^{-\beta l}}{\beta l} \qquad (2.51)$$

where l is the mean penetration chord length given by

$l = 4V/S$ for simple, convex regions

and V = volume (cm^3)

S = Surface Area (cm^2)

β = Attenuation Coefficient = $\frac{-\ln(0.01)}{R(E_{max})}$

where R = Range of the electron of energy

Emax

Two equations are used to calculate the range of electrons in materials:

$$R = 0.412E^{(1.265 - 0.0945 \ln E)} \qquad \text{for } E \leq 3 \text{ MEV}$$

$$R = 0.530E - 0.106 \qquad \text{for } E \geq 3 \text{ MEV} \qquad (2.52)$$

With this correction we can write a new expression for the dose received by a TLD in the cavity from electrons produced in the sleeve material. From small cavity theory the cavity dose is:

$$m^{D_c} = \int_0^{\infty} dE\, E\, \phi(E) \left\{ d(E) \left(\frac{en\mu^z_{tot}}{\rho_z}\right) \int_0^E dT_o\, Q_z(E, T_o) \int_0^{T_o} \frac{\frac{1}{\rho_c}\left|\frac{dT}{dx}\right|_c}{\frac{1}{\rho_z}\left|\frac{dT}{dx}\right|_z} dT \right\} \quad \frac{\text{MEV}}{\text{gm. sec.}} \qquad (2.53)$$

Next the dose in the cavity which is due to the absorption of gamma rays directly by the cavity material must be considered. This dose is equal to

$$ {}_{m}D_{c} = \int_{o}^{\infty} E\,\phi(E)\left(\frac{en\mu_{tot}^{c}}{\rho_{c}}\right)dE\,, \quad \frac{MEV}{gm.\ sec.} \tag{2.54} $$

This value is then weighted by $\left[1 - d(E)\right]$ and added to Eq. 2.53 to get the total dose received by a TLD in the cavity. The dose in a cavity/TLD of any size is

$$ {}_{m}D_{c} = \int_{o}^{\infty} dE\ E\,\phi(E)\left\{d(E)\,\frac{en\mu_{tot}^{z}}{\rho_{z}}\int_{o}^{E} dT_{o}\,Q_{z}(E,T_{o})\int_{o}^{T_{o}} \frac{\frac{1}{\rho_{c}}\left|\frac{dT}{dx}\right|_{c}}{\frac{1}{\rho_{z}}\left|\frac{dT}{dx}\right|_{z}}\,dT + \left[1 - d(E)\right]\frac{en\mu_{tot}^{c}}{\rho_{c}}\right\}\,, \quad \frac{MEV}{gm.\ sec.} \tag{2.55} $$

To simplify Eq. (2.55) we define two new quantities. The first is the relative external dose (RED)

$$ RED \equiv d(E)\int_{o}^{E} dT_{o}\ Q_{z}(E,T_{o})\int_{o}^{T_{o}} \frac{\frac{1}{\rho_{c}}\left|\frac{dT}{dx}\right|_{c}}{\frac{1}{\rho_{z}}\left|\frac{dT}{dx}\right|_{z}}\,dT \tag{2.56} $$

The second equation is the relative internal dose (RID given by

$$ RID \equiv \left[1 - d(E)\right]\frac{\left(\frac{en\mu_{tot}^{c}}{\rho_{c}}\right)}{\left(\frac{en\mu_{tot}^{z}}{\rho_{z}}\right)} \tag{2.57} $$

A new expression for the dose ratio can now be obtained through the substitution of RED and RID:

$$\frac{{}_{m}D_{c}}{{}_{m}D_{z}} = \frac{\int_{o}^{\infty} dE\ E\phi(E)\left(\frac{en\mu^{z}_{tot}}{\rho_{z}}\right)\ (RED + RID)}{\int_{o}^{\infty} \phi(E)\left(\frac{en\mu^{z}_{tot}}{\rho_{z}}\right) dE} \qquad (2.58)$$

The last step in this derivation is to define a new quantity R_D. R_D is merely the dose ratio ${}_{m}D_{c} / {}_{m}D_{c}$. T. E. Burlin uses the notation $(1/\overline{\overline{\overline{S}}})$ for this quantity. The three bars indicate that the stopping power ratio has been average over three spectra, ie. electron slowing down, initial electron energy, and gamma photon. Thus R_D is defined as

$$R_D = \frac{{}_{m}D_{c}}{{}_{m}D_{z}} = \frac{\int_{o}^{\infty} dE\ E\phi(E)\left(\frac{en\mu^{z}_{tot}}{\rho_{z}}\right)\ (RED + RID)}{\int_{o}^{\infty} E\phi(E)\ \left(\frac{en\mu^{z}_{tot}}{\rho_{z}}\right) dE} \qquad (2.59)$$

Equation 2.59 can be rearranged to give

$${}_{m}D_{z} = \left(\frac{1}{R_D}\right){}_{m}D_{c} \qquad (2.60)$$

In this prescription $1/R_D$ is similar to a quantity labeled $1/f$ and called the "f" factor by various workers in the field. (S3)(K,1) The method by which these $1/R_D$ factors are used to correct raw TLD data is explained in section 2.8.2.

2.5.5 Secondary Electrons

The cavity theory described in the last two sections does not allow for the possibility that fast secondary electrons may be produced by the primary electrons. Should enough of these secondary electrons be produced and leak out of the cavity/TLD, the dose ratio predicted in Equation 2.5 9 will produce values which are too large. Spencer and Attix (S, 7) modified the simple small cavity theory outlined, in Section 2.5.3, to take into account the production of these fast secondary electrons. In their modification inelastic collisons were considered dissipative only if they result in energy transfers less than a cutoff energy Δ. Then the stopping power $(1/\rho_c \, |dT/dx|_c)$, was replaced with a modified stopping power which includes only energy losses less than Δ. The parameter Δ was chosen to be equal to the kinetic energy which an electron must have to cross the cavity's TLD. Then calculations were made for a few cases. (More cases were not used because this modification greatly increased the difficulty of the computation) the results of the calculations indicated that even when there is a large difference in atomic numbers, density, etc. between the cavity material and the surrounding medium, the difference between the two theories is less than a few percent if Δ is larger than about one-hundred KEV. The dosimeters which were used in the present experiments were cylindrical crystals of L_iF. With an outside diameter of lmm. This corresponds to a thickness of 0.27 $gm./cm^2$. An electron requires 436 KEV to cross this cavity. Since this is significantly larger than one hundred KEV only a very small error is made by ignoring the effect of secondary electrons in the M.I.T. dosimeter capsules. Therefore, secondary electrons were not considered further in the present work.

2.6 EFFECT OF NEUTRONS

Thermoluminescent dosimeters do exhibit a thermoluminescent response due to ions ejected as recoil products in elastic scattering collisions with fast neutrons. As these ions move through the lattice they create electrons and electron-hole pairs. These electrons may then become trapped, and responsible for a thermoluminescent response attributable to neturons when the TLD is readout. The neutron response for some thermoluminescent materials has been investigated. (S, 11) (R, 1) (S, 7) The major problem encountered in the determination of neutron response is that any experiment which uses neutrons is generally accompanied by gammas which arise from captured neutrons.

When a gamma photon interacts with matter, free, energetic electrons are produced. When a fast neutron interacts, atoms are ejected from the lattice. These recoiling lattice atoms create a much higher ionization density along their track than an electron does along its track. The ionization caused by the heavy, highly charged recoil atom is generally subject to considerable recombination, whereas the primary and secondary electrons from gammas are far more likely to be caught in impurity traps . This means that the response of a TLD is much larger for a 3 MEV gamma ray than for a 3 MEV neutron.

There have only been a few studies completed which determine neutron response as a function of the incoming neutron energy. (S, 11) (W, 1) Most of these experiments have been of the integral type. The results of this work are shown in Fig. 2.20. The solid line in this plot was calculated considering only elastic scattering recoils due to fast neutrons. The scattering was assumed to be isotropic in the center of mass system. The calibration of the dosimeters which establishes the relationship between dose and the thermoluminescent output was

^{7}LiF Response to Neutrons

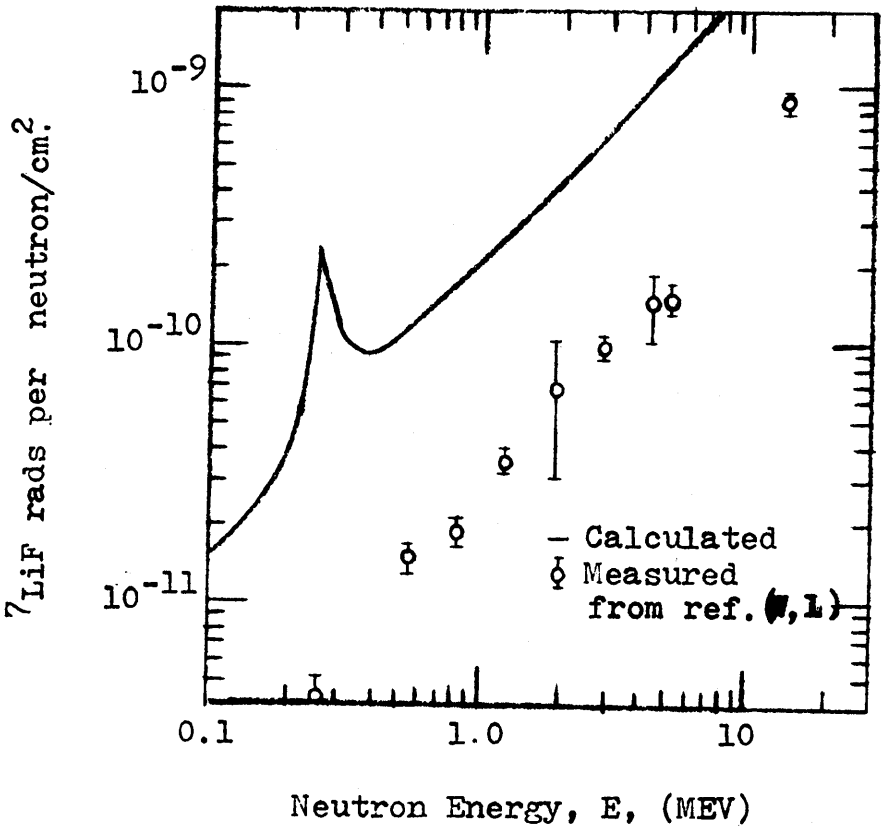

Fig. 2.20 Dose Per Unit Neutron Fluence for ^{7}LiF as a Function of Neutron Energy.

established with gamma rays. Figure 2.20 shows that there is generally good agreement between the slopes of the two curves but that the calculated curve is an order of magnitude higher. This is probably due to the reduced ability of low-energy ions to produce ionization and the high probability for re-combination.

In addition to the thermoluminescent (TL) response caused by neutron-induced production of electron-hole pairs, a TL response might also be caused by lattice-ion displacements and lattice vibrations. A one MEV neutron will produce, on the average, several hundred displacements and many times more replacements in the crystaline lattice. Simons and Yule state, (S, 6)

> "However, it has been found that for moderate fast neutron fluences (10^{15} n/cm^2) the gamma ray response and fast neutron reponse are additive, so that even though there are a sizeable number of defects introduced (a number comparable with the number of impurity traps associated with the thermoluminescence), the thermoluminescent output is not affected."

Values, found by interpolating between the MEASURED values of Fig. 2.20, and a calculated neutron spectrum were used to estimate the neutron response in the TLD's irradiated in the M.I.T. blanket mockups. The results are shown in the first column of Table 2.7. The second column in the table shows the measured dose of the ^{7}LiF TLDs in stainless steel capsules. The percentage of the dose caused by neutrons is shown in the last column of Table 2.7. This can be used to correct the experimental data for neutron response. The effect of this correction is shown in Chapter 4 where the experimentally determined dose curves are discussed.

LiF TLD's composed of natural lithium (7.42% ^{6}Li) exhibit a large neutron response due to the ^{6}Li (n, α) reaction. The cross section for this reaction varies between 0.1 and 3.5 barn in the neutron

TABLE 2.7 Estimated TLD-700 Neutron Response in Blanket No. 4

Distance from Converter Interface	Dneutron (rads)	Dtotal (rads) (in S.S.)	$\frac{\text{Dneutron}}{\text{D total}} \times 100\%$
BLANKET			
0.0 cm.	31.6	310.2	10.2
3.76 "	22.2	243.7	9.1
7.52 "	15.9	201.5	7.9
11.28 "	11.5	164.6	7.0
15.04 "	8.28	133.6	6.2
18.80 "	6.04	107.8	5.6
22.56"	4.42	86.6	5.1
26.31 "	3.20	69.6	4.6
30.07"	2.36	56.2	4.2
33.83"	1.73	45.6	3.8
37.59"	1.32	38.8	3.4
41.35 "	0.963	30.1	3.2
REFLECTOR			
45.11 cm.	0.662	17.9	3.7
48.92"	0.442	13.4	3.3
52.73"	0.305	10.9	2.8
56.54"	0.215	9.35	2.3
60.35"	0.154	8.09	1.9
64.16 "	0.116	6.80	1.7
67.97"	0.0840	5.60	1.5
71.78 "	0.0578	4.45	1.3
75.59"	0.0433	3.41	1.3
79.40"	0.0305	2.44	1.2
83.21 "	0.0203	1.55	1.3
87.02"	0.0111	0.74	1.5

energy range from 0.01 to 5 MEV. The particle product is highly ionizing and hence quite capable of causing a response in a LiF TLD. Therefore TLD's which were enriched to 99.997% in ^{7}LiF (Harshaw TLD-700) were used in the present study to avoid this problem.

The scarcity of data points and large differences between the measured and calculated values in Fig. 2.20 indicate that a better understanding of the neutron response of ^{7}LiF is required.

2.7 CAPSULE DESIGN

2.7.1 General Requirements

The TLD capsule is to be designed so that the most accurate results possible may be obtained. In order to do this certain factors must be kept in mind. First the TLD capsule is used to approximate a point detector. Thus a small TLD should be used and the smaller the better. The proper material must be selected for both the sleeve and TLD material. The capsule construction details also have to be considered.

There were several constraints which governed the selection of capsule design features. There are a total of 18 test positions in the blanket and reflector regions of the facility. Each of these test positions is made of tubing or recesses having a 3/8 in. ($\sim$ 9 mm.) inside diameter. Commercially available TLD's having satisfactory characteristics for the present use have an outside diameter of 1 mm. (0.039 in.). The space between the TLD and the inside wall of the test position can then be used for sleeve material. This puts an upper limit on the sleeve wall thickness of about 4 mm. The minimum wall thickness is governed by charged particle equilibrium requirements.

This will be discussed in section 2.7.2 which follows. Therefore one major design criteria is to use only capsules which will both fit in the test positions and establish charged particle equilibrium.

Nominally identical TLD's vary substantially in their TL outputs. This variation is often 20% or more between two TLD's exposed to the same dose under identical conditions. The standard deviation from the mean ($\pm 1\sigma$) of the 48 ^{7}LiF TLD's which were used in the present work was $\pm 5.5\%$ for equal dose and dose rate exposures to a Co-60 source. In order to minimize this uncertainty, three TLD's were used in each capsule. The same three TLD's were always located in the same position in the same capsule for every exposure of that capsule. This required that the capsule sleeves all be long enough to contain three TLDs. In order to keep the TLD's from sliding past each other within the capsule's central hole, a fairly tight tolerance is required. However, enough room must be left so the TLD slides through the hole easily because these crystals break easily if they become stuck inside. In this work all capsules used were found to behave satisfactorily when a No. 52 drill was used. This produces a hole size of 1.2 mm. (0.046 in.) leaving sufficient but not excessive clearance for the TLD.

The TLDs were sealed in the capsules using machine screws for end plugs in the stainless steel and aluminum capsules. In the remaining capsules (made of lead, zirconium, tungsten, teflon, and tin) end plugs were taped on with mylar tape. Once the end plugs were in place the capsules were put into holders.

The holders for the blanket region were long rods which had notches cut in them for the TLD capsules. The capsules were taped to the rod with a piece of mylar tape. In the reflector region the test

positions were holes drilled into the two-inch diameter steel plug, which penetrates the reflector. Therefore the length of the TLD capsules could not be longer than the depth of the hole in the plug. (i.e. 2 in.).

Finally each TLD capsule was numbered using an engraving tool. The overall design of the stainless steel dosimeter capsules used in this work is shown in Fig. 2.21. The sleeves made from the other materials irradiated were identical to the design in Fig. 2.21 except for wall thickness.

2.7.2 Sleeve Wall Thickness

One of the most important factors affecting the performance of any cavity ionization dosimeter is the thickness of the surrounding sleeve. In general the sleeve material is the material in which the gamma dose rate is desired. For example, if the gamma dose rate in stainless steel is desired at any point in a reactor a TLD with a sleeve of stainless steel will be used. Sometimes sleeves which simulate gamma absorption in other materials may be used. Lead sleeves were used to simulate gamma absorption in uranium dioxide and aluminum sleeves to simulate sodium in the present work. The basis for this simulation is discussed in detail in section 2.8.5.

In order to use Bragg-Gray Theory as applied to TLD capsules the TLD must see an electron spectrum which is characteristic of the sleeve material. In stainless steel for example, the TLD must be subjected to an electron spectrum characteristic of stainless steel.

To establish this spectrum Charged Particle Equilibrium (CPE) must exist. When this condition exists the electron spectrum retains its shape throughout the sleeve material and the small internal cavity/TLD. The actual sleeve thickness required to establish CPE is not well defined. It is generally accepted (C, 1) that charged particle

TLD Capsule

Stainless Steel Wall

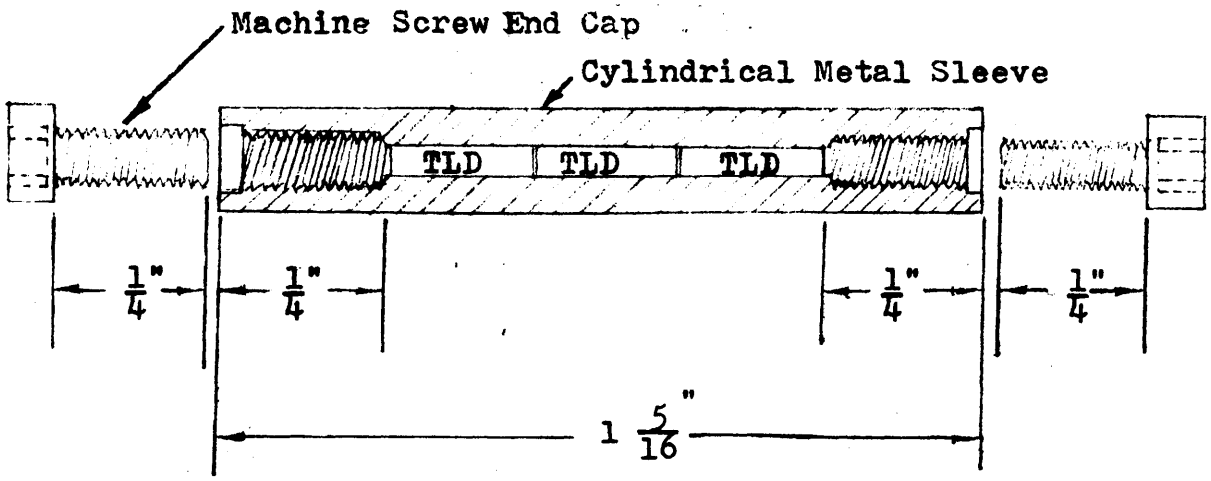

A. 3/16" Outside Diameter

B. 0.064 Inside Diameter;
0.070" Wall Thickness

C. End Screws; 1/4" deep x 4-40

Features

A. Bragg-Gray Cavity Design

B. Holds three 1mm. Dia. x 6mm. TLD-700's

C. Establishes Charged Particle Equilibrium

Fig. 2.21 Stainless Steel TLD Capsule

equilibrium will be established in any material having a thickness equal to the range of the most energetic electron found in that material. However, it has been found (B, 5) that much less than the full electron range is actually needed and for the vast majority of applications. 50% of the range of the most energetic electron is adequate. In summary then, the charged particle equilibrium requirement places a minimum thickness restriction on the sleeve wall of about one half the range of the most energetic electrons present.

There is also an important maximum wall thickness restriction. If the wall thickness is too thick, low energy gammas and electrons will be attenuated by the wall. This may alter the electron spectrum in the TLD cavity . To minimize this attenuation as much as possible the sleeve wall thickness should be just large enough to establish charged particle equilibrium and no larger. Since charged particle equilibrium is established in a thickness equal to the range of the most energetic electron, no sleeve should be thicker than this range . Wall thicknesses were therefore kept between 50% and the full range of the most energetic electron for each sleeve material used. This criterion determined the range of allowable outside diameters. In order to simplify fabrication , standard stock which had an outside diameter within the required limits was used whenever possible.

The range of the most energetic electron must now be determined, a task conveniently done in two steps: First, determining the energy of the most energetic electron, and then determining the range of this electron.

It would be impractical to base the design on the range of the single most energetic electron which actually occurs in the sleeve wall. In actuality the most energetic electrons which occur in significant numbers should be used. The method used to select this population in the present work involved first identifying the most energetic gammas

which are present in significant quantities from the multigroup ANISN, results shown in Table 2.2. In the blanket region the first group which has a significant gamma contribution is group 26. In the reflector it is group 24. These gamma energies range between 4 and 8 MEV. Once the gamma energy is known the electron's energy may be estimated by considering the photoelectric effect, pair production, and the compton effect. The photoelectric cross section for 4 to 8 MEV gammas is so small that this process need not be considered. Pair production and the compton effect are significant at these energies. However, electrons produced by pair production have energies which are less than half of the gamma energy, and thus the most energetic compton electrons are used as the most energetic electrons. Compton scattering may produce electrons with energies up to 80 to 90 percent of the original gamma energies (E, 2). Based on the above considerations a 4 MEV electron was chosen to design the sleeve wall thicknesses. The range of electrons between 1 MEV and 20 MEV is given by (T, 3).

$$R(gm./cm^2) = 0.530\,T_o - 0.106 \tag{2.61}$$

All capsules used in the Blanket Test Facility were therefore based on $R_{max} = 2.0(gm./cm^2)$, the result of substituting $T_o = 4$ MEV into Eq. 2.61. Table 2.8 gives the actual diameters and wall thicknesses of the capsules used in the experimental work; all satisfy the relation $1.0 \leq R \leq 2.0$ gm./cm.^{2}

TABLE 2.8 I. Capsule Criteria (Inches)

Material	Minimum Allowable Wall Thickness (50% Ele. Range)	Maximum Allowable Wall Thickness (100% Ele. Range)
Lead	0.349	0.0699
Stainless Steel	0.0503	0.1007
Aluminum	0.1469	0.2938
Tungsten	0.0205	0.0411
Tin	0.0544	0.1089
Zirconium	0.0609	0.1219
Teflon	0.187	0.374

II. As Built Dimensions (Inches)

Material	Wall Thickness	Capsule Diameter
Lead	0.070	0.125
Stainless Steel	0.070	0.187
Aluminum	0.152	0.350
Tungsten	0.036	0.118
Tin	0.102	0.250
Zirconium	0.099	0.244
Teflon	0.177	0.400

At Argonne National Laboratory (S, 3) a sensitivity study was made to determine what effect changes in sleeve wall thickness would have on the output from a TLD. Their results showed that large variations in sleeve thickness resulted in small changes in the TLD response. For example, the wall thickness of a stainless steel sleeve was varied during exposures in the ZPPR critical facility. The TLD readouts relative to a 0.894 gm/cm^2 teflon sleeve were then determined. When the sleeve wall thickness was 0.400 g/cm^2, the response was 1.027 ± 0.087, and for the thickness 1.959 g/cm^2 the response was 1.067 ± 0.091. This is a small change indeed: approximately 4% less than the experimental error of ± 9%. An out-of-pile experiment using Co-60 gamma rays and stainless steel capsules of 0.400 gm/cm^2 and 2.579 gm/cm^2 was also performed with only air between the source and TLD capsules. The variation in TLD response was 2%, which is also within the experimental error of ± 9%. This result is particularly significant due to the great dissimilarity in gamma absorption between the stainless steel sleeve and the air which surrounded it. These results indicate that wall thickness may be varied through a wide range without affecting capsule performance. This is pertinent to work at M.I.T., because it confirms that any sleeve thickness between half and the full electron range may be used without affecting TLD response.

2.7.3 Selection of Thermoluminescent Material

There are currently two thermoluminescent materials which are being used to measure gamma energy absorption in fast critical facilities: Lithium fluoride and calcium fluoride. Either one of these materials may be used in criticals and both can give consistent and reproducible results. In any gamma heating measurements with TLD's an ideal dosimeter capsule would behave as a "matched" cavity, namely one which has no spectral dependence. In order to have a "matched"

cavity the atomic number, Z, of the TLD and the wall material must be very close. The concept of a "matched" cavity is developed more fully in section 2.8.3. Since gamma heating is to be measured in fuel, coolant, and clad, the ideal situation would required use of three different thermoluminescent materials, each matched to one of the three components. However, such thermoluminescent materials do not exist. Calcium fluoride may be used as a "matched" cavity with aluminum or sodium. This is satisfactory for measuring the heating which occurs in the coolant; but, only about 4% of the gamma heating occurs in the coolant (see Table 2.6).

Lithium fluoride has an average Z of 6. This makes it an excellent dosimeter for personnel dosimetry, ie. is it very close to the average Z of human tissue. Therefore it will not behave as a "matched" cavity with the heavy Z materials found in a fast reactor blanket.

Since no ideal thermoluminescent material has been developed for reactor blankets LiF or CaF_2: M_n must be used in unmatched dosimeters. As previously noted, experience has shown that the most consistent results for ^7LiF are obtained by integrating the area under the glow curve. The Harshaw 2000 TL analyzer available at M.I.T. does this automatically. The CaF_2: M_n results on the other hand are most consistent when the peak value of the glow curve is used. Thus CaF_2: M_n requires an X-Y plotter, a feature not available with the present M.I.T. setup. Even more importantly, ^7LiF has been successfully used in ZPPR, and ZPR-9. Also, ^7LiF does not fade readily as does CaF_2:M_n. Tappendorf (T, 1) states that LIF is reported to lose only 5% of its stored signal in a year, but CaF_2:M_n loses 20 to 30% in the first 24 hours after exposure. For these reasons ^7LiF was used at M.I.T.

Both ^{7}LiF and $CaF_2:M_n$ are commercially available in crystaline form in convenient-to-use geometries, which permits higher precision than powder.

2.8 CAPSULE USE

So far the experimental methods discussed have focused on TLD capsule theory and its relation to performance limitations and design. This section integrates the preceeding information to explain how the capsule is actually used, detailing the process in which a thermoluminescent response from the TLD is converted into a gamma dose rate for the sleeve material.

2.8.1 Capsule Calibration Procedures

In order to use a TLD, a relation between the thermoluminescent output and the gamma dose received by the capsule must be determined. This is done experimentally: the TLD capsules are exposed to a known gamma flux produced by a radioactive source which has sufficient strength to impart a reasonable dose to the capsule in a reasonable amount of time. Cobalt-60 was used for this purpose. Knowing the geometry of the source, its activity, gamma energy, and where the TLD capsule is placed in relation to the source, the dose rate, (rads/hr), can readily be determined. Attendant problems concerning dose rate determination are discussed in much greater detail in Chapter 3.

In order to perform the TLD calibrations 50 TLDs were used. All calibrations were done in stainless steel sleeves. Each sleeve contained three TLD's (except one sleeve which contained two). The capsules were numbered one through seventeen.

The TLD's were ordered such that in every capsule exposure the same TLD's were in the same location in the same stainless steel

sleeve. This insured that each capsule behaved as an independent reproducible measuring instrument of known calibration.

Calibration was completed in two steps. The first step established the consistency of the entire measurement procedure. This was done by giving the capsules the same Co-60 gamma dose in several exposures and comparing the thermoluminescent responses. In this step four runs were completed. Each capsule absorbed a dose of 252.3 rads. This dose was chosen because it is representative of the doses received by the capsules in a blanket exposure. After the exposure the TLD's were readout in the Harshaw 2000 thermoluminescent analyzer. The readouts from the three TLD's in one capsule were then averaged to obtain the "detector" response for the capsule/detector. The averaged responses in nanocoulombs have been entered in Table 2.9. The average values and the standard deviations are taken to represent the experimental uncertainty ($\pm 1\sigma$) of the entire measurement process.

It has been suggested that normalizing the readouts by the weight of the TLD might help decrease this uncertainty. This would involve determining the TL response in nanocoulombs per gram of ^{7}LiF. However, in the present experiment the same TLD's were placed in the same position of the same capsule for every exposure. Thus the normalization weight remains the same from run to run. Normalization by weight, under these circumstances would cancel out in so far as any bias or error are concerned. Placing the same TLD's in the same capsules eliminates variations due to capsule differences as well as those due to TLD differences.

The second step necessary in calibration is the establishment of the relationship between thermoluminescent output and capsule dose. The capsules were exposed to several different total doses and the

TABLE 2.9 Results of Constant-Dose TLD Calibration Runs

Total Dose = 252.31 RADs

Capsule No.	Run 1	Run 2	Run 3	Run 4	Average	Standard Deviation, % ($\pm 1\sigma$)
1	501.5	612.5	590.9	618.7	580.9	± 9.3%
2	515.4	621.4	592.2	613.3	585.6	± 8.3"
3	487.7	586.5	555.6	577.7	551.9	± 8.1"
4	549.9	653.6	596.0	634.3	608.4	± 7.5"
5	548.6	648.8	616.7	609.0	605.8	± 6.9"
6	551.6	636.6	619.7	595.9	600.9	± 6.1"
7	577.8	649.7	645.4	583.5	614.1	± 6.3"
8	562.4	607.8	628.2	573.0	592.8	± 5.1"
9	550.0	572.8	605.7	573.1	560.4	± 7.0"
10	589.2	586.2	659.1	525.7	590.0	± 9.2"
11	631.0	614.3	707.1	563.5	629.0	± 9.4"
12	616.8	589.5	691.0	545.0	610.6	± 10.0"
13	611.6	624.6	691.8	551.0	619.8	± 9.3"
14	575.8	540.0	653.3	524.9	573.5	± 10.0"
15	570.7	554.4	658.5	558.9	585.6	± 8.4"
16	563.1	550.8	646.5	563.3	580.9	± 7.6"
17	569.8	592.2	666.5	604.1	608.2	± 6.8"
Average	563.1	602.4	636.7	574.2	594.1	± 5.5%

*For each run, each capsule response is the average of the readouts of the three TLD's it contains

corresponding readouts were obtained. Again the three TLD responses for each capsule were averaged. The results were then correlated: thermoluminescent output in nanocoulombs versus the total dose in rads for each capsule. This correlation was used to find doses in all experimental work. This method calibrates the whole TLD response system. This includes the effect of annealing, readout, and irradiation procedures. The calibration curve for capsule No. 1 is typical of all capsules and is shown in Fig. 2.22. The differences between this curve and the curves for the sixteen other capsules was generally less than ±5%.

This curve shows a break at approximately 1000 rads. This is a direct result of the calibration point obtained at 1800 rads. This point falls above the slope of the straight line fit through the other five points. Other investigators (T,1) (S,3) (S,2) have reported this supralinearity effect to occur between 700 and 1000 rads total exposure to Co-60 gamma rays. This, phenomena, however, has little impact on the results of the present work because of all TLD exposures performed at M.I.T. Only two data points (~2000 rads) were above the 1800 rad point. At this exposure level the difference between the results obtained with the supralinear fit and an extrapolation of the straight line through the other points is less than the experimental error (±10%).

2.8.2 Spectral Response Factors

When a TLD capsule, which has been calibrated with a Co-60 source is placed in an experimental assembly, the nominal "dose" in the sleeve must be corrected for the difference in reactor and Co-60 spectra. This becomes very obvious from consideration of Fig. 2.23, a plot of the ratio of the gamma dose in the sleeve material to that in an ^{7}LiF TLD cavity. For monoenergetic gammas this ratio is given

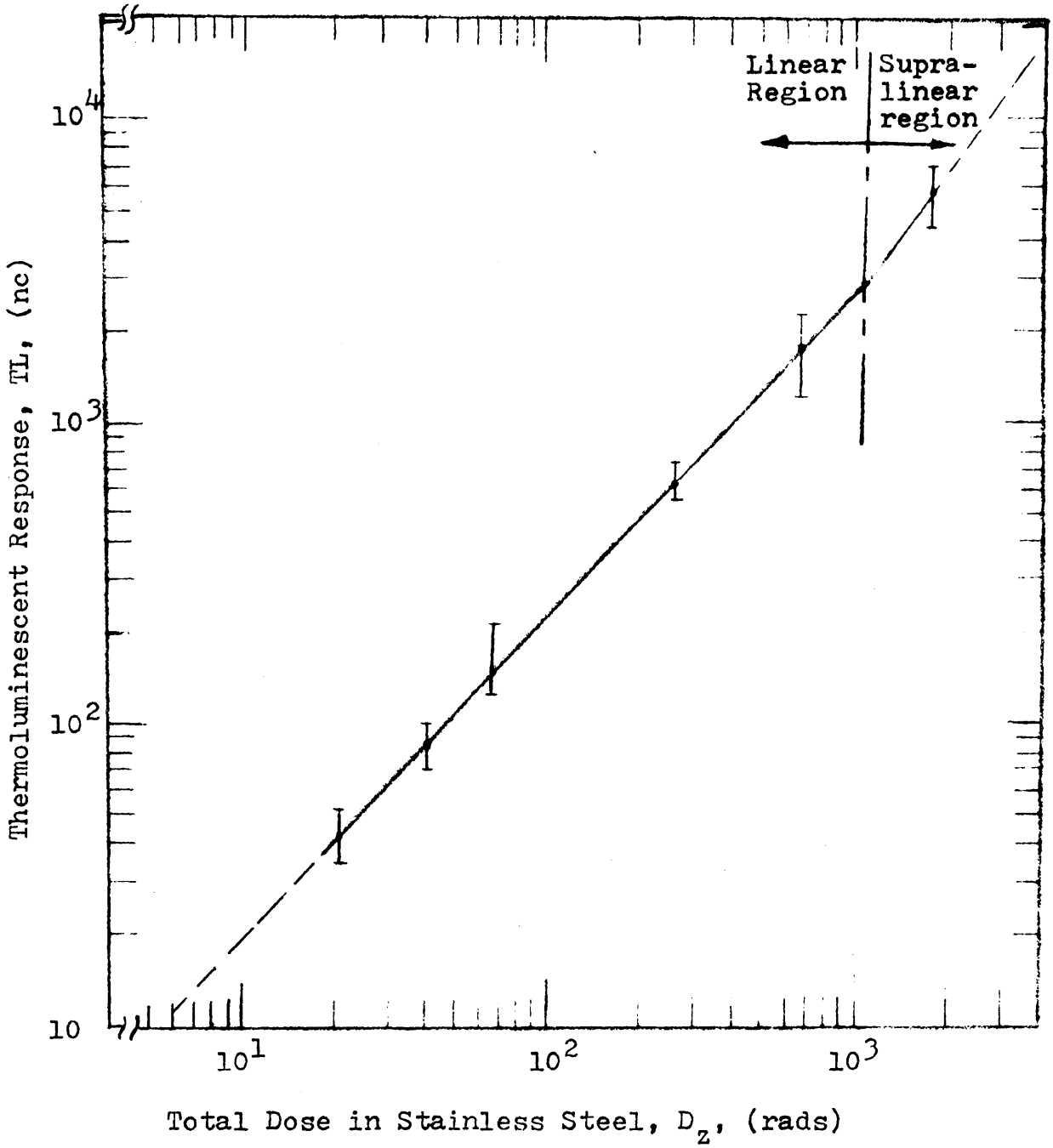

Fig. 2.22 Typical Calibration Curve for ^{7}LiF in Stainless Steel Capsules

Sleeve Dose Rates Relative to ^{7}LiF

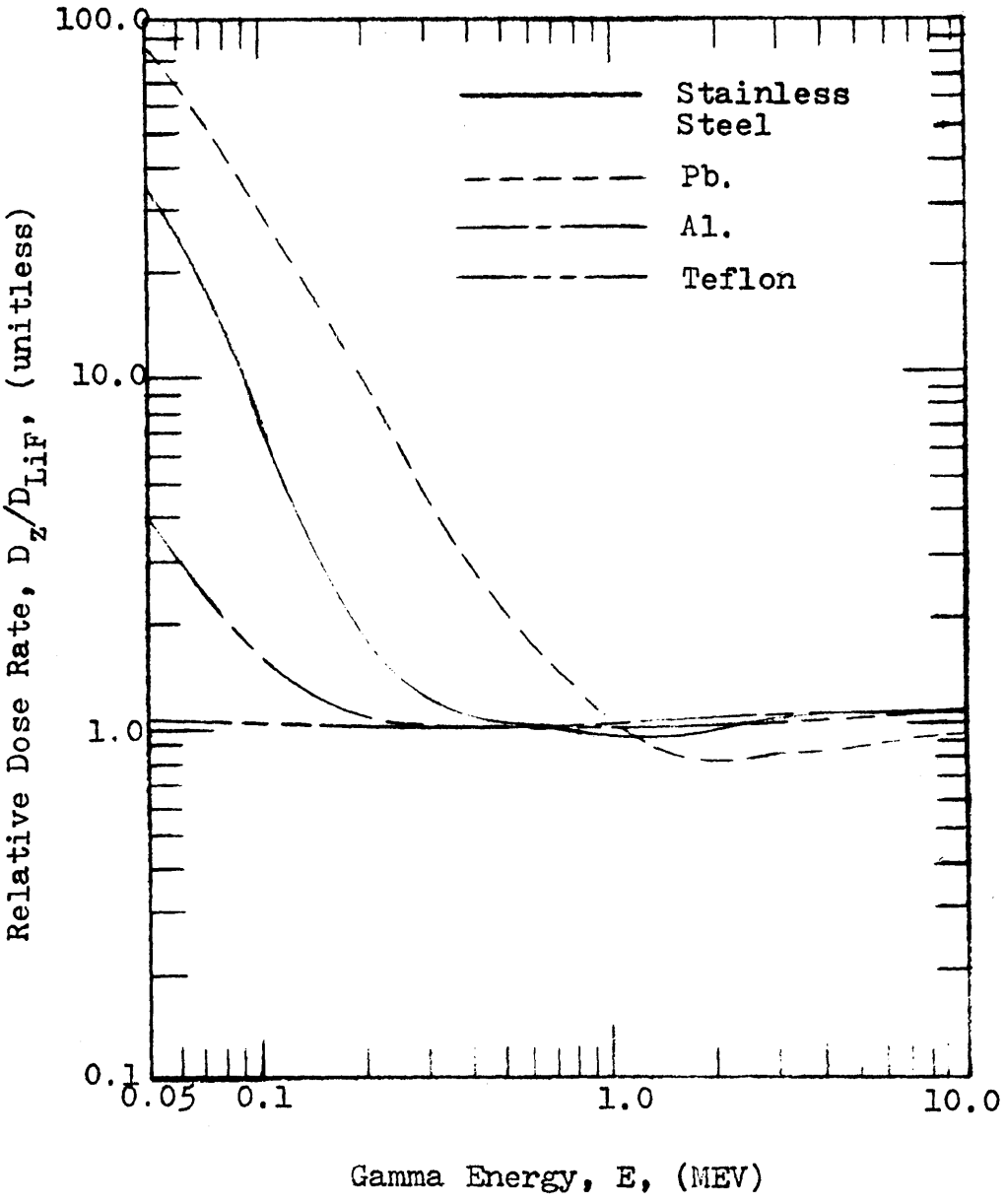

Fig. 2.23 Dose Rate Relative to ^{7}LiF for Four Major Sleeve Materials

by:

$$\frac{D_z(E)}{D_z(E)} = \frac{1}{RED + RID} \qquad (2.62)$$

RED and RID are defined in Eqs. 2.56 and 2.57. $D_z(E)$ and $D_c(E)$ are the doses in the sleeve and cavity due to gamma photons of energy (E). The figure shows that in the gamma energy range between 0.05 and 0.6 MEV there are very significant differences between the dose in the sleeve material and that in ^7LiF, with the exception of teflon. In Blanket No. 4 a significant gamma flux exists in this region. (See Fig. 2.6 and Table 2.2). Therefore, the uncorrected dose rates in Co-60 calibrated capsules for steel, lead, and aluminum sleeves will yield an underestimate of the true dose. However, the correct value may be found by multiplying the uncorrected dose by spectral response factors.

To find the required spectral response factors, recall Eq. 2.60.

$$_mD_z = \frac{1}{R_D}\, _mD_c \qquad (2.63)$$

Where $_mD_z$ = Dose in Sleeve Material

$_mD_c$ = Dose in Cavity Material

$1/R_D$ = Proportionality Constant

In this equation, $_mD_c$ is the dose in the cavity material or in this case the dose in the TLD. The dose in the cavity can be related to the thermoluminescent output of the TLD by a proportionality constant. This constant depends on the TLD analyzer, the annealing procedures, and other details of TLD handling procedures. However, as long as the procedure remains identical for every run the proportionality constant should be the same for every run. Thus, we can write a relation for the thermoluminescent response and the TLD dose as follows.

$$ {}^{m}D_{c} = (TL) \times C $$

where

$${}^{m}D_{c} = \text{Dose in Cavity/TLD, (rads)} \qquad (2.64)$$

$$TL = \text{Thermoluminescent Reponse (nc)}$$

$$C = \text{Proportionality Constant (rads/nc)}$$

This expression may then be substituted into Eq. 2.63 to give

$$ {}^{m}D_{z} = \left(\frac{1}{R_D}\right)(TL)C \qquad (2.65) $$

This gives a relation between the actual thermoluminescent output and the dose in the sleeve.

The next step in arriving at spectral response factors is to set up a ratio of Eq. 2.65 for two different situations. That is, for calibration exposure Eq. 2.65 may be written:

$$ {}^{cal}D_{z} = \left(\frac{1}{R_D}\right)_{cal}(TL)_{cal}\, C \text{ , rads} \qquad (2.66) $$

And, for an experimental run, Eq. 2.65 may be written:

$$ {}^{exp}D_{z} = \left(\frac{1}{R_D}\right)_{exp}(TL)_{exp}\, C, \text{ rads} \qquad (2.67) $$

The ratio of Eq. 2.66 to 2.67 is

$$ \frac{{}^{cal}D_{z}}{{}^{exp}D_{z}} = \frac{\left(\frac{1}{R_D}\right)_{cal}(TL)_{cal}\, C}{\left(\frac{1}{R_D}\right)_{exp}(TL)_{exp}\, C} \qquad (2.68) $$

Since the proportionality constant, C, is the same for every run, it cancels. The thermoluminescent output is the response in nanocoulombs for the two cases. $1/R_D$ is the factor which was developed in section 2.5.4. It is important to remember that these $1/R_D$ factors are dependent upon their respective spectra and sleeve walls. For example the $(1/R_D)_{cal}$ factor is dependent upon the Co-60 spectrum and stainless steel sleeves, and the $(1/R_D)_{exp}$ factor is dependent upon the spectrum in the Blanket Test Facility and sleeve wall material, be it stainless steel, lead, aluminium, etc.

In order to make use of Eq. 2.54, assume that a TLD capsule has been irradiated in the Blanket Test Facility and the capsule average TL response has been found. This quantity can then be substituted into Eq. 2.54 for $(TL)_{exp}$. Secondly the $1/R_D$ factors for the calibration and experimental spectra and sleeves can be substituted into Eq. 2.58. They are calculated by Eq. 2.59. Now Eq. 2.58 will be correct as long as both Eqs. 2.56 and 2.57 are satisfied. This means that ANY calibration thermoluminescent response and the corresponding dose rate may be substituted into Eq. 2.68; we pick the case such that:

$$(TL)_{cal} = (TL)_{exp} \tag{2.69}$$

The dose rate for this particular $(TL)_{cal}$ is substituted into Eq. 2.68. The thermoluminescent responses cancel. Thus Eq. 2.59 becomes

$$exp^{D}z = \left[\frac{(1/R_D)_{exp}}{(1/R_D)_{cal}}\right] \; cal^{D}z \tag{2.70}$$

And the spectral response factor is

$$\text{Spectral Response Factor} = \left[\frac{\left(\frac{1}{R_D}\right)_{exp}}{\left(\frac{1}{R_D}\right)_{cal}}\right] \qquad (2.71)$$

Now, to find the dose in the sleeve of a TLD capsule in a reactor blanket, first find the thermoluminescent response in nanocoulombs. Second, from the calibration curve find ${}_{cal}D_z$. Then find ${}_{exp}D_z$ by multiplying ${}_{cal}D_z$ by the proper spectral response factor of Eq. 2.71. This result is the actual dose occurring in the sleeve.

2.8.3 Teflon-Encased TLD Capsules

In section 2.8.2 a general method was developed for finding doses in the sleeve materials of any thermoluminescent dosimeter capsule. This is based on the assumption that the spectral response factors can be accurately calculated. These factors cannot necessarily be accurately calculated because $(1/R_D)_{exp}$ depends on the spectrum in the Blanket Test Facility. This spectrum has been calculated by ANISN and its accuracy is not well known. This is a problem which has faced most groups working on fast reactor gamma heating measurements.

There is one method which may be used to get around this problem. This method uses a "matched capsule." This is a capsule in which the wall material is the same, or behaves very nearly the same, as the cavity material in its response to gamma radiation. When this is the case the stopping powers of the cavity and wall material are similar at all electron energies. Thus we have

$$\left(\frac{1}{\rho_c}\left|\frac{dT}{dx}\right|_c\right) \approx \left(\frac{1}{\rho_z}\left|\frac{dT}{dx}\right|_z\right) \tag{2.72}$$

When this condition exists Eq. 2.64 for the relative external dose reduces to

$$RED = d(E)\int_0^E T_o Q_z(E,T_o)\, dT_o \tag{2.73}$$

or

$$RED = d(E) \tag{2.74}$$

When this result is substituted into Eq. 2.59 along with the definition for RID (Eq. 2.57), R_D becomes:

$$R_D = \frac{\displaystyle\int_0^\infty dE\ E\phi(E)\left(\frac{en\mu_{tot}^z}{\rho_z}\right)\left\{d(E) + \left[1 - d(E)\right]\left[\frac{\left(\frac{en\mu_{tot}^c}{\rho_c}\right)}{\left(\frac{en\mu_{tot}^z}{\rho_z}\right)}\right]\right\}}{\displaystyle\int_0^\infty dE\ E\phi(E)\left(\frac{en\mu_{tot}^z}{\rho_z}\right)} \tag{2.75}$$

The mass energy absorption coefficients for both sleeve and cavity are similar in the matched cavity or

$$\left(\frac{en\mu_{tot}^c}{\rho_c}\right) \approx \left(\frac{en\mu_{tot}^z}{\rho_z}\right) \tag{2.76}$$

When substituted into Eq. 2.75, the value in the curly brackets reduces to unity and the expression for becomes

$$R_D = \frac{\int_0^\infty dE\ E\phi(E)\left(\frac{en\mu^z_{tot}}{\rho_z}\right)}{\int_0^\infty dE\ E\phi(E)\left(\frac{en\mu^z_{tot}}{\rho_z}\right)} = 1.0 \qquad (2.77)$$

What this development shows is that for any spectrum the R_D factor for the matched cavity is unity; there is no spectral dependence for a matched cavity.

The above considerations make it obvious that the ideal way to perform gamma heating measurements is to use a "matched" cavity/TLD. When ^{7}LiF TLD's are encased in teflon a "matched cavity does in fact exist. This is shown by the teflon curve in Fig. 2.23, which is almost constant at a value of unity at all energies. In other words, the ratio of the dose in teflon to that in ^{7}LiF is very close to unity at all energies:

$$\frac{1}{R_D} = \frac{D_{tef}(E)}{D_{LiF}(E)} \approx 1.0 \qquad (2.78)$$

In work which involves testing the accuracy of calculational techniques and experimental procedures the teflon-encased TLD capsule can be very valuable. This is discussed further in section 4.4.4.

When one desires to measure gamma heating in metal with a large atomic number (Z) a teflon sleeve is not very practical: the sleeve is is instead made of the material in which the gamma absorption rates are desired. Unfortunately with ^{7}LiF a "matched cavity" with heavy Z materials cannot be constructed. Thus an unmatched cavity MUST be used.

2.8.4 Stainless-Steel-Encased TLD's

Stainless steel is a first choice for a TLD sleeve material since current LMFBR designs use stainless cladding. These sleeves also have several other desirable properties. They do not become excessively radioactively "hot" during irradiation in the BTF blankets; they protect the TLD's well, and are not difficult to make.

Stainless sleeves are also excellent when used in conjunction with a Co-60 calibration source. At the gamma energy of Co-60 (1.17 and 1.33 MEV) the dose rate in stainless steel is practically identical to that in ^{7}LiF. This can be seen in figure 2.23. The $(1/R_D)$ factor was calculated to be 1.054. Since this is very close to unity it will not make a large difference in the spectral response factor. This removes the uncertainty which would occur when otherwise calculating the $(1/R_D)$ factor for a source having lower gamma energies.

It is important to note that in a fast reactor gamma spectrum the $(1/R_D)$ values are also small. They were found to range from 1.0532 at the front of the blanket to 0.9684 at the rear of the reflector; thus the overall spectral response factor $[(1/R_D)_{exp} / (1/R_D)_{cal}]$ will have very little effect on the gamma dose measurement. This correction is, for example, less than the standard deviation characteristic of the results, as established in Table 2.8. In other words, a

Co-60 calibrated stainless steel TLD capsule is not highly dependent upon the details of the gamma spectra in fast reactors. They behave sufficiently like "matched" cavity dosimeters, and thus are well suited for fast reactor work.

2.8.5 Aluminum and Lead Sleeves

The bulk of the material which makes up the blanket region of the fast reactor is sodium coolant and U-238 fuel, and, as shown in Table 2.6, gamma absorption by fuel dominates. It then becomes very apparent that gamma heating rates must be measured in materials other than steel. The normal method of measurement would require that TLD capsules be constructed with sodium and uranium dioxide sleeves. This is not practical because sodium is reactive and UO_2 fragile. Also, fissioning in the UO_2 would cause ionization about the fission product track which affects the TLD response adversly. The next best thing is to use materials which simulate sodium and UO_2. Aluminum and lead were chosen for this purpose. A comparison of the mass energy absorption coefficients of aluminum vs. sodium and lead vs. uranium and UO_2 have been plotted in Fig. 2.24.

The value of the (Z/A) also provides a good comparison of the simulation. (Z/A) for sodium is 0.478 and for aluminum 0.482. An effective Z for compounds is given by (B,2):

$$\bar{Z}^3 = \frac{\sum_i a_i Z_i^4}{\sum_i a_i Z_i} \qquad (2.79)$$

where a_i is the atom fraction and Z_i the atomic number of element i. The average effective atomic weight, A, is found by (S,3);

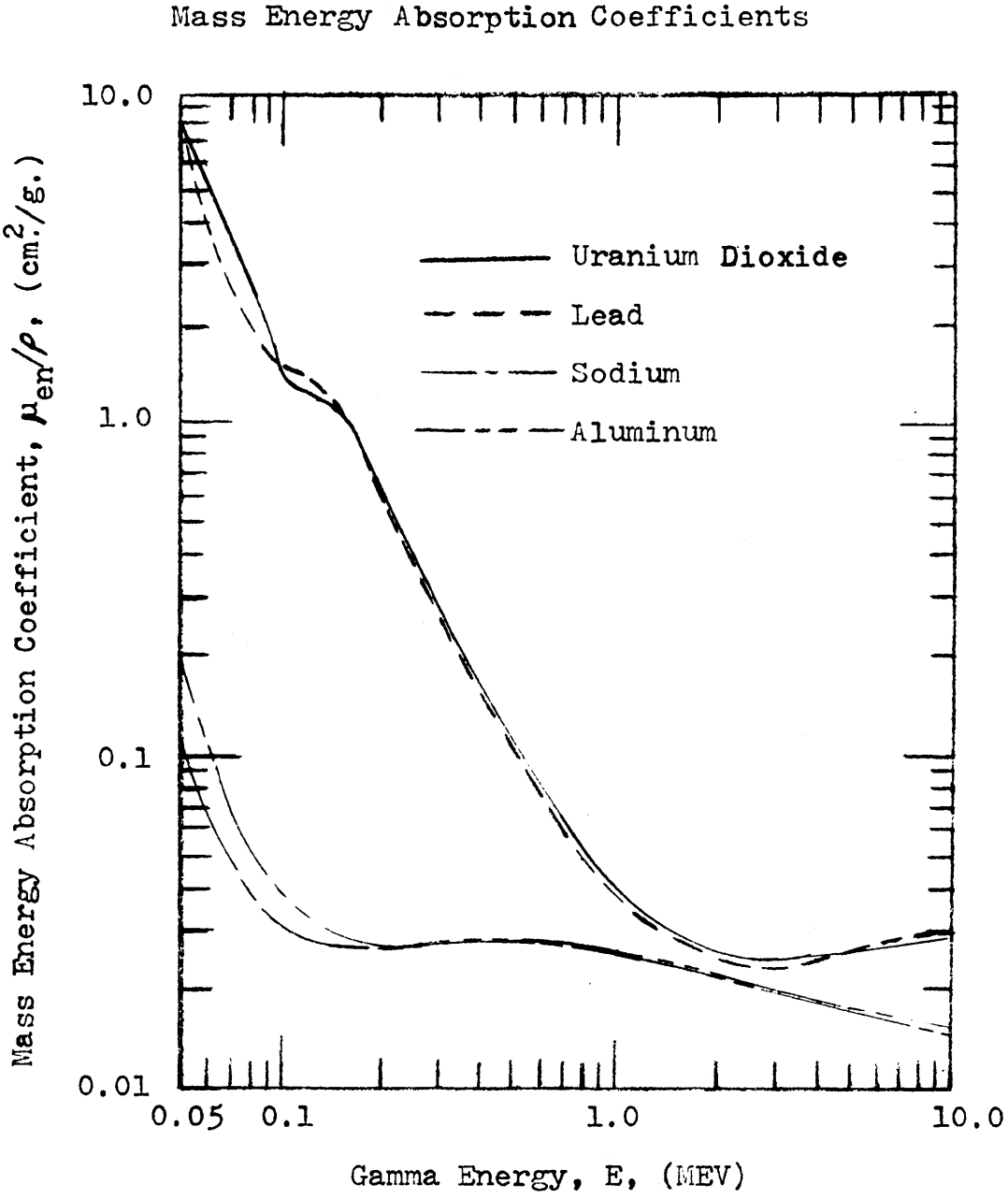

Fig. 2.24 Mass Energy Absorption Coefficients for Uranium Dioxide, Lead, Sodium, and Aluminum

$$\bar{A} = (5.55 \times 10^{-3})\ Z^2 + 2.079\ Z - 0.89 \qquad (2.78)$$

For UO_2, $(\bar{Z}/\bar{A})$ is 0.392; and Z/A for lead is 0.402.

The comparison of both mass energy absorption coefficients and average (Z/A) ratios shows the simulation to be quite good.

In addition to their ability to simulate sodium and UO_2, both aluminum and lead are relatively easy to machine , and are readily available.

The results obtained with these capsules and with the stainless steel capsules are presented in Chapter 4.

2.9 CHAPTER SUMMARY

This Chapter has dealt with the theoretical considerations underlying gamma heating measurements . This necessarily included an analysis of the BTF Blanket No. 4. to ascertain its adequacy as a mockup for a fast reactor, and thereby establish the validity of gamma heating results obtained from it. As was shown, Blanket No. 4. is a good simulation for gamma spectra, flux distributions, and gamma absorption rates. Transverse leakage was found not to be a problem.

The major considerations in TLD capsule design and use were then developed. This includes cavity ionization theory which is necessary for development of spectral correction factors. Sleeve design and calibration procedures were then outlined to establish proper design methods and capsule use. Finally, the simulation of gamma absorption in sodium and UO_2 using aluminum and lead was shown to be a good one.

These considerations lay the groundwork on which the experiments performed at M.I.T. were based. The result of this work is the topic of the remainder of this report.

Chapter 3
CALIBRATION FACILITIES

The most important single step in obtaining accurate, absolute gamma heating results is the calibration of the dosimeter capsules. In section 2.8.1 we went into some detail on how to obtain a calibration curve. The key requirement is that the gamma flux and spectrum be known at the point where the dosimeter capsule is placed. Perhaps the best way to achieve this goal is to place the capsule a known distance from a known source in a clean geometry: e.g. a well-defined source (point, line, plane) in an effectively infinite medium.

In the present work two gamma sources were investigated; both Cobalt-60. The first was approximately 4400 curies, and was located at Massachusetts General Hospital. The second source was used in a facility constructed at M.I.T. The detailed particulars and the results of this work are the subject of this chapter.

3.1 COBALT-60 SOURCE AT MASSACHUSETTS GENERAL HOSPITAL

This Cobalt-60 source had a strength of approximately 6000 curies during the period in which the calibration work was done. The source was composed of several pencils of Cobalt-60 mounted in the form of an open ring, and contained inside a large circular lead shield. This assembly was in turn mounted on a cart which could be rolled over-top the TLD capsules which were to be exposed to the source. The arrangement of this facility was such that both the TLD capsules and the source were very close to the lead shielding. This provides an excessive amount of compton scattered

photons which degrade the pure cobalt-60 spectrum. In spite of this known shortcoming several TLD capsules were calibrated with this source. These calibrations showed poor reproducibility (±20%) and thus it was decided that a new calibration facility should be constructed at M.I.T.

3.2 CONSTRUCTION OF THE M.I.T. CALIBRATION FACILITY

The major objective was to provide a system which was easy to use and interpret. The design developed in response to these requirements is discussed in the following sections.

3.2.1 Selection of Source Material

There are several calibrated radioactive sources available commercially. Therefore the first key decision is which source material should be used. The first and foremost factor in source selection is that only gammas should be emitted and that the energies and yields of the photons are well known. Co-60 and Cs-137 both fit into this category and were the only two considered seriously.

In section 2.8.4 the advantage of using stainless steel LiF dosimeter capsules was discussed in that the ratio of the energy absorption coefficient of stainless steel to that of LiF was unity in the energy range just above one MEV. Since the 1.17 and 1.33 MEV gammas of cobalt-60 fall in this range the $1/R_D$ for Co-60 calibration was well known and close to 1.0. This is a strong argument for the use of cobalt-60.

When doing gamma heating measurements in an experimental facility whose spectrum is different from the calibration spectrum,

spectral response factors must be used. However, if the calibration source had a spectrum identical to that of the experiment no correction would be required. To obtain a spectrum which is identical to that in the blanket would be very difficult. However, one method to approximate this is to find the average energy of the gammas absorbed in the various blanket materials and then use a calibration source which emits a gamma near this average energy. To find this average energy the following equation may be used.

$$\bar{E}_{ab} = \frac{\int_0^\infty \phi(E)\left(\frac{en\mu_{tot}}{\rho}\right) E \, dE}{\int_0^\infty \phi(E)\left(\frac{en\mu_{tot}}{\rho}\right) dE} \text{, MEV} \qquad (3.1)$$

where $\bar{E}_{ab}$ = Average Energy of Absorbed Gamma

$\phi(E)$ = Gamma Flux

$\frac{en\mu_{tot}}{\rho}$ = Total Energy Absorption Coefficient

E = Gamma Energy

An 18-group ANISN-calculated blanket gamma spectrum was used to find $\bar{E}_{ab}$ of Eq. 3.1 for cladding, coolant, and fuel materials, yielding the following results: in sodium 1.344 MEV, in stainless steel 1.263 MEV, and in uranium 0.6272 MEV. The total overall average energy of the absorbed gammas in the blanket was found to be 1.115 MEV. Considering that the gammas absorbed in uranium have an average energy of 0.6270 MEV and that a large percentage of the gammas are absorbed in UO_2 it would be worthwhile to consider using cesium-137 (0.66 MEV gamma) as a calibration source. However, the average overall absorbed gamma has an energy of 1.115 MEV which

is closer to the average of the cobalt-60 gamma energies (1.25 MEV).

Based on the consideration of the ($1/R_D$) factor, and the match to average absorbed energy, a cobalt-60 source was chosen for use in all calibration work in the present study.

A source whose strength was approximately 70mc. of cobalt-60 was obtained through the M.I.T. radiation protection office. It was contained in a sealed steel capsule having a diameter of 3/4 in. and a height of 1 in. The exact strength of the source was not well known (~ 70 mc.) and thus a calibration of the source was required. The calibration method used is described in section 3.2.4.

3.2.2 Dose Rate Calculations

Once a source which has adequate strength has been obtained, the dose rate as a function of distance from the source must be determined. There are two areas of concern in this determination. The first is merely to find the dose rate distribution, and the second deals with error analysis.

The most direct way to find the dose rate at any distance, r, from the source is to specify that it be a point source, in which case:

$$D(r) = \frac{A \sum_{i=1}^{N} E_i y_i \left(\frac{en\mu}{\rho}\right)_i C}{4\pi r^2} \qquad (3.2)$$

where A = Activity in curies

E = Energy of ith gamma of yield y_i per disintegration

N = Total number of gammas per disintegration

$\frac{en\mu}{\rho}$ = Mass energy absorption coefficient, cm^2/gm

r = Distance from source, cm

C = Conversion factor, 2.135×10^6

According to this equation, as the radial distance from the source, r, increases, the spatial gradient in the dose rate, $(\frac{dD}{dr})$ decreases very rapidly. A plot of the dose rate in stainless steel vs. r is shown in Figs. 3.1 for a 70 mc. point source - the calibrated source available to, and used in the present work. It is obvious that close to the source, where the dose rate is changing most rapidly, a small change in r (e.g. positioning error) will produce a significant change in the dose rate received by a detector located at r. As the detector is moved farther and farther away from the source, the slope of the curve flattens considerably. Thus a detector could be moved over a large distance with very little change in the dose rate. If a detector were placed too close to the source the positioning error would be large. If it were too far away the dose rate would be very small. Based upon a tradeoff between the competing effects of dose rate and positioning error, a minimum useful distance of roughly 3cm was selected, and the design described below in section 3.2.3 developed in response.

During calibration irradiations the TLD's were supported by a holder machined to fairly high accuracy. However, there will nevertheless be an error in the capsule position. This error should certainly be less than ±0.01 in. To make doubly sure, the allowance for the machining error was generously assumed to be ±0.02 in. Thus, the criteria for the location of the detectors is that a change in, r, of ±0.02 in. (±0.51mm) should result in a change in the dose rate which

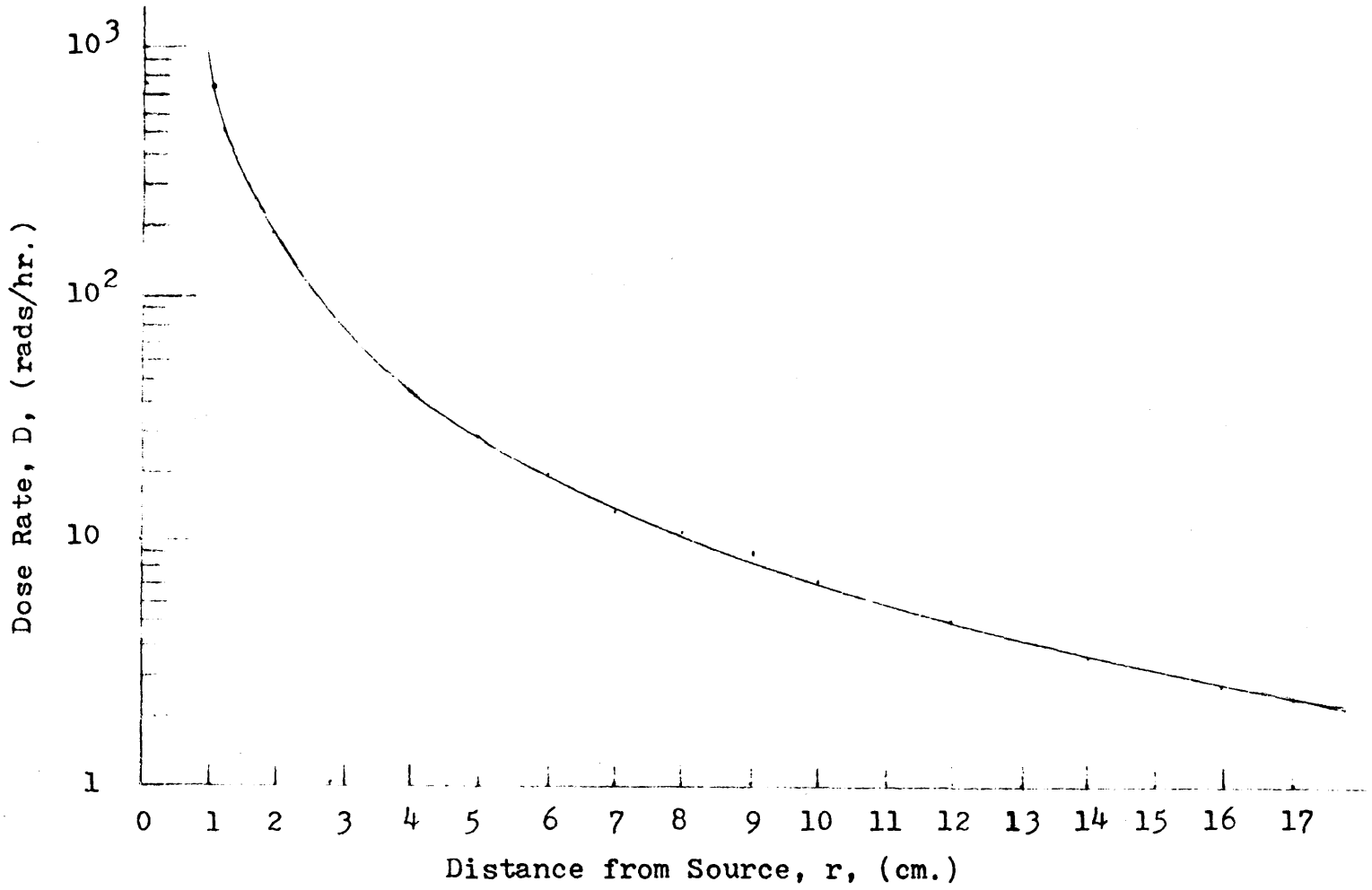

Fig. 3.1 Dose Rate in Stainless Steel as a Function of Distance from a 70 mCi Co-60 Point Source

which is less than 1.0%. This criterion is met where $r \geq 1$ 3/32 in. (2.78cm). The capsule holder was then constructed to hold the capsules at a distance of 1 3/32 in. from the center of the source. At this r the gamma dose for a 70mc. Cobalt-60 point source is 95.4 rad / hr . This is a useful dose rate, because the TLD capsules can receive acceptable doses, similar to those achieved in the blanket mockup, in just a few hours. The overall calibration of an entire library of TLD's can then be completed in two weeks time.

The use of Eq. 3.2 implies use of both a point source and a point detector. However, for the TLD capsules used during this calibration (shown in Fig. 2.21) the height within the capsule occupied by TLD's is 0.75 in (1.91 cm). When this capsule is placed 3 cm. from the source, the TLD's at either end should receive a smaller dose than the central TLD because they are, on the average, farther away. However, during actual calibration runs this effect could not be seen in the experimental data, probably due to the fact that the source used was not truely a point source.

3.2.3 Detector Holder

The detector holder fulfils three basic requirements. It must support TLD capsules, and ionization chamber dosimeters, and scattering by the holder must be negligible.

The design selected (see Fig. 3.2) involved an aluminum tube mounted vertically, through which the source slides. The source is suspended by a metal chain which can be reproducibly latched to suspend the source at the axial mid-plane of the TLD capsules or ICD's. Mounted on the outside of the tube is an aluminum disk having a 10.2 in. (26 cm) diameter. The dosimeters can be mounted securely on

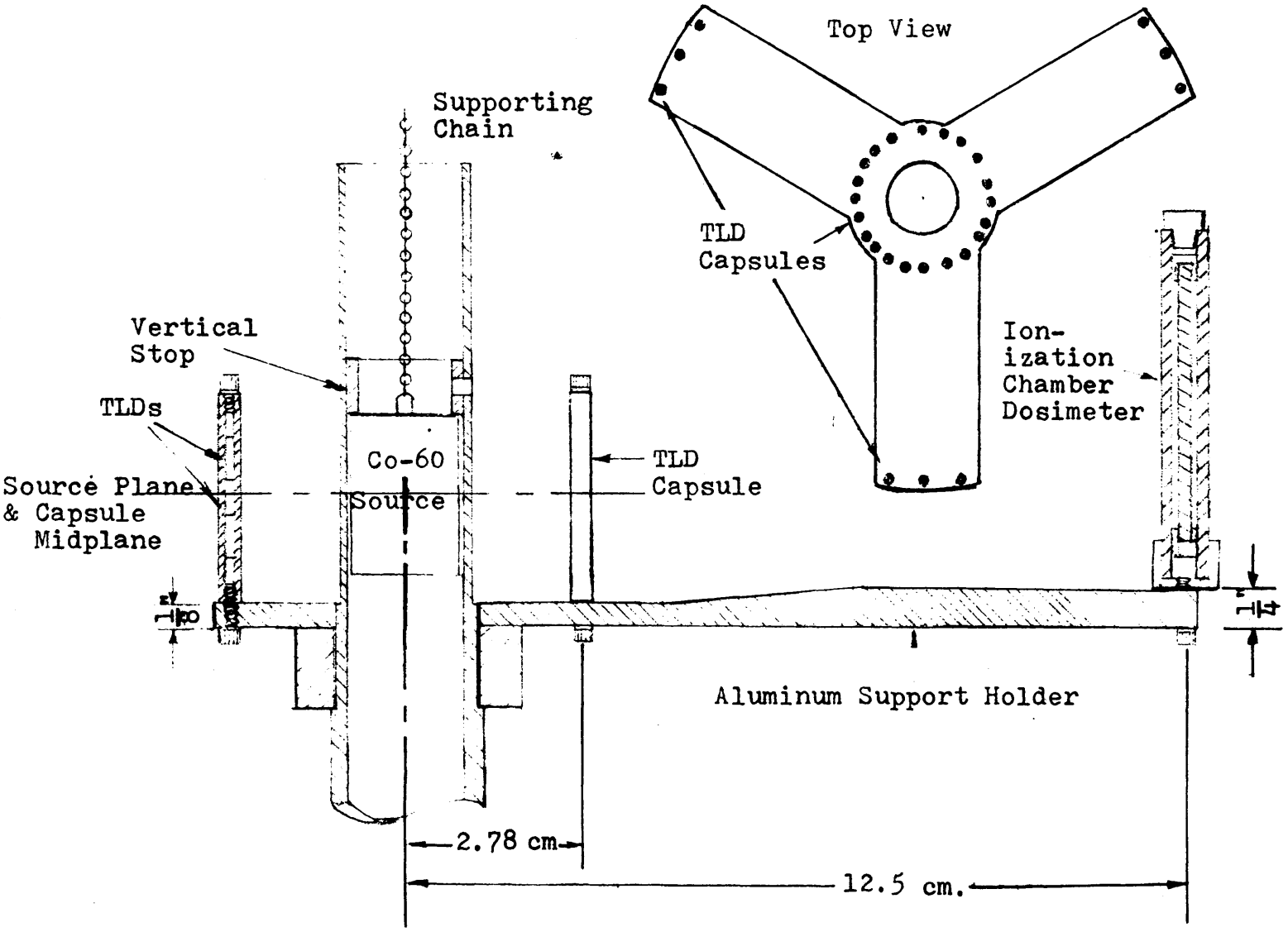

Fig. 3.2 Aluminum Irradiation Holder Used in M.I.T. Calibration Facility

this disk, with machine screws, at radii of 1 3/32 in. (2.78 cm) and 4.92 in. (12.5 cm). To use this holder the source is lifted up from its storage pig, through the tube, into position, and the dosimeters are thereby irradiated. Irradiations were timed with an ordinary electric clock. Runs were performed for specific time intervals (1/2 hr., 1, hr., etc.) with an accuracy of ±2 sec.

Aluminum was chosen as the construction material because it has a relatively low Z and density, and good machining properties. The disk was made from 1/4 in. aluminum plate. This thickness also provides sufficient strength to prevent warping and bending.

As noted above, the source has been used for calibration of both TLD capsules and ICD's. Certain differences in the calibration procedure for ICD's must be noted. There are two positions shown in Fig. 3.2. Both inner and outer positions were used for TLD capsules, but only the outer ones were used for the ICD's. This is because a maximum dose of 30 rads will completely drain the charge from the ion chamber, and thus the lower dose rates at the outer positions are more suitable for ICD calibration. The ICD's also required a special supporting cap which could be fastened to the machine screws (see Fig. 3.2). One final modification was required for ICD calibration: the vertical stop which positioned the source was raised so that the mid-plane of the source and the ICD coincided. These modifications allowed complete calibration of the change in voltage on the dosimeter as a function of the total gamma dose received.

Before proceeding further we must determine the effect of scattered gammas from this structure upon the detector. To do this the ratio of scattered gamma flux to that arriving directly from the source at the detector's location must be established. To determine this ratio,

consider a solid ring around the gamma source, with the detector located outside this ring. This arrangement is shown in Fig. 3.3. The source is located **c** centimeters above the plane of the ring and the detector is **d** centimeters above the ring's plane. Some of the gamma's emitted by the source will be Compton-Scattered by the solid ring. Then, if **S** photons per second are emitted from the source, the amount which are scattered per unit length of the ring may be represented as;

$$S' = \begin{matrix}\text{Ring Scattering} \\ \text{Source}\end{matrix} = \frac{S\mu_c t\, da}{4\pi f^2}, \quad \frac{\text{photons}}{\text{cm./sec.}} \tag{3.3}$$

where **S** = Source Strength (photons/sec)

μ_c = Compton Scattering Coefficient, $(cm.^{-1})$

t = Thickness of Ring, cm.

a = Radius of Ring, cm.

f = Distance from Source to Ring, cm.;

$$f^2 = a^2 + c^2$$

The differential unit of scattered flux reaching a point detector at **c** due to a small ring segment specified by $d\theta$ is

$$d\phi_s = \frac{S'ad\theta'}{4\pi e^2} = \frac{S'ad\theta}{4\pi(l^2 + d^2)}, \quad \frac{\text{photons}}{cm.^2\ \text{sec}} \tag{3.4}$$

Thus the total scattered flux reaching the detector is the integral of Eq. 3.6. around the ring:

$$\phi_s = 2\int_0^{\pi} \frac{S'ad\theta}{4\pi(d^2 + l^2)}, \quad \frac{\text{photons}}{cm.^2\ \text{sec}} \tag{3.5}$$

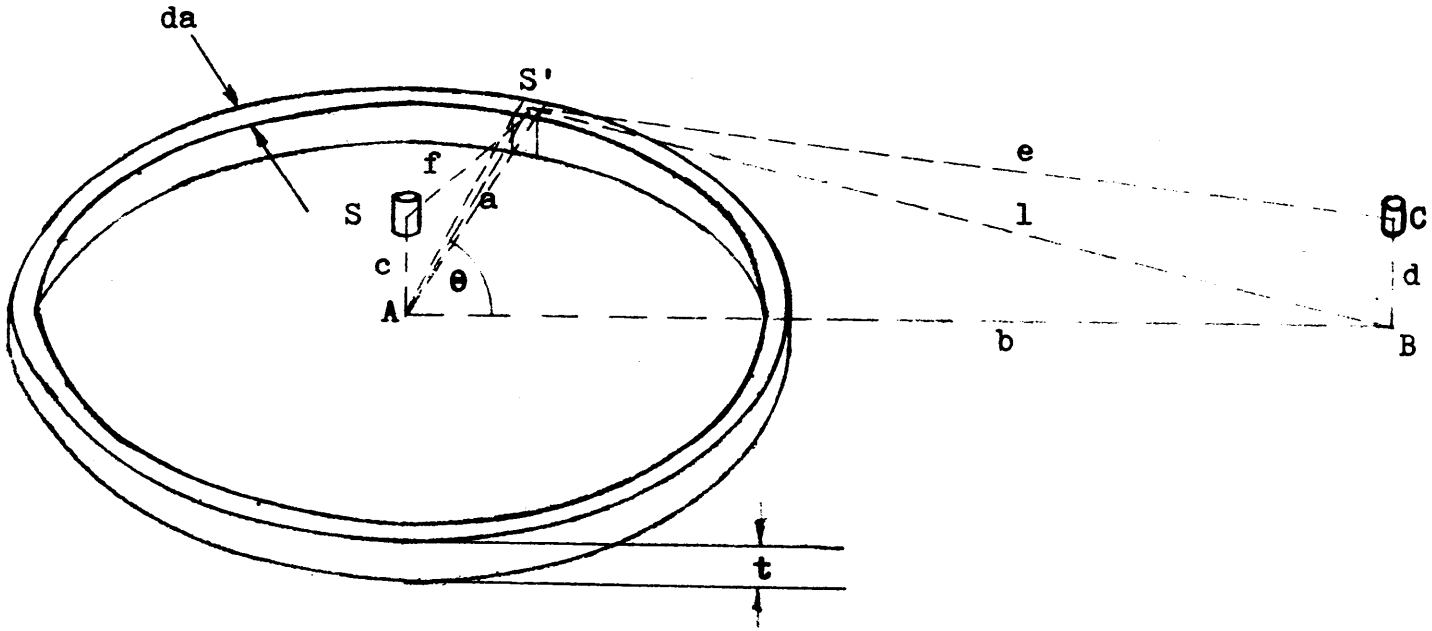

Fig. 3.3 Model for TLD Holder Scattering Calculation

With the law of cosines l can be written:

$$l^2 = a^2 + b^2 - 2ab \cos \theta \tag{3.6}$$

When this is substituted into Eq. 3.5 and the integration performed, the result is:

$$\phi_s = \frac{S' a}{2\sqrt{(a^2 - b^2)^2 + 2d^2(a^2 + b^2) + d^4}} \quad , \quad \frac{\text{photons}}{\text{sec. cm}^2} \tag{3.7}$$

Now by substituting Eq. 3.3 for S' and integrating over the radius of the disk with respect to a, the scattered flux at C from an entire disk of radius b is found.

$$\phi_s = \frac{S\mu_c t}{8} \int_o^b \frac{a\, da}{(a^2+c^2)\sqrt{(a^2-b^2)^2+2d^2(a^2+b^2)+d^4}} \quad , \quad \frac{\text{photons}}{\text{cm}^2 \text{ sec.}} \tag{3.8}$$

The flux which reaches the detector directly from the source is given by:

$$\phi_D = \frac{S}{4\pi b^2} \quad , \quad \frac{\text{photons}}{\text{cm}^2 \text{ sec.}} \tag{3.9}$$

The ratio of the scattered flux to the direct flux is therefore

$$\frac{\phi_s}{\phi_D} = \frac{b^2 \mu_c t}{2} \int_0^b \frac{a\,da}{(a^2+c^2)\sqrt{(a^2-b^2)^2+2d^2(a^2+b^2)+d^4}} \qquad (3.10)$$

This equation was evaluated numerically, using Simpson's Rule, for two aluminum disks. The first disk was 1/8 in. thick and had a diameter of 2 3/16 in. (5.66 cm.). The ratio of the scattered to direct flux was found to be 0.01. Thus scattering provides a negligible portion of the absorbed flux for a TLD capsule placed on the outside edge of this disk. The second disk was 10.2 in. (26 cm) in diameter and 1/4 in. thick. The scattering component was found to be 6.3% of the direct flux. To rectify this situation, sections of this disk were removed so that the holder assumed the hub and spoke shape shown in Fig. 3.2. This left approximately 28% of the original material. Thus, the scattrered flux was reduced to approximately 1.8% of the direct flux, which is considered small enough to be negligible.

This exercise demonstrates that scattering should not be a problem with the source holder. It is also a conservative calculation because Compton Scattering is predominantly forward scattering (E,2). Therefore in this model the isotropic scattering assumation provides an overestimate of the flux at the detector.

3.2.4 Source Calibration

Up to this point in the discussion of the calibration source, all dose rate calculations have been based on the assumption that the

source strength was exactly 70 mc. and that it behaved as a point source. As noted earlier the exact source strength was not known with sufficient accuracy for present purposes. The problem was further complicated by the actual size of the source (3/4 in. (1.90 cm) diameter and 1.0 in. (2.54 cm) high). The problem is that when a detector is placed 1 3/32" (1.78 cm) from the center of this cylinder, the assumption that the contents behaves as a point source is not necessarily a good one. Therefore, some method had to be found to determine what the dose actually is at this location from the source.

To calibrate the source two calibrated ionization chamber instruments were used. One was a Technical Associates "Juno" Model 7 and the second a Nuclear Chicago "High Range Cutie Pie." These instruments were both calibrated against a national Bureau of Standards Cesium-137 source (accuracy ±3%) immediately before exposure to the cobalt-60 source. These instruments have an accuracy of ±5% immediately after calibration. When placed 100 cm. (39.4 in.) from the cobalt-60 source the positioning error of the instrument is easily kept within ±3%. Both instruments agreed that at 100 cm. from the source the exposure rate was 100 milliroentgens. Combination of the various uncertainty involved give this measurement an accuracy of ±6.5%. Further measurements of dose as a function of distance from the source determined that the dose rates were characteristic of a point source up to a point 12.5 cm (4.92 in.) from the source. The exposure rate at 100 cm. (39.4 in.) converted to a dose rate in stainless steel by the following

$$D = Ex\ (10^{-3}\ R/mR)\left(\frac{87.6\ ergs/gm.\ R.}{100\ ergs/gm.\ R.}\right)\left(\frac{\frac{en\mu_{S.S.}}{\rho}}{\frac{en\mu_{air}}{\rho}}\right),$$

rads/hr. (3.11)

where Ex = Exposure, Milliroentgens

$\frac{en}{\rho}\mu$ = Mass Energy Absorption Coefficient, $\frac{cm^2}{gm}$

The dose rate was then measured at 100 cm and using the inverse square law characteristic of a point source the dose at 12.5 cm (10.2 in.) was calculated to be 5.258 rads/hr. Again the uncertainty in this calculation, based on the accuracy of the instruments, is ± 6.5%.

The next task is the determination of the gamma dose at 1 3/32 in. (2.78 cm) from the source. Since the point source approximation cannot be considered valid apriori, a comparative technique was employed. Several stainless steel TLD capsules were exposed in the holder at both 1 3/32 in. (2.78 cm) and the 10.2 in. (12.5 cm) positions for an hour and readout. Forty-eight TLD's in all were used, twenty four in both inner and outer rings. The standard deviation of the readouts of the inner 24 TLD's was ±6.1% The ratio of the average response of the inner TLD's to the outer TLD's was found to be 16.43:1. the dose rate at 12.5 cm. was then multiplied by this ratio to arrive at the dose rate in stainless steel at 2.78 cm. from the source: 86.39 rads / hr. This value was the standard dose rate used for calibration of all TLD capsules in the present work. The dose at 12.5 cm (5.258 rads / hr) was used for ICD calibration. Error analysis shows that the calibration-induced uncertainty in absolute dose rates for irradiations at the outer ring are approximately ±6.5% and at the inner ring ±8.9 %.

TLD capsule calibrations were carried out for all capsules with the source facility. The responses of all TLD's were checked against each other to determine if the central TLD's of a capsule were receiving

significantly higher dose rates than the outer TLD's. This effect could not be noticed. During any single calibration the standard deviation of all the TLD data was determined and found to range between ± 5.5 and ± 6.0% indicating that there was not a great mismatch in nominally identical doses received by any two TLD's.

The simple calibration facility described above was found to be satisfactory for all TLD work done at M.I.T. The results of traverses using TLD's calibrated in this manner are presented in the following chapter.

Chapter 4
EXPERIMENTAL PROCEDURE AND RESULTS

Experimental work was carried out in three areas: measurement of dose traverses in stainless steel, aluminum , and lead capsules; application of spectral unfolding techniques; and verification of spectrum response corrections. The dose traverses establish gamma heating rates in the M.I.T. Blanket Test Facility and are compared against results calculated using the ANISN program. In the spectral unfolding work a gamma spectrum is unfolded from experimentally determined dose rates, and again compared to ANISN calculations. Finally, a teflon-sheathed TLD experiment was carried out to assess the accuracy with which spectral response factors can be determined.

4.1 EXPERIMENTAL PROCEDURE

There are several important aspects of procedure which must be observed in order to establish reliable experimental data. These points are outlined in this section to clarify how the irradiations were performed and why they were done in the manner prescribed.

4.1.1 Annealing

Annealing history directly affects the total thermoluminescence of the TLD during readout. Both annealing temperature and the time at temperature must remain consistent from run to run. Although the best annealing scheme for any thermoluminescent material is difficult to determine, Harshaw Chemical Company recommends one

hour at 400°C followed by two hours at 100°C for the ^{7}LiF pre-irradiation anneal. ^{7}LiF exhibits spurious peaks in the glow curve around 80°C, therefore a post-irradiation pre-readout anneal of ten minutes at 100°C is recommended. This removes electrons from the unstable traps which cause these spurious peaks.

In the annealing process two ovens were used: one operated at 400°C and the other at 100°C. During annealing the 1 mm. diameter by 6 mm. long extruded TLD rods were supported by a holder which consisted of an aluminum plate (4 in. x 4 in x 1/4 in) in which holes were drilled to contain the TLD's. The pre-irradiation anneal was carried out in three steps: one hour in the 400°C oven; a two minute cool down under ambient room conditions; followed by two hours in the 100°C oven. When the TLD's and their holders were placed in the 400°C oven the temperature in the oven dropped approximately 3°C. This was recovered within ten minutes. There was no perceptible change in oven temperature when the TLD's were placed in the 100°C oven. The results obtained with this procedure were found to be adequate: ie. no large changes were measured in TLD response when they were subjected to several repetitive equal doses from the cobalt-60 calibration source; and the response from an annealed unirradiated TLD produced no statistically detectable background signal.

4.1.2 TLD Handling

TLD readouts become inconsistent when the crystal surface is dirty. Therefore, tweezers were always used to handle TLD's. Stainless steel tweezers with teflon coated tips were used because they were easy to manipulate and did not scratch the TLD surfaces.

The TLD's were also cleaned after every third use in a methanol bath. Any TLD's which inadvertently became dirty either through contact with human skin or dirty surfaces were cleaned with trichloroethylene, followed by methanol.

The TLD's were normally stored in their aluminum annealing plate, which was fitted with a lid. They were kept in a dark drawer between uses.

4.1.3 Bookkeeping

Bookkeeping is important to any experimental work but particularly so with TLD's because they are small, cannot be marked for identification, and many are used during an experiment. It is important to keep track of each TLD throughout the history of its exposure in order to interpret its results accurately. This was accomplished by associating each TLD with a number by numbering each of the fifty holes in the annealing plate in which the TLD's were stored. The stainless steel, aluminum , and lead capsules were also numbered by scribing one end with an engraving tool. During irradiations, TLD's 1, 2, and 3 were placed in capsule 1; 4, 5, and 6 in capsule 2, etc.. The capsules were also marked such that the position of each TLD in the capsule (top, middle, bottom) was known with respect to the mark, which thereby ensured that each TLD was in the same location in the same capsule during all irradiations.

During readouts the response of each TLD was recorded together with its number. This along with a log book record of every capsule's history permitted an accurate compilation of all data points.

4.1.4 Length of Blanket Exposures

Ideally a dosimeter capsule would be inserted into the blanket and withdrawn while the blanket was operating normally, similar to the blanket of an actual reactor during full power operation. Since the concrete shielding at the rear of the Blanket Test Facility must be removed to gain access to the blanket test positions, the blanket could not be in operation during loading or withdrawal of the TLD capsules. In fact, because of a problem with the lead shutter isolating the hohlraum region, the M.I.T. reactor had to be shut down during retrieval. After a run was completed a cooling-down time of approximately 45 minutes was required. Therefore, a run duration which is as long as practical is desirable so that the TLD dose due to background, received both before and after a run, would be negligible with respect to the dose received during the run. The background levels were measured, and found to be 0.075 rads/hr. in stainless steel, and on this basis a 5 hour run was found to be quite satisfactory, also, the doses received during a five hour run avoided high exposures in the LiF supra-linearity region.

4.1.5 Assignment of Dose Rates

After completion of an irradiation in either the Blanket Test Facility or the calibration facility the capsule-averaged response (in nanocoulombs) was converted to a total dose in the sleeve material using that capsule's calibration curve and the appropriate spectral response factors. For aluminium the spectral corrections ranged between 1.07 and 1.09; for stainless steel, 0.98 to 0.92; and for lead, 1.20 to 1.50. This procedure produces a total dose in rads which may then be divided by the run length to obtain a dose rate (rads/hr.). For example, in stainless steel the response for capsule three is found to be 850 nanocoulombs. The calibration curve shows this corresponds to 345 rads.

At capsule three's position in the BTF blanket $(1/R_D)_{exp.}$ is found to be 0.97677 and $(1/R_D)_{cal}$ is 0.9486. (The $(1/R_D)$ factors were obtained from RESPOND), the dose rate from Eq. 2.70 is then found to be 352 rads. Run time was 5 hours, hence the dose rate is 70.4 rads /hr. Identical procedures were applied to all capsule responses.

The experimental error assigned to a capsule dose rate calculation is the standard deviation which was obtained for that capsule. (See section 4.3.1). These errors ranged between 6 and 10 percent. It is important to note that the spectral response factor for aluminum and stainless steel capsules mentioned above are within or very close to the experimental error. However, for lead capsules the spectral response factors were between 1.2 and 1.5 and thus play an important role in dose rate determination. Therefore the accuracy of this calculation is discussed later in section 4.3.3.

4.2 NORMALIZATION

If absolute dose rates are to be calculated, measured and compared, a normalization scheme is required. In the ANISN blanket problem this was accomplished by specifying the strength of the thermal neutron plane source located in the converter's graphite region. The value chosen for the source strength was determined by irradiating a calibrated gold foil in the hohlraum, from which the total thermal flux was found to be 3.0×10^9 $(n/cm^2 sec)$. The total source in ANISN was then adjusted so that the thermal driving flux matched this value. Thus the gamma dose rates calculated by ANISN could be compared on an absolute basis. It should be noted that this is a severe test of the calculation method since the converter must be calculated accurately

in addition to the blanket.

The actual dose rates obtained with the TLD's also had to be adjusted for changes in reactor power. The thermal flux value found using the gold foil was determined while the reactor was at a full power of 5.0 megawatts. All subsequent runs normalized to this run by use of a stainless steel TLD monitor placed at the blanket's center in each run (see appendix C.2). Here again some uncertainty is introduced, since the reactor power calibration is precise only to within about ± 5%, and furthermore the shim rod position also affects hohlraum flux at constant reactor power.

With this normalization scheme, all measured and calculated values represent blanket heating rates at a nominal reactor power of 5.0 megawatts. The various sources of error in this figure make comparisons in the blanket on an absolute basis less precise than those on a relative basis. However, even so, these comparisons were found to be rather good, particularly for the key material - UO_2 as will be discussed in the next section.

4.3 COMPARISON OF CALCULATIONS AND EXPERIMENTAL RESULTS

4.3.1 Radial Dose Traverses

Three sets of dose traverses (set #1 in stainless steel, set #2 in aluminum, set #3 in lead) were performed and compared to calculations; (each set consisted of two runs).

Figure 4.1 compares calculated and measured data for stainless steel on a relative basis. The calculated data has been normalized

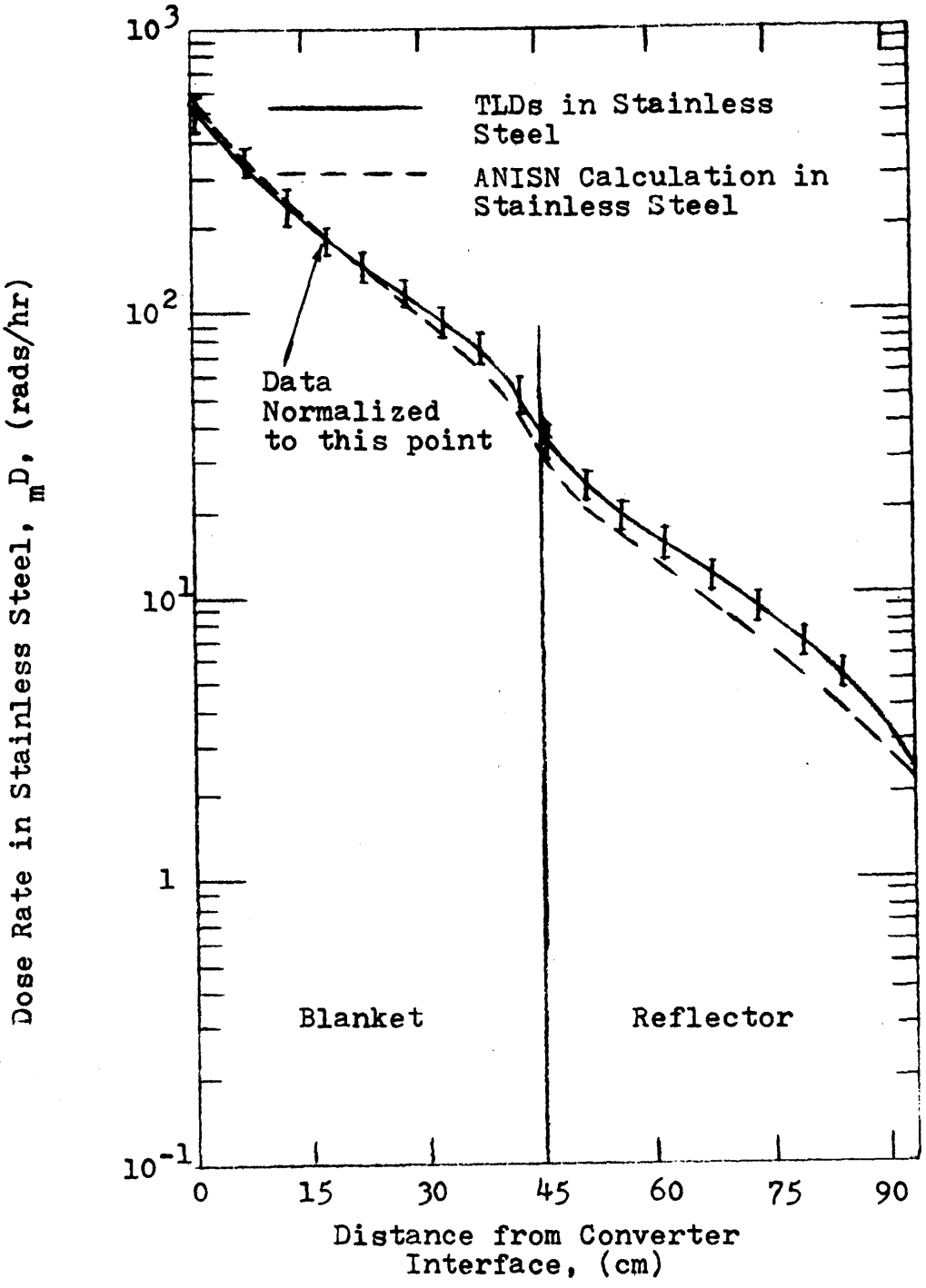

Fig. 4.1 Comparison of Relative Dose Rate Traverses in Stainless Steel

to the experimental data at the location of the fourth TLD capsule. Again the error bars represent the standard deviation ($\pm 1\sigma$) for each capsule. The comparison shows good agreement in the blanket: generally within the limits of experimental error. The agreement in the reflector, however, is not quite as good . The calculation gives results which are between 35 and 40 percent low. Figure 4. 2 shows the comparison of absolute stainless steel dose rates in the blanket and reflector. This shows that the measured dose rates are higher at all points. The difference is approximately 27 to 30 percent in the blanket, and grows to approximately 60% in the reflector.

The corresponding sodium dose comparisons are shown in Figs. 4.3(relative) and 4.4 (absolute). Again the comparison is very good in the blanket but poorer in the reflector, where the discrepancy ranges between 40 and 45%. In the absolute comparison shown in Fig. 4.4, the calculation also falls below the measurement as was the case in the stainless steel comparison. This difference ranges between 42 and 45% in the blanket. In the reflector it is between 70 and 80%.

Figure 4.5 shows the corresponding comparison for UO_2 on an ABSOLUTE basis. The agreement here is very good in the blanket and fairly good in the reflector. In the blanket all dose rates agree within the limits of experimental error. The differences in the reflector are between 11.5 and 12.5%. Again, error estimates are derived from a statistical analysis of the data. Two runs were made for each sleeve type so that at every test position two data points are available. The reported uncertainty this is found by first evaluating the standard deviation from the mean:

$$SDM = \sum_{i=1}^{N} [(A_m - A_i)^2/(N - 1)]^{\frac{1}{2}} \qquad (4.1)$$

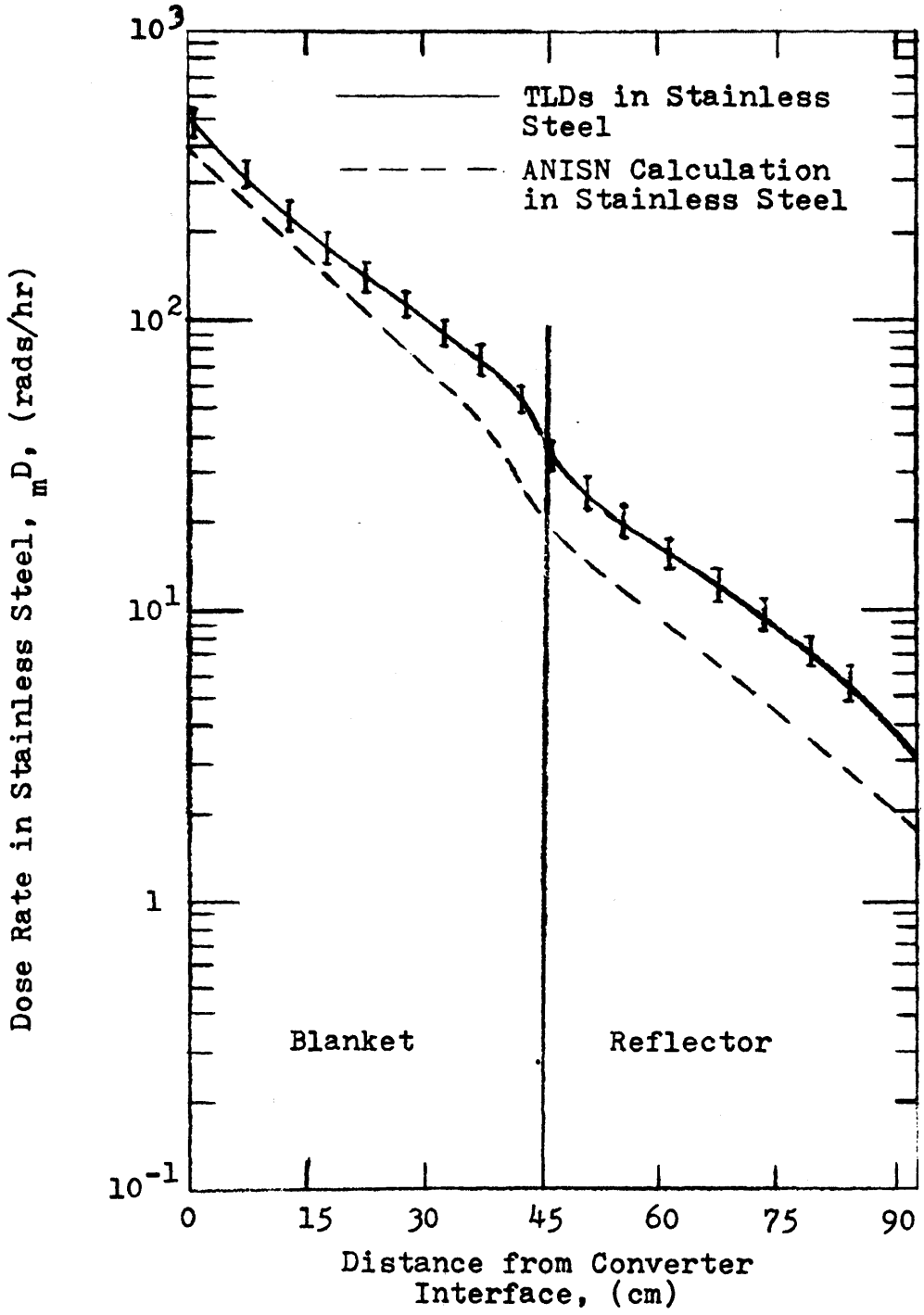

Fig. 4.2 Comparison of Absolute Dose Rate Traverses in Stainless Steel

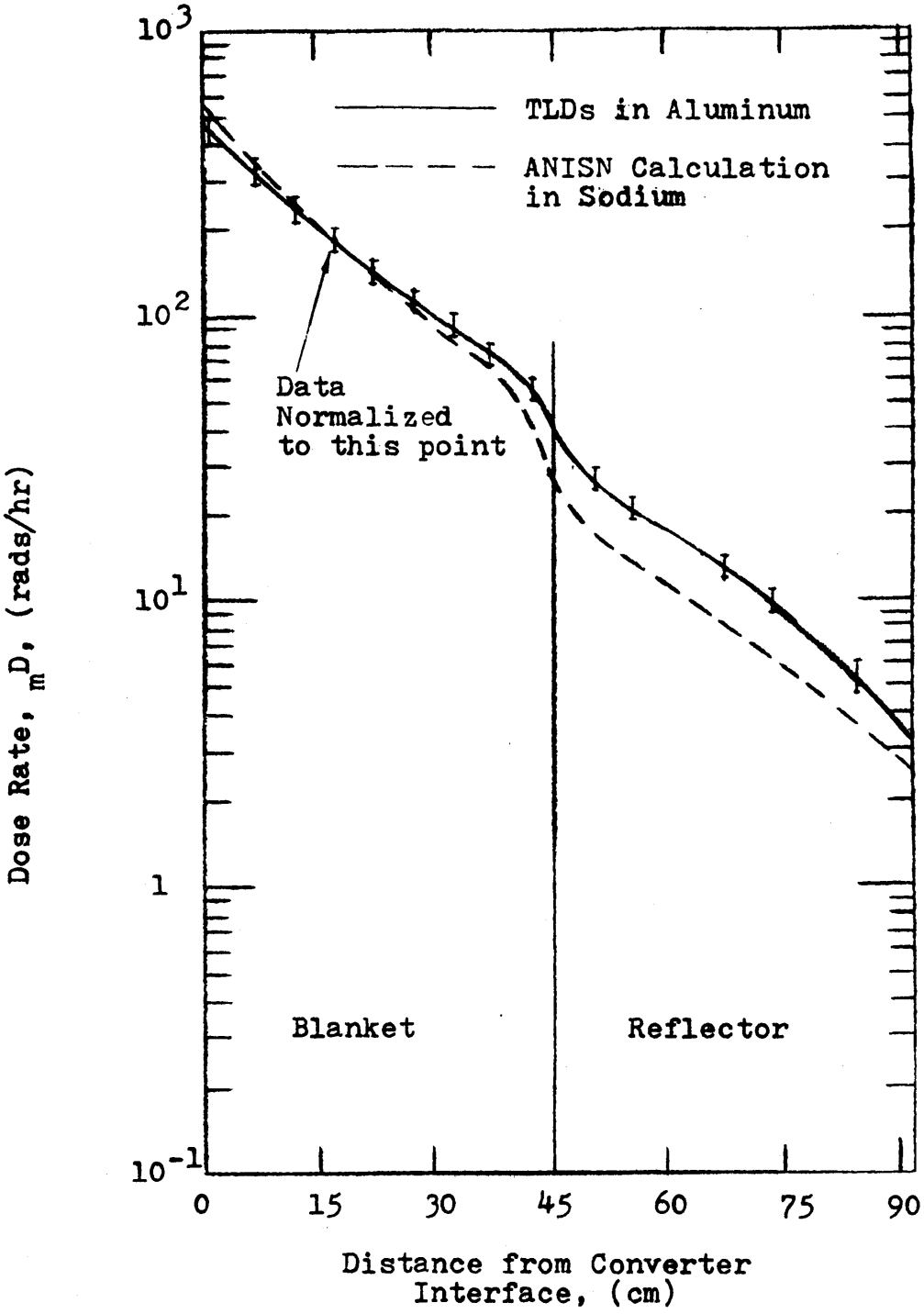

Fig. 4.3 Comparison of Relative Dose Rate Traverses in Sodium (Aluminum)

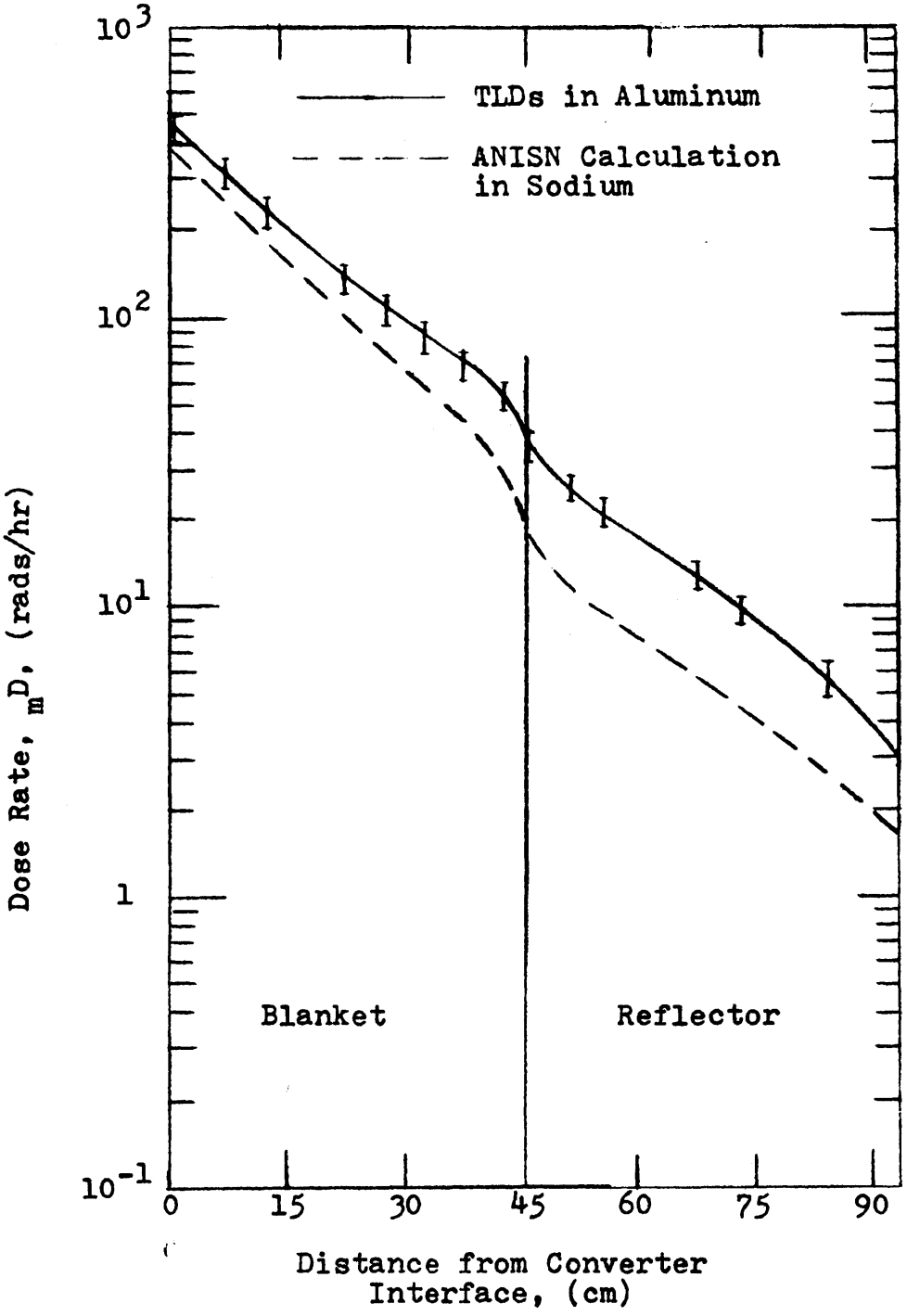

Fig. 4.4 Comparison of Absolute Dose Rate Traverses in Sodium (Aluminum)

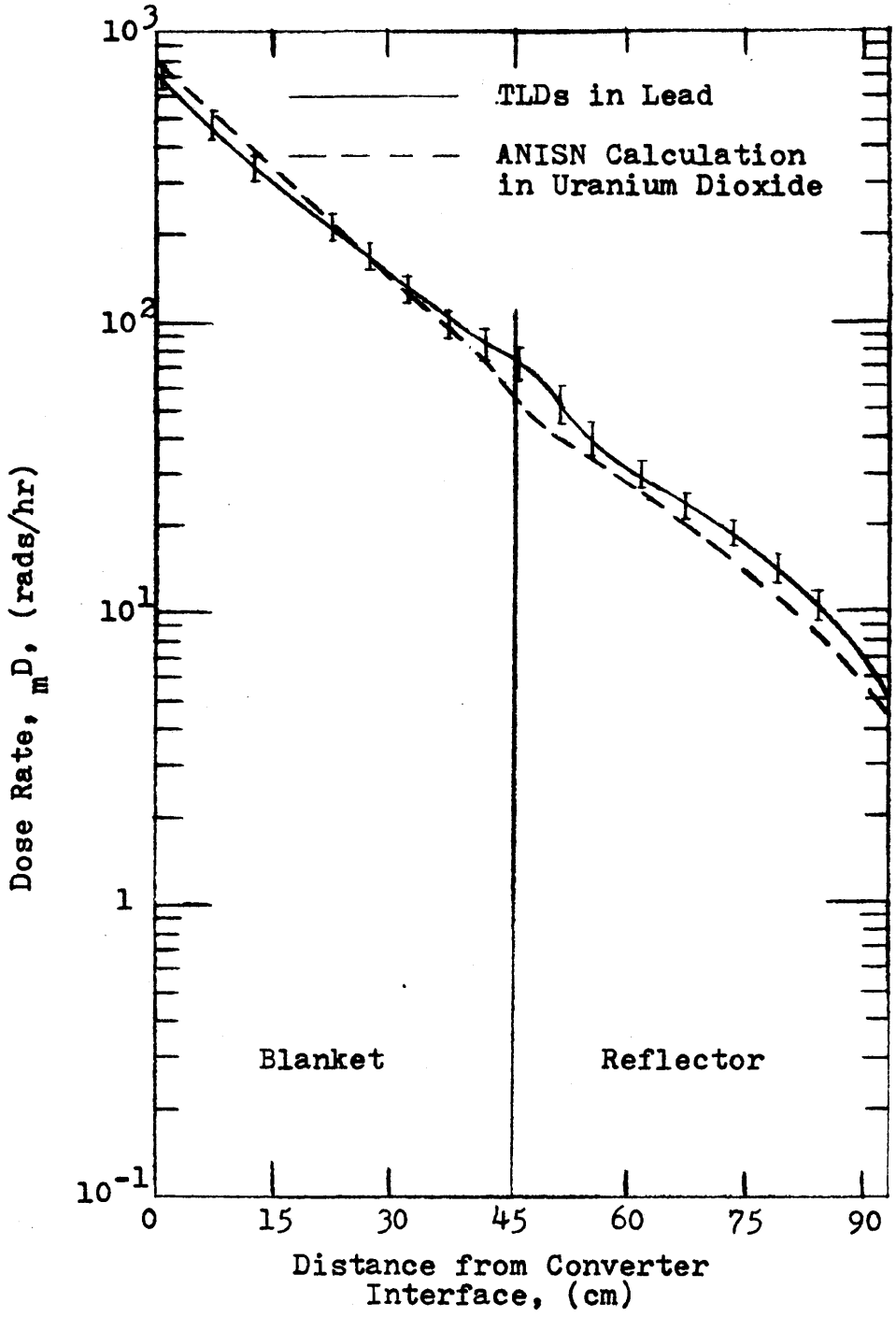

Fig. 4.5 Comparison of Absolute Dose Rate Traverses in Uranium Dioxide (lead)

Where Am = Arithmetic mean value of the N different individual repetitions, Ai

The reported error, ± (the "one-sigma" value - namely, the range about the reported value into which 68% of further repetitions would be expected to tall), is then obtained from

$$\sigma = t \times SDM \ , \qquad (4.2)$$

where t is Student's - Factor (M,2) which accounts for the fact that a small sample does not constitute a normal population. For example, t = 1.84 for a two-sample population and approaches 1.0 for a large number of samples.

This adjusted deviation has been found to range between 1.0 and 11.0% and the average for all capsules was 6.5% . The dose traverses all exhibit the same general pattern, ie. the calculations fall below TLD measurements. The size of this discrepancy appears to decrease as the atomic number of the material increases. The UO_2 (lead) comparisons exhibit the best agreement, which is very significant because UO_2 absorbs over 80% of the gamma energy deposited in the blanket, as was shown in Table 2.6. The sodium (aluminum) and stainless steel comparisons, on the other hand, suggest that additional calculational refinements are necessary for these materials.

Figure 4.6 presents a comparison of homogenized total dose rates. To obtain the data plotted, the values of the dose rates for the three major materials, fuel, coolant and structure were weighted by their corresponding concentrations (weight percent) in Blanket No. 4. These weighted doses were then added together to obtain the homogenized total dose rates throughout the blanket and reflector. The homogenized TLD data was prepared in the same manner, except that lead and aluminum dose rates were substituted for UO_2 and sodium.

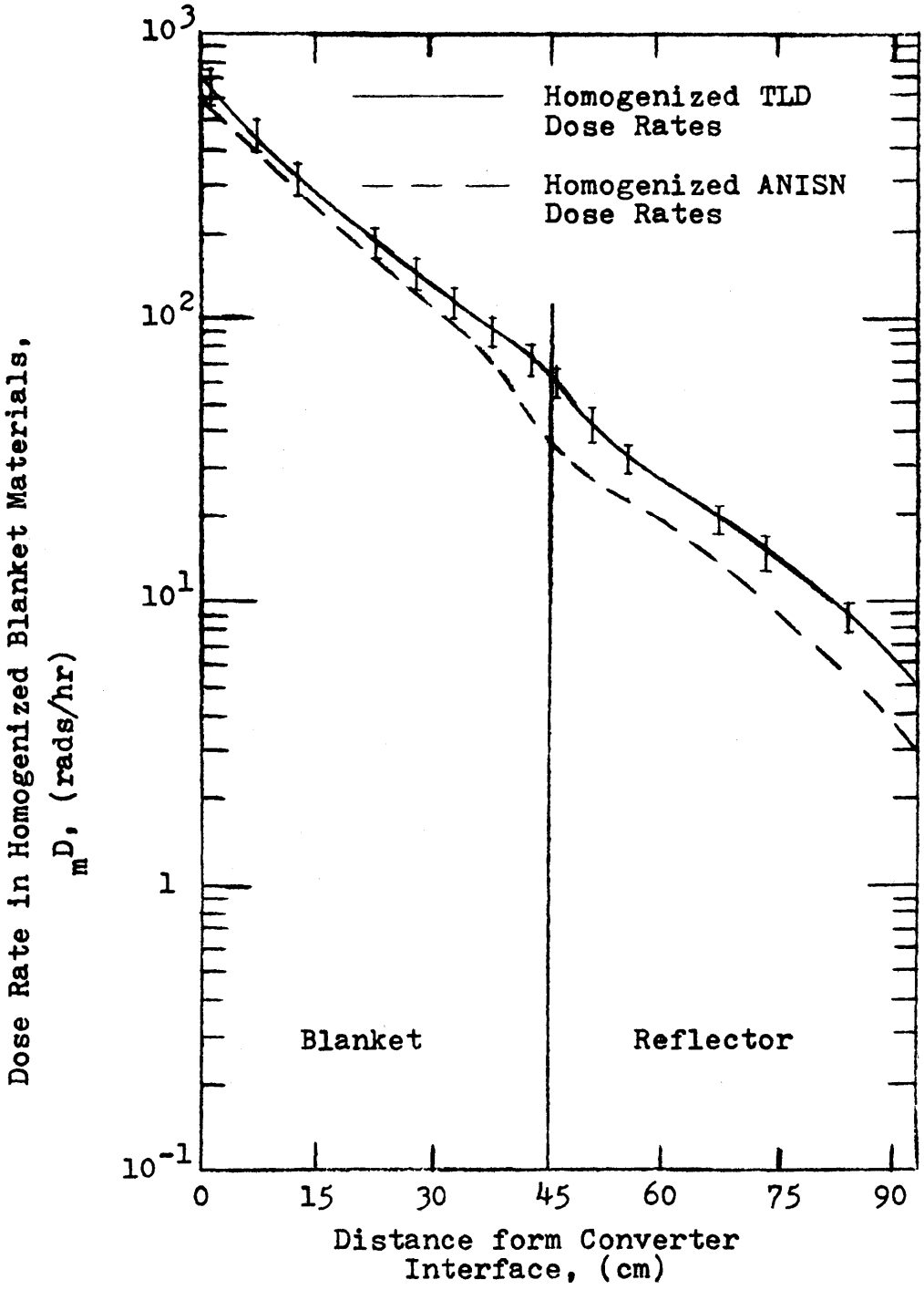

Fig. 4.6 Comparison of Homogenized Total Dose Rates

The comparison is in general good in the blanket region. The discrepancy in the reflector, however, ranges between 35 and 40%.

In all the figures, (Fig. 4.1 through 4.6) the measured TLD data has been corrected for the estimated effects of neutron irradiation on TLD's. The neutron correction was obtained by subtracting out of the TLD-measured dose rate the calculated dose rate due to neutrons (see discussion pertaining to Table 2.7). The uncorrected data and the corrections are both tabulated in Appendix C2.

Figure 4.7 presents a comparison of dose rate ratios (ie. spectral indices). At the bottom of the figure the measured aluminum to-stainless steel ratio is compared with the calculated sodium-to-stainless steel ratio. At the top of the figure the calculated UO_2-to-stainless steel ratio is compared with the measured lead-to-stainless steel ratio. The sodium-to-stainless steel comparison shows fairly good agreement. In the top two curves the shapes agree rather well, but the ANISN results for the UO_2 vs. stainless steel values are much higher than the measured data. This figure shows that there are significant discrepancies between the calculated and experimental results which need to be explained.

In addition to the dose rate traverses shown in Figs. 4.1 through 4.6, horizontal and vertical dose rate traverses were made with TLD's in stainless steel capsules to determine the transverse buckling characterizing gamma leakage. These results were obtained in the same manner as outlined in section 4.1. The results of these runs have already been presented in Figs. 2.13 and 2.14 of Chapter 2.

4.3.2 Spectrum Unfolding

The process of determining a multigroup gamma spectrum from a

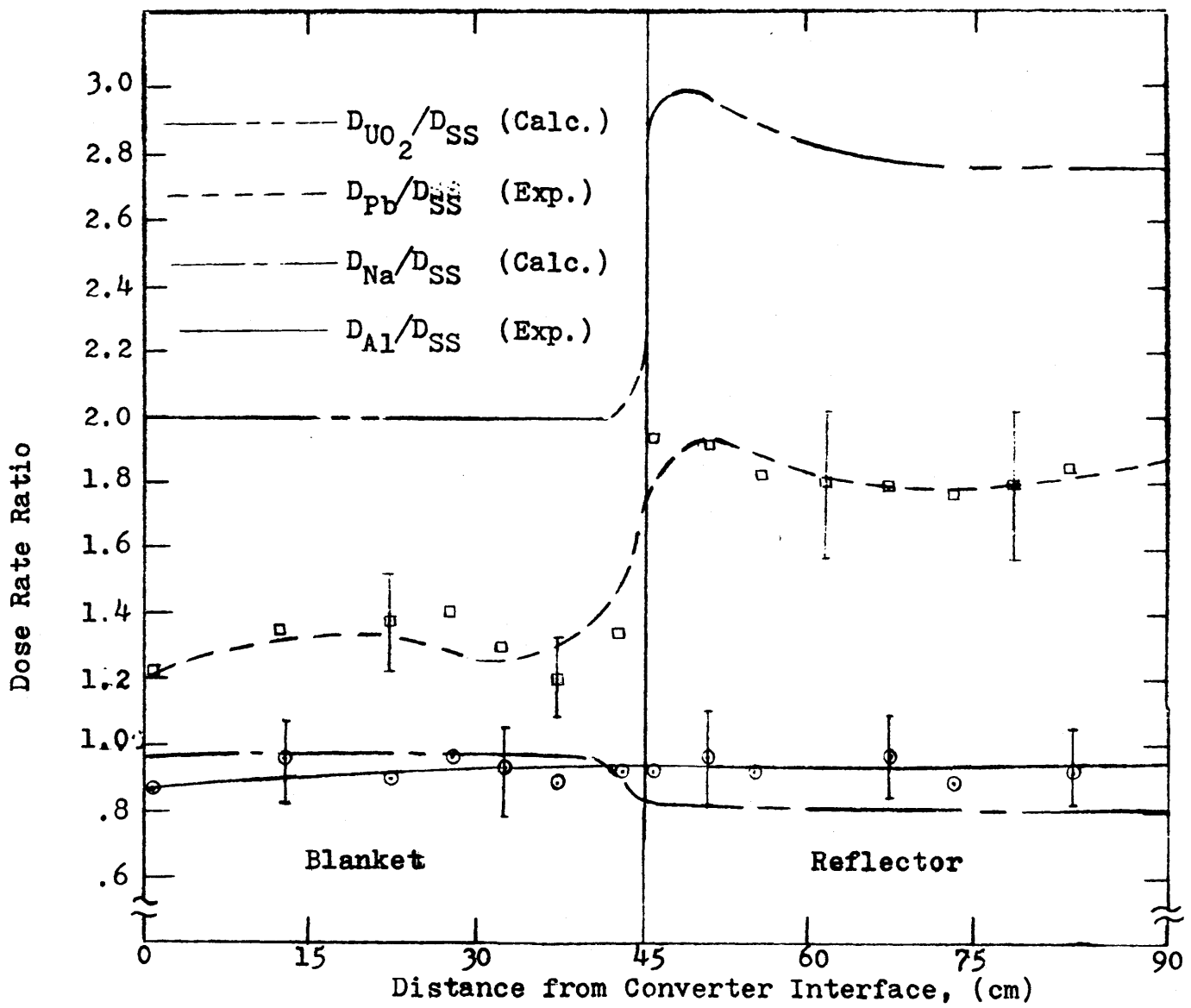

Fig. 4.7 Comparison of Dose Rate Ratios Relative to Stainless Steel

series of measured activities is called spectrum unfolding. In short, if the activities or heating rates of several materials and their appropriate multigroup cross sections are known, the gamma spectrum may be found in a manner entirely analogous to the familiar unfolding of neutron spectra from foil activation data. Such unfolding processes are performed at M.I.T. with the MITSPECTRA code, which is a simplified version of the RFSP code (F,1), which is inturn an improved version of the SPECTRA code (G,1).

To unfold the gamma spectrum at the midpoint of the Blanket Mock-up No. 4 the gamma heating rates in several materials were measured using TLD's. The capsule materials used were stainless steel, tin, zirconium, tungsten, and lead. In addition to the dose rates in these materials, the appropriate cross sections must also be input to MIT-SPECTRA. These cross sections were obtained from the GAMLEG 69 code, as mentioned in section 2.3.1. Cross sections were calculated in the same 18 group structure as used in the standard ANISN problem. This the gamma spectrum calculated from the activities can be compared against the ANISN transport results.

Capsules of stainless steel, tin, zirconium, tungsten, and lead were prepared with sleeve wall thicknesses in accordance with the specifications of Table 2.8. All irradiations were performed at the same time at the midplane of the central three test positions of the row of 18 test positions running across the width of the blanket. (See Fig. 2.3) In these positions the flux is quite uniform spatially, as can be seen in the dose traverse of Fig. 2.13. In addition the dose rates of Fig. 2.13 were used to normalize all values to the centermost test position. The raw TLD data was converted to dose rates using the TLD calibrations and appropriate spectral response factors.

The spectrum calculated by ANISN at the blanket midpoint is compared to the MITSPECTRA unfolding results in Table 4.1 and Fig. 4.8. The comparison is adequate: the calculated dose rates are within, or very close to, the experimental uncertainty, however, the difference in the individual group fluxes (up to 101.52%) is of some concern and indicates that additional work is required in this area.

4.3.4 Teflon Sleeve Experiment

In Chapter 2 cavity ionization theory and the development of ($1/R_D$) factors was dealt with at some length. Since these ($1/R_D$) factors play such an important role in determining dose rates, it is of direct interest to determine the accuracy of their calculation.

Before discussing the experiment, a few relations must be developed. With Eq. 2.53, and the definitions of RID and RED, the ratio of the dose in a TLD cavity in lead to that in teflon can be written as:

$$\frac{{}^{Pb}D_c}{{}^{Tef}D_c} = \frac{\left\{\int_0^\infty dE\ E\phi(E)\left(\frac{en\mu^z_{tot}}{\rho_z}\right)(RED + RID)\right\}_{Pb}}{\left\{\int_0^\infty dE\ E\phi(E)\left(\frac{en\mu^z_{tot}}{\rho_z}\right)(RED + RID)\right\}_{Tef}} \tag{4.1}$$

Since ^7LiF in teflon is a matched cavity, the expression for the dose in the cavity/TLD may be replaced by the dose in teflon, and Eq. 4.1 reduces to:

TABLE 4.1 Gamma Spectrum Unfolded at Blanket Midpoint

1. Gamma Spectrum

Gamma Group	E_{Max} (MeV)	MITSPECTRA	ANISN*	% DEV.
1	10.0	0.00131146	0.00101	+37.876
2	8.0	0.0128947	0.00640	+100.160
3	6.5	0.00678541	0.00463	+53.549
4	5.0	0.0210559	0.01218	+70.198
5	4.0	0.0869786	0.04171	+101.522
6	3.0	0.121072	0.06707	+70.838
7	2.5	0.171627	0.11238	+44.220
8	2.0	0.120574	0.10424	+10.252
9	1.66	0.0707146	0.06847	+4.242
10	1.33	0.103370	0.13662	-25.291
11	1.0	0.0737837	0.09804	-21.572
12	0.8	0.0613845	0.10531	-39.560
13	0.6	0.0441173	0.14949	-69.203
14	0.4	0.0479146	0.04861	+3.751
15	0.3	0.0373710	0.03201	+22.407
16	0.2	0.0175028	0.01091	+62.410
17	0.1	0.00146931	0.00085	+88.896
18	0.05	0.00007259	0.00006	+22.491
Total		1.0000	1.00000	

2. Capsule Dose Rates

TLD Sleeve Material	Experimental Dose Rates (rads/hr.)	Calculated Dose Rates (rads/hr.)	% Dev.
Fe	54.1	56.7	-4.82
Zr	56.9	59.5	-4.58
Sn	72.2	63.5	12.09
W	96.1	84.3	12.31
Pb	85.3	93.9	-10.11

*Calculated value used as initial guess to unfolding program

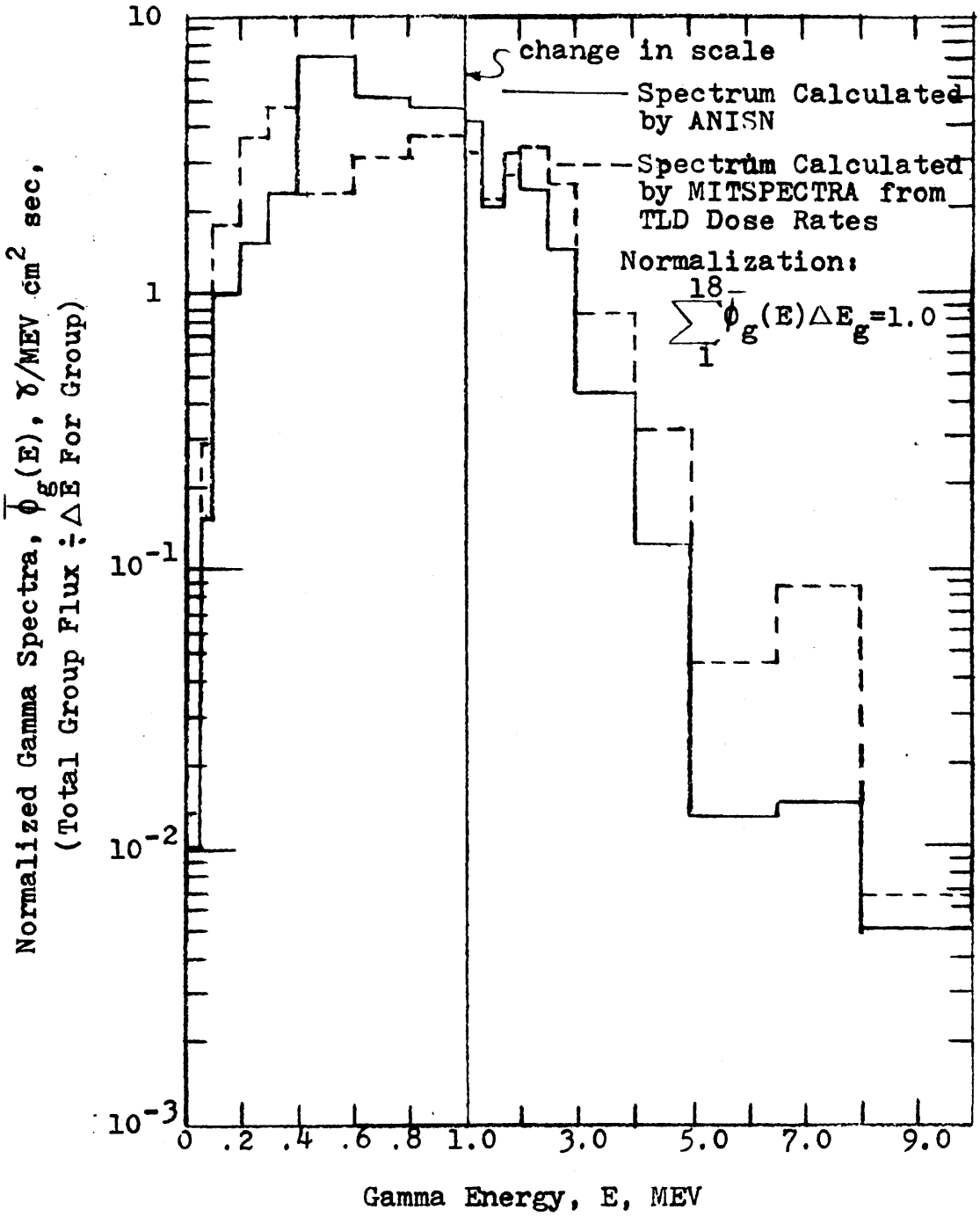

Fig. 4.8 Comparison of Spectra Calculated by ANISN and Unfolded by MITSPECTRA from Experimental Data

$$\frac{{}^{Pb}D_c}{{}^{Tef}D_c} = \frac{\left\{\int_0^\infty dE\ E\phi(E)\left(\frac{en\mu^z_{tot}}{\rho_z}\right)(RED + RID)\right\}_{Pb}}{\int_0^\infty dE\ \phi(E)\left(\frac{en\mu^{Tef}_{tot}}{\rho_{Tef}}\right)} \qquad (4.2)$$

The RESPOND program calculates the values in both numerator and denominator in the process of calculating R_D factors. Since teflon/LiF form a matched cavity, the calculated dose rate is thereby known with a much higher accuracy than the dose in an unmatched cavity. Also, teflon has a relatively low atomic number (8.57), and thus is not nearly as sensitive to the hard-to-calculate low energy p ortion of the spectrum as lead.

Thus Eq. 4.2 provides a basis for comparison. The ratio on the left can be obtained by irradiating two ^{7}LiF TLD capsules, one lead and one teflon, at the same location in the BTF blanket and finding the ratio of their responses. The quantity on the right can be obtained from the results of a RESPOND calculation. Since lead do ses are highly spectrally dependent this constitutes a very good test of how well RESPOND calculates these values.

The subject comparison was carried out for both lead and stainless steel sleeves. Table 4.2 shows the calculated and measured values and their difference.

TABLE 4.2 Comparison of ^{7}LiF Cavity Dose Ratios

Sleeve Material	Measured Ratio	Calculated Ratio	Percent Difference
Stainless Steel	0.970± 0.136	1.056	9%
Lead	1.333± 0.187	1.480	10%

The measured values in this table represent the ratio of the response from the TLD's in either stainless steel or lead to the TLD's in teflon, both are ±10%. Therefore the combined errors for the measured ratios is ±14%. The calculated values differ by 9% and 10% both of which are within the ±14% experimental uncertainty. On this basis the RESPOND results were concluded to be satisfactory.

4.4 CHAPTER SUMMARY

The experimental results presented in this chapter are fairly encouraging. The relative dose rate comparisons were very good throughout the blanket. In the reflector the ANISN calculation appears to underestimate the TLD measurements. To find if the measurement or the calculation was at fault, an independent experimental verification using ionization chambers was carried out, as discussed in the following chapter. The results of the spectrum unfolding work also appears to be encouraging in that a fairly good comparison was obtained between both ANISN and MISPECTRA spectra and capsule dose rate calculations. Finally the experimental verification of the response function values calculated by RESPOND indicates that accuracy within the experimental capability for verification can be expected. Further discussion of some of the points raised in this chapter will be presented in Chapter 6, where recommended future work is outlined.

Chapter 5

COMPARISON WITH OTHER GAMMA MEASUREMENT TECHNIQUES

In addition to the use of TLD's in the M.I.T. BlanketTest Facility, ionization chamber dosimeters (ICD's) and Radiophotoluminescent (RPL) dosimeters have been investigated. Dose traverses have been completed with the ICD's, but the RPL technique is still under development. In this chapter the techniques for using these devices, and the available results are discussed.

5.1 IONIZATION CHAMBER DOSIMETERS

The miniature ionization dosimeters which were used in the BTF blanket and reflector, operated as an integrating dosimeter. These dosimeters were initially charged to 300 volts and placed in the BTF. As gamma ray photons interact with the wall material, energetic electrons are liberated and move through the air in the chamber's cavity. The air in the cavity is then ionized along the path of the primary electrons. The secondary electrons are then attracted to the central anode and thereby reduce the charge on the dosimeter. Therefore the change in charge is proportional to the total number of electrons reaching the anode. As was discussed in Chapter 2, the total number of electrons is proportional to the gamma energy deposited in the wall material. Thus a properly designed ionization dosimeter behaves much as an "air" TLD in the cavity of a dosimeter capsule. Thus, through application of spectral response factors and accurate calibration, the change in charge can be converted into

a dose rate in the wall material of the ionization chamber.

Based on ionization chamber design principles described by Boag (B, 6), a set of ion chambers were designed and built. Figure 5.1 shows a sketch of one of these chambers. Unfortunately a dosimeter of this type cannot receive a very large total dose before it is completely discharged: approximately 30 rads for the design shown. The total dose which the dosimeter may receive increases as the gap between the internal electrode and wall decreases. Thus a small gap is desired. The gap in the present design is only 0.018 in(0.45 mm) and thus a good insulator is required at the ends of the dosimeter. Ceresin wax was found to adequately fill this requirement. End caps were also required to prevent ingress of dirt and dust, which otherwise causes enough leakage of charge to completely discharge the ICD in a matter of a few hours.

The ICD's were readout using an electrometer, which determined the voltage difference between the central anode and the chamber wall. The voltage was subtracted from the pre-irradiation value (300 volts) to obtain a change in voltage (ΔV), which is proportional to the energy deposited in the dosimeter.

These capsules were also calibrated with the same cobalt-60 source used for TLD capsule calibrations. During calibration the ICD's were each given a total dose of 0.877 rads during a 10 minute exposure in the outer ring of the aluminium calibration holder. To establish the calibration curve the following relation was used:

$$D_z = (1/R_D)_{cal} C(\Delta V/\Delta T) \text{ , rads/hr.} \qquad (5.1)$$

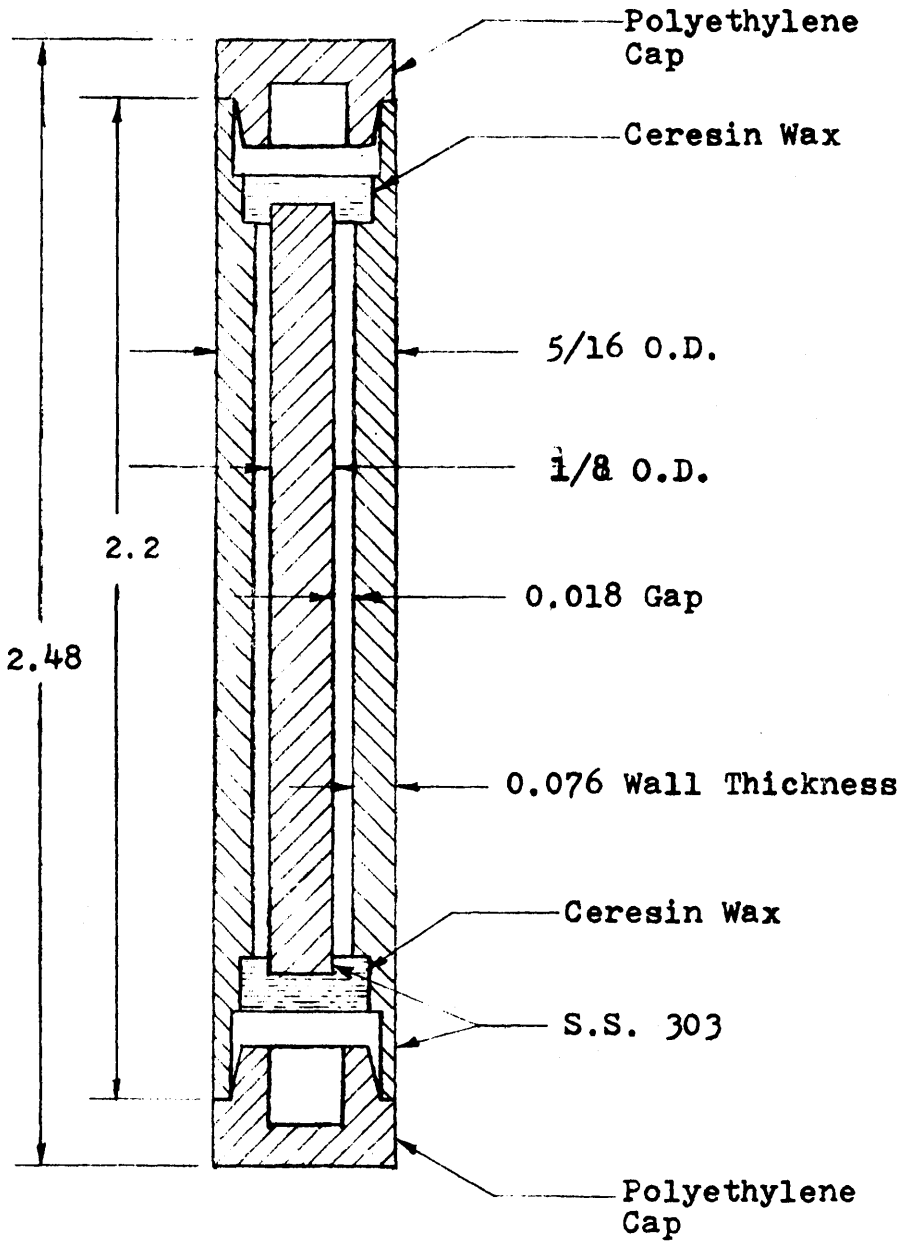

Fig. 5.1 Schematic of Ionization Chamber Dosimeter (All Dimensions in Inches)

where

D_z = Dose to stainless steel wall, RADs/Hr

R_D = Response Factor

C = Proportionality Constant Between the Chamber Change in Charge and Gamma Dose received (D_c), RADS/Volt

ΔV = Voltage change, volts

ΔT = Irradiation Time, Hours

This equation is completely analogous to the corresponding TLD equation (Eq. 2.65). The linearity of response implied in Eq. 5.1 was verified experimentally. Calibration was completed by performing a series of irradiations, each ten minutes in length, to determine ($\Delta V/\Delta T$) corresponding to D_z = 5.258 RADs per hour. The factor $(1/R_D)_{cal}$ was calculated using the RESPOND code. From these values the proportionality factor, C, was determined for each ICD. The product of C and $(1/R_D)_{cal}$ is the slope of the desired calibration curve. Equation 5.1 was then used to convert measured ($\Delta V/\Delta T$) values to a dose rate using the C, found from calibration.

Spectral response factors must also be applied to experimental data in the same manner as in TLD work. These factors again enter as the ratio $(1/R_D)_{exp}/(1/R_D)_{cal}$, and are derived in the same manner as was developed in Chapter 2. In the stainless steel ICD's these factors ranged between 1.01 and 1.05, and therefore had very little effect on the experimental data - much less than the experimental error ($\pm 1\sigma$) which ranged between 8 and 10 percent

Several duplicate dose traverses were performed with these dosimeters. As previously noted, the maximum dose which can be recorded by the ICD's before total discharge is approximately 30 rads. Therefore the M.I.T. reactor power had to be lowered to

perform an irradiation. Also, when the dose rates in the blanket were at an acceptable level the doses in the reflector were too low to be measured. Thus two runs were required to make a complete dose traverse.

The results of the dose traverse measured with ICD's is shown in Fig. 5.2 and compared to the results obtained with the TLD's. Both sets of data are absolute values. The agreement is very good. All discrepancies are within the limits of overlapping experimental error: no error bars are shown for the ICD traverse to avoid confusing the figure. However, the experimentally determined errors are near ±10% for all ICD's, about the same as for the TLD data.

A major point of interest is that the ICD should not be as neutron sensitive as a TLD. The air in the cavity is much less dense than a TLD, and therefore many fewer recoil atoms are produced. Also, the heavy recombination which occurs about the track of the recoil atom further mitigates against any significant effect upon the charge on the dosimeter. Therefore, the ICD should not be affected by neutrons. (The effect of protons recoiling from the wax insulators at the ends is not considered significant). This makes the comparison in Fig. 5.2 of significant value because it indicates that the neutron corrections applied to the TLD data yields values which are very close to the ICD data.

The comparison of the TLD and ICD data also indicates that the experimentally determined dose rates are indeed higher than the dose rates predicted by ANISN, as can be seen by referring back to Fig. 4.2.

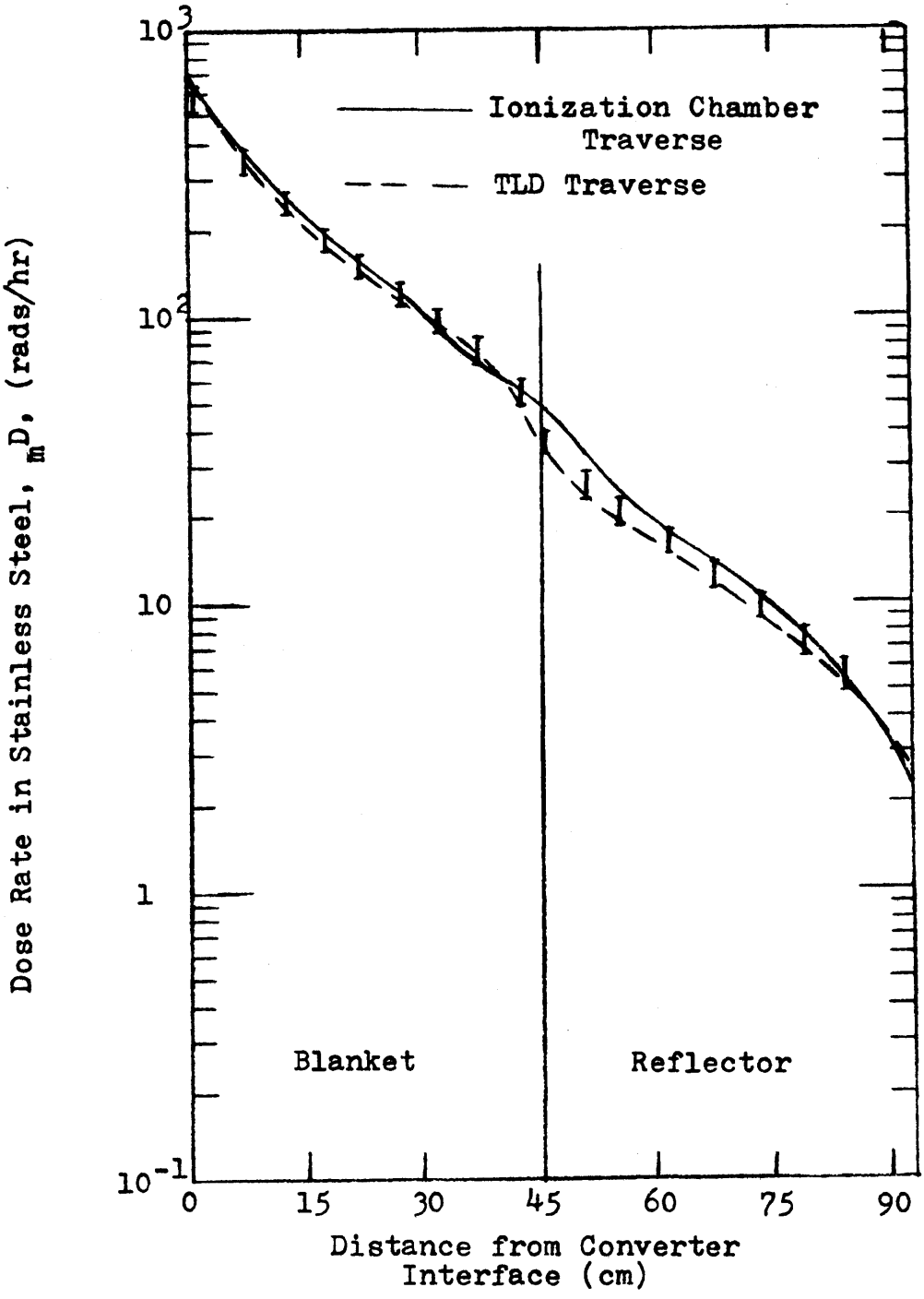

Fig. 5.2 Comparison of Absolute Dose Rates in Stainless Steel Measured with TLDs and Ionization Chamber Dosimeters.

5.2 RADIOPHOTOLUMINESCENT DOSIMETERS

A rather special variation of the technique of RPL dosimetry is currently being investigated at M.I.T. using ^{7}LiF for the RPL material, based on work by Regulla (R,2). Although the ICD results have adequately verified the TLD method, and conventional RPL glass methods have well-recognized drawbacks (e.g. neutron sensitivity) for the present application, the use of LiF RPL's offers the intriguing possibility of obtaining both TLD and RPL data from the same set of detectors.

In an RPL material exposed to gamma or X-radiation, "F" and "H" centers are formed in the same manner as was outlined in section 2.4.1. When these luminescent centers are exposed to light of the proper wave length, the electrons forming the "F" centers are excited to a higher energy level. As they de-excite, they emit light photons at a different wave length than that of the light causing the excitation. The key difference from thermoluminescence is that in a TLD the applied thermal energy raises the electron out of the "F" center and into the conduction band, whereas the excitation light of the RPL material only raises the electron to a higher energy level of the "F" center. In the TLD the electron falls into an electron hole and the "F" center is destroyed. In RPL material the electron returns to the "F" center and thus preserves the "F" center intact. RPL dosimeters therefore constitute a permanent record, with considerable resistance to fading under long term storage. In the present case this implies that one can readout the LiF RPL response first in a non-destructive manner, followed by the usual TLD readout. The light intensity which is emitted from an RPL material when exposed to the proper excitation light, is proportional to the number of "F" centers.

The total number of "F" centers is inturn proportional to the gamma energy deposition. Thus, in order to readout an RPL dosimeter, one need only to expose it to light of the proper wave length and then measure the emitted light with a photomultiplier tube.

A schematic of the readout device which is being assembled at M.I.T. is shown in Fig. 5.3. Excitation light is provided by the slide-projector light source. This light is passed through a blue filter which has a peak light transmission at 450 mm., the peak excitation spectrum and emission (RPL) spectrum are shown in Fig. 5.4. Thus only blue light reaches the RPL dosimeter, which is held in a glass holder. The mirrors in this chamber reflect the excitation (and emitted) light to help increase the signal intensity. Once the LiF "F" centers have been excited, the RPL emitted light, which has peaks near 520 and 630 mm., is given off. The blue-green filter permits transmission for all wavelengths above 500 nm. Thus the RPL-emitted light may reach the photo-tube, and all scattered excitation light will be filtered out. Once the RPL dosimeter is excited its luminescence will continue as long as the exciting light is present. This will then provide a constant current from the photo-tube, which can be monitored with the picoammeter. Since the output current from the photo-tube is proportional to the emitted light intensity, the current measured by the picoammeter is a measure of the gamma energy received by the RPL material. At the present time the proper light source, filtration scheme and associated electronics are still being developed. It is clear, however, that the signal to be measured is very weak, and that its measurement will require an increase in sophistication over the simple device sketched in Fig. 5.3.

Assuming that the capability for reading out ^{7}LiF as an RPL material can be achieved, an intercomparison of RPL and TLD dose

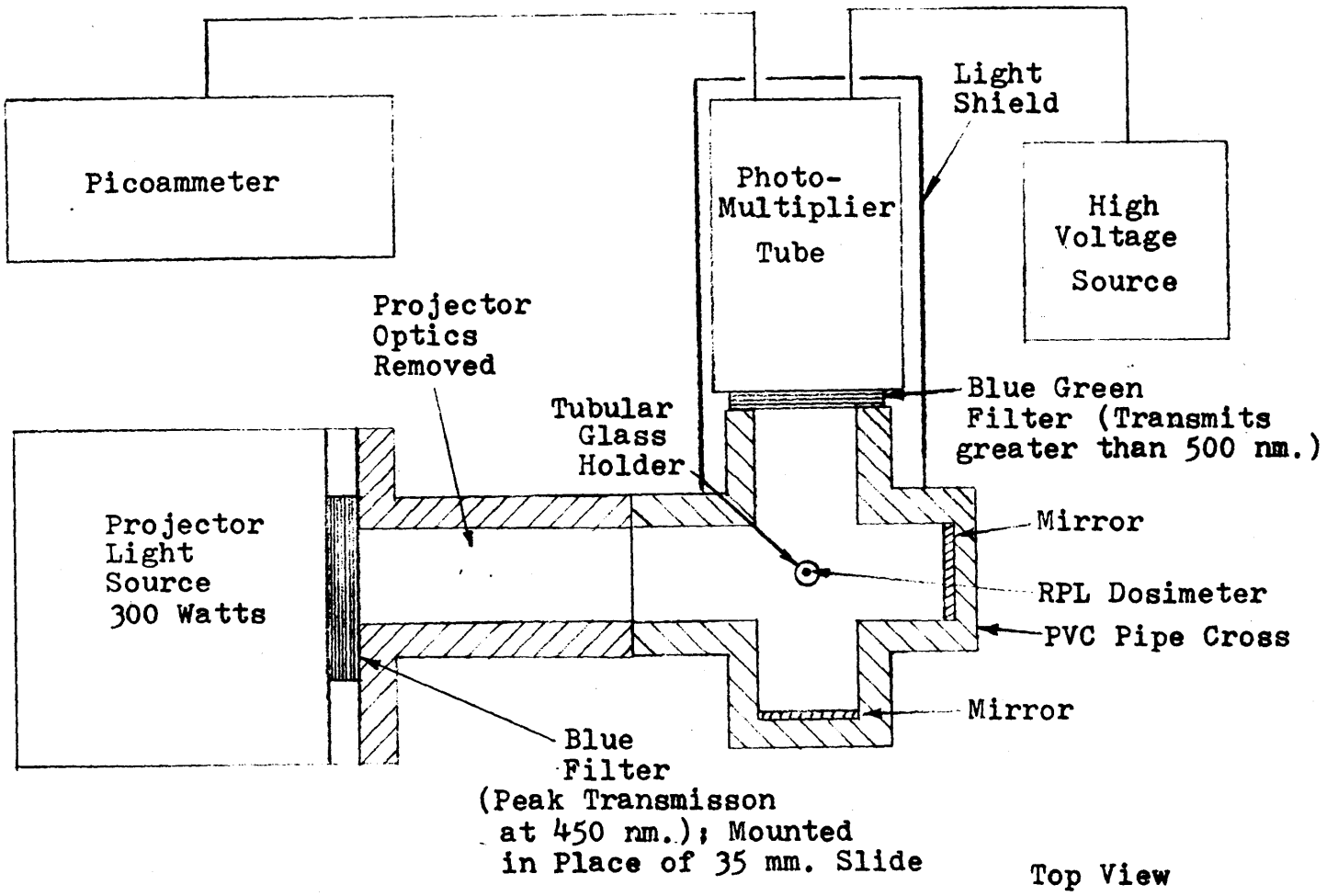

Fig. 5.3 Schematic of RPL Readout Device for ^{7}LiF Dosimeters

calibrations will be made to assess the compatibility of the projected dual use of LiF detectors.

On the basis of the work reported in this chapter it is concluded that TLD dosimetry is an acceptable approach to measurement of gamma heating in FBR blankets in that it gives data comparable to ICD measurements, a well understood approach of long-standing, but far less convenient to apply.

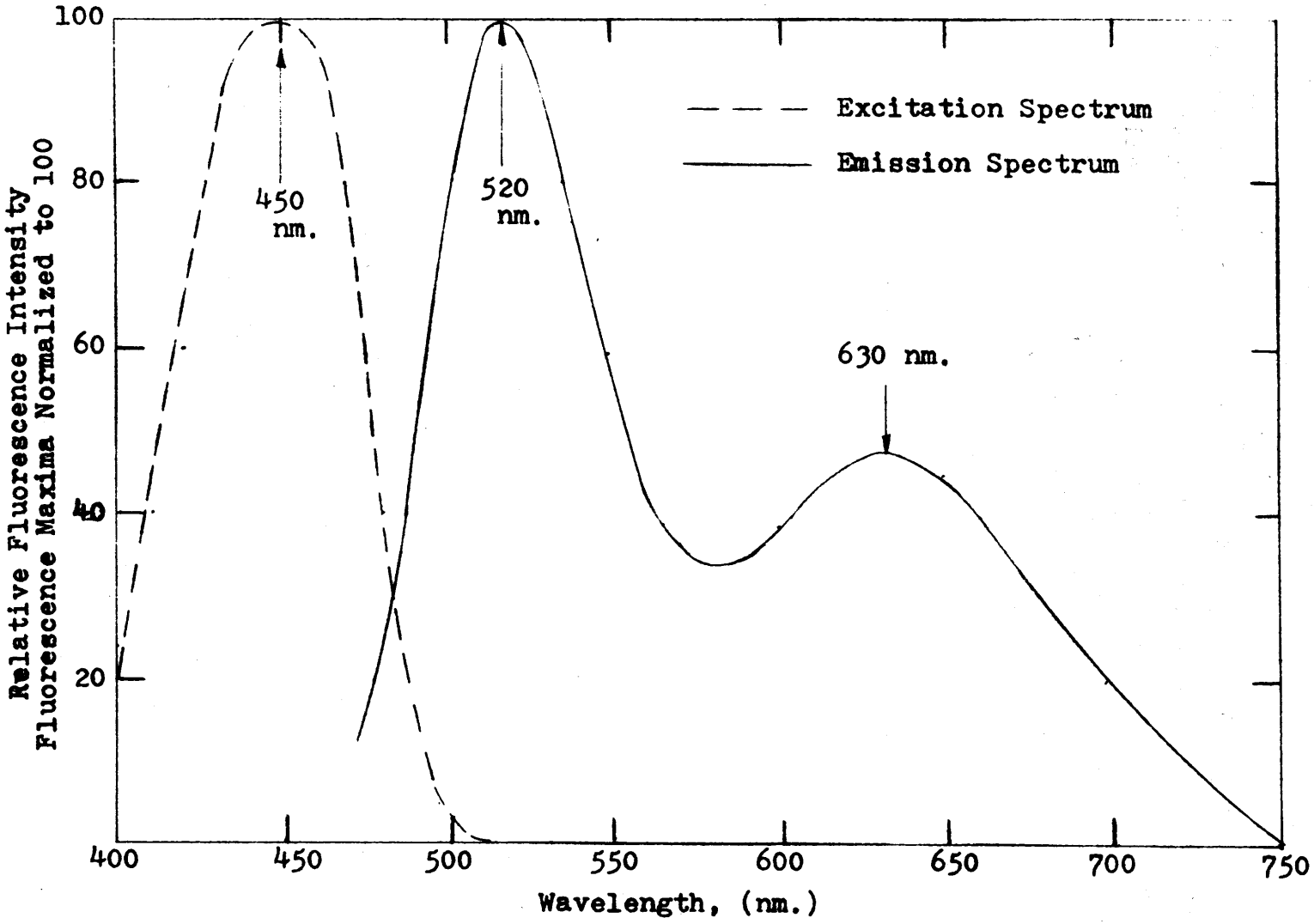

Fig. 5.4 Excitation and Emission Spectra of Radiophotoluminescence of LiF Crystals (From Ref. 1,2)

Chapter 6
SUMMARY AND CONCLUSIONS

6.1 INTRODUCTION

The work presented in this report deals with the measurement and calculation of gamma heating distributions in a fast reactor blanket mockup. Two types of dosimeters, thermoluminescent (TLD) and ionization chamber (ICD), were intercompared, and good agreement observed. A third method, employing ^{7}LiF as a radiophotoluminescent (RPL) dosimeter is currently under investigation. Dose traverses of the type under discussion are valuable as benchmark data against which current calculational techniques may be compared. In this work traverses were compared with dose rates calculated using the ANISN discrete ordinant transport code and a coupled neutron gamma cross section set. The results of these experiments and calculations are recapitulated in the following sections.

6.2 TLD APPLICATIONS TO BLANKET MEASUREMENTS

6.2.1 ^{7}LiF Performance

^{7}LiF thermoluminescent dosimeters were used to perform dose rate traverses in the blanket test facility. These solid state dosimeters trap primary and secondary electrons which are produced by gamma rays through the photoelectric effect, the compton effect, and pair production. When a crystal of this material is placed in a gamma absorbing medium it may be used as a Bragg-Gray gamma detector.

^{7}LiF TLD's were found to have several desirable qualities:

1. They are small and approximate a point detector.
2. They hold their response and do not fade significantly over long time periods.
3. They may absorb high doses (up to 10,000 rads), which are often encountered in reactor work.
4. The neutron response of ^{7}LiF appears to be small and ultimately amenable to mitigation through the use of calculated correction factors.
5. They are readily available in conveniently handled forms.
6. Adequate readout equipment is commercially available.

The only major drawbacks to the use of TLD's are the somewhat complicated corrections necessary to account for sheath and TLD energy response, the sensitivity of TLD response to annealing procedures, and the somewhat high standard deviation of the overall process. Since the average Z of ^{7}LiF is 8.21 and the Z values of reactor materials, particularly uranium dioxide (which has an average Z of 87.2) are so different, their gamma absorption characteristics will be quite different. Thus, significant spectral corrections are required when measuring gamma heating in heavy reactor materials. For UO_2 these factors were found to range between 1.2 in the blanket to 1.5 in the reflector, the difference being due to changes in the gamma spectrum. These corrections can be calculated sufficiently well with the computer code RESPON D (modified as described in section 2.5.3).

Although ^{7}LiF TLD response is fairly sensitive to such things as annealing procedures and handling between use, practical handling and annealing procedures have been evolved to minimize the effect

of human factors on the results.

The dose rates obtained in Blanket Mockup No. 4 at M.I.T. were found to be reproducible with an experimental precision (± one sigma) of 8%. On this basis, and in view of the advantages, listed above, ^{7}LiF is concluded to be an acceptable TLD material for use in reactor applications.

6.2.2 Energy Response

Due to the sensitivity of the response of dosimeter capsules composed of ^{7}LiF TLD's sheathed in heavy materials to the shape of the ambient gamma energy spectra, a significant portion of this study has been devoted to the determination of accurate spectral response factors. Cavity ionization theory has been applied to ^{7}LiF TLD capsules to permit the use of line spectrum (Co-60) calibration facility doses to convert TLD response measured after irradiation in a blanket mock-up into a dose in the TLD's sheath material.

The computer program RESPOND was used to calculate the spectral response factors derived in Chapter 2. The differences between the equations employed here and those in Tuttle's (T, 3) original version of RESPOND are presented. The calculated ratios of sleeve dose to cavity /TLD dose have been compared to the original version and some significant differences observed. For example, for ^{7}LiF TLD's in lead Tuttle's version predicts a "Burlin's Factor" of 0.7268 for the ZPR-6-6 gamma spectrum, while the modified version predicts 0.6096. For monoenergetic gammas sources (Co-60) the difference is generally between 2 and 6 percent. To confirm the accuracy of the modified RESPOND calculation a teflon sleeve experiment was conducted. In this experiment, the ratio of the dose in an

^{7}LiF TLD surrounded by a high Z material to the dose in one encapsulated in teflon was both calculated and measured. This comparison was made for both stainless steel and lead sleeves. The calculated/measured ratios for the stainless steel sleeves differed by 9 percent, and for lead by 10 percent. These deviations are within the experimental accuracy of the TLD measurements. On this basis the modified version of RESPOND was considered acceptable.

6.2.3 Neutron Effects

The presence of a fast neutron spectrum causes recoiling heavy ions to be produced in a TLD crystal when it is placed in a fast reactor blanket mockup. However, since these recoiling nuclei are heavily ionizing, a large amount of recombination occurs along their track, which reduces the sensitivity of a TLD to these heavy ion recoils. In section 2.6 the response of the TLD's to neutrons was calculated. For stainless steel and aluminum this dose constituted 10% of the gamma-induced response at the front of the blanket, decreasing to 2% deeper into the blanket and reflector. In the lead encased TLD, the neutron effects are only 4.5% of the total induced gamma dose and decrease to less than one percent deeper into the blanket and reflector. For all three sleeve materials (aluminum, stainless steel, and lead) the neutron effect is within the experimental accuracy of state-of-the-art TLD methodology, and thus was not considered a major source of error in experimental dose rate determination.

The estimate of neutron response was based on experimental results presented by Wingate et. al (W, 1). At present this response function is not well known. Therefore, additional work is required to further establish an accurate knowledge of the neutron response of ^{7}LiF TLD's.

6.3 BLANKET MOCKUP NO. 4

6.3.1 Comparison With Cylindrical Reactor

If the measurements obtained in the M.I.T. Blanket Test Facility are going to provide benchmark data relevant to the U.S. fast breeder reactor program, it must be shown that the Blanket Test Facility's gamma-related characteristics are in good agreement with those of a fast reactor. In this study a comparison was performed using ANISN, in which both the Blanket Test Facility and a cylindrical fast reactor were modeled. These ANISN calculations were performed with an S_8 discrete ordinant approximation. Comparison of P_0, P_1 and P_3 calculations showed that P_1 order-of-scattering was adequate for gamma heating predictions. All calculations were performed using a 40 group coupled neutron (22 group) and gamma (18 group) cross section set (M, 1). Total gamma flux distributions, gamma spectra, U-238 capture rates, and the ratio of total gamma to neutron fluxes were compared throughout the facility. These comparisons all showed excellent agreement. It was thus concluded that Blanket Mockup No. 4 provides a good simulation of the photonic behavior of an LMFBR blanket.

A sensitivity study was also conducted to determine the effect, if any, of transverse leakage on spectra or flux distributions. Stainless steel TLD dosimeters were used to make vertical and horizontal dose traverses in the blanket to determine the effective extrapolated height and width of the facility by fitting the data to the theoretical cosine distributions. These values are used in ANISN to characterize the transverse leakage using a buckling type formulation. ANISN results using the measured height and width values were compared against results for a semi-infinite slab (infinite height and width). No

significant differences were obtained. Therefore transverse leakage was shown not to affect gamma heating traverses in the present application. This result is similar to that found previously for assembly neutronics.

6.3.2 Comparison of Experiments and Calculations

Calculations were compared to TLD measurements in two categories: dose traverses and gamma spectra. Gamma dose rate traverses were measured in aluminum, stainless steel, and lead. Aluminum was shown to have gamma absorption characteristics similar to sodium, and lead was shown to be similar to UO_2. Thus the measured gamma dose rates were compared to calculated dose rates in sodium, stainless steel and UO_2. The relative dose rate comparisons showed good agreement for all materials in the blanket region. However, in the reflector the experimental data for aluminum (sodium) exceeded calculated results by 45%; for stainless steel TLD data was 40% higher than the ANISN calculation. The lead (UO_2) comparison showed very good agreement throughout the entire facility.

The dose traverses were also compared on an absolute basis. Here the errors became larger for both aluminum (sodium) and stainless steel; 80% for aluminum and 60% for stainless steel. However, the absolute lead (UO_2) results compared quite well. These results show an overall pattern, in that the errors became larger as the atomic numbers of the materials decreased. In view of these discrepancies, other experimental methods employing ionization chamber dosimeters and radiophotoluminescent dosimeters were investigated as a means for obtaining independent verification.

A gamma spectrum unfolded from gamma dose rates measured with TLD's sheathed in stainless steel, tin, zirconium, tungsten, and

lead resulted in fair agreement with the spectrum calculated by ANISN. However, the discrepancies in several groups, particularly the above 3 MEV, are large enough to be of concern (as much as 101.5%).

6.3.3 Comparison With Ionization Chamber Dosimeters

The dose traverses made with stainless steel ionization chamber dosimeters are of particular value because they are demonstrably small-cavity devices, and are considered not to be greatly affected by neutrons. They therefore, provide a good standard, based on a totally different principle of operation, against which steel-sheathed ^{7}LiF TLD's may be compared. This comparison was found to be quite good, with discrepancies never being larger than the experimental uncertainty of the TLD or the ICD measurements. The two experiments were performed independently, and as such they verify each other; since both predict heating rates which are greater than the ANISN calculations it would appear that these calculations are in error.

6.4 TLD APPLICATIONS IN LMFBR BLANKETS: CONCLUSIONS

In the gamma heating work conducted at M.I.T., the ^{7}LiF TLD capsules have been found to be quite suitable for providing good benchmark data which is reproducible within ± 8 percent. The dose traverses consistently show, however, that the experimental data are higher than coupled neutron-gamma transport calculations. Discrepancies are particularly evident in the blanket's reflector region. Calculations have also been made to compare the BTF mock-ups at M.I.T. to the blanket and reflector regions of an actual cylindrical LMFBR, both neutronically (prior work L,1) and photonically (present work) and good agreement has been obtained. There-

fore, on this basis, higher-than-predicted gamma heating rates are also to be expected in the blanket and reflector regions of actual LMFBR reactors. The experimental TLD results are confirmed by ionization chamber dosimeter results. From all of this evidence it is concluded that it is primarily the calculational methods which require further investigation and refinement. The large discrepancy between certain measured and calculated "spectral index" traverses (ratios of dose rates) is one of the areas requiring follow-up.

6.5 RECOMMENDATIONS FOR FUTURE WORK

There are several areas in which additional work should be performed involving improvements in experimental methodology, calculational methods, and gamma spectrum determination.

The experimental reproducibility achieved in this work was on the order of ±10% for several dosimeter capsules. This can be seen in Appendix C.2. This can probably be reduced. The TLD's used in this work were ordinary Harshaw TLD-700 extruded dosimeters (1mm. diam. x 6mm. long). "High-sensitivity" TLD's from Harshaw Chemical Company are available having standard deviations which are typcially 2.0 to 4.0% at 10 roentgens exposure. These TLD's should considerably reduce the large variations often obtained using the present dosimeters. Once can also presumbaly reduce the SDM by using only TLD's which exhibit the smallest stardard deviations during repetitive calibrations. For example, if we had selected the best one-third of our TLD library and discarded the rest, the SDM observed

during calibration would have been reduced from ± 10% to ± 7% for the worst capsule and from 5.5% to 4.4% for the entire library.

Several techniques should be investigated to help improve calculational methods. Cross sections are a likely source of error, and therefore other coupled cross section sets should be tried, or new improved sets developed. Since most of the gammas are produced locally, neutron capture calculations also have to be improved: the comparison of measured and calculated neutron rates in blanket mockups reported by Leung (L, 1) and others, are in no better agreement than reported here. Therefore the fault may well lie in nuetronic calculations rather than in the photonics.

The major discrepancies observed in the present work occurred in the blanket's reflector. In the calculation unshielded iron cross sections were used. Use of a self-shielded iron cross section set should therefore be investigated.

One area of uncertainty in the present work is the effect of the boundary condition at the rear of the reflector used as imput to the ANISN calculation. In much of the prior ANISN calculations at M.I.T. a "black" or total-absorption boundary condition was used based upon measurements which showed that this was appropriate for neutronics calculations. However, several calculations were made with a steel reflector which was thicker than the actual BTF reflector. (To simulate backscatter from the shield doors). This provided much better agreement with the gamma heating measurements in the outer half of the reflector. Therefore better boundary conditions should be explored. This could include input of group albedos to ANISN or adding an additional zone to the

calculation to include the effects of the concrete shielding at the rear of the BTF.

The effect of bremsstrahlung should also be investigated. In the reflector region of the BTF approximately 10% of the gamma spectrum is contained in the region between 5 and 10 MEV. These gammas can give rise to a large number of energetic electrons which, due to reradiation can alter the gamma spectrum as they decelerate. Therefore, this effect should be investigated.

A gamma spectrum is required for input to RESPOND in order to calculate spectral response factors. All gamma spectra used in the present work were obtained from ANISN calculations. However, the gamma spectrum unfolding work showed some large discrepancies. Therefore, the unfolding technique should be improved to determine gamma spectra more accurately. Once perfected, the unfolding technique should be extended to the reflector region. The use of more sleeve materials, higher precision TLD's and a larger number of repetitive runs is recommended. If the calculated gamma spectra can be corrected in this manner, better spectral response factors may in turn be calculated.

In conclusion, the present work indicates that total gamma heating rates can be calculated to within about 8% in the blanket and 40% in the reflector regions of LMFBR's. Work is continuing at M.I.T. in several areas: a closer investigation of calculational methods in particular; additional experimental measurements, including work during FY 1975 on Blanket Mockup

No. 5, which will have a better reflector region design than Mockup No. 4; and continued work on methods development including spectrum unfolding, and a general effort to increase precision all-around.

Appendix A Nomenclature (In order of appearance)

D_j = dose rate, material j, rads/hr.

ϕ_g = group flux, photons/cm^2 sec.

$(\sigma_j E)_g$ = group absorption cross section, calories barns/atom (or molecule)

ρ_j = density, material j, gm./cm^3

N_j = density, material j, atoms/cm^3

$\phi_g(E)$ = average differential gamma flux in group g, photons/MEV cm^2 sec.

ΔE_g = width of energy group g, MEV

W = extrapolated width of blanket, cm

H = extrapolated height of blanket, cm.

B = buckling, $in.^{-1}$

$\phi(E)$ = differential gamma spectrum, photons/MEV cm^2 sec

K = kerma rate, ergs/gm. sec

$en\mu_{tot}$ = total energy absorption coefficient, cm^{-1}

$\frac{en\mu_{tot}}{\rho}$ = total mass energy absorption coefficient, cm^2/gm.

$\left|\frac{dT}{dx}\right|$ = stopping power, MEV/cm.

x_1 = point of electron birth

x_2 = point of electron departure from unit volume

dl	=	differential element of electron range, cm.
$n(T_o)\, dT_o$	=	number of electrons born about T_o (per unit volume per unit time), electrons/cm^3 sec
R	=	total energy deposition rate, ergs/gm. sec.
$I(T_o, T)$	=	electron spectrum, electrons/MEV cm^2 sec.
T	=	electron energy, MEV
T_o	=	initial electron energy, MEV
v	=	velocity of electron, cm/sec.
c	=	subscript denoting cavity/TLD
z	=	subscript denoting medium/sleeve
$N(T_o T)dT$	=	number of electrons born at T_o which appear in dT about T per unit time, electrons/sec
$Q(E, T_o)$	=	initial number of electrons produced per unit absorbed energy, electrons/MEV
E	=	energy of gamma photon, MEV
E_{avail}	=	available gamma energy
D	=	energy deposition rate density, MEV/cm^3 sec.
m^D	=	mass energy deposition rate, MEV/gm sec.
$(1/_m\bar{S})$	=	Burlin "S" factor, averaged over electron slowing down spectrum
$(1/_m\bar{\bar{S}})$	=	Burlin "S" factor, averaged over initial electron spectrum.

$A(E, T_o)$	=	Burlin's initial electron spectrum
Z	=	atomic number
$\overline{Z}$	=	average atomic number
A	=	mass number
$\overline{A}$	=	average mass number
B	=	relativistic velocity
I	=	geometric mean ionization potential, MEV/electrons
r_o	=	electron radius, cm.
W_i	=	weight fraction, material i
$\psi(E, T_o)$	=	spectral shape function
CE	=	subscript denoting the compton effect
PP	=	subscript denoting pair production
PE	=	subscript denoting the photoelectric effect
$N_\alpha(E, T)$	=	shape function for scattered electrons, cm^2/MEV electron
m_o	=	electron rest mass, gms
h	=	Planck's constant, 6.625×10^{-27} erg-sec
$\hbar$	=	Planck's constant divided by 2π
ν_o	=	frequency of gamma radiation, sec^{-1}
l	=	mean chord length, cm
V	=	volume of cavity, cm^2
S	=	Surface area of cavity, cm^2
β	=	Attenuation coefficient, cm^{-1}

R	=	electron range, cm
d(E)	=	Burlin's weighting factor, unitless
RED	=	relative external dose, MEV/gm.sec
R/D	=	relative internal dose, MEV/gm. sec.
$(1/R_D)$	=	ratio of dose in cavity/TLD to dose in medium/ sleeve
a_i	=	atom fraction, material i
D(r)	=	dose rate, rads/hr.
E_i	=	energy of ith gamma emitted from source, MEV
N	=	number of source gammas per disintegration
r	=	distance from source, cm
S	=	source strength, photons/sec
S'	=	ring source strength, photons/cm
u_c	=	compton effect energy absorption coefficient, cm^{-1}
t	=	thickness of ring, cm.
a	=	radius of ring, cm.
f	=	distance from source to ring, cm.
D_c	=	dose in cavity/TLD, MEV/gm. sec
ΔV	=	change in voltage, volts
ΔT	=	change in time, sec

Appendix B Gamma Cross Sections

Gamma mass energy absorption cross sections are required for input to RESPOND for both the cavity and sleeve material. These were obtained from the document "Photon Cross Sections from 0.001 to 100 MEV for Elements/Through 100", LA-3753 (1967). This listing includes mass energy coefficients for the photoelectric effect, the compton effect, and pair production.

ANISN also required input of multigroup gamma heating cross sections. These were supplied by the GAMLEG 69 (R, 3) program and are listed in Table B.1.

B. 1 Gamma Cross Sections for Multigroup Heating Rates

The cross sections in this Table were developed by the Computer Program GAMLEG 69 (R, 3) in a suitable group structure for gamma heating calculations performed using ANISN (E, 1).

$E\sigma_a$, Calory barns/atom(or molecule)

E_{max} (MEV)	Group	Na	Fe
10.0	23	0.2174 (-12)	0.7443 (-12)
8.0	24	0.1783 (-12)	0.5743 (-12)
6.5	25	0.1459 (-12)	0.4384 (-12)
5.0	26	0.1197 (-12)	0.3345 (-12)
4.0	27	0.9896(-13)	0.2596 (-12)
3.0	28	0.8311 (-13)	0.2081 (-12)
2.5	29	0.7201 (-13)	0.1758 (-12)
2.0	30	0.6210 (-13)	0.1492 (-12)
1.65	31	0.5354 (-13)	0.1278 (-12)
1.33	32	0.4423 (-13)	0.1057 (-12)
1.0	33	0.3584 (-13)	0.8614 (-13)
0.8	34	0.2872 (-13)	0.6988 (-13)
0.6	35	0.2082 (-13)	0.5255 (-13)
0.4	36	0.1439 (-13)	0.3989 (-13)
0.3	37	0.9899 (-14)	0.3438 (-13)
0.2	38	0.5742 (-14)	0.4650 (-13)
0.1	39	0.5302 (-14)	0.1512 (-12)
0.05	40	0.4038 (-13)	0.1383 (-11)

Table B.1 Gamma Cross Sections for Multigroup Heating Rates (Continued)

		$E\sigma_g$, Calories -barns/atom(or molecule)	
E_{max}(MEV)	Group	UO_2	Al.
10.0	23	0.5949 (-11)	0.2718 (-12)
8.0	24	0.4384 (-11)	0.2216 (-12)
6.5	25	0.3174 (-11)	0.1794 (-12)
5.0	26	0.2275 (-11)	0.1453 (-12)
4.0	27	0.1655 (-11)	0.1188 (-12)
3.0	28	0.1258 (-11)	0.9893 (-13)
2.5	29	0.1041 (-11)	0.8538 (-13)
2.0	30	0.8954 (-12)	0.7348 (-13)
1.66	31	0.8141 (-12)	0.6330 (-13)
1.33	32	0.7803 (-12)	0.5229 (-13)
1.0	33	0.8039(-12)	0.4238 (-13)
0.8	34	0.8921 (-12)	0.3397 (-13)
0.6	35	0.1138 (-11)	0.2467 (-13)
0.4	36	0.1619 (-11)	0.1711 (-13)
0.3	37	0.2508 (-11)	0.1192 (-13)
0.2	38	0.4736(-11)	0.7499 (-14)
0.1	39	0.4892 (-11)	0.9141 (-14)
0.05	40	0.1747 (-10)	0.8368 (-13)

B.1 Gamma Cross Sections for Multigroup Heating Rates (Continued)

		$E\sigma_a$ Calories - Barns/atom (or molecule)	
E_{max} (MEV)	Group	Sn	Zr
10.0	23	0.2124 (-11)	0.1470 (-11)
8.0	24	0.1573 (-11)	0.1100 (-11)
6.5	25	0.1138 (-11)	0.8086 (-11)
5.0	26	0.8142 (-12)	0.5914 (-12)
4.0	27	0.5922 (-12)	0.4406 (-12)
3.0	28	0.4497 (-12)	0.3414 (-12)
2.5	29	0.3684 (-12)	0.2827 (-12)
2.0	30	0.3076 (-12)	0.2371 (-12)
1.66	31	0.2638 (-12)	0.2026 (-12)
1.33	32	0.2238 (-12)	0.1692 (-12)
1.0	33	0.1927 (-12)	0.1414 (-12)
0.8	34	0.1715 (-12)	0.1199 (-12)
0.6	35	0.1621 (-12)	0.1011 (-12)
0.4	36	0.1836 (-12)	0.9628 (-13)
0.3	37	0.2607 (-12)	0.1156 (-12)
0.2	38	0.6145 (-12)	0.2484 (-12)
0.1	39	0.2054 (-11)	0.9328 (-12)
0.05	40	0.5111 (-11)	0.4108 (-11)

B. 1 Gamma Cross Sections for Multigroup Heating Rates (Continued)

		$E\sigma_a$ Calories - Barns/atom(or molecule)	
E_{max} (MEV)	Group	W	Pb
10.0	23	0.3969 (-11)	0.4691 (-11)
8.0	24	0.2902 (-11)	03.428 (-11)
6.5	25	0.2076 (-11)	0.2454 (-11)
5.0	26	0.1467 (-11)	0.1734 (-11)
4.0	27	0.1051 (-11)	0.1242 (-11)
3.0	28	0.7865 (-12)	0.9299 (-12)
2.5	29	0.6404 (-12)	0.7602 (-12)
2.0	30	0.5382 (-12)	0.6448 (-12)
1.66	31	0.4742 (-12)	0.5777 (-12)
1.33	32	0.4314 (-12)	0.5424 (-12)
1.0	33	0.4131 (-12)	0.5433 (-12)
0.8	34	0.4232 (-12)	0.5852 (-12)
0.6	35	0.5056 (-12)	0.7328 (-12)
0.4	36	0.7165 (-12)	0.1056 (-11)
0.3	37	0.1160 (-11)	0.1722 (-11)
0.2	38	0.2820 (-11)	0.4078 (-11)
0.1	39	0.5202 (-11)	0.4439 (-11)
0.05	40	0.1136 (-10)	0.1398 (-10)

Appendix C Intermediate Data

This appendix presents intermediate and raw data for the experiments and analyses presented in this report. Section C.1 presents TLD raw data from calibration runs. C.2 presents the TLD dose traverse data. C.2 also presents other data, which includes intermediate dose rate calculations, dose rate measurements, both uncorrected and corrected for neutron response The ionization chamber calibration and dose traverse data is also presented. C.3 presents a table of TLD capsule standard deviations.

C.1 Calibration Data

Table C.1.1 Constant-Dose Irradiation Data

The data presented here are the results of the four constant-dose irradiations. The capsule averaged standard deviation (from the mean of the 4 runs) is shown at the right.

Capsule No.	TLD No.	Response (nc) Run 1	Run 2	Run 3	Run 4	($\pm 1\sigma$)
	1	506.7	569.0	629.9	650.5	
1	2	468.0	603.8	512.4	528.6	±9.3%
	3	529.8	664.8	630.5	677.0	
	4	439.1	525.5	508.3	516.8	
2	5	574.9	698.2	657.4	693.0	±8.3%
	6	532.2	640.4	611.0	630.0	
	7	465.9	573.1	543.9	555.6	
3	8	562.7	661.6	625.4	663.8	±8.1%
	9	434.5	524.9	497.4	513.6	
4	11	513.8	612.6	561.9	608.3	±7.5%
	12	586.6	694.5	630.1	660.3	
5	14	501.5	592.5	567.7	565.1	±6.9%
	15	595.6	705.1	665.7	653.0	
	16	567.9	651.8	632.7	607.8	
6	17	494.4	569.3	559.7	511.4	±6.1%
	18	592.4	688.6	666.6	668.4	
	19	620.6	692.3	691.1	644.3	
7	20	587.4	668.8	659.3	572.4	±6.3%
	21	525.4	587.9	585.7	533.9	

Table C.1.1 Constant-Dose Irradiation Data (Continued)

Capsule No.	TLD No.	Run 1	Run 2	Run 3	Run 4	($\pm 1\sigma$)
	22	538.7	579.3	607.2	539.2	
8	23	602.7	663.4	672.6	650.0	±5.1%
	24	545.8	580.7	604.7	529.8	
	25	479.2	502.7	540.3	455.8	
9	26	560.5	585.4	596.0	527.2	±7.0%
	27	610.4	630.4	680.9	556.4	
	28	634.5	631.0	710.4	553.9	
10	29	555.9	560.1	623.4	508.7	±9.2%
	30	577.1	567.6	643.5	514.5	
	31	550.6	544.4	621.2	492.5	
11	32	698.0	676.1	782.2	615.9	9.4%
	33	644.3	622.3	718.0	582.1	
	34	538.5	518.5	603.3	481.5	
12	35	638.4	608.9	719.2	560.4	±10.0%
	36	673.4	641.1	750.5	593.0	
	37	672.7	663.7	767.1	600.9	
13	38	533.1	590.1	591.8	481.6	±9.3%
	39	629.0	620.0	716.6	570.5	
	40	518.4	487.9	604.4	429.5	
14	41	546.1	510.0	587.1	545.5	±10.0%
	42	662.9	622.0	768.5	599.8	
	43	592.2	558.6	680.8	654.3	
15	44	533.9	526.8	617.2	532.4	±8.4%
	45	585.9	577.7	677.5	580.1	
	46	511.1	518.5	584.0	510.7	
16	47	606.4	578.3	690.6	604.0	
	48	571.7	555.7	664.8	575.3	
17	49	552.1	574.0	643.5	580.8	±6.8%
	50	587.5	610.5	689.5	627.4	

Table C.1.2 Calibration Data (TLD Response vs. Total Dose)

The data presented here establishes the relation between total dose and TLD response (nc).

Capsule No.	TLD No.	Response (nc) Run 1 (44.6/Rads)	Run 2 (70.6/Rads)	Run 3 (252./Rads)	Run 4 (386.Rads)	Run 5 (701 Rads)	Run 6 (1822 Rads)
	1	100.3	148.7	629.9	902.2	1860	6120
1	2	94.6	140.9	512.4	850.1	1640	5920
	3	105.7	150.1	630.5	982.3	2000	5830
	4	89.6	127.7	508.3	807.1	1590	5290
2	5	116.9	165.7	657.4	1080	2140	5944
	6	109.3	154.7	611.0	984.1	1990	5650
	7	85.8	142.1	543.9	902.4	1600	4880
3	8	117.3	154.8	625.4	988.5	2090	5560
	9	101.8	121.4	497.4	753.8	1780	4500
4	11	100.9	145.4	561.9	899.3	1930	5290
	12	108.0	151.3	630.1	959.1	2040	5630
5	14	93.8	133.9	567.7	834.8	1780	5220
	15	110.8	156.3	665.7	982.4	2180	5650
	16	105.3	131.1	632.7	919.4	1950	5450
6	17	91.1	149.9	559.7	793.2	1700	5490
	18	109.2	154.4	666.6	960.7	2100	5580
	19	108.6	158.3	691.1	964.9	2140	6150
7	20	103.3	153.8	569.3	916.1	2030	5790
	21	91.1	140.2	585.7	824.1	1820	5580
	22	90.8	143.3	607.2	909.9	1740	5270
8	23	101.0	156.2	672.6	838.7	1930	6030
	24	90.3	145.5	604.7	801.8	1810	5360

Table C.1.2 Calibration Data (TLD Response vs. Total Dose), (Continued)

Capsule No.	TLD No.	Run 1	Run 2	Run 3	Run 4	Run 5	Run 6
	25	79.3	127.6	540.3	718.3	1470	5380
9	26	91.2	146.5	596.0	818.7	1720	5420
	27	99.3	154.2	680.9	904.7	1880	5490
	28	97.6	150.1	710.4	916.2	1860	5380
10	29	86.7	164.1	623.4	809.9	1620	5900
	30	89.2	143.4	643.5	837.1	1690	5240
	31	89.3	149.2	621.2	831.5	1600	5470
11	32	105.2	189.5	782.2	1030	2010	5850
	33	95.4	169.6	718.0	956.3	1850	5650
	34	83.7	147.4	603.3	813.4	1510	5630
12	35	98.9	176.1	719.2	961.6	1800	5810
	36	104.1	184.9	750.5	1000	1900	5940
	37	101.9	186.7	767.1	1020	1860	5770
13	38	82.3	153.6	591.8	812.9	1510	5360
	39	95.5	176.0	716.6	948.7	1730	5580
	40	84.1	153.3	604.4	819.8	1490	5400
14	41	87.4	161.4	587.1	859.3	1550	5470
	42	105.2	171.7	768.5	1050	1910	5650
	43	89.1	176.7	680.8	945.1	1720	5240
15	44	95.7	158.0	617.3	884.3	1550	5020
	45	98.8	177.6	679.5	983.9	1710	5760
	46	86.7	159.2	584.0	884.4	1560	5510
16	47	104.4	187.8	690.6	1040	1820	5880
	48	98.9	175.8	664.8	894.4	1730	5540
	49	98.2	181.7	643.5	1000	176	5400
17	50	105.9	182.0	689.5	1060	188	5700

Table C.1.3 Ionization Chamber Data

Ion-Chamber	V(mV)*	C**
L2	28.56 ± 2.39	32.59 ± 2.73
L4	29.56 ± 2.43	33.73 ± 2.77
L5	30.42 ± 2.47	34.71 ± 2.82
L7	30.20 ± 2.46	34.46 ± 2.81
L8	30.34 ± 2.46	34.62 ± 2.81
L9	28.92 ± 2.41	33.00 ± 2.75
L11	27.35 ± 2.34	31.21 ± 2.67
L12	29.10 ± 2.41	33.21 ± 2.75
L15	31.13 ± 2.50	35.52 ± 2.85
L16	27.42 ± 2.34	31.29 ± 2.67
L17	32.05 ± 2.53	36.57 ± 2.89
S0	24.94 ± 2.23	28.46 ± 2.54
S1	36.15 ± 2.69	41.25 ± 3.07
S3	33.92 ± 2.60	28.71 ± 2.97
S5	32.96 ± 2.57	37.61 ± 2.93
S6	30.67 ± 2.48	35.00 ± 2.83
S7	37.35 ± 2.73	46.62 ± 3.12
S8	36.00 ± 2.68	41.08 ± 3.06
S9	28.03 ± 2.37	31.99 ± 2.70
S12	35.12 ± 2.65	40.08 ± 3.02
S18	33.39 ± 2.58	38.10 ± 2.94

*Average of Calibration Runs $\pm 1\sigma$

**Linear Constant for Straight Line Calibration Curve.

C.2 Dose Traverse Data

Table C.2.1 Raw TLD Dose Traverse Data

This table presents the averaged values of the TLD responses in each capsule.

Capsule Averaged Response (nc)*

Capsule No.	Distance into Blanket (cm)	Stainless Steel		Aluminum	
		Run 1	Run 2	Run 1	Run 2
1	2.34	6350	9130	6820	6540
2	7.50	4020	5570	4350	4130
3	12.70	2700	3580	2820	2750
4	17.40	2020	2810	2300	2120
5	22.60	1600	2040	1670	1570
6	27.80	1250	1640	1300	1260
7	32.60	987	1280	1010	969
8	37.60	809	948	783	732
9	42.80	581	788	590	559
10	46.27	387	512	358	349
11	51.67	273	335	254	246
12	50.06	214	263	194	188
13	62.46	121	207		
14	67.86	128	152	120	116
15	73.32	98.5	117	87.1	87.1
16	78.65	72.5	88.5		
17	84.05	53.6	66.1	48.4	47.1

*Data has not been corrected for reactor power, neutron effects, or energy response.

Table C.2.1 Raw TLD Dose Traverse Data (Continued)

Capsule No.	Distance into Blanket (cm)	TLD Capsule-Averaged Response (nc)* Lead Run 1	Lead Run 2
1	2.34	9640	12010
2	7.50	5930	7450
3	12.70	3810	4570
4	17.40	2390	2710
5	22.60	2190	2560
6	27.80	1750	2040
7	32.60	1360	1570
8	37.60	1000	1160
9	42.80	805	904
10	46.27	490	557
11	51.67	371	406
12	57.06	290	318
13	62.46	232	257
14	67.86	171	185
15	73.32	133	143
16	78.65	98.4	106
17	87.05	74.6	79.3

* Data has not been corrected for reactor power, neutron effects, or energy response.

Table C.2.2 Dose Rate Traverses Uncorrected for Neutron Response*

Capsule No.	Distance into Blanket	S.S.	Al.	Pb
1	2.34	563. ± 24	487 ± 24	694 ± 81
2	7.50	456 ± 2	347 ± 13	474 ± 55
3	12.70	252 ± 16	242 ± 17	342 ± 24
4	17.40	192. 25	192.25	192.25
5	22.60	154 ± 17	149 ± 4.3	212 ± 8.3
6	27.80	122 ± 9.5	117 ± 7.5	171 ± 6.2
7	32.60	100 ± 9.4	93.0 ± 4.7	130 ± 3.0
8	37.60	82.2 ± 9.0	73.0 ± 1.3	99.2 ± 1.2
9	42.80	60.0 ± 2.0	55.6 ± 1.9	80.5 ± 1.3
10	46.27	38.5 ± 2.5	35.4 ± 2.5	74.7 ± 3.5
11	51.67	27.2 ± 1.9	26.2 ± 1.6	52.3 ±2.3
12	57.06	21.8 ± 1.02	20.1 ± 1.3	39.4 ± 1.2
13	62.46	17.6 ± 0.86		31.7 ± 2.0
14	67.86	13.3 ± 0.82	12.9 ± 0.77	23.9 ± 1.5
15	73.32	10.8 ± 0.79	9.51 ± 0.56	19.0 ± 1.35
16	78.65	7.92 ± 0.69		14.3 ± 0.97
17	84.05	5.90 ± 0.55	5.45 ± 0.37	10.9 ± 0.95

*Capsule No. 4 has a stainless steel sleeve for all runs (including Pb. and Al.). All runs were then normalized to the capsule No. 4 dose rate (192.25 rads /hr.) at a reactor power of 5 MW. Values listed are averages of two runs. Error represents standard deviation from mean times student's factor. (SDM x t)

Table C.2.3 Dose Rate Traverses Corrected for Neutron Response*

Capsule No.	Neutron Contribution to TLD Dose Rate (rads /Hr)	S.S.	Al.	Pb
1	22.2	512 ± 21	443 ± 22	667 ± 77
2	15.9	420 ± 2.1	320 ± 12	455 ± 53
3	11.5	236 ± 1	227 ± 16	328 ± 23
4	6.04	181	181	181
5	4.42	146 ± 20	141 ± 3.5	207 ± 8.1
6	3.20	116 ± 9.0	112 ± 7.2	168 ± 6.0
7	2.36	96.2 ± 9.0	89.5 ± 4.6	127 ± 2.9
8	1.73	79.4 ± 8.7	70.6 ± 1.3	97.2 ± 2.8
9	1.32	58.1 ± 1.9	53.8 ± 1.9	78.9 ± 0.95
10	0.963	37.1 ± 2.4	34.1 ± 2.4	73.0 ± 1.2
11	0.305	26.4 ± 1.8	25.5 ± 1.6	51.8 ± 2.4
12	0.215	21.3 ± 1.0	19.6 ± 1.3	39.1 ± 1.7
13	0.154	17.3 ± 0.85		31.5 ± 0.94
14	0.0840	13.1 ± 0.81	12.7 ± 0.76	23.8 ± 0.15
15	0.0578	10.6 ± 0.77	9.39 ± 0.55	18.9 ± 1.3
16	0.0433	7.82 ± 0.68		14.2 ± 0.96
17	0.0305	5.83 ± 0.55	5.38 ± 0.37	10.8 ± 0.94

*Capsule No. 4 used for normalization. A stainless steel sleeve was used in every run (including Al. and Pb.) values listed are averages of two runs. Errors are ± 1 σ (SDM x t)

Table C.2.4 Standard Deviation from Mean for TLD Capsules,*

Capsule No.	Distance into Blk. (cm.)	S.S.	Al.	Pb.
1	2.34	4.2%	5.0%	11.6%
2	7.50	0.5%	3.8%	11.6%
3	12.70	6.4%	7.1%	7.1%
4	17.40			
5	22.60	11.0%	2.5%	3.9%
6	27.80	7.8%	6.4%	3.6%
7	32.60	9.4%	5.1%	2.3%
8	37.60	11.0%	1.8%	2.9%
9	42.80	3.3%	3.5%	1.2%
10	46.27	6.4%	7.1%	1.6%
11	51.67	7.0%	6.3%	4.7%
12	57.06	4.7%	6.4%	4.4%
13	62.46	4.9%		3.0%
14	67.86	6.2%	6.0%	6.2%
15	73.32	7.3%	5.9%	7.1%
16	78.65	8.7%		6.8%
17	84.05	9.4%	6.9%	8.7%

*SDM x t, where t = 1.84, Student t-factor for two repetitions

Table C.2.5 Ionization Chamber Dose Rate Traverse Data

Test Position	Distance in Blanket (cm)	Dose Rate (rads/hr)*
1	2.34	547.0 ± 61.5
2	7.50	344.0 ± 42.0
3	12.70	251.0 ± 33.0
4	17.40	186.5 ± 27.5
5	22.26	152.0 ± 18.5
6	27.80	119.5 ± 15.5
7	32.60	78.5 ± 11.5
8	37.60	61.5 ± 9.0
9	42.80	55.0 ± 6.0
10	46.27	40.5 ± 5.0
11	51.67	26.5 ± 3.5
12	57.06	22.5 ± 3.0
13	62.46	15.5 ± 2.5
14	67.86	13.5 ± 2.5
15	73.32	10.0 ± 2.0
16	78.65	7.0 ± 2.0
17	84.05	5.5 ± 2.0
18	88.45	3.0 ± 2.0

*Average of BTF irradiations ± 1 σ.

C.3 Other Data

Table C.3.1 Spectral Response Factors,

Capsule No.	Distance into Blanket (cm)	Stainless Steel	Al.	Pb
1	2.34	0.980	1.07	1.20
2	7.50	0.980	1.07	1.20
3	12.70	0.980	1.07	1.20
4	17.40	0.980	1.07	1.20
5	22.60	0.980	1.07	1.20
6	27.80	0.980	1.07	1.20
7	32.60	0.982	1.07	1.17
8	37.60	0.982	1.07	1.17
9	42.80	0.979	1.07	1.72
10	46.27	0.923	1.08	1.58
11	51.67	0.915	1.09	1.50
12	57.06	0.919	1.10	1.50
13	62.46	0.919	1.10	1.50
14	67.86	0.919	1.10	1.50
15	73.32	0.919	1.10	1.50
16	78.65	0.919	1.10	1.50
17	84.05	0.919	1.10	1.50

Appendix D Computer Programs

This appendix has been included to briefly describe and show sample problems for the computer programs which were used. A brief description of the modifications made to the RESPOND program is included.

D.1 RESPOND Modifications

There were two areas in which the RESPOND program was modified. The first dealt with inconsistencies with cavity ionization theory, and is discussed in section 2.5.3 of Chapter 2. The second area of modification dealt with expanding the program to handle gamma spectra which had a significant portion of the spectrum between 5 and 10 MEV. The only difficulty encountered in increasing this energy range is that the collision stopping power relation used in Eq. 2.26 must be corrected for the density of the TLD cavity and for bremsstrahlung. The density correction is merely subtra cted from the stopping power of Eq. 2.26. It is given by (S, 11).

$$\Delta \left|\frac{dT}{dx}\right| = \frac{2\pi e^4}{m_o v^2} NZ \left[\ln \frac{4\pi e^2 h^2 NZ}{m_o(1-\beta^2)I^2} - 1\right], \quad \frac{MEV}{cm.} \tag{D.1.1}$$

Where

e = electron charge

m_o = electron rest mass

v = electron velocity

N = atomic number density

Z = atomic number

I = mean ionization potential

$\hbar$ = Planck's constant divided by 2π

β = v/c

C = speed of light

The radiation correction acts as an increase in the electron stopping power and is therefore added to the normal stopping power relation of Eq. 2.26 this correction is given by (J,1).

$$\frac{dT}{dx} = \frac{TZ}{1600\, m_o c^2}\left[\left|\frac{dT}{dx}\right|_{col}\right], \frac{MEV}{cm.} \qquad (D.1.2)$$

Where

T = electron energy

Z = atomic number

m_o = electron rest mass

c = speed of light

$\left|\frac{dT}{dx}\right|_{col}$ = collision stopping power (Eq. 2.26)

RESPOND was modified by including these corrections in its stopping power calculation. The stopping powers calculated by the code were then compared against stopping powers tabulated by Bichsel (B,4) and were found to differ by less than 1.0% at all electron energies.

D.2 RESPOND Sample Problem

The computer code RESPOND calculates the R_D factors which were developed in Chapter 2. The sample problem shown here includes a program listing, sample input, and output. There are three categories of input data: the first involves input of material properties such as atomic number, atomic mass, mean ionization potential, and the density of both sleeve and TLD materials; mass energy absorption coefficients for both cavity/TLD and sleeve materials; and the third involves specification of a gamma spectrum. RESPOND then finds the R_D factor for all input gamma spectra supplied to it.

```
C                                   RESPOND                                    00000010 MAIN0001
C     CALCULATES THE RELATIVE ENERGY RESPONSE OF A CAVITY IN A MEDIUM.         00000020 MAIN0002
C          BASED ON T. E. BURLIN'S GENERAL THEORY OF CAVITY IONIZATION,        00000030 MAIN0003
C                T. E. BURLIN, 'RAD. DOS.' 2ND. ED. P.332                     00000040 MAIN0004
C                                                                             00000050 MAIN0005
C                SEPTEMBER 27, 1971.                                          00000060 MAIN0006
C                OCTOBER 7, 1971        STRUCTURAL DEBUGGING COMPLETED.       00000070 MAIN0007
C                OCTOBER 19, 1971       FUNCTIONAL DEBUGGING CONTINUING.      00000080 MAIN0008
C                OCTOBER 21, 1971       STOPPING POWER CHECKED,               00000090 MAIN0009
C                G. N. WHYTE, 'PRINC. RAD. DOS.' P.15                         00000100 MAIN0010
C                                       ELECTRON RANGE CHECKED,               00000110 MAIN0011
C                J. B. MARION, '1960 NUCL. DATA TABLES PT.3' P.6              00000120 MAIN0012
C                OCTOBER 27, 1971       ELECTRON SPECTRA CHECKED,             00000130 MAIN0013
C                R. D. EVANS, 'PRINC. RAD. DOS.' P.107                        00000140 MAIN0014
C                H. A. BETHE + J. ASHKIN, 'EXP. NUCL. PHYS.' P.328            00000150 MAIN0015
C                NOVEMBER 1, 1971.                                            00000160 MAIN0016
C                NOVEMBER 30, 1971      FINE ENERGY MESH USED FOR             00000170 MAIN0017
C                                       STOPPING POWER CALCULATION.           00000180 MAIN0018
C                                                                             00000190 MAIN0019
C                          ROBERT J. TUTTLE                 AI/NAR            00000200 MAIN0020
C                                                                             00000210 MAIN0021
      REAL                                                                    00000220 MAIN0022
     6  D(200),RANGE(200),RED(200),RID(200),FGAM(200),                                MAIN0023
     5  SINT1(200),SINT2(200),UNITY(200),                                             MAIN0024
     4  SPC(10000),SPM(10000),EEO(200),SPCM(200),EG(200),SOURCE(200),                 MAIN0025
     3  SIGPEC(200),SIGCOC(200),SIGPPC(200),SIGTC(200),SC(200),SP(200),               MAIN0026
     2  SIGPEM(200),SIGCOM(200),SIGPPM(200),SIGTM(200),                               MAIN0027
     1  DATE(2),RUN(20),TITLE(12),GAMMA(12),CAVITY(12),MEDIUM(12),IC,IM,00000280 MAIN0028
     7  TOT(200),GAMS(200)                                                           MAIN0029
C                                                                             00000290 MAIN0030
      DE=0.05                                                                 00000340 MAIN0031
C                                                                             00000350 MAIN0032
      DO 20 I=1,200                                                           00000360 MAIN0033
        EG(I)=DE*I                                                            00000370 MAIN0034
        EEO(I)=EG(I)                                                          00000380 MAIN0035
        SOURCE(I)=0.0                                                         00000390 MAIN0036
```

```
      TOT(I)=0.0                                                                MAIN0037
      UNITY(I)=1.0                                                  00000400    MAIN0038
   20 CONTINUE                                                      00000410    MAIN0039
C                                                                   00000420    MAIN0040
      READ (5,2) TITLE,CLT                                          00000430    MAIN0041
    2 FORMAT (1X,12A4,12X,F12.6)                                                MAIN0042
      WRITE (6,2) TITLE,CLT                                         00000450    MAIN0043
      READ (5,3) CAVITY,ZC,AC,IC,PC                                 00000460    MAIN0044
    3 FORMAT (1X,12A4,4F6.0)                                                    MAIN0045
      WRITE (6,4) CAVITY,ZC,AC,IC,PC                                00000480    MAIN0046
    4 FORMAT (10X,12A4/20X,'ATOMIC NUMBER =',F10.4/                 00000490    MAIN0047
     1                  20X,'ATOMIC MASS   =',F10.4/                00000500    MAIN0048
     2                  20X,'MEAN IONIZATION POTENTIAL =',F10.4/    00000510    MAIN0049
     3                  20X,'DENSITY =',F10.4/)                     00000515    MAIN0050
      READ (5,5) (SIGPEC(I),I=1,200)                               00000520    MAIN0051
      READ (5,5) (SIGCOC(I),I=1,200)                               00000530    MAIN0052
      READ (5,5) (SIGPPC(I),I=1,200)                               00000540    MAIN0053
    5 FORMAT (12F6.0)                                              00000550    MAIN0054
C                                                                   00000560    MAIN0055
      DO 30 I=1,200                                                 00000570    MAIN0056
        SIGTC(I)=SIGPEC(I)+SIGCOC(I)+SIGPPC(I)                      00000580    MAIN0057
   30 CONTINUE                                                      00000590    MAIN0058
C                                                                   00000600    MAIN0059
      READ (5,3) MEDIUM,ZM,AM,IM,PM                                 00000610    MAIN0060
      WRITE (6,4) MEDIUM,ZM,AM,IM,PM                                00000620    MAIN0061
      READ (5,5) (SIGPEM(I),I=1,200)                               00000630    MAIN0062
      READ (5,5) (SIGCOM(I),I=1,200)                               00000640    MAIN0063
      READ (5,5) (SIGPPM(I),I=1,200)                               00000650    MAIN0064
C                                                                   00000660    MAIN0065
      DO 40 I=1,200                                                 00000670    MAIN0066
        SIGTM(I)=SIGPEM(I)+SIGCOM(I)+SIGPPM(I)                      00000680    MAIN0067
   40 CONTINUE                                                      00000690    MAIN0068
C                                                                   00000700    MAIN0069
      WRITE (6,6)                                                   00000710    MAIN0070
    6 FORMAT ('1'///10X,'PHOTON MASS ENERGY ABSORPTION COEFFICIENTS'/ 00000720    MAIN0071
     1  10X,'PHOTON ENERGY',9X,'PHOTO',15X,'COMPTON',15X,'PAIR',      00000730    MAIN0072
```

```
     2  14X,'TOTAL'/                                                          00000740 MAIN0073
     3  14X,'(MEV)',12X,'ELECTRIC',13X,'EFFECT',13X,'PRODUCTION'/)            00000750 MAIN0074
      WRITE (6,7) CAVITY                                                     00000760 MAIN0075
    7 FORMAT (10X,12A4/)                                                     00000770 MAIN0076
C                                                                            00000780 MAIN0077
      DO 50 I=1,200                                                          00000790 MAIN0078
      WRITE (6,8) I,EG(I),SIGPEC(I),SIGCOC(I),SIGPPC(I),SIGTC(I)             00000800 MAIN0079
    8 FORMAT (I4,10X,F5.2,4F20.5)                                            00000810 MAIN0080
   50 CONTINUE                                                               00000820 MAIN0081
C                                                                            00000830 MAIN0082
      WRITE (6,6)                                                            00000840 MAIN0083
      WRITE (6,7) MEDIUM                                                     00000850 MAIN0084
C                                                                            00000860 MAIN0085
      DO 60 I=1,200                                                          00000870 MAIN0086
      WRITE (6,8) I,EG(I),SIGPEM(I),SIGCOM(I),SIGPPM(I),SIGTM(I)             00000880 MAIN0087
   60 CONTINUE                                                               00000890 MAIN0088
C                                                                            00000900 MAIN0089
C     THIS COMPLETES INITIAL INPUT                                           00000910 MAIN0090
C     CALCULATE MASS STOPPING POWER AS FUNCTION OF ELECTRON ENERGY.          00000920 MAIN0091
C                                                                            00000930 MAIN0092
        IC=0.000001*IC                                                       00000940 MAIN0093
        IM=0.000001*IM                                                       00000950 MAIN0094
        CC=0.1535311*ZC/AC                                                   00000960 MAIN0095
        CM=0.1535311*ZM/AM                                                   00000970 MAIN0096
C                                                                            00000980 MAIN0097
      DO 70 K=1,10000                                                        00000990 MAIN0098
        EE=0.001*K                                                           00001000 MAIN0099
        B1=0.511006/(EE+0.511006)                                            00001010 MAIN0100
        B2=B1**2                                                             00001020 MAIN0101
        B21=1.0-B2                                                           00001030 MAIN0102
      A1=ALOG(0.255503*EE*B21/B2)                                                   MAIN0103
        A2=-0.6931472*(2.0*B1-B2)+B2+0.125*(1.0-B1)**2                       00001050 MAIN0104
      SPCOC=CC*(A1-2.0*ALOG(IC)+A2)/B21                                             MAIN0105
      SPCOM=CM*(A1-2.0*ALOG(IM)+A2)/B21                                             MAIN0106
      SPRC=1.2231E-3*EE*ZC*SPCOC                                                    MAIN0107
      SPRM=1.2231E-3*EE*ZM*SPCOM                                                    MAIN0108
```

```
C                                                                                MAIN0109
      QC=8.30498E-10*PC*ZC/(AC*B2*IC**2)                                         MAIN0110
      QM=8.30498E-10*PM*ZM/(AM*B2*IM**2)                                         MAIN0111
      ALQC=ALOG(QC)                                                              MAIN0112
      ALQM=ALOG(QM)                                                              MAIN0113
      IF (ALQC.LT.1.0) GO TO 71                                                  MAIN0114
      SPPC=CC*(ALQC-1.0)                                                         MAIN0115
      GO TO 74                                                                   MAIN0116
   71 SPPC=0.0                                                                   MAIN0117
   74 IF(ALQM.LT.1.0) GO TO 76                                                   MAIN0118
      SPPM=CM*(ALQM-1.0)                                                         MAIN0119
      GO TO 77                                                                   MAIN0120
   76 SPPM=0.0                                                                   MAIN0121
C                                                                                MAIN0122
   77 SPC(K)=SPCCC+SPRC-SPPC                                                     MAIN0123
      SPM(K)=SPCCM-SPPM+SPRM                                                     MAIN0124
   70 CONTINUE                                                                   MAIN0125
C                                                                   00001090     MAIN0126
C     CALCULATE RELATIVE (CAVITY/MEDIUM) AVERAGE MASS STOPPING POWER 00001100    MAIN0127
C     AS A FUNCTION OF INITIAL ELECTRON ENERGY.                     00001110     MAIN0128
C                                                                   00001120     MAIN0129
      DO 80 I=1,200                                                 00001130     MAIN0130
        K1=(I-1)*50+1                                               00001140     MAIN0131
        K2=I*50                                                     00001150     MAIN0132
        SINT1(I)=0.0                                                00001160     MAIN0133
      DO 85 K=K1,K2                                                 00001170     MAIN0134
        SINT1(I)=SINT1(I)+SPC(K)/SPM(K)                             00001180     MAIN0135
   85 CONTINUE                                                      00001190     MAIN0136
        SINT1(I)=0.02*SINT1(I)                                      00001200     MAIN0137
        CALL TRAP(SINT1,DE,I,S1)                                    00001210     MAIN0138
        CALL TRAP(UNITY,DE,I,EINT)                                  00001220     MAIN0139
        SPCM(I)=S1/EINT                                             00001230     MAIN0140
   80 CONTINUE                                                      00001240     MAIN0141
C                                                                   00001250     MAIN0142
C     CALCULATE AVERAGE OF STOPPING POWER WITH RESPECT TO ELECTRON  00001260     MAIN0143
C     SOURCE SPECTRUM AS A FUNCTION OF PHOTON ENERGY.               00001270     MAIN0144
```

```
C                                                                       00001280 MAIN0145
C     CALCULATE ELECTRON RANGE AND WEIGHTING FUNCTION, D(EEO).          00001290 MAIN0146
C                                                                       00001300 MAIN0147
      DO 110 I=1,200                                                    00001310 MAIN0148
        POW=1.265-0.0954*ALOG(EEO(I))                                   00001320 MAIN0149
        RANGE(I)=0.412*EEO(I)**POW                                      00001330 MAIN0150
        KEEP=I                                                          00001340 MAIN0151
      IF (EEO(I).EQ.3.0) GO TO 120                                      00001350 MAIN0152
  110 CONTINUE                                                          00001360 MAIN0153
C                                                                       00001370 MAIN0154
  120   R1=RANGE(KEEP)                                                 00001380 MAIN0155
C                                                                       00001390 MAIN0156
      DO 130 I=KEEP,200                                                 00001400 MAIN0157
        RANGE(I)=0.530*EEO(I)-0.106                                     00001410 MAIN0158
  130 CONTINUE                                                          00001420 MAIN0159
C                                                                       00001430 MAIN0160
        RANGE(KEEP)=(R1+RANGE(KEEP))*0.5                                00001440 MAIN0161
C                                                                       00001450 MAIN0162
      DO 140 I=1,200                                                    00001460 MAIN0163
       BETAL=4.605/RANGE(I)*CLT                                         00001470 MAIN0164
      IF (BETAL.GT.174.0) GO TO 135                                     00001480 MAIN0165
        D(I)=(1.0-EXP(-BETAL))/BETAL                                    00001490 MAIN0166
      GO TO 140                                                         00001500 MAIN0167
  135   D(I)=1.0/BETAL                                                  00001510 MAIN0168
  140 CONTINUE                                                          00001520 MAIN0169
C                                                                       00001610 MAIN0170
C     CALCULATE ELECTRON SOURCE SPECTRUM                                00001620 MAIN0171
C                                                                       00001630 MAIN0172
      DO 90 J=1,200                                                     00001640 MAIN0173
        SC(J)=0.0                                                       00001650 MAIN0174
        SP(J)=0.0                                                       00001660 MAIN0175
        EP=EG(J)                                                        00001670 MAIN0176
      CALL COMP (EP,DE,SC,NE)                                           00001680 MAIN0177
      CALL TRAP (SC,DE,NE,CINT)                                         00001690 MAIN0178
      CALL PAIR (EP,DE,SP,NE)                                           00001700 MAIN0179
      CALL TRAP (SP,DE,NE,PINT)                                         00001710 MAIN0180
```

```
C                                                                       00001720 MAIN0181
      DO 100 I=1,J                                                              MAIN0182
        SOURCE(I)=SC(I)/CINT*SIGCOM(J)+SP(I)/PINT*SIGPPM(J)             00001740 MAIN0183
  100 CONTINUE                                                                  MAIN0184
C                                                                               MAIN0185
        SOURCE(J)=SOURCE(J)+SIGPEM(J)/DE                                00001770 MAIN0186
C                                                                       00001780 MAIN0187
C     ELECTRON SOURCE SPECTRUM HAS BEEN CALCULATED, NOW AVERAGE.        00001790 MAIN0188
C                                                                       00001800 MAIN0189
      DO 150 I=1,J                                                      00001810 MAIN0190
        I1=I                                                            00001820 MAIN0191
        SINT2(I)=SPCM(I)*SOURCE(I)                                      00001830 MAIN0192
  150 CONTINUE                                                          00001840 MAIN0193
C                                                                       00001850 MAIN0194
      CALL TRAP(SINT2,DE,I1,S2)                                         00001860 MAIN0195
      CALL TRAP(SOURCE,DE,I1,S1)                                        00001870 MAIN0196
        RED(J)=S2/S1*D(J)                                               00001880 MAIN0197
        RID(J)=(SIGTC(J)/SIGTM(J))*(1.0-D(J))                           00001890 MAIN0198
        TOT(J)=RED(J)+RID(J)                                                    MAIN0199
C                                                                       00001950 MAIN0200
   90 CONTINUE                                                          00001960 MAIN0201
C                                                                       00001530 MAIN0202
      WRITE (6,12) TITLE                                                00001540 MAIN0203
   12 FORMAT ('1'///10X,12A4//                                          00001550 MAIN0204
     1  5X,'ELECTRON',2X,'STOPPING POWER',3X,'RELATIVE AVERAGE',        00001560 MAIN0205
     2  3X,'RANGE',7X,'PHOTON',3X,'WEIGHT',9X,'RELATIVE DOSES'/         00001570 MAIN0206
     3  6X,'ENERGY',2X,'CAVITY',4X,'MEDIUM',3X,'STOPPING POWER',        00001580 MAIN0207
     4  3X,'(G/CM2)',6X,'ENERGY',3X,'FACTOR',                           00001590 MAIN0208
     5  3X,'EXTERNAL   INTERNAL   TOTAL'/)                              00001600 MAIN0209
      DO 125 J=1,200                                                            MAIN0210
      WRITE (6,13) J,EEO(J),SPC(50*J),SPM(50*J),SPCM(J),RANGE(J),EEO(J),00001910 MAIN0211
     1  D(J),RED(J),RID(J),TOT(J)                                                MAIN0212
   13 FORMAT (I4,F7.2,F9.4,F10.4,4X,F10.5,3X,F10.4,4X,F7.2,F10.5,F9.4,  00001930 MAIN0213
     1  2F10.4)                                                         00001940 MAIN0214
  125 CONTINUE                                                                  MAIN0215
C                                                                       00001970 MAIN0216
```

```
      WRITE (6,14) TITLE                                                00001980 MAIN0001
   14 FORMAT ('1'///12A4)                                               00001990 MAIN0002
   10 READ (5,9,END=999) GAMMA                                          00002000 MAIN0003
    9 FORMAT (12A4)                                                     00002010 MAIN0004
      READ (5,5) (FGAM(I),I=1,200)                                      00002020 MAIN0005
C                                                                       00002030 MAIN0006
C     AVERAGE RED+RID OVER PHOTON SPECTRUM.                             00002040 MAIN0007
C                                                                       00002050 MAIN0008
      DO 160 I=1,200                                                    00002060 MAIN0009
      ENG=DE*I                                                                   MAIN0010
      GAMS(I)=FGAM(I)*SIGTM(I)*ENG                                               MAIN0011
      SINT1(I)=(RED(I)+RID(I))*GAMS(I)                                           MAIN0012
  160 CONTINUE                                                                   MAIN0013
C                                                                                MAIN0014
      I100=200                                                                   MAIN0015
      CALL TRAP (SINT1,DE,I100,S1)                                               MAIN0016
      CALL TRAP (GAMS,DE,I100,S2)                                                MAIN0017
        BF=S1/S2                                                        00002130 MAIN0018
      WRITE (6,11) GAMMA,BF                                             00002140 MAIN0019
   11 FORMAT (/2X,'FOR THE PHOTON SPECTRUM - ',12A4,                    00002150 MAIN0020
     1  5X,'BURLIN/S FACTOR =',F8.4)                                    00002160 MAIN0021
      WRITE (6,17) S1,S2                                                         MAIN0022
   17 FORMAT (/10X,'CAVITY DOSE',5X,E10.3,10X,'SLEEVE DOSE',5X,E10.3)            MAIN0023
C                                                                       00002170 MAIN0024
C     THIS COMPLETES THE CALCULATION FOR ONE CASE. RETURN FOR MORE.     00002180 MAIN0025
C                                                                       00002190 MAIN0026
      GO TO 10                                                          00002200 MAIN0027
  999 STOP                                                              00002205 MAIN0028
      END                                                               00002210 MAIN0029
```

```
      SUBROUTINE TRAP(Y,H,NPTS,SUM)                                    00002220 SUB10001
C                  SEPTEMBER 27, 1971.                                  00002230 SUB10002
      DIMENSION Y(200)                                                 00002240 SUB10003
        SUM=0.0                                                        00002250 SUB10004
      DO 10 J=1,NPTS                                                   00002260 SUB10005
   10   SUM=SUM+Y(J)                                                   00002270 SUB10006
        SUM=H*(SUM-0.5*(Y(1)+Y(NPTS)))                                 00002280 SUB10007
      IF (NPTS.EQ.1) SUM=H*Y(1)                                        00002290 SUB10008
      IF (NPTS.EQ.2) SUM=H*(Y(1)+Y(2))                                 00002300 SUB10009
      RETURN                                                           00002310 SUB10010
      END                                                              00002320 SUB10011
```

```
      SUBROUTINE COMP (E,DT,S,N)                                        00002330 SUB20001
      DIMENSION S(200)                                                  00002340 SUB20002
        A=E/0.511006                                                    00002350 SUB20003
        TMAX=E*(2.0*A/(1.0+2.0*A))                                      00002360 SUB20004
        K=TMAX/DT                                                       00002370 SUB20005
        TEND=0.0                                                                 SUB20006
      DO 10 I=1,K                                                       00002380 SUB20007
        N=K                                                             00002390 SUB20008
        T=I*DT                                                          00002400 SUB20009
      IF (K.LT.1) GO TO 15                                              00002410 SUB20010
        D=E-T                                                           00002420 SUB20011
        TEND=T                                                          00002430 SUB20012
10      S(I)=(4.88129E-04*(2.0+(T/D)**2*((1.0/A**2)+D/E-2.0*D/(A*T)))            SUB20013
     1        /A**2)*T                                                           SUB20014
      IF (TMAX.LE.T) GO TO 20                                           00002460 SUB20015
15      N=K+1                                                           00002470 SUB20016
        T=TMAX                                                          00002480 SUB20017
        D=E-T                                                           00002490 SUB20018
      S(K+1)=(4.88129E-04*(2.0+(T/D)**2*((1.0/A**2)+D/E-2.0*D/(A*T)))           SUB20019
     1        /A**2)*(TMAX-TEND)*T/DT                                            SUB20020
20    RETURN                                                            00002520 SUB20021
      END                                                               00002530 SUB20022
```

```
      SUBROUTINE PAIR (E,DE,S,N)                                        00002540 SUB30001
      DIMENSION S(200)                                                  00002550 SUB30002
        EK=E-1.022012                                                   00002560 SUB30003
      IF (EK.LE.0.0) GO TO 30                                           00002570 SUB30004
        K=EK/DE                                                         00002580 SUB30005
      IF (K.LE.1) GO TO 30                                              00002590 SUB30006
        R=1.4+0.1*E                                                     00002600 SUB30007
      DO 10 I=1,K                                                       00002610 SUB30008
      ENE=DE*I                                                                   SUB30009
        N=K                                                             00002620 SUB30010
        X=I*DE/EK                                                       00002630 SUB30011
        XR=3.141593*X                                                   00002640 SUB30012
   10   S(I)=4.0*ENE*SQRT(0.25-(X-0.5)**2)/(R+(2.0-R)*SIN(XR))                  SUB30013
      GO TO 20                                                          00002660 SUB30014
   30   S(1)=1.0                                                         00002670 SUB30015
        N=1                                                             00002680 SUB30016
   20 RETURN                                                            00002690 SUB30017
      END                                                               00002700 SUB30018
```

LIF CAVITY IN LEAD 0.249000

LITHIUM-7 FLUORIDE
ATOMIC NUMBER = 6.0000
ATOMIC MASS = 13.0070
MEAN IONIZATION POTENTIAL = 86.4700
DENSITY = 2.6575

LEAD
ATOMIC NUMBER = 82.0000
ATOMIC MASS = 207.1900
MEAN IONIZATION POTENTIAL = 788.0000
DENSITY = 11.3400

PHOTON MASS ENERGY ABSORPTION COEFFICIENTS

	PHOTON ENERGY (MEV)	PHOTO ELECTRIC	COMPTON EFFECT	PAIR PRODUCTION	TOTAL
	LITHIUM-7 FLUORIDE				
1	0.05	0.02880	0.01200	0.0	0.04080
2	0.10	0.00360	0.01860	0.0	0.02160
3	0.15	0.00080	0.02220	0.0	0.02300
4	0.20	0.00030	0.02430	0.0	0.02460
5	0.25	0.00020	0.02530	0.0	0.02550
6	0.30	0.00010	0.02640	0.0	0.02650
7	0.35	0.00010	0.02680	0.0	0.02690
8	0.40	0.0	0.02720	0.0	0.02720
9	0.45	0.0	0.02740	0.0	0.02740
10	0.50	0.0	0.02760	0.0	0.02760
11	0.55	0.0	0.02740	0.0	0.02740
12	0.60	0.0	0.02720	0.0	0.02720
13	0.65	0.0	0.02700	0.0	0.02700
14	0.70	0.0	0.02680	0.0	0.02680
15	0.75	0.0	0.02670	0.0	0.02670
16	0.80	0.0	0.02650	0.0	0.02650
17	0.85	0.0	0.02630	0.0	0.02630
18	0.90	0.0	0.02610	0.0	0.02610
19	0.95	0.0	0.02590	0.0	0.02590
20	1.00	0.0	0.02570	0.0	0.02570
21	1.05	0.0	0.02550	0.0	0.02550
22	1.10	0.0	0.02520	0.0	0.02520
23	1.15	0.0	0.02500	0.0	0.02500
24	1.20	0.0	0.02480	0.0	0.02480
25	1.25	0.0	0.02460	0.0	0.02460
26	1.30	0.0	0.02430	0.0	0.02430
27	1.35	0.0	0.02410	0.0	0.02410
28	1.40	0.0	0.02390	0.0	0.02390
29	1.45	0.0	0.02360	0.0	0.02360
30	1.50	0.0	0.02340	0.0	0.02340
31	1.55	0.0	0.02320	0.0	0.02320
32	1.60	0.0	0.02300	0.00010	0.02310
33	1.65	0.0	0.02280	0.00010	0.02290
34	1.70	0.0	0.02260	0.00010	0.02270
35	1.75	0.0	0.02250	0.00010	0.02260
36	1.80	0.0	0.02230	0.00010	0.02240
37	1.85	0.0	0.02210	0.00010	0.02220
38	1.90	0.0	0.02190	0.00010	0.02200
39	1.95	0.0	0.02170	0.00020	0.02190
40	2.00	0.0	0.02150	0.00020	0.02170
41	2.05	0.0	0.02130	0.00020	0.02150
42	2.10	0.0	0.02120	0.00020	0.02140
43	2.15	0.0	0.02100	0.00030	0.02130
44	2.20	0.0	0.02090	0.00030	0.02120
45	2.25	0.0	0.02070	0.00030	0.02100
46	2.30	0.0	0.02050	0.00030	0.02080
47	2.35	0.0	0.02040	0.00040	0.02080
48	2.40	0.0	0.02020	0.00040	0.02060
49	2.45	0.0	0.02010	0.00040	0.02050
50	2.50	0.0	0.01990	0.00040	0.02030
51	2.55	0.0	0.01970	0.00050	0.02020
52	2.60	0.0	0.01960	0.00050	0.02010
53	2.65	0.0	0.01940	0.00050	0.01990
54	2.70	0.0	0.01930	0.00050	0.01980

56	2.80	0.0	0.01890	0.00060	0.01950
57	2.85	0.0	0.01880	0.00060	0.01940
58	2.90	0.0	0.01860	0.00060	0.01920
59	2.95	0.0	0.01850	0.00070	0.01920
60	3.00	0.0	0.01830	0.00070	0.01900
61	3.05	0.0	0.01820	0.00070	0.01890
62	3.10	0.0	0.01810	0.00080	0.01890
63	3.15	0.0	0.01800	0.00080	0.01880
64	3.20	0.0	0.01780	0.00080	0.01860
65	3.25	0.0	0.01770	0.00090	0.01860
66	3.30	0.0	0.01760	0.00090	0.01850
67	3.35	0.0	0.01750	0.00090	0.01840
68	3.40	0.0	0.01740	0.00090	0.01830
69	3.45	0.0	0.01730	0.00100	0.01830
70	3.50	0.0	0.01710	0.00100	0.01810
71	3.55	0.0	0.01700	0.00100	0.01800
72	3.60	0.0	0.01690	0.00110	0.01800
73	3.65	0.0	0.01680	0.00110	0.01790
74	3.70	0.0	0.01670	0.00110	0.01780
75	3.75	0.0	0.01660	0.00120	0.01780
76	3.80	0.0	0.01650	0.00120	0.01770
77	3.85	0.0	0.01630	0.00120	0.01750
78	3.90	0.0	0.01620	0.00130	0.01750
79	3.95	0.0	0.01610	0.00130	0.01740
80	4.00	0.0	0.01600	0.00130	0.01730
81	4.05	0.0	0.01590	0.00130	0.01720
82	4.10	0.0	0.01580	0.00140	0.01720
83	4.15	0.0	0.01570	0.00140	0.01710
84	4.20	0.0	0.01560	0.00140	0.01700
85	4.25	0.0	0.01550	0.00150	0.01700
86	4.30	0.0	0.01550	0.00150	0.01700
87	4.35	0.0	0.01540	0.00150	0.01690
88	4.40	0.0	0.01530	0.00160	0.01690
89	4.45	0.0	0.01520	0.00160	0.01680
90	4.50	0.0	0.01510	0.00160	0.01670
91	4.55	0.0	0.01500	0.00160	0.01660
92	4.60	0.0	0.01490	0.00170	0.01660
93	4.65	0.0	0.01480	0.00170	0.01650
94	4.70	0.0	0.01470	0.00170	0.01640
95	4.75	0.0	0.01460	0.00180	0.01640
96	4.80	0.0	0.01460	0.00180	0.01640
97	4.85	0.0	0.01450	0.00180	0.01630
98	4.90	0.0	0.01440	0.00180	0.01620
99	4.95	0.0	0.01430	0.00190	0.01620
100	5.00	0.0	0.01420	0.00190	0.01610
101	5.05	0.0	0.01410	0.00190	0.01600
102	5.10	0.0	0.01410	0.00200	0.01610
103	5.15	0.0	0.01400	0.00200	0.01600
104	5.20	0.0	0.01390	0.00200	0.01590
105	5.25	0.0	0.01390	0.00200	0.01580
106	5.30	0.0	0.01380	0.00210	0.01590
107	5.35	0.0	0.01370	0.00210	0.01580
108	5.40	0.0	0.01360	0.00210	0.01570
109	5.45	0.0	0.01360	0.00210	0.01570
110	5.50	0.0	0.01350	0.00220	0.01570
111	5.55	0.0	0.01340	0.00220	0.01560
112	5.60	0.0	0.01340	0.00220	0.01560
113	5.65	0.0	0.01330	0.00220	0.01550
114	5.70	0.0	0.01320	0.00230	0.01550
115	5.75	0.0	0.01310	0.00230	0.01540
116	5.80	0.0	0.01310	0.00230	0.01540
117	5.85	0.0	0.01300	0.00240	0.01540
118	5.90	0.0	0.01290	0.00240	0.01530
119	5.95	0.0	0.01290	0.00240	0.01530
120	6.00	0.0	0.01280	0.00240	0.01520

122	6.10	C.0	0.01270	0.00250	0.01520
123	6.15	C.0	0.01260	0.00250	0.01510
124	6.20	0.0	0.01250	0.00250	0.01500
125	6.25	C.0	0.01250	0.00250	0.01500
126	6.30	C.0	0.01240	0.00260	0.01500
127	6.35	C.0	0.01240	0.00260	0.01500
128	6.40	C.0	0.01230	0.00260	0.01490
129	6.45	C.0	0.01220	0.00260	0.01480
130	6.50	C.0	0.01220	0.00270	0.01490
131	6.55	C.0	0.01210	0.00270	0.01480
132	6.60	C.0	0.01200	0.00270	0.01470
133	6.65	C.0	0.01200	0.00270	0.01470
134	6.70	0.0	0.01190	0.00280	0.01470
135	6.75	C.0	0.01190	0.00280	0.01470
136	6.80	C.0	0.01180	0.00280	0.01460
137	6.85	C.0	0.01170	0.00280	0.01450
138	6.90	0.0	0.01170	0.00290	0.01460
139	6.95	0.0	0.01160	0.00290	0.01450
140	7.00	C.0	0.01150	0.00290	0.01440
141	7.05	C.0	0.01150	0.00290	0.01440
142	7.10	C.0	0.01140	0.00300	0.01440
143	7.15	C.0	0.01140	0.00300	0.01440
144	7.20	0.0	0.01130	0.00300	0.01430
145	7.25	C.0	0.01120	0.00300	0.01420
146	7.30	C.0	0.01120	0.00310	0.01430
147	7.35	C.0	0.01110	0.00310	0.01420
148	7.40	C.0	0.01100	0.00310	0.01410
149	7.45	0.0	0.01100	0.00310	0.01410
150	7.50	C.0	0.01090	0.00310	0.01400
151	7.55	C.0	0.01090	0.00320	0.01410
152	7.60	C.0	0.01080	0.00320	0.01400
153	7.65	0.0	0.01070	0.00320	0.01390
154	7.70	C.0	0.01070	0.00320	0.01390
155	7.75	C.0	0.01060	0.00330	0.01390
156	7.80	C.0	0.01050	0.00330	0.01380
157	7.85	C.0	0.01050	0.00330	0.01380
158	7.90	C.0	0.01040	0.00330	0.01370
159	7.95	0.0	0.01040	0.00340	0.01380
160	8.00	C.0	0.01030	0.00340	0.01370
161	8.05	C.0	0.01030	0.00340	0.01370
162	8.10	0.0	0.01030	0.00340	0.01370
163	8.15	C.0	0.01020	0.00350	0.01370
164	8.20	C.0	0.01020	0.00350	0.01370
165	8.25	C.0	0.01020	0.00350	0.01370
166	8.30	0.0	0.01020	0.00350	0.01370
167	8.35	C.0	0.01010	0.00350	0.01360
168	8.40	C.0	0.01010	0.00360	0.01370
169	8.45	C.0	0.01010	0.00360	0.01370
170	8.50	C.0	0.01010	0.00360	0.01370
171	8.55	0.0	0.01010	0.00360	0.01370
172	8.60	0.0	0.01000	0.00360	0.01360
173	8.65	C.0	0.01000	0.00370	0.01370
174	8.70	C.0	0.01000	0.00370	0.01370
175	8.75	0.0	0.01000	0.00370	0.01370
176	8.80	C.0	0.00990	0.00370	0.01360
177	8.85	C.0	0.00990	0.00370	0.01360
178	8.90	C.0	0.00990	0.00380	0.01370
179	8.95	C.0	0.00990	0.00380	0.01370
180	9.00	C.0	0.00980	0.00380	0.01360
181	9.05	0.0	0.00980	0.00380	0.01360
182	9.10	0.0	0.00980	0.00380	0.01360
183	9.15	C.0	0.00980	0.00390	0.01370
184	9.20	C.0	0.00980	0.00390	0.01370
185	9.25	0.0	0.00970	0.00390	0.01360
186	9.30	C.0	0.00970	0.00390	0.01360

188	9.40	0.0	0.00970	0.00400	0.01370
189	9.45	0.0	0.00960	0.00400	0.01360
190	9.50	0.0	0.00960	0.00400	0.01360
191	9.55	0.0	0.00960	0.00400	0.01360
192	9.60	0.0	0.00960	0.00400	0.01360
193	9.65	0.0	0.00960	0.00410	0.01370
194	9.70	0.0	0.00950	0.00410	0.01360
195	9.75	0.0	0.00950	0.00410	0.01360
196	9.80	0.0	0.00950	0.00410	0.01360
197	9.85	0.0	0.00950	0.00410	0.01360
198	9.90	0.0	0.00940	0.00420	0.01360
199	9.95	0.0	0.00940	0.00420	0.01360
200	10.00	0.0	0.00940	0.00420	0.01360

PHOTON MASS ENERGY ABSORPTION COEFFICIENTS

	PHOTON ENERGY (MEV)	PHOTO ELECTRIC	COMPTON EFFECT	PAIR PRODUCTION	TOTAL
	LEAD				
1	0.05	5.9[illegible]C	0.03770	0.0	9.98770
2	0.10	1.98000	0.01380	0.0	1.99380
3	0.15	1.15100	0.01750	0.0	1.16850
4	0.20	0.59000	0.01970	0.0	0.60970
5	0.25	0.41050	0.02080	0.0	0.43130
6	0.30	0.23100	0.02190	0.0	0.25290
7	0.35	0.17500	0.02220	0.0	0.19720
8	0.40	0.11900	0.02250	0.0	0.14150
9	0.45	0.09570	0.02260	0.0	0.11830
10	0.50	0.07240	0.02280	0.0	0.09520
11	0.55	0.05610	0.02270	0.0	0.07880
12	0.60	0.04830	0.02270	0.0	0.07100
13	0.65	0.04280	0.02250	0.0	0.06530
14	0.70	0.03730	0.02230	0.0	0.05960
15	0.75	0.03180	0.02220	0.0	0.05400
16	0.80	0.02630	0.02200	0.0	0.04830
17	0.85	0.02390	0.02170	0.0	0.04560
18	0.90	0.02160	0.02140	0.0	0.04300
19	0.95	0.01930	0.02110	0.0	0.04040
20	1.00	0.01690	0.02080	0.0	0.03770
21	1.05	0.01600	0.02060	0.0	0.03660
22	1.10	0.01520	0.02050	0.00010	0.03580
23	1.15	0.01430	0.02030	0.00010	0.03470
24	1.20	0.01340	0.02010	0.00020	0.03370
25	1.25	0.01260	0.01990	0.00020	0.03270
26	1.30	0.01170	0.01990	0.00030	0.03190
27	1.35	0.01080	0.01960	0.00030	0.03070
28	1.40	0.00990	0.01940	0.00040	0.02970
29	1.45	0.00910	0.01930	0.00040	0.02880
30	1.50	0.00820	0.01910	0.00050	0.02780
31	1.55	0.00750	0.01890	0.00070	0.02750
32	1.60	0.00760	0.01870	0.00080	0.02710
33	1.65	0.00730	0.01860	0.00090	0.02680
34	1.70	0.00700	0.01840	0.00120	0.02660
35	1.75	0.00660	0.01820	0.00140	0.02620
36	1.80	0.00630	0.01800	0.00160	0.02590
37	1.85	0.00600	0.01780	0.00170	0.02550
38	1.90	0.00570	0.01770	0.00190	0.02530
39	1.95	0.00540	0.01750	0.00210	0.02500
40	2.00	0.00510	0.01730	0.00230	0.02470
41	2.05	0.00480	0.01710	0.00250	0.02440
42	2.10	0.00490	0.01700	0.00280	0.02470
43	2.15	0.00470	0.01680	0.00300	0.02450
44	2.20	0.00460	0.01670	0.00320	0.02450
45	2.25	0.00450	0.01650	0.00340	0.02440
46	2.30	0.00440	0.01630	0.00370	0.02440
47	2.35	0.00430	0.01620	0.00390	0.02440
48	2.40	0.00420	0.01600	0.00410	0.02430
49	2.45	0.00400	0.01590	0.00440	0.02430
50	2.50	0.00390	0.01570	0.00460	0.02420
51	2.55	0.00380	0.01550	0.00480	0.02410
52	2.60	0.00370	0.01540	0.00510	0.02420
53	2.65	0.00360	0.01520	0.00530	0.02410
54	2.70	0.00350	0.01510	0.00550	0.02410

55	2.75	0.00330	0.01490	0.00580	0.02430
56	2.80	0.00320	0.01470	0.00600	0.02390
57	2.85	0.00310	0.01460	0.00620	0.02390
58	2.90	0.00300	0.01440	0.00650	0.02390
59	2.95	0.00290	0.01430	0.00670	0.02390
60	3.00	0.00280	0.01410	0.00690	0.02330
61	3.05	0.00270	0.01400	0.00710	0.02330
62	3.10	0.00270	0.01390	0.00730	0.02390
63	3.15	0.00260	0.01380	0.00760	0.02400
64	3.20	0.00260	0.01370	0.00780	0.02410
65	3.25	0.00250	0.01350	0.00800	0.02400
66	3.30	0.00250	0.01340	0.00820	0.02410
67	3.35	0.00240	0.01330	0.00840	0.02410
68	3.40	0.00240	0.01320	0.00860	0.02420
69	3.45	0.00240	0.01310	0.00880	0.02430
70	3.50	0.00230	0.01300	0.00910	0.02440
71	3.55	0.00230	0.01290	0.00930	0.02450
72	3.60	0.00220	0.01280	0.00950	0.02450
73	3.65	0.00220	0.01270	0.00970	0.02460
74	3.70	0.00210	0.01260	0.00990	0.02460
75	3.75	0.00210	0.01240	0.01010	0.02460
76	3.80	0.00200	0.01230	0.01030	0.02460
77	3.85	0.00200	0.01220	0.01060	0.02480
78	3.90	0.00190	0.01210	0.01080	0.02480
79	3.95	0.00190	0.01200	0.01100	0.02490
80	4.00	0.00190	0.01190	0.01120	0.02500
81	4.05	0.00190	0.01180	0.01140	0.02500
82	4.10	0.00180	0.01170	0.01160	0.02510
83	4.15	0.00180	0.01170	0.01170	0.02520
84	4.20	0.00180	0.01160	0.01190	0.02530
85	4.25	0.00170	0.01150	0.01210	0.02530
86	4.30	0.00170	0.01140	0.01230	0.02540
87	4.35	0.00170	0.01130	0.01250	0.02550
88	4.40	0.00170	0.01130	0.01260	0.02560
89	4.45	0.00160	0.01120	0.01280	0.02560
90	4.50	0.00160	0.01110	0.01300	0.02570
91	4.55	0.00160	0.01100	0.01320	0.02580
92	4.60	0.00160	0.01090	0.01340	0.02590
93	4.65	0.00150	0.01090	0.01350	0.02590
94	4.70	0.00150	0.01080	0.01370	0.02600
95	4.75	0.00150	0.01070	0.01390	0.02610
96	4.80	0.00150	0.01060	0.01410	0.02620
97	4.85	0.00140	0.01050	0.01430	0.02620
98	4.90	0.00140	0.01050	0.01440	0.02630
99	4.95	0.00140	0.01040	0.01460	0.02640
100	5.00	0.00140	0.01030	0.01480	0.02650
101	5.05	0.00140	0.01020	0.01490	0.02650
102	5.10	0.00130	0.01020	0.01510	0.02660
103	5.15	0.00130	0.01010	0.01520	0.02660
104	5.20	0.00130	0.01000	0.01540	0.02670
105	5.25	0.00130	0.01000	0.01550	0.02680
106	5.30	0.00130	0.00990	0.01560	0.02680
107	5.35	0.00130	0.00980	0.01580	0.02690
108	5.40	0.00120	0.00980	0.01590	0.02690
109	5.45	0.00120	0.00970	0.01610	0.02700
110	5.50	0.00120	0.00970	0.01620	0.02710
111	5.55	0.00120	0.00960	0.01630	0.02710
112	5.60	0.00120	0.00950	0.01650	0.02720
113	5.65	0.00120	0.00950	0.01660	0.02730
114	5.70	0.00120	0.00940	0.01680	0.02740
115	5.75	0.00110	0.00930	0.01690	0.02730
116	5.80	0.00110	0.00930	0.01700	0.02740
117	5.85	0.00110	0.00920	0.01720	0.02750
118	5.90	0.00110	0.00910	0.01730	0.02750
119	5.95	0.00110	0.00910	0.01750	0.02770
120	6.00	0.00110	0.00900	0.01760	0.02770

121	6.15	0.00110	0.00900	0.01770	0.02780
122	6.16	0.00110	0.00890	0.01780	0.02780
123	6.15	0.00100	0.00890	0.01790	0.02780
124	6.20	0.00100	0.00830	0.01800	0.02760
125	6.25	0.00100	0.00840	0.01810	0.02790
126	6.30	0.00100	0.00870	0.01820	0.02790
127	6.35	0.00100	0.00870	0.01830	0.02800
128	6.40	0.00100	0.00860	0.01840	0.02800
129	6.45	0.00100	0.00860	0.01850	0.02810
130	6.50	0.00100	0.00860	0.01860	0.02820
131	6.55	0.00100	0.00850	0.01870	0.02820
132	6.60	0.00100	0.00850	0.01880	0.02830
133	6.65	0.00100	0.00840	0.01890	0.02830
134	6.70	0.00100	0.00840	0.01900	0.02840
135	6.75	0.00090	0.00830	0.01910	0.02830
136	6.80	0.00090	0.00830	0.01920	0.02840
137	6.85	0.00090	0.00820	0.01930	0.02840
138	6.90	0.00090	0.00820	0.01940	0.02850
139	6.95	0.00090	0.00810	0.01950	0.02850
140	7.00	0.00090	0.00810	0.01960	0.02860
141	7.05	0.00090	0.00800	0.01980	0.02870
142	7.10	0.00090	0.00800	0.01990	0.02880
143	7.15	0.00090	0.00800	0.02000	0.02890
144	7.20	0.00090	0.00790	0.02010	0.02890
145	7.25	0.00090	0.00790	0.02020	0.02900
146	7.30	0.00090	0.00790	0.02030	0.02900
147	7.35	0.00080	0.00780	0.02040	0.02900
148	7.40	0.00080	0.00770	0.02050	0.02900
149	7.45	0.00080	0.00770	0.02060	0.02910
150	7.50	0.00080	0.00760	0.02070	0.02910
151	7.55	0.00080	0.00760	0.02080	0.02920
152	7.60	0.00080	0.00750	0.02090	0.02920
153	7.65	0.00080	0.00750	0.02100	0.02930
154	7.70	0.00080	0.00750	0.02110	0.02940
155	7.75	0.00080	0.00740	0.02120	0.02940
156	7.80	0.00080	0.00740	0.02130	0.02950
157	7.85	0.00080	0.00730	0.02140	0.02950
158	7.90	0.00080	0.00730	0.02150	0.02960
159	7.95	0.00070	0.00720	0.02160	0.02950
160	8.00	0.00070	0.00720	0.02170	0.02960
161	8.05	0.00070	0.00710	0.02180	0.02960
162	8.10	0.00070	0.00710	0.02190	0.02970
163	8.15	0.00070	0.00710	0.02200	0.02980
164	8.20	0.00070	0.00710	0.02210	0.02990
165	8.25	0.00070	0.00700	0.02220	0.02990
166	8.30	0.00070	0.00700	0.02230	0.03000
167	8.35	0.00070	0.00700	0.02230	0.03000
168	8.40	0.00070	0.00690	0.02240	0.03000
169	8.45	0.00070	0.00690	0.02250	0.03010
170	8.50	0.00070	0.00690	0.02260	0.03020
171	8.55	0.00070	0.00680	0.02270	0.03020
172	8.60	0.00070	0.00680	0.02280	0.03030
173	8.65	0.00070	0.00680	0.02290	0.03040
174	8.70	0.00070	0.00670	0.02300	0.03040
175	8.75	0.00070	0.00670	0.02310	0.03050
176	8.80	0.00070	0.00670	0.02320	0.03060
177	8.85	0.00070	0.00660	0.02330	0.03060
178	8.90	0.00070	0.00660	0.02340	0.03070
179	8.95	0.00070	0.00660	0.02350	0.03080
180	9.00	0.00070	0.00660	0.02350	0.03080
181	9.05	0.00070	0.00650	0.02360	0.03090
182	9.10	0.00060	0.00650	0.02370	0.03090
183	9.15	0.00060	0.00650	0.02380	0.03090
184	9.20	0.00060	0.00640	0.02390	0.03090
185	9.25	0.00060	0.00640	0.02400	0.03100
186	9.30	0.00060	0.00640	0.02410	0.03110

187	9.35	0.00060	0.00630	0.02420	0.03110
188	9.40	0.00060	0.00630	0.02430	0.03120
189	9.45	0.00060	0.00630	0.02440	0.03130
190	9.50	0.00060	0.00620	0.02450	0.03130
191	9.55	0.00060	0.00620	0.02460	0.03140
192	9.60	0.00060	0.00620	0.02470	0.03150
193	9.65	0.00060	0.00610	0.02480	0.03150
194	9.70	0.00060	0.00610	0.02480	0.03150
195	9.75	0.00060	0.00610	0.02490	0.03160
196	9.80	0.00060	0.00610	0.02500	0.03170
197	9.85	0.00060	0.00600	0.02510	0.03170
198	9.90	0.00060	0.00600	0.02520	0.03180
199	9.95	0.00060	0.00600	0.02530	0.03190
200	10.00	0.00060	0.00590	0.02540	0.03190

LIF CAVITY IN LEAD

	ELECTRON ENERGY	STOPPING POWER CAVITY	STOPPING POWER MEDIUM	RELATIVE AVERAGE STOPPING POWER	RANGE (G/CM2)	PHOTON ENERGY	WEIGHT FACTOR	RELATIVE DOSES EXTERNAL	INTERNAL	TOTAL
1	0.05	5.3709	3.0448	2.10266	0.0040	0.05	0.00345	0.0073	0.0041	0.0113
2	0.10	3.3552	2.0029	1.90733	0.0135	0.10	0.01177	0.0225	0.0107	0.0332
3	0.15	2.6433	1.6220	1.79421	0.0265	0.15	0.02313	0.0416	0.0192	0.0608
4	0.20	2.2827	1.4287	1.73998	0.0420	0.20	0.03664	0.0641	0.0389	0.1030
5	0.25	2.0679	1.3140	1.70476	0.0594	0.25	0.05179	0.0893	0.0561	0.1454
6	0.30	1.9277	1.2412	1.67863	0.0782	0.30	0.06823	0.1163	0.0976	0.2139
7	0.35	1.8306	1.1925	1.65775	0.0983	0.35	0.08571	0.1444	0.1247	0.2691
8	0.40	1.7606	1.1590	1.64025	0.1193	0.40	0.10405	0.1748	0.1722	0.3470
9	0.45	1.7087	1.1359	1.62511	0.1412	0.45	0.12309	0.2051	0.2031	0.4082
10	0.50	1.6694	1.1199	1.61170	0.1638	0.50	0.14268	0.2363	0.2486	0.4849
11	0.55	1.6392	1.1091	1.59960	0.1869	0.55	0.16266	0.2677	0.2764	0.5441
12	0.60	1.6157	1.1021	1.58854	0.2106	0.60	0.18287	0.2994	0.3130	0.6124
13	0.65	1.5974	1.0982	1.57833	0.2347	0.65	0.20315	0.3305	0.3295	0.6600
14	0.70	1.5830	1.0964	1.56881	0.2592	0.70	0.22336	0.3614	0.3492	0.7107
15	0.75	1.5717	1.0965	1.55987	0.2841	0.75	0.24336	0.3920	0.3741	0.7661
16	0.80	1.5630	1.0981	1.55144	0.3092	0.80	0.26305	0.4219	0.4043	0.8263
17	0.85	1.5562	1.1007	1.54343	0.3346	0.85	0.28232	0.4506	0.4139	0.8645
18	0.90	1.5510	1.1044	1.53590	0.3602	0.90	0.30112	0.4784	0.4242	0.9026
19	0.95	1.5472	1.1088	1.52856	0.3860	0.95	0.31939	0.5060	0.4363	0.9423
20	1.00	1.5445	1.1138	1.52149	0.4120	1.00	0.33709	0.5319	0.4519	0.9838
21	1.05	1.5427	1.1194	1.51475	0.4381	1.05	0.35420	0.5564	0.4499	1.0064
22	1.10	1.5417	1.1254	1.50825	0.4644	1.10	0.37071	0.5802	0.4430	1.0232
23	1.15	1.5413	1.1318	1.50196	0.4908	1.15	0.38662	0.6028	0.4419	1.0447
24	1.20	1.5415	1.1385	1.49586	0.5172	1.20	0.40194	0.6250	0.4401	1.0651
25	1.25	1.5421	1.1454	1.48995	0.5438	1.25	0.41666	0.6462	0.4388	1.0840
26	1.30	1.5432	1.1527	1.48420	0.5704	1.30	0.43082	0.6651	0.4349	1.1000
27	1.35	1.5445	1.1601	1.47861	0.5971	1.35	0.44441	0.6836	0.4361	1.1197
28	1.40	1.5462	1.1676	1.47315	0.6238	1.40	0.45747	0.7016	0.4366	1.1382
29	1.45	1.5481	1.1753	1.46783	0.6506	1.45	0.47001	0.7185	0.4343	1.1528
30	1.50	1.5502	1.1832	1.46263	0.6774	1.50	0.48205	0.7350	0.4360	1.1709
31	1.55	1.5525	1.1911	1.45755	0.7042	1.55	0.49361	0.7506	0.4272	1.1778
32	1.60	1.5549	1.1992	1.45257	0.7311	1.60	0.50472	0.7652	0.4222	1.1874
33	1.65	1.5575	1.2073	1.44770	0.7579	1.65	0.51539	0.7795	0.4125	1.1920
34	1.70	1.5602	1.2155	1.44292	0.7848	1.70	0.52564	0.7930	0.4048	1.1978
35	1.75	1.5630	1.2237	1.43824	0.8116	1.75	0.53550	0.8060	0.4007	1.2067
36	1.80	1.5661	1.2320	1.43362	0.8385	1.80	0.54498	0.8184	0.3935	1.2119
37	1.85	1.5693	1.2404	1.42904	0.8653	1.85	0.55410	0.8298	0.3882	1.2180
38	1.90	1.5726	1.2487	1.42447	0.8922	1.90	0.56287	0.8411	0.3801	1.2212
39	1.95	1.5762	1.2571	1.41992	0.9190	1.95	0.57132	0.8518	0.3755	1.2273
40	2.00	1.5800	1.2656	1.41540	0.9458	2.00	0.57945	0.8621	0.3695	1.2315
41	2.05	1.5838	1.2743	1.41089	0.9726	2.05	0.58729	0.8717	0.3607	1.2324
42	2.10	1.5882	1.2829	1.40642	0.9993	2.10	0.59485	0.8811	0.3510	1.2321
43	2.15	1.5927	1.2918	1.40197	1.0260	2.15	0.60213	0.8900	0.3459	1.2359
44	2.20	1.5973	1.2995	1.39755	1.0527	2.20	0.60917	0.8983	0.3382	1.2365
45	2.25	1.6019	1.3081	1.39316	1.0793	2.25	0.61595	0.9063	0.3305	1.2368
46	2.30	1.6066	1.3166	1.38880	1.1060	2.30	0.62251	0.9142	0.3218	1.2360
47	2.35	1.6073	1.3251	1.38448	1.1325	2.35	0.62884	0.9215	0.3164	1.2379
48	2.40	1.6081	1.3337	1.38018	1.1591	2.40	0.63496	0.9284	0.3095	1.2379
49	2.45	1.6089	1.3422	1.37592	1.1856	2.45	0.64088	0.9354	0.3030	1.2384
50	2.50	1.6098	1.3508	1.37170	1.2120	2.50	0.64661	0.9418	0.2964	1.2382
51	2.55	1.6107	1.3593	1.36751	1.2384	2.55	0.65215	0.9479	0.2916	1.2395
52	2.60	1.6116	1.3679	1.36335	1.2648	2.60	0.65752	0.9539	0.2845	1.2384
53	2.65	1.6126	1.3764	1.35922	1.2911	2.65	0.66271	0.9595	0.2785	1.2380
54	2.70	1.6136	1.3850	1.35513	1.3173	2.70	0.66775	0.9648	0.2730	1.2378
55	2.75	1.6146	1.3935	1.35108	1.3436	2.75	0.67263	0.9703	0.2687	1.2391

56	2.50	1.5754	1.4021	1.34736	1.3697	2.80	0.67737	0.9753	0.2632	1.2385
57	2.55	1.5767	1.4105	1.34307	1.3958	2.85	0.68196	0.9799	0.2582	1.2381
58	2.60	1.5777	1.4191	1.33911	1.4219	2.90	0.68642	0.9847	0.2519	1.2366
59	2.65	1.5788	1.4277	1.33519	1.4479	2.95	0.69075	0.9890	0.2484	1.2374
60	3.00	1.5799	1.4362	1.33136	1.4739	3.00	0.69577	0.9943	0.2429	1.2372
61	3.05	1.5811	1.4448	1.32745	1.5105	3.05	0.70071	0.9995	0.2377	1.2372
62	3.10	1.5822	1.4533	1.32363	1.5370	3.10	0.70474	1.0032	0.2335	1.2367
63	3.15	1.5833	1.4618	1.31984	1.5635	3.15	0.70866	1.0071	0.2282	1.2354
64	3.20	1.5845	1.4703	1.31608	1.5900	3.20	0.71249	1.0105	0.2219	1.2324
65	3.25	1.5857	1.4788	1.31235	1.6165	3.25	0.71620	1.0141	0.2199	1.2340
66	3.30	1.5868	1.4873	1.30866	1.6430	3.30	0.71983	1.0172	0.2151	1.2323
67	3.35	1.5880	1.4958	1.30499	1.6695	3.35	0.72337	1.0204	0.2112	1.2316
68	3.40	1.5892	1.5043	1.30136	1.6960	3.40	0.72682	1.0233	0.2066	1.2298
69	3.45	1.5904	1.5128	1.29776	1.7225	3.45	0.73019	1.0260	0.2032	1.2292
70	3.50	1.5916	1.5213	1.29418	1.7490	3.50	0.73348	1.0291	0.1977	1.2268
71	3.55	1.5928	1.5298	1.29064	1.7755	3.55	0.73669	1.0316	0.1935	1.2251
72	3.60	1.5940	1.5383	1.28713	1.8020	3.60	0.73982	1.0342	0.1912	1.2254
73	3.65	1.5953	1.5467	1.28364	1.8285	3.65	0.74298	1.0366	0.1871	1.2237
74	3.70	1.5965	1.5552	1.28019	1.8550	3.70	0.74587	1.0390	0.1839	1.2229
75	3.75	1.5977	1.5637	1.27676	1.8815	3.75	0.74880	1.0413	0.1818	1.2230
76	3.80	1.5989	1.5721	1.27336	1.9080	3.80	0.75165	1.0435	0.1787	1.2222
77	3.85	1.6002	1.5806	1.26998	1.9345	3.85	0.75445	1.0457	0.1733	1.2190
78	3.90	1.6014	1.5890	1.26664	1.9610	3.90	0.75718	1.0478	0.1713	1.2191
79	3.95	1.6027	1.5974	1.26332	1.9875	3.95	0.75985	1.0496	0.1678	1.2174
80	4.00	1.6039	1.6059	1.26003	2.0140	4.00	0.76246	1.0514	0.1644	1.2157
81	4.05	1.6051	1.6143	1.25676	2.0405	4.05	0.76502	1.0532	0.1617	1.2149
82	4.10	1.6064	1.6227	1.25352	2.0670	4.10	0.76753	1.0548	0.1593	1.2141
83	4.15	1.6076	1.6312	1.25031	2.0935	4.15	0.76998	1.0561	0.1561	1.2121
84	4.20	1.6089	1.6396	1.24711	2.1200	4.20	0.77238	1.0575	0.1529	1.2105
85	4.25	1.6101	1.6480	1.24395	2.1465	4.25	0.77473	1.0591	0.1514	1.2105
86	4.30	1.6114	1.6564	1.24081	2.1730	4.30	0.77704	1.0605	0.1492	1.2097
87	4.35	1.6126	1.6648	1.23769	2.1995	4.35	0.77930	1.0617	0.1463	1.2080
88	4.40	1.6139	1.6732	1.23460	2.2260	4.40	0.78151	1.0627	0.1442	1.2069
89	4.45	1.6151	1.6816	1.23153	2.2525	4.45	0.78368	1.0640	0.1420	1.2060
90	4.50	1.6163	1.6900	1.22848	2.2790	4.50	0.78581	1.0652	0.1392	1.2043
91	4.55	1.6176	1.6984	1.22546	2.3055	4.55	0.78789	1.0662	0.1365	1.2027
92	4.60	1.6188	1.7067	1.22246	2.3320	4.60	0.78994	1.0672	0.1346	1.2019
93	4.65	1.6201	1.7151	1.21949	2.3585	4.65	0.79195	1.0681	0.1325	1.2006
94	4.70	1.6213	1.7235	1.21652	2.3850	4.70	0.79392	1.0690	0.1300	1.1990
95	4.75	1.6226	1.7319	1.21359	2.4115	4.75	0.79585	1.0699	0.1283	1.1982
96	4.80	1.6238	1.7402	1.21068	2.4380	4.80	0.79775	1.0707	0.1266	1.1973
97	4.85	1.6251	1.7486	1.20779	2.4645	4.85	0.79961	1.0717	0.1247	1.1964
98	4.90	1.6263	1.7569	1.20491	2.4910	4.90	0.80144	1.0722	0.1223	1.1945
99	4.95	1.6275	1.7653	1.20206	2.5175	4.95	0.80324	1.0729	0.1207	1.1936
100	5.00	1.6288	1.7736	1.19923	2.5440	5.00	0.80500	1.0736	0.1185	1.1920
101	5.05	1.6300	1.7820	1.19642	2.5705	5.05	0.80673	1.0741	0.1167	1.1908
102	5.10	1.6312	1.7903	1.19363	2.5970	5.10	0.80844	1.0747	0.1159	1.1907
103	5.15	1.6325	1.7987	1.19087	2.6235	5.15	0.81011	1.0751	0.1142	1.1894
104	5.20	1.6337	1.8070	1.18811	2.6500	5.20	0.81175	1.0757	0.1121	1.1878
105	5.25	1.6349	1.8154	1.18538	2.6765	5.25	0.81337	1.0759	0.1100	1.1859
106	5.30	1.6362	1.8237	1.18267	2.7030	5.30	0.81496	1.0762	0.1098	1.1860
107	5.35	1.6374	1.8320	1.17998	2.7295	5.35	0.81652	1.0767	0.1078	1.1844
108	5.40	1.6386	1.8403	1.17730	2.7560	5.40	0.81806	1.0770	0.1062	1.1832
109	5.45	1.6399	1.8487	1.17464	2.7825	5.45	0.81957	1.0774	0.1049	1.1823
110	5.50	1.6411	1.8570	1.17201	2.8090	5.50	0.82105	1.0774	0.1037	1.1811
111	5.55	1.6423	1.8653	1.16938	2.8355	5.55	0.82251	1.0776	0.1022	1.1798
112	5.60	1.6435	1.8736	1.16678	2.8620	5.60	0.82395	1.0779	0.1010	1.1789
113	5.65	1.6447	1.8819	1.16420	2.8885	5.65	0.82537	1.0779	0.0992	1.1771
114	5.70	1.6459	1.8903	1.16163	2.9150	5.70	0.82676	1.0782	0.0980	1.1762
115	5.75	1.6472	1.8986	1.15907	2.9415	5.75	0.82813	1.0785	0.0970	1.1755
116	5.80	1.6484	1.9069	1.15654	2.9680	5.80	0.82948	1.0784	0.0958	1.1742
117	5.85	1.6496	1.9152	1.15402	2.9945	5.85	0.83081	1.0786	0.0947	1.1734
118	5.90	1.6508	1.9235	1.15152	3.0210	5.90	0.83212	1.0787	0.0934	1.1721
119	5.95	1.6520	1.9319	1.14903	3.0475	5.95	0.83340	1.0786	0.0920	1.1706
120	6.00	1.6532	1.9401	1.14656	3.0740	6.00	0.83467	1.0786	0.0907	1.1694
121	6.05	1.6544	1.9484	1.14411	3.1005	6.05	0.83592	1.0784	0.0897	1.1691

122	6.10	1.6953	1.9567	1.14167	3.1270	6.10	0.83715	1.0784	0.0890	1.1675
123	6.15	1.6993	1.9650	1.13925	3.1535	6.15	0.83836	1.0784	0.0878	1.1662
124	6.20	1.7033	1.9733	1.13684	3.1800	6.20	0.83956	1.0784	0.0866	1.1649
125	6.25	1.7072	1.9816	1.13445	3.2065	6.25	0.84074	1.0781	0.0856	1.1637
126	6.30	1.7112	1.9898	1.13207	3.2330	6.30	0.84190	1.0780	0.0850	1.1630
127	6.35	1.7151	1.9981	1.12971	3.2595	6.35	0.84304	1.0777	0.0841	1.1618
128	6.40	1.7191	2.0064	1.12736	3.2860	6.40	0.84417	1.0776	0.0829	1.1605
129	6.45	1.7230	2.0147	1.12503	3.3125	6.45	0.84529	1.0772	0.0815	1.1587
130	6.50	1.7269	2.0230	1.12271	3.3390	6.50	0.84637	1.0769	0.0812	1.1581
131	6.55	1.7308	2.0313	1.12040	3.3655	6.55	0.84745	1.0767	0.0801	1.1568
132	6.60	1.7347	2.0395	1.11811	3.3920	6.60	0.84852	1.0764	0.0787	1.1550
133	6.65	1.7387	2.0478	1.11584	3.4185	6.65	0.84957	1.0762	0.0781	1.1543
134	6.70	1.7426	2.0561	1.11357	3.4450	6.70	0.85060	1.0758	0.0773	1.1531
135	6.75	1.7711	2.0644	1.11132	3.4715	6.75	0.85162	1.0758	0.0771	1.1529
136	6.80	1.7722	2.0727	1.10909	3.4980	6.80	0.85263	1.0754	0.0758	1.1511
137	6.85	1.7734	2.0809	1.10686	3.5245	6.85	0.85363	1.0752	0.0747	1.1499
138	6.90	1.7746	2.0892	1.10465	3.5510	6.90	0.85461	1.0747	0.0745	1.1492
139	6.95	1.7758	2.0975	1.10246	3.5775	6.95	0.85558	1.0745	0.0735	1.1480
140	7.00	1.7769	2.1057	1.10027	3.6040	7.00	0.85653	1.0740	0.0722	1.1462
141	7.05	1.7781	2.1140	1.09810	3.6305	7.05	0.85747	1.0739	0.0715	1.1454
142	7.10	1.7793	2.1223	1.09594	3.6570	7.10	0.85840	1.0734	0.0708	1.1442
143	7.15	1.7804	2.1306	1.09380	3.6835	7.15	0.85932	1.0728	0.0701	1.1429
144	7.20	1.7816	2.1388	1.09166	3.7100	7.20	0.86023	1.0726	0.0692	1.1417
145	7.25	1.7828	2.1471	1.08954	3.7365	7.25	0.86112	1.0720	0.0680	1.1400
146	7.30	1.7839	2.1554	1.08743	3.7630	7.30	0.86201	1.0717	0.0690	1.1398
147	7.35	1.7851	2.1636	1.08534	3.7895	7.35	0.86288	1.0714	0.0671	1.1386
148	7.40	1.7862	2.1719	1.08325	3.8160	7.40	0.86374	1.0711	0.0663	1.1374
149	7.45	1.7874	2.1802	1.08118	3.8425	7.45	0.86459	1.0706	0.0656	1.1362
150	7.50	1.7885	2.1884	1.07912	3.8690	7.50	0.86543	1.0702	0.0647	1.1350
151	7.55	1.7897	2.1967	1.07706	3.8955	7.55	0.86626	1.0697	0.0646	1.1342
152	7.60	1.7908	2.2049	1.07503	3.9220	7.60	0.86708	1.0693	0.0637	1.1330
153	7.65	1.7920	2.2132	1.07300	3.9485	7.65	0.86789	1.0687	0.0627	1.1314
154	7.70	1.7931	2.2215	1.07098	3.9750	7.70	0.86869	1.0681	0.0621	1.1302
155	7.75	1.7943	2.2297	1.06898	4.0015	7.75	0.86948	1.0678	0.0617	1.1295
156	7.80	1.7954	2.2380	1.06698	4.0280	7.80	0.87026	1.0672	0.0607	1.1279
157	7.85	1.7966	2.2463	1.06500	4.0545	7.85	0.87103	1.0668	0.0603	1.1271
158	7.90	1.7977	2.2545	1.06303	4.0810	7.90	0.87180	1.0662	0.0593	1.1255
159	7.95	1.7989	2.2628	1.06106	4.1075	7.95	0.87255	1.0660	0.0596	1.1257
160	8.00	1.8000	2.2710	1.05911	4.1340	8.00	0.87330	1.0654	0.0586	1.1241
161	8.05	1.8011	2.2793	1.05717	4.1605	8.05	0.87403	1.0650	0.0583	1.1233
162	8.10	1.8023	2.2876	1.05524	4.1870	8.10	0.87476	1.0644	0.0578	1.1221
163	8.15	1.8034	2.2958	1.05332	4.2135	8.15	0.87548	1.0637	0.0572	1.1210
164	8.20	1.8045	2.3041	1.05141	4.2400	8.20	0.87619	1.0631	0.0567	1.1198
165	8.25	1.8057	2.3123	1.04951	4.2665	8.25	0.87689	1.0627	0.0564	1.1191
166	8.30	1.8068	2.3206	1.04762	4.2930	8.30	0.87759	1.0620	0.0559	1.1179
167	8.35	1.8079	2.3289	1.04574	4.3195	8.35	0.87828	1.0612	0.0552	1.1164
168	8.40	1.8090	2.3371	1.04387	4.3460	8.40	0.87896	1.0608	0.0553	1.1161
169	8.45	1.8102	2.3454	1.04201	4.3725	8.45	0.87963	1.0602	0.0548	1.1149
170	8.50	1.8113	2.3536	1.04015	4.3990	8.50	0.88029	1.0595	0.0543	1.1138
171	8.55	1.8124	2.3619	1.03831	4.4255	8.55	0.88095	1.0590	0.0540	1.1130
172	8.60	1.8135	2.3701	1.03648	4.4520	8.60	0.88160	1.0584	0.0531	1.1115
173	8.65	1.8146	2.3784	1.03466	4.4785	8.65	0.88224	1.0577	0.0531	1.1107
174	8.70	1.8158	2.3867	1.03284	4.5050	8.70	0.88288	1.0572	0.0528	1.1100
175	8.75	1.8169	2.3949	1.03104	4.5315	8.75	0.88351	1.0565	0.0523	1.1088
176	8.80	1.8180	2.4032	1.02924	4.5580	8.80	0.88413	1.0558	0.0515	1.1073
177	8.85	1.8191	2.4114	1.02746	4.5845	8.85	0.88475	1.0554	0.0512	1.1066
178	8.90	1.8202	2.4197	1.02568	4.6110	8.90	0.88536	1.0547	0.0512	1.1059
179	8.95	1.8213	2.4280	1.02391	4.6375	8.95	0.88596	1.0540	0.0507	1.1047
180	9.00	1.8224	2.4362	1.02215	4.6640	9.00	0.88656	1.0532	0.0501	1.1032
181	9.05	1.8236	2.4445	1.02040	4.6905	9.05	0.88715	1.0527	0.0498	1.1025
182	9.10	1.8247	2.4528	1.01866	4.7170	9.10	0.88773	1.0522	0.0496	1.1018
183	9.15	1.8258	2.4610	1.01692	4.7435	9.15	0.88831	1.0515	0.0495	1.1010
184	9.20	1.8269	2.4693	1.01520	4.7700	9.20	0.88889	1.0510	0.0493	1.1003
185	9.25	1.8280	2.4775	1.01349	4.7965	9.25	0.88945	1.0503	0.0485	1.0988
186	9.30	1.8291	2.4858	1.01178	4.8230	9.30	0.89001	1.0496	0.0481	1.0977
187	9.35	1.8302	2.4941	1.01007	4.8495	9.35	0.89057	1.0491	0.0479	1.0970

188	9.40	1.7313	2.5023	1.CC838	4.8760	9.40	0.89112	1.0484	0.0478	1.0962
189	9.45	1.7324	2.5186	1.CC870	4.9025	9.45	0.89166	1.0476	0.0471	1.0947
190	9.50	1.7335	2.5189	1.CC502	4.9290	9.50	0.89220	1.0472	0.0468	1.0940
191	9.55	1.7346	2.5271	1.CC336	4.9555	9.55	0.89274	1.0464	0.0465	1.0929
192	9.60	1.7357	2.5354	1.CC170	4.9820	9.60	0.89326	1.0457	0.0461	1.0918
193	9.65	1.7368	2.5436	1.CC004	5.0085	9.65	0.89379	1.0452	0.0462	1.0914
194	9.70	1.7379	2.5519	C.99840	5.0350	9.70	0.89431	1.0444	0.0456	1.0900
195	9.75	1.7389	2.5602	C.99676	5.0615	9.75	0.89482	1.0436	0.0453	1.0889
196	9.80	1.7400	2.5684	C.99514	5.0880	9.80	0.89533	1.0429	0.0449	1.0878
197	9.85	1.7411	2.5767	C.99351	5.1145	9.85	0.89583	1.0424	0.0447	1.0871
198	9.90	1.7422	2.5850	C.99190	5.1410	9.90	0.89633	1.0416	0.0443	1.0860
199	9.95	1.7433	2.5932	C.99030	5.1675	9.95	0.89682	1.0409	0.0440	1.0849
200	10.00	1.7444	2.6015	C.98870	5.1940	10.00	0.89731	1.0404	0.0438	1.0842

IF CAVITY IN LEAD

FOR THE PHOTON SPECTRUM - MONOENERGETIC PHOTONS AT 0.15 MEV				BURLIN/S FACTOR = 0.0608
CAVITY DOSE	0.533E-03	SLEEVE DOSE	0.876E-02	
FOR THE PHOTON SPECTRUM - MONOENERGETIC PHOTONS AT 0.25 MEV				BURLIN/S FACTOR = 0.1454
CAVITY DOSE	0.784E-03	SLEEVE DOSE	0.539E-02	
FOR THE PHOTON SPECTRUM - MONOENERGETIC PHOTONS AT 0.4 MEV				BURLIN/S FACTOR = 0.3470
CAVITY DOSE	0.982E-03	SLEEVE DOSE	0.283E-02	
FOR THE PHOTON SPECTRUM - MONOENERGETIC PHOTONS AT 0.6 MEV				BURLIN/S FACTOR = 0.6124
CAVITY DOSE	0.130E-02	SLEEVE DOSE	0.213E-02	
FOR THE PHOTON SPECTRUM - MONOENERGETIC PHOTONS AT 1.0 MEV				BURLIN/S FACTOR = 0.9838
CAVITY DOSE	0.185E-02	SLEEVE DOSE	0.188E-02	
FOR THE PHOTON SPECTRUM - MONOENERGETIC PHOTONS AT 1.5 MEV				BURLIN/S FACTOR = 1.1709
CAVITY DOSE	0.244E-02	SLEEVE DOSE	0.208E-02	
FOR THE PHOTON SPECTRUM - PURE CO-60 SPECTRUM				BURLIN/S FACTOR = 1.0829
CAVITY DOSE	0.220E-02	SLEEVE DOSE	0.203E-02	
FOR THE PHOTON SPECTRUM - CO-60 SOURCE SPECTRUM				BURLIN/S FACTOR = 0.8624
CAVITY DOSE	0.692E-01	SLEEVE DOSE	0.802E-01	
FOR THE PHOTON SPECTRUM - LMFBR P. ROSE				BURLIN/S FACTOR = 0.8819
CAVITY DOSE	0.459E-01	SLEEVE DOSE	0.521E-01	
FOR THE PHOTON SPECTRUM - ZPPR SIMONS + HUNTSMAN				BURLIN/S FACTOR = 1.0514
CAVITY DOSE	0.545E-01	SLEEVE DOSE	0.518E-01	
FOR THE PHOTON SPECTRUM - ZPR-6-6 R. GOLD				BURLIN/S FACTOR = 0.6096
CAVITY DOSE	0.307E-01	SLEEVE DOSE	0.503E-01	
FOR THE PHOTON SPECTRUM - FISSION SOURCE MAIENSCHEIN + PEELLE				BURLIN/S FACTOR = 0.3372
CAVITY DOSE	0.278E-01	SLEEVE DOSE	0.825E-01	
FOR THE PHOTON SPECTRUM - GOLD-198 (0.41)				BURLIN/S FACTOR = 0.3587
CAVITY DOSE	0.100E-02	SLEEVE DOSE	0.280E-02	
FOR THE PHOTON SPECTRUM - CESIUM-137 (0.66)				BURLIN/S FACTOR = 0.6720
CAVITY DOSE	0.142E-02	SLEEVE DOSE	0.211E-02	
FOR THE PHOTON SPECTRUM - COBALT-60 (AVERAGE, 1.25)				BURLIN/S FACTOR = 1.0840

CAVITY DOSE	0.222E-02	SLEEVE DOSE	0.204E-02	
FOR THE PHOTON SPECTRUM - MITR BTF		POSITIONS 1-6 (ANISN)		BURLIN/S FACTOR = 0.8756
CAVITY DOSE	0.484E-01	SLEEVE DOSE	0.553E-01	
FOR THE PHOTON SPECTRUM - MITR BTF		POSITIONS 7-8 (ANISN)		BURLIN/S FACTOR = 0.9031
CAVITY DOSE	0.502E-01	SLEEVE DOSE	0.556E-01	
FOR THE PHOTON SPECTRUM - MITR BTF		POSITION 9 (ANISN)		BURLIN/S FACTOR = 0.8956
CAVITY DOSE	0.516E-01	SLEEVE DOSE	0.576E-01	
FOR THE PHOTON SPECTRUM - MITR BTF		POSITION 10 (ANISN)		BURLIN/S FACTOR = 0.6150
CAVITY DOSE	0.505E-01	SLEEVE DOSE	0.822E-01	
FOR THE PHOTON SPECTRUM - MITR BTF		POSITION 11 (ANISN)		BURLIN/S FACTOR = 0.6674
CAVITY DOSE	0.673E-01	SLEEVE DOSE	0.101E+00	
FOR THE PHOTON SPECTRUM - MITR BTF		POSITIONS 12-17 (ANISN)		BURLIN/S FACTOR = 0.7051
CAVITY DOSE	0.748E-01	SLEEVE DOSE	0.106E+00	

D.2. INTERP Sample Problem

INTERP is a small program written at M.I.T. which merely interpolates and punches the mass energy absorption coefficients in a suitable format for input to RESPOND. For the modified version of RESPOND, mass energy absorption coefficients at 200 points between 0.05 and 10.0 MEV are required as input. INTERP provided this data using a simple linear interpolation of the values given for the photoelectric effect, the compton effect, and pair production mass energy absorption coefficients given in the document "Photon Cross Sections from 0.001 to 100 MEV for Elements 1 through 100", LA-3753, (1967).

```
C      INTERPOLATE                                                        SUB10001
C      AUTHOR: PAUL A. SCHEINERT                                          SUB10002
C                                                                         SUB10003
       DIMENSION ENERGY(200),DAT1(200),DAT2(200),EE(200),TITLE(12)        SUB10004
C                                                                         SUB10005
       DO 5 I=1,200                                                       SUB10006
       ENERGY(I)=0.0                                                      SUB10007
       DAT1(I)=0.0                                                        SUB10008
       DAT2(I)=0.0                                                        SUB10009
       EE(I)=0.05*I                                                       SUB10010
     5 CONTINUE                                                           SUB10011
C                                                                         SUB10012
    40 READ (5,2,END=999) TITLE,N                                         SUB10013
     2 FORMAT (12A4,12X,I5)                                               SUB10014
       READ (5,3) (ENERGY(I),I=1,N)                                       SUB10015
       READ (5,3) (DAT2(I),I=1,N)                                         SUB10016
     3 FORMAT (12F6.0)                                                    SUB10017
C                                                                         SUB10018
       DO 10 I=1,200                                                      SUB10019
       EGG=I*0.05                                                         SUB10020
       DO 20 J=1,N                                                        SUB10021
       IF (ENERGY(J)-EGG) 15,16,15                                        SUB10022
    15 JJ=J+1.0                                                           SUB10023
       IF (ENERGY(JJ)-EGG) 20,19,17                                       SUB10024
    20 CONTINUE                                                           SUB10025
    16 DAT1(I)=DAT2(J)                                                    SUB10026
       GO TO 10                                                           SUB10027
    19 DAT1(I)=DAT2(JJ)                                                   SUB10028
       GO TO 10                                                           SUB10029
    17 DIF=ENERGY(JJ)-ENERGY(J)                                           SUB10030
       DIFF=EGG-ENERGY(J)                                                 SUB10031
       FRACT=DIFF/DIF                                                     SUB10032
       REMAIN=DAT2(JJ)-DAT2(J)                                            SUB10033
       DAT1(I)=FRACT*REMAIN+DAT2(J)                                       SUB10034
    10 CONTINUE                                                           SUB10035
C                                                                         SUB10036
```

```
      WRITE (6,24) TITLE                                                SUB10037
   24 FORMAT ('1'/10X,12A4/)                                            SUB10038
C                                                                       SUB10039
      DO 30 II=1,200,10                                                 SUB10040
      KK=II+9                                                           SUB10041
      WRITE (6,21) (EE(I),I=II,KK)                                      SUB10042
   21 FORMAT (1X/4X,'ENERGY',10X,10(4X,F4.2,2X))                        SUB10043
      WRITE (6,22) (DAT1(I),I=II,KK)                                    SUB10044
   22 FORMAT (4X,'COEFFICIENT',5X,10(2X,F8.4))                          SUB10045
   30 CONTINUE                                                          SUB10046
      DO 50 II=1,181,12                                                 SUB10047
      KK=II+11                                                          SUB10048
      PUNCH 25, (DAT1(I),I=II,KK)                                       SUB10049
   25 FORMAT (12F6.4)                                                   SUB10050
   50 CONTINUE                                                          SUB10051
      PUNCH 26, (DAT1(I),I=193,200)                                     SUB10052
   26 FORMAT (8F6.4)                                                    SUB10053
C                                                                       SUB10054
C     THIS COMPLETES CALCULATION FOR ONE CASE                           SUB10055
C                                                                       SUB10056
      GO TO 40                                                          SUB10057
  999 STOP                                                              SUB10058
      END                                                               SUB10059
```

```
0.05  0.06  0.08  0.1   0.15  0.2   0.3   0.4   0.5   0.6   0.8   1.0
1.5   2.0   3.0   4.0   5.0   6.0   8.0   10.0
  5.01  3.41  3.01  2.15 0.957 0.491 0.1850.09210.05470.03600.01920.0122
.00593.00360.00197.00131.00097.00077.00054.00041
COMPTON EFFECT ENERGY ABS. COEFF. FOR TUNGSTEN                    20
0.05  0.06  0.08  0.1   0.15  0.2   0.3   0.4   0.5   0.6   0.8   1.0
1.5   2.0   3.0   4.0   5.0   6.0   8.0   10.0
.00799.009570.01210.01420.01800.02010.02230.02310.02320.02320.02260.0212
0.01960.01760.01450.01240.0106.00934.00747.00619
PAIR PROD. ENERGY ABS. COEFF. FOR TUNGSTEN                        20
0.05  0.06  0.08  0.1   0.15  0.2   0.3   0.4   0.5   0.6   0.8   1.0
1.5   2.0   3.0   4.0   5.0   6.0   8.0   10.0

.00041.00200.006260.01030.01380.01650.02080.0242
```

PHOTO-ELECTRIC ENERGY ABS. COEFF. FOR TUNGSTEN

ENERGY	0.05	0.10	0.15	0.20	0.25	0.30	0.35	0.40	0.45	0.50
COEFFICIENT	5.0100	2.1500	0.5570	0.4910	0.3380	0.1850	0.1386	0.0921	0.0734	0.0547
ENERGY	0.55	0.60	0.65	0.70	0.75	0.80	0.85	0.90	0.95	1.00
COEFFICIENT	0.0454	0.0360	0.0318	0.0276	0.0234	0.0192	0.0175	0.0157	0.0140	0.0122
ENERGY	1.05	1.10	1.15	1.20	1.25	1.30	1.35	1.40	1.45	1.50
COEFFICIENT	0.0116	0.0109	0.0103	0.0097	0.0091	0.0084	0.0078	0.0072	0.0066	0.0059
ENERGY	1.55	1.60	1.65	1.70	1.75	1.80	1.85	1.90	1.95	2.00
COEFFICIENT	0.0057	0.0055	0.0052	0.0050	0.0048	0.0045	0.0043	0.0041	0.0038	0.0036
ENERGY	2.05	2.10	2.15	2.20	2.25	2.30	2.35	2.40	2.45	2.50
COEFFICIENT	0.0035	0.0034	0.0034	0.0033	0.0032	0.0031	0.0030	0.0029	0.0029	0.0028
ENERGY	2.55	2.60	2.65	2.70	2.75	2.80	2.85	2.90	2.95	3.00
COEFFICIENT	0.0027	0.0026	0.0025	0.0025	0.0024	0.0023	0.0022	0.0021	0.0021	0.0020
ENERGY	3.05	3.10	3.15	3.20	3.25	3.30	3.35	3.40	3.45	3.50
COEFFICIENT	0.0019	0.0019	0.0019	0.0018	0.0018	0.0018	0.0017	0.0017	0.0017	0.0016
ENERGY	3.55	3.60	3.65	3.70	3.75	3.80	3.85	3.90	3.95	4.00
COEFFICIENT	0.0016	0.0016	0.0015	0.0015	0.0015	0.0014	0.0014	0.0014	0.0013	0.0013
ENERGY	4.05	4.10	4.15	4.20	4.25	4.30	4.35	4.40	4.45	4.50
COEFFICIENT	0.0013	0.0013	0.0013	0.0012	0.0012	0.0012	0.0012	0.0012	0.0012	0.0011
ENERGY	4.55	4.60	4.65	4.70	4.75	4.80	4.85	4.90	4.95	5.00
COEFFICIENT	0.0011	0.0011	0.0011	0.0011	0.0011	0.0010	0.0010	0.0010	0.0010	0.0010
ENERGY	5.05	5.10	5.15	5.20	5.25	5.30	5.35	5.40	5.45	5.50
COEFFICIENT	0.0010	0.0010	0.0009	0.0009	0.0009	0.0009	0.0009	0.0009	0.0009	0.0009
ENERGY	5.55	5.60	5.65	5.70	5.75	5.80	5.85	5.90	5.95	6.00
COEFFICIENT	0.0009	0.0008	0.0008	0.0008	0.0008	0.0008	0.0008	0.0008	0.0008	0.0008
ENERGY	6.05	6.10	6.15	6.20	6.25	6.30	6.35	6.40	6.45	6.50
COEFFICIENT	0.0008	0.0008	0.0008	0.0007	0.0007	0.0007	0.0007	0.0007	0.0007	0.0007
ENERGY	6.55	6.60	6.65	6.70	6.75	6.80	6.85	6.90	6.95	7.00
COEFFICIENT	0.0007	0.0007	0.0007	0.0007	0.0007	0.0007	0.0007	0.0007	0.0007	0.0007
ENERGY	7.05	7.10	7.15	7.20	7.25	7.30	7.35	7.40	7.45	7.50
COEFFICIENT	0.0006	0.0006	0.0006	0.0006	0.0006	0.0006	0.0006	0.0006	0.0006	0.0006
ENERGY	7.55	7.60	7.65	7.70	7.75	7.80	7.85	7.90	7.95	8.00
COEFFICIENT	0.0006	0.0006	0.0006	0.0006	0.0006	0.0006	0.0006	0.0006	0.0005	0.0005
ENERGY	8.05	8.10	8.15	8.20	8.25	8.30	8.35	8.40	8.45	8.50
COEFFICIENT	0.0005	0.0005	0.0005	0.0005	0.0005	0.0005	0.0005	0.0005	0.0005	0.0005
ENERGY	8.55	8.60	8.65	8.70	8.75	8.80	8.85	8.90	8.95	9.00
COEFFICIENT	0.0005	0.0005	0.0005	0.0005	0.0005	0.0005	0.0005	0.0005	0.0005	0.0005
ENERGY	9.05	9.10	9.15	9.20	9.25	9.30	9.35	9.40	9.45	9.50
COEFFICIENT	0.0005	0.0005	0.0005	0.0005	0.0005	0.0005	0.0005	0.0004	0.0004	0.0004
ENERGY	9.55	9.60	9.65	9.70	9.75	9.80	9.85	9.90	9.95	****
COEFFICIENT	0.0004	0.0004	0.0004	0.0004	0.0004	0.0004	0.0004	0.0004	0.0004	0.0004

COMPTON EFFECT ENERGY ABS. COEFF. FOR TUNGSTEN

ENERGY	0.05	0.10	0.15	0.20	0.25	0.30	0.35	0.40	0.45	0.50
COEFFICIENT	0.0080	0.0142	0.0180	0.0201	0.0212	0.0223	0.0227	0.0231	0.0232	0.0232
ENERGY	0.55	0.60	0.65	0.70	0.75	0.80	0.85	0.90	0.95	1.00
COEFFICIENT	0.0232	0.0232	0.0230	0.0229	0.0227	0.0226	0.0222	0.0219	0.0215	0.0212
ENERGY	1.05	1.10	1.15	1.20	1.25	1.30	1.35	1.40	1.45	1.50
COEFFICIENT	0.0210	0.0209	0.0207	0.0206	0.0204	0.0202	0.0201	0.0199	0.0198	0.0196
ENERGY	1.55	1.60	1.65	1.70	1.75	1.80	1.85	1.90	1.95	2.00
COEFFICIENT	0.0194	0.0192	0.0190	0.0188	0.0186	0.0184	0.0182	0.0180	0.0178	0.0176
ENERGY	2.05	2.10	2.15	2.20	2.25	2.30	2.35	2.40	2.45	2.50
COEFFICIENT	0.0174	0.0173	0.0171	0.0170	0.0168	0.0167	0.0165	0.0164	0.0162	0.0160
ENERGY	2.55	2.60	2.65	2.70	2.75	2.80	2.85	2.90	2.95	3.00
COEFFICIENT	0.0159	0.0157	0.0156	0.0154	0.0153	0.0151	0.0150	0.0148	0.0147	0.0145
ENERGY	3.05	3.10	3.15	3.20	3.25	3.30	3.35	3.40	3.45	3.50
COEFFICIENT	0.0144	0.0143	0.0142	0.0141	0.0140	0.0139	0.0138	0.0137	0.0136	0.0135
ENERGY	3.55	3.60	3.65	3.70	3.75	3.80	3.85	3.90	3.95	4.00
COEFFICIENT	0.0133	0.0132	0.0131	0.0130	0.0129	0.0128	0.0127	0.0126	0.0125	0.0124
ENERGY	4.05	4.10	4.15	4.20	4.25	4.30	4.35	4.40	4.45	4.50
COEFFICIENT	0.0123	0.0122	0.0121	0.0120	0.0120	0.0119	0.0118	0.0117	0.0116	0.0115
ENERGY	4.55	4.60	4.65	4.70	4.75	4.80	4.85	4.90	4.95	5.00
COEFFICIENT	0.0114	0.0113	0.0112	0.0111	0.0111	0.0110	0.0109	0.0108	0.0107	0.0106
ENERGY	5.05	5.10	5.15	5.20	5.25	5.30	5.35	5.40	5.45	5.50
COEFFICIENT	0.0105	0.0105	0.0104	0.0103	0.0103	0.0102	0.0102	0.0101	0.0100	0.0100
ENERGY	5.55	5.60	5.65	5.70	5.75	5.80	5.85	5.90	5.95	6.00
COEFFICIENT	0.0099	0.0098	0.0098	0.0097	0.0097	0.0096	0.0095	0.0095	0.0094	0.0093
ENERGY	6.05	6.10	6.15	6.20	6.25	6.30	6.35	6.40	6.45	6.50
COEFFICIENT	0.0093	0.0092	0.0092	0.0092	0.0091	0.0091	0.0090	0.0090	0.0089	0.0089
ENERGY	6.55	6.60	6.65	6.70	6.75	6.80	6.85	6.90	6.95	7.00
COEFFICIENT	0.0088	0.0088	0.0087	0.0087	0.0086	0.0086	0.0085	0.0085	0.0085	0.0084
ENERGY	7.05	7.10	7.15	7.20	7.25	7.30	7.35	7.40	7.45	7.50
COEFFICIENT	0.0084	0.0083	0.0083	0.0082	0.0082	0.0081	0.0081	0.0080	0.0080	0.0079
ENERGY	7.55	7.60	7.65	7.70	7.75	7.80	7.85	7.90	7.95	8.00
COEFFICIENT	0.0079	0.0078	0.0078	0.0078	0.0077	0.0077	0.0076	0.0076	0.0075	0.0075
ENERGY	8.05	8.10	8.15	8.20	8.25	8.30	8.35	8.40	8.45	8.50
COEFFICIENT	0.0074	0.0074	0.0074	0.0073	0.0073	0.0073	0.0072	0.0072	0.0072	0.0071
ENERGY	8.55	8.60	8.65	8.70	8.75	8.80	8.85	8.90	8.95	9.00
COEFFICIENT	0.0071	0.0071	0.0071	0.0070	0.0070	0.0070	0.0069	0.0069	0.0069	0.0068
ENERGY	9.05	9.10	9.15	9.20	9.25	9.30	9.35	9.40	9.45	9.50
COEFFICIENT	0.0068	0.0068	0.0067	0.0067	0.0067	0.0066	0.0066	0.0066	0.0065	0.0065
ENERGY	9.55	9.60	9.65	9.70	9.75	9.80	9.85	9.90	9.95	****
COEFFICIENT	0.0065	0.0064	0.0064	0.0064	0.0063	0.0063	0.0063	0.0063	0.0062	0.0062

PAIR PROD. ENERGY ABS. COEFF. FOR TUNGSTEN

ENERGY	0.05	0.10	0.15	0.20	0.25	0.30	0.35	0.40	0.45	0.50
COEFFICIENT	0.0	0.0	0.0	0.0	0.0	0.0	0.0	0.0	0.0	0.0
ENERGY	0.55	0.60	0.65	0.70	0.75	0.80	0.85	0.90	0.95	1.00
COEFFICIENT	0.0	0.0	0.0	0.0	0.0	0.0	0.0	0.0	0.0	0.0
ENERGY	1.05	1.10	1.15	1.20	1.25	1.30	1.35	1.40	1.45	1.50
COEFFICIENT	0.0000	0.0001	0.0001	0.0002	0.0002	0.0002	0.0003	0.0003	0.0004	0.0004
ENERGY	1.55	1.60	1.65	1.70	1.75	1.80	1.85	1.90	1.95	2.00
COEFFICIENT	0.0006	0.0007	0.0009	0.0010	0.0012	0.0014	0.0015	0.0017	0.0018	0.0020
ENERGY	2.05	2.10	2.15	2.20	2.25	2.30	2.35	2.40	2.45	2.50
COEFFICIENT	0.0022	0.0024	0.0026	0.0029	0.0031	0.0033	0.0035	0.0037	0.0039	0.0041
ENERGY	2.55	2.60	2.65	2.70	2.75	2.80	2.85	2.90	2.95	3.00
COEFFICIENT	0.0043	0.0046	0.0048	0.0050	0.0052	0.0054	0.0056	0.0058	0.0060	0.0063
ENERGY	3.05	3.10	3.15	3.20	3.25	3.30	3.35	3.40	3.45	3.50
COEFFICIENT	0.0065	0.0067	0.0069	0.0071	0.0073	0.0075	0.0077	0.0079	0.0081	0.0083
ENERGY	3.55	3.60	3.65	3.70	3.75	3.80	3.85	3.90	3.95	4.00
COEFFICIENT	0.0085	0.0087	0.0089	0.0091	0.0093	0.0095	0.0097	0.0099	0.0101	0.0103
ENERGY	4.05	4.10	4.15	4.20	4.25	4.30	4.35	4.40	4.45	4.50
COEFFICIENT	0.0105	0.0106	0.0108	0.0110	0.0112	0.0113	0.0115	0.0117	0.0119	0.0120
ENERGY	4.55	4.60	4.65	4.70	4.75	4.80	4.85	4.90	4.95	5.00
COEFFICIENT	0.0122	0.0124	0.0126	0.0127	0.0129	0.0131	0.0133	0.0134	0.0136	0.0138
ENERGY	5.05	5.10	5.15	5.20	5.25	5.30	5.35	5.40	5.45	5.50
COEFFICIENT	0.0139	0.0141	0.0142	0.0143	0.0145	0.0146	0.0147	0.0149	0.0150	0.0151
ENERGY	5.55	5.60	5.65	5.70	5.75	5.80	5.85	5.90	5.95	6.00
COEFFICIENT	0.0153	0.0154	0.0156	0.0157	0.0158	0.0160	0.0161	0.0162	0.0164	0.0165
ENERGY	6.05	6.10	6.15	6.20	6.25	6.30	6.35	6.40	6.45	6.50
COEFFICIENT	0.0166	0.0167	0.0168	0.0169	0.0170	0.0171	0.0173	0.0174	0.0175	0.0176
ENERGY	6.55	6.60	6.65	6.70	6.75	6.80	6.85	6.90	6.95	7.00
COEFFICIENT	0.0177	0.0178	0.0179	0.0180	0.0181	0.0182	0.0183	0.0184	0.0185	0.0186
ENERGY	7.05	7.10	7.15	7.20	7.25	7.30	7.35	7.40	7.45	7.50
COEFFICIENT	0.0188	0.0189	0.0190	0.0191	0.0192	0.0193	0.0194	0.0195	0.0196	0.0197
ENERGY	7.55	7.60	7.65	7.70	7.75	7.80	7.85	7.90	7.95	8.00
COEFFICIENT	0.0198	0.0199	0.0200	0.0202	0.0203	0.0204	0.0205	0.0206	0.0207	0.0208
ENERGY	8.05	8.10	8.15	8.20	8.25	8.30	8.35	8.40	8.45	8.50
COEFFICIENT	0.0209	0.0210	0.0211	0.0211	0.0212	0.0213	0.0214	0.0215	0.0216	0.0216
ENERGY	8.55	8.60	8.65	8.70	8.75	8.80	8.85	8.90	8.95	9.00
COEFFICIENT	0.0217	0.0218	0.0219	0.0220	0.0221	0.0222	0.0222	0.0223	0.0224	0.0225
ENERGY	9.05	9.10	9.15	9.20	9.25	9.30	9.35	9.40	9.45	9.50
COEFFICIENT	0.0226	0.0227	0.0228	0.0228	0.0229	0.0230	0.0231	0.0232	0.0233	0.0233
ENERGY	9.55	9.60	9.65	9.70	9.75	9.80	9.85	9.90	9.95	****
COEFFICIENT	0.0234	0.0235	0.0236	0.0237	0.0238	0.0239	0.0239	0.0240	0.0241	0.0242

D.4 GAMRE Sample Problem

GAMRE is a short program written at M.I.T., which merely converts a multi-group gamma spectrum into suitable format for input into RESPOND. In the present study the only input spectra were provided by ANISN. GAMRE divides the total group flux from ANISN by the width of its energy group and then finds the value of the gamma spectrum at 200 points between 0.05 and 10.0 MEV (again by simple LINEAR interpolation). These values are then punched on cards for input to RESPOND.

```
C      GAMRE1                                                          SUB20001
C      AUTHOR PAUL A. SCHEINERT                                        SUB20002
C      INPUT GAMMA SPECTRUM TO RESPOND                                 SUB20003
C                                                                      SUB20004
       DIMENSION EN1(50),GROLD(50),GRNEW(200),EN2(200),TITLE(12),      SUB20005
      1  FLUX1(50)                                                     SUB20006
C                                                                      SUB20007
       DO 5 I=1,50                                                     SUB20008
       FLUX1(I)=0.0                                                    SUB20009
       GROLD(I)=0.0                                                    SUB20010
       EN1(I)=0.0                                                      SUB20011
     5 CONTINUE                                                        SUB20012
C                                                                      SUB20013
       DO 8 I=1,200                                                    SUB20014
       GRNEW(I)=0.0                                                    SUB20015
       EN2(I)=0.05*I                                                   SUB20016
     8 CONTINUE                                                        SUB20017
C                                                                      SUB20018
    60 READ (5,2,END=999) TITLE,N                                      SUB20019
     2 FORMAT (12A4,12X,I5)                                            SUB20020
       READ (5,3) (EN1(I),I=1,N)                                       SUB20021
       READ (5,3) (GROLD(I),I=1,N)                                     SUB20022
     3 FORMAT (10F7.0)                                                 SUB20023
C                                                                      SUB20024
       DO 9 II=1,N,9                                                   SUB20025
       KK=II+8                                                         SUB20026
       WRITE (6,51) (EN1(I),I=II,KK)                                   SUB20027
    51 FORMAT (1X/4X,'ENERGY',10X,9(4X,F4.2,2X))                       SUB20028
       WRITE (6,52) (GROLD(I),I=II,KK)                                 SUB20029
    52 FORMAT (4X,'SPECTRUM',8X,9(2X,F8.5))                            SUB20030
     9 CONTINUE                                                        SUB20031
C                                                                      SUB20032
       DO 10 I=1,N                                                     SUB20033
       IF (I-1) 11,12,11                                               SUB20034
    12 DELE=EN1(I)                                                     SUB20035
       FLUX1(I)=GROLD(I)/DELE                                          SUB20036
```

```
      GO TO 10                                                          SUB20037
   11 II=I-1                                                            SUB20038
      DELE=EN1(I)-EN1(II)                                               SUB20039
      FLUX1(I)=GROLD(I)/DELE                                            SUB20040
   10 CONTINUE                                                          SUB20041
C                                                                       SUB20042
      DO 20 I=1,200                                                     SUB20043
      ANUM=0.05*I                                                       SUB20044
      EEO=ANUM+0.025                                                    SUB20045
      EE1=EEO-0.05                                                      SUB20046
      DO 30 J=1,N                                                       SUB20047
      IF (EEO-EN1(J)) 24,24,21                                          SUB20048
   21 IF (EE1-EN1(J)) 25,30,30                                          SUB20049
   30 CONTINUE                                                          SUB20050
   24 GRNEW(I)=FLUX1(J)                                                 SUB20051
      GO TO 20                                                          SUB20052
   25 JJ=J+1                                                            SUB20053
      DIFF=EEO-EN1(J)                                                   SUB20054
      REM=EN1(J)-EE1                                                    SUB20055
      A1=DIFF*FLUX1(JJ)                                                 SUB20056
      A2=REM*FLUX1(J)                                                   SUB20057
      TOT=A1+A2                                                         SUB20058
      GRNEW(I)=TOT/0.05                                                 SUB20059
   20 CONTINUE                                                          SUB20060
C                                                                       SUB20061
      WRITE (6,42) TITLE                                                SUB20062
   42 FORMAT ('1'/10X,12A4/)                                            SUB20063
C                                                                       SUB20064
      DO 40 II=1,200,10                                                 SUB20065
      KK=II+9                                                           SUB20066
      WRITE (6,41) (EN2(I),I=II,KK)                                     SUB20067
   41 FORMAT (1X/4X,'ENERGY',10X,10(3X,F5.2,2X))                        SUB20068
      WRITE (6,43) (GRNEW(I),I=II,KK)                                   SUB20069
   43 FORMAT (4X,'SPECTRUM',8X,10(1X,F9.5))                             SUB20070
   40 CONTINUE                                                          SUB20071
C                                                                       SUB20072
```

```
      DO 50 II=1,181,12                                                  SUB20073
      KK=II+11                                                           SUB20074
      PUNCH 53, (GRNEW(I),I=II,KK)                                       SUB20075
   53 FORMAT (12F6.4)                                                    SUB20076
   50 CONTINUE                                                           SUB20077
      PUNCH 54, (GRNEW(I),I=193,200)                                     SUB20078
   54 FORMAT (8F6.4)                                                     SUB20079
C                                                                        SUB20080
C     THIS COMPLETES CALCULATION FOR ONE SPECTRUM                        SUB20081
C                                                                        SUB20082
      GO TO 60                                                           SUB20083
  999 STOP                                                               SUB20084
      END                                                                SUB20085
```

```
200 POINT GAMMA SPECTRUM  1-6                                          18
0.05    0.1     0.2     0.3     0.4     0.6     0.8     1.0     1.33    1.66
2.0     2.5     3.0     4.0     5.0     6.5     8.0     10.0
0.000060.000850.010910.032010.048610.149490.105310.098040.136620.06847
0.104240.112380.067070.041710.012180.004630.006400.00101
200 POINT GAMMA SPECTRUM  7-8                                          18
0.05    0.1     0.2     0.3     0.4     0.6     0.8     1.0     1.33    1.66
2.0     2.5     3.0     4.0     5.0     6.5     8.0     10.0
0.000050.000700.010510.029140.042840.138760.098530.090170.139780.06586
0.113660.124710.074280.044700.012930.004810.007540.00102
```

200 POINT GAMMA SPECTRUM 12-17

ENERGY	0.05	0.10	0.15	0.20	0.25	0.30	0.35	0.40	0.45	0.50
SPECTRUM	0.06270	0.67690	1.23200	1.22845	1.22490	1.03125	0.83760	0.79330	0.75900	0.75900
ENERGY	0.55	0.60	0.65	0.70	0.75	0.80	0.85	0.90	0.95	1.00
SPECTRUM	0.75900	0.47908	0.19915	0.19915	0.19915	0.17660	0.15405	0.15405	0.15405	0.13119
ENERGY	1.05	1.10	1.15	1.20	1.25	1.30	1.35	1.40	1.45	1.50
SPECTRUM	0.10833	0.10833	0.10833	0.10833	0.10833	0.10833	0.08785	0.08558	0.08558	0.08558
ENERGY	1.55	1.60	1.65	1.70	1.75	1.80	1.85	1.90	1.95	2.00
SPECTRUM	0.08558	0.08558	0.08475	0.08282	0.08282	0.08282	0.08282	0.08282	0.08282	0.07249
ENERGY	2.05	2.10	2.15	2.20	2.25	2.30	2.35	2.40	2.45	2.50
SPECTRUM	0.06216	0.06216	0.06216	0.06216	0.06216	0.06216	0.06216	0.06216	0.06216	0.06353
ENERGY	2.55	2.60	2.65	2.70	2.75	2.80	2.85	2.90	2.95	3.00
SPECTRUM	0.06490	0.06490	0.06490	0.06490	0.06490	0.06490	0.06490	0.06490	0.06490	0.05807
ENERGY	3.05	3.10	3.15	3.20	3.25	3.30	3.35	3.40	3.45	3.50
SPECTRUM	0.05124	0.05124	0.05124	0.05124	0.05124	0.05124	0.05124	0.05124	0.05124	0.05124
ENERGY	3.55	3.60	3.65	3.70	3.75	3.80	3.85	3.90	3.95	4.00
SPECTRUM	0.05124	0.05124	0.05124	0.05124	0.05124	0.05124	0.05124	0.05124	0.05124	0.04708
ENERGY	4.05	4.10	4.15	4.20	4.25	4.30	4.35	4.40	4.45	4.50
SPECTRUM	0.04292	0.04292	0.04292	0.04292	0.04292	0.04292	0.04292	0.04292	0.04292	0.04292
ENERGY	4.55	4.60	4.65	4.70	4.75	4.80	4.85	4.90	4.95	5.00
SPECTRUM	0.04292	0.04292	0.04292	0.04292	0.04292	0.04292	0.04292	0.04292	0.04292	0.03999
ENERGY	5.05	5.10	5.15	5.20	5.25	5.30	5.35	5.40	5.45	5.50
SPECTRUM	0.03706	0.03706	0.03706	0.03706	0.03706	0.03706	0.03706	0.03706	0.03706	0.03706
ENERGY	5.55	5.60	5.65	5.70	5.75	5.80	5.85	5.90	5.95	6.00
SPECTRUM	0.03706	0.03706	0.03706	0.03706	0.03706	0.03706	0.03706	0.03706	0.03706	0.03706
ENERGY	6.05	6.10	6.15	6.20	6.25	6.30	6.35	6.40	6.45	6.50
SPECTRUM	0.03706	0.03706	0.03706	0.03706	0.03706	0.03706	0.03706	0.03706	0.03706	0.05919
ENERGY	6.55	6.60	6.65	6.70	6.75	6.80	6.85	6.90	6.95	7.00
SPECTRUM	0.08132	0.08132	0.08132	0.08132	0.08132	0.08132	0.08132	0.08132	0.08132	0.08132
ENERGY	7.05	7.10	7.15	7.20	7.25	7.30	7.35	7.40	7.45	7.50
SPECTRUM	0.08132	0.08132	0.08132	0.08132	0.08132	0.08132	0.08132	0.08132	0.08132	0.08132
ENERGY	7.55	7.60	7.65	7.70	7.75	7.80	7.85	7.90	7.95	8.00
SPECTRUM	0.08132	0.08132	0.08132	0.08132	0.08132	0.08132	0.08132	0.08132	0.08132	0.04427
ENERGY	8.05	8.10	8.15	8.20	8.25	8.30	8.35	8.40	8.45	8.50
SPECTRUM	0.00722	0.00722	0.00722	0.00722	0.00722	0.00722	0.00722	0.00722	0.00722	0.00722
ENERGY	8.55	8.60	8.65	8.70	8.75	8.80	8.85	8.90	8.95	9.00
SPECTRUM	0.00722	0.00722	0.00722	0.00722	0.00722	0.00722	0.00722	0.00722	0.00722	0.00722
ENERGY	9.05	9.10	9.15	9.20	9.25	9.30	9.35	9.40	9.45	9.50
SPECTRUM	0.00722	0.00722	0.00722	0.00722	0.00722	0.00722	0.00722	0.00722	0.00722	0.00722
ENERGY	9.55	9.60	9.65	9.70	9.75	9.80	9.85	9.90	9.95	10.00
SPECTRUM	0.00722	0.00722	0.00722	0.00722	0.00722	0.00722	0.00722	0.00722	0.00722	0.00361

ENERGY	0.05	0.10	0.20	0.30	0.40	0.60	0.80	1.00	1.33
SPECTRUM	0.00018	0.00669	0.12320	0.12245	0.08376	0.15180	0.03983	0.03081	0.03575
ENERGY	1.66	2.00	2.50	3.00	4.00	5.00	6.50	8.00	****
SPECTRUM	0.02824	0.02816	0.03108	0.03245	0.05124	0.04292	0.05559	0.12198	0.01443

D.5 MITSPECTRA Sample Problem

MITSPECTRA was used in this study to unfold a gamma spectrum from measured experimental data. The code itself is identical to the code used for unfolding neutron spectra from foil activities, as described and listed in Ref. (C, 2), thus only the input/output are shown here.

```
(6E12.5)
(6E12.5)
(6E12.5)
(15E4.2)
 FE   ZR   SN    W   PB
 4.12889E+04 2.79641E+05 1.91821E+05 5.37016E+05 1.87352E+06 3.07627E+06
 5.16568E+06 4.74719E+06 2.94464E+06 6.00610E+06 4.08372E+06 4.40862E+06
 6.21824E+06 2.00467E+06 1.32525E+06 4.67803E+05 3.37644E+04 2.57262E+03
   1.209E-05   9.330E-06   7.121E-06   5.433E-06   4.217E-06   3.380E-06  FE
   2.855E-06   2.424E-06   2.076E-06   1.716E-06   1.399E-06   1.135E-06  FE
   8.537E-07   6.481E-07   5.585E-07   7.554E-07   2.457E-06   2.246E-05  FE
   1.462E-05   1.093E-05   8.042E-06   5.882E-06   4.382E-06   3.395E-06  ZR
   2.811E-06   2.358E-06   2.015E-06   1.683E-06   1.406E-06   1.192E-06  ZR
   1.006E-06   9.575E-07   1.150E-06   2.470E-06   9.277E-06   4.086E-05  ZR
   1.624E-05   1.202E-05   8.699E-06   6.223E-06   4.526E-06   3.437E-06  SN
   2.816E-06   2.351E-06   2.016E-06   1.711E-06   1.473E-06   1.311E-06  SN
   1.239E-06   1.403E-06   1.992E-06   4.697E-06   1.570E-05   3.906E-05  SN
   1.959E-05   1.432E-05   1.025E-05   7.241E-06   5.187E-06   3.881E-06   W
   3.160E-06   2.656E-06   2.340E-06   2.129E-06   2.039E-06   2.088E-06   W
   2.495E-06   3.536E-06   5.726E-06   1.392E-05   2.567E-05   5.603E-05   W
   2.054E-05   1.501E-05   1.074E-05   7.592E-06   5.438E-06   4.072E-06  PB
   3.328E-06   2.823E-06   2.529E-06   2.375E-06   2.379E-06   2.562E-06  PB
   3.208E-06   4.622E-06   7.540E-06   1.786E-05   1.944E-05   6.122E-05  PB
    5.41E+01    5.69E+01    7.22E+01    9.61E+01    8.53E+01
 .10 .10 .10 .10 .10
```

```
NO. OF REGIS   5  NO. OF GROUPS  18
(6E1  2.5)
(6E1  2.5)
(6E1  2.5)
(15E  4.2)
FLUX GUESS
  0.4124690+05     0.2796410+06     0.1518210+06     0.5370160+06     0.1873520+07
  0.3076270+07     0.5165610+07     0.4747190+07     0.2944640+07     0.6006160+07
  0.4083720+07     0.4406620+07     0.6218240+07     0.2004670+07     0.1325250+07
  0.4678630+06     0.3376440+05     0.2572620+04

CROSS SECTION DATA

     0.00001     0.00001     0.00001     0.00001     0.00000     0.00000     0.00000     0.00000     0.00000     0.00000
     0.00000     0.00000     0.00000     0.00000     0.00000     0.00000     0.00000     0.00002
     0.00001     0.00001     0.00001     0.00001     0.00000     0.00000     0.00000     0.00000     0.00000     0.00000
     0.00000     0.00000     0.00000     0.00000     0.00000     0.00000     0.00001     0.00004
     0.00002     0.00001     0.00001     0.00001     0.00000     0.00000     0.00000     0.00000     0.00000     0.00000
     0.00000     0.00000     0.00000     0.00000     0.00000     0.00000     0.00002     0.00004
     0.00002     0.00001     0.00001     0.00001     0.00001     0.00000     0.00000     0.00000     0.00000     0.00000
     0.00000     0.00000     0.00000     0.00000     0.00001     0.00001     0.00003     0.00006
     0.00002     0.00002     0.00001     0.00001     0.00001     0.00000     0.00000     0.00000     0.00000     0.00000
     0.00000     0.00000     0.00000     0.00000     0.00001     0.00002     0.00002     0.00006

NORMALIZATION VECTOR

     0.2234750-06     0.2569420-06     0.2249300-06     0.2038500-06     0.2407970-06
     0.1726580-06     0.1925130-06     0.1664810-06     0.1490110-06     0.1759570-06
     0.1316260-06     0.1413350-06     0.1204840-06     0.1066590-06     0.1259080-06
     0.1004250-06     0.1023740-06     0.8615110-07     0.7534850-07     0.8900350-07
     0.7794920-07     0.7701230-07     0.6268690-07     0.5397500-07     0.6375140-07
     0.6247080-07     0.5966680-07     0.4780380-07     0.4038500-07     0.4773730-07
     0.5277260-07     0.4940240-07     0.3990270-07     0.3436240-07     0.4057520-07
     0.4486090-07     0.4144110-07     0.3256230-07     0.2763780-07     0.3309490-07
     0.3137330-07     0.3541300-07     0.2792240-07     0.2434960-07     0.2964330-07
     0.3171900-07     0.2957820-07     0.2369800-07     0.2215400-07     0.2784290-07
     0.2545050-07     0.2471000-07     0.2040160-07     0.2121740-07     0.2788980-07
     0.2027960-07     0.2094000-07     0.1315780-07     0.2172730-07     0.3003510-07
     0.1578030-07     0.1768010-07     0.1716060-07     0.2596250-07     0.3760340-07
     0.1197960-07     0.1662770-07     0.1943210-07     0.3679500-07     0.5418520-07
     0.1037340-07     0.2021100-07     0.2759000-07     0.5958370-07     0.8839390-07
     0.1376030-07     0.4340540-07     0.6501550-07     0.1448490-06     0.2093780-06
     0.4541580-07     0.1630400-06     0.2174510-06     0.2671170-06     0.2279010-06
     0.4151970-06     0.7181010-06     0.5490970-06     0.5830380-06     0.7177020-06

NORMALIZED INITIAL CALCULATED ACTIVITY RATIOS

0.1666730+01  0.1660020+01  0.1354500+01  0.1417070+01  0.1423550+01
```

ITERATION NO. 8

	INIT FLUX GUESS	8TH ITER FLUX	WGHTD FLUX	NORM INIT FLUX	NORM 8TH ITER FLUX	NORM WGHTD FLUX	PCT. DEV.
GROUP 1	0.2416680+05	0.2341110+05	0.2943510+05	0.9511860-03	0.1237810-02	0.1237810-02	-30.134
GROUP 2	0.1772220+06	0.2735960+06	0.2742200+06	0.6442180-02	0.1153150-01	0.1153150-01	-79.001
GROUP 3	0.1216670+06	0.1496460+06	0.1497680+06	0.4419040-02	0.6298090-02	0.6298090-02	-42.521
GROUP 4	0.3403340+06	0.4596560+06	0.4594690+06	0.1237140-01	0.1927960-01	0.1927960-01	-55.846
GROUP 5	0.1187340+07	0.1866910+07	0.1862430+07	0.4316090-01	0.7831910-01	0.7831910-01	-81.459
GROUP 6	0.1943590+07	0.2566150+07	0.2668330+07	0.7086900-01	0.1122090+00	0.1122090+00	-58.333
GROUP 7	0.3273750+07	0.3923380+07	0.3926580+07	0.1190030+00	0.1651210+00	0.1651210+00	-38.753
GROUP 8	0.3006530+07	0.2392640+07	0.2895000+07	0.1093630+00	0.1217410+00	0.1217410+00	-11.319
GROUP 9	0.1866160+07	0.1693810+07	0.1695190+07	0.6783560-01	0.7126640-01	0.7128640-01	-5.095
GROUP 10	0.3806360+07	0.2685190+07	0.2691390+07	0.1383650+00	0.1131790+00	0.1131790+00	18.202
GROUP 11	0.2584060+07	0.1858300+07	0.1859810+07	0.9397800-01	0.7820920-01	0.7820920-01	16.969
GROUP 12	0.2793560+07	0.1627780+07	0.1629110+07	0.1015630+00	0.6850770-01	0.6850770-01	32.546
GROUP 13	0.3946810+07	0.1334260+07	0.1335290+07	0.1432520+00	0.5615180-01	0.5615190-01	60.802
GROUP 14	0.1275460+07	0.1086490+07	0.1085860+07	0.4618220-01	0.4566290-01	0.4566290-01	1.125
GROUP 15	0.8398770+06	0.8155170+06	0.8161920+06	0.3053020-01	0.3432230-01	0.3432230-01	-12.421
GROUP 16	0.2964760+06	0.3695750+06	0.3698760+06	0.1077690-01	0.1555410-01	0.1555410-01	-44.328
GROUP 17	0.2139820+05	0.2135160+05	0.2137720+05	0.7778420-03	0.1319480-02	0.1319480-02	-69.634
GROUP 18	0.1638400+04	0.1662040+04	0.1664200+04	0.5926630-04	0.6998320-04	0.6998320-04	-18.093
TOTAL	0.2750570+08	0.2376060+08	0.2378300+08	0.1000000+01	0.1000000+01	0.1000000+01	0.0

	ACTIVITY INPUT	CALC ACTIVITY	PCT. DEV.	INPUT ERROR
FE	0.5410000+02	0.5648660+02	-5.005	0.1000
ZR	0.5690000+02	0.5946650+02	-4.501	0.1000
SN	0.7220000+02	0.6333850+02	12.274	0.1000
W	0.9610000+02	0.8416540+02	12.398	0.1000
PB	0.8530000+02	0.9401840+02	-10.221	0.1000

ITERATION NO. 10

	INIT FLUX GUESS	10TH ITER FLUX	WGHTD FLUX	NORM INIT FLUX	NORM 10TH ITER FLUX	NORM WGHTD FLUX	PCT. DEV.
GROUP 1	0.261669D+05	0.302035D+05	0.302306D+05	0.951186D-03	0.131146D-02	0.131146D-02	-37.876
GROUP 2	0.177222D+06	0.236570D+06	0.237236D+06	0.644218D-02	0.102947D-01	0.102947D-01	-100.160
GROUP 3	0.121567D+06	0.156271D+06	0.156411D+06	0.441904D-02	0.678541D-02	0.678541D-02	-53.549
GROUP 4	0.340334D+06	0.484927D+06	0.485362D+06	0.123714D-01	0.210559D-01	0.210559D-01	-70.193
GROUP 5	0.116734D+07	0.200316D+07	0.200495D+07	0.431609D-01	0.869786D-01	0.869786D-01	-101.522
GROUP 6	0.194959D+07	0.278933D+07	0.279083D+07	0.708690D-01	0.121072D+00	0.121072D+00	-70.838
GROUP 7	0.327375D+07	0.395265D+07	0.395620D+07	0.119003D+00	0.171627D+00	0.171627D+00	-44.220
GROUP 8	0.350853D+07	0.277638D+07	0.277937D+07	0.109363D+00	0.120574D+00	0.120574D+00	-10.252
GROUP 9	0.186616D+07	0.162859D+07	0.163005D+07	0.678366D-01	0.707146D-01	0.707146D-01	-4.242
GROUP 10	0.380636D+07	0.238067D+07	0.238230D+07	0.138365D+00	0.103370D+00	0.103370D+00	25.291
GROUP 11	0.254806D+07	0.169927D+07	0.170079D+07	0.940780D-01	0.737837D-01	0.737837D-01	21.572
GROUP 12	0.279356D+07	0.141371D+07	0.141498D+07	0.101563D+00	0.613845D-01	0.613845D-01	39.560
GROUP 13	0.394381D+07	0.131604D+07	0.131695D+07	0.143252D+00	0.441173D-01	0.441173D-01	69.203
GROUP 14	0.127046D+07	0.110350D+07	0.110449D+07	0.461822D-01	0.479146D-01	0.479146D-01	-3.751
GROUP 15	0.839677D+06	0.860671D+06	0.861443D+06	0.305302D-01	0.373710D-01	0.373710D-01	-22.407
GROUP 16	0.296470D+06	0.403097D+06	0.403458D+06	0.107769D-01	0.175028D-01	0.175028D-01	-62.410
GROUP 17	0.213932D+05	0.338395D+05	0.338693D+05	0.777842D-03	0.146931D-02	0.146931D-02	-88.896
GROUP 18	0.163640D+04	0.167191D+04	0.167341D+04	0.592663D-04	0.725957D-04	0.725957D-04	-22.491
TOTAL	0.275697D+08	0.230304D+08	0.230511D+08	0.100000D+01	0.100000D+01	0.100000D+01	0.0

	ACTIVITY INPUT	CALC ACTIVITY	PCT. DEV.	INPUT ERROR
FE	0.541000D+02	0.567676D+02	-4.820	0.1000
ZR	0.569000D+02	0.595085D+02	-4.584	0.1000
SN	0.722000D+02	0.634705D+02	12.091	0.1000
W	0.961000D+02	0.842657D+02	12.310	0.1000
PB	0.853000D+02	0.939247D+02	-10.111	0.1000

Appendix E References

(A1) Atomics International, "Fuels, Materials, and Control Rod Development Programs", AI-AEC-13109, p.59 (1973)

(A2) Atomics International, "Fuels, Materials, and Control Rod Development Programs", AI-AEC-13119, pp. 31, (Feb. 15, 1974).

(A3) Attix, Frank H., "Luminescence Dosimetery", Proceedings of International Conference on Luminescence Dosimetry, Stanford, California (April 1967).

(B1) Becker, K., Solid State Dosimetry, CRC Press, Cleveland, Ohio (1973).

(B2) Becker, K. "Some Characteristics of RPL Dosimeter Glasses," Solid State and Chemical Radiation Dosimetry in Medicine and Biology, pp. 131-146, (1967).

(B3) Bethe, N.A., and Ashkin, J., "Experimental Nuclear Physics", Segre E., Editor, Vol. I, Wiley, New York, pp. 325, (1953).

(B4) Bichsel, H.,"Radiation Dosimetry", Attix, F.H., and Roesch, W.C., Editors, Vol. I , Academic Press, New York, (1968).

(B5) Boag, J.W.,"Radiation Dosimetry", Attix, F. H., and Roesch, W. C., Editors, Vol. II, Academic Press, New York, (1968).

(B6) Boag, J.W., "Radiation Dosimetry", Hine, G. J., Brownell, G. L. , Editors, Academic Press, New York, pp. 153, (1956).

(B7) Boulette, E.T., Marr, D.R., Bunch, W.L., "Analysis of the Measured Gamma Dose Distribution in the FTR/EMC", HEDL-TME 73-40, (April 1973).

(B8) Burlin, T.E., "Radiation Dosimetry", Vol. 1, Attix, Frank H., Roesch, William C., Editors, Academic Press, New York, (1968).

(C1) Cameron, J.R., Suntharalingam, N., and Kenny, G.N., Thermoluminescent Dosimetry, The University of Wisconsin Press, Madison, Wisconsin, (1968).

(C2) Chan, J.K., , "A Foil-Method for Neutron Spectrometry in Fast Reactors", S.M. Thesis, M.I.T. Nucl. Eng. Dept., (January 1974).

References Cond't

(D1) Deward, L. A., Stoebe, T.G., "Thermoluminescent Properties of Solids and their Applications", American Scientist, Vol. 60, Num. 3, pp. 303, (May-June, 1972).

(D2) Doerfel, "Determination of Gamma Heating in the Structural Materials of Fast Critical Assemblies by Radiophotoluminescence Glasses", EURFNR-1041, (June 1972).

(E1) Engle, W. W., Jr., "A Users Manual for ANISN, A One Dimensional Discrete Ordinates Transport Code with Anisotropic Scattering", K-1693 (March 30, 1967).

(E2) Evans, R.D., The Atomic Nucleus, McGraw Hill, New York (1955).

(E3) Evans, R.D., "Radiation Dosimetry", Attix, F.H., and Roesch, W.C., Editors, Vol, I, Academic Press, New York, pp. 100, (1968).

(F1) Fischer, A. and Turi, A., "The RFSP Programme for Unfolding Neutron Spectra from Activation Data," INDC(HUN)-8/U, (May, 1972).

(F2) Forbes, I. A., Driscoll, M. J., Thompson, T.J., Kaplan, I., and Lanning, D.D., "Design, Construction, and Evaluation of a Facility for the Simulation of Fast Reactor Blankets", M.I.T.-4105-2, MITNE-110 (Feb. 1970).

(F3) Ford, Walter E., Wallace, David M., "POPOP 4, A Code for Converting Gamma Ray Spectra to Secondary Gamma-Ray Production Cross Sections", Oak Ridge National Laboratory, CTC-12, (May 23, 1969).

(G1) Green, C.R., Halbleib, J.H., Walker, J.V., "A Technique for Unfolding Neutron Spectra from Activation Measurements", SC-PR-67-746, (Dec., 1967).

(G2) Gregory, Driscoll, M.J., Lanning, D.D., "Heterogeneous Effects in Fast Breeder Reactors", MITNE-143, C00-2250-1, (January 1973).

References Cond't

(J1) Johns, H.E., Laughlin, J.S., "Radiation Dosimetry", Hine, G.J., and Brownell, G.L., Editors, Academic Press, New York, (1956).

(K1) Kam, F.B.K., "Calculations of Gamma Ray Heating in Iron: Analysis of TSF Measurements with Thermoluminescent Dosimeters (TLD's)", Fast Reactor Analytical Shielding Progress Report, ORNL-TM-4482, pp. 55, (May 1974).

(K2) Knight, J.R., and Mynatt, "MUG, a Program for Generating Multigroup Photon Cross Sections", Oak Ridge National Laboratory, CTC-17, (1970).

(L1) Leung, T.C., Driscoll M.J., Kaplan I., Lanning, D.D. "Neutronics of an LMFBR Blanket Mockup", MITNE-127, C00-3060-1, (January 1972).

(M1) Morrison, G. W., E.A. Straker, and R. H. Ode Garden, " A Coupled Neutron and Gamma Ray Multigroup Cross Section Library for use in Shielding Calculations", Trans Am Nuc. Soc. , 15, 1, pp. 535, (June 1972).

(M2) Maksoudian, Leon Y., Probability and Statistics with Applications, International Textbook co, Scranton, Pa., (1969).

(N1) NCRP, "Stopping Powers for use with Cavity Chambers" National Committee on Radiation Protection and Measurements, NBS Handbook 79, (1961).

(R1) Reddy, A.R., Ayyangar, K., and G.L. Brownell, "Thermoluminescence Response of LiF to Reactor Neutrons", Radiation Res., 40, pp. 522 (1969).

(R2) Regulla, D.F., "Lithium Flouride Dosimetry Based on Radiophotoluminescence", Health Physics, 22, pp. 491 (1972).

(R3) Renken, James H., Adams, Kenneth G., "An Improved Capability for Solution of Photon Transport Problems by the Method of Discrete Ordinates", Sandia Laboratories, SC-RP-69-739, (December 1969).

(S1) Schulman, J. H., "Solid State Dosimetry", Amelinckx, S., Batz, B., Strumane, R., Editors. Proceedings of the NATO Summer School, Brussels, Belgium; Gordon and Breach Science Publishers, New York, pp. 107-152 (1967).

References Cond't

(S2) Schulman, J. H., Kirk, R.D., and West, E.J., "Luminescence Dosimetry", Attix, Frank H. Editor, Stanford University, pp. 113 (April 1967).

(S3) Simons, G.G. and Huntsman, T.S., "Evaluation of ^{7}LiF Thermoluminescent Dosimeters for Gamma Ray Dose Measurements in ZPPR", Argonne National Laboratory, ZPR-TM-68, (January 27, 1971).

(S4) Simons, G.G., Olson, A.P., "Analysis and Measurements of Gamma Ray Heating in the Demonstration Benchmark Plutonium Fueled Critical Assembly", Nuclear Science and Engineering, Vol. 53, Num. 2, pp. 176-196 (February 1974).

(S5) Simons, G.G., Yule, T.J., Presentation of Results at AEC/RRD Conference on Gamma Heating Measurements, (April 1974).

(S6) Simons, G.G., Yule, T.J., "Gamma Heating Measurements in Zero Power Fast Reactors with Thermoluminescent Dosimeters", Argonne National Laboratory, ZPR-TM-128, (December 1972).

(S7) Simpson, R.E., "Response of Lithium Fluoride to Reactor Neutrons", Attix, Frank H., Editor, Stanford University, (April 1967).

(S8) Spencer, L.V. and Attix, F.H., "A Theory of Cavity Ionization", Rad. Res., Vol. 3, No. 3, pp. 239-254 (1955).

(S9) Spiers, F.W., "Radiation Dosimetry", Hine, G.J., and Brownell, G.L., Editors, Academic Press, New York, pp. 27, (1958).

(S10) Springer, T.H., "Gamma Ray Heating Rate Measurements by Direct Calorimetric Methods", Atomics International Report for AEC/RRD Conference on Gamma Heating Measurements (April 1974).

(S11) Sternheimer, R.M., Phys. Rev., 88, 851, (1952).

(T1) Tappendorf, "Reactor Gamma Heat Measurements with Thermoluminescent Phosphors", Aerojet Nuclear Company UC-80, (March 1972).

References Cond't

(T2) Thompson, J.J., Ziemer, P.L., "Thermoluminescent Properties of Lithium Borate Activated by Silver", Health Physics; 25; No. 4, pp. 435-441, (October 1973).

(T3) Tuttle, R.J., "Measurements of Gamma Ray Heating by Thermoluminescent Dosimeters", Atomics International, TI-707-140-022 (May 5, 1972).

(W1) Wingate, C.L., Tochilin, E., and Goldstein, N., "Response of Lithium Fluoride to Neutrons and Charged Particles", Attix, Frank H. Editor, Stanford University, pp. 421, (April 1967).

(W2) Wood, P.J., and Driscoll, M.J., "Assessment of Thorium Blankets for Fast Breeder Reactors", MITNE-148, C00-2250-2, (July 1973).

(Y1) Yule, T.J., "A Survey of Techniques, Including the Gas Filled Ionization Counter, for Measuring Gamma-Ray Heating in Low-Power Fast Reactor Environments", Argonne National Laboratory, ZPR-TM-140, (April 26, 1973).